



Martin O'Malley, *Governor*
Anthony G. Brown, *Lt. Governor*

James T. Smith, Jr., *Secretary*
Melinda B. Peters, *Administrator*

Maryland Department of Transportation

STATE HIGHWAY ADMINISTRATION

RESEARCH REPORT

Effective Implementation of Ground Penetrating Radar (GPR) for Condition Assessment & Monitoring of Critical Infrastructure Components of Bridges and Highways

**PROF. DIMITRIOS GOULIAS
UNIVERSITY OF MARYLAND
&
DR. MICHAEL L. SCOTT
ADOJAM**

**Project number SP309B4R
FINAL REPORT**

January, 2015

The contents of this report reflect the views of the author who is responsible for the facts and the accuracy of the data presented herein. The contents do not necessarily reflect the official views or policies of the Maryland State Highway Administration. This report does not constitute a standard, specification, or regulation.

Technical Report Documentation Page

1. Report No. MD-15-SHA-UM-3-11	2. Government Accession No.	3. Recipient's Catalog No.	
4. Title and Subtitle Effective Implementation of Ground Penetrating Radar (GPR) for Condition Assessment & Monitoring of Critical Infrastructure Components of Bridges and Highways.	5. Report Date January, 2015		6. Performing Organization Code
	8. Performing Organization Report No.		
7. Author/s Dimitrios Goulias ¹ , & Michael Scott ² .	10. Work Unit No. (TRAIS)		
9. Performing Organization Name and Address ¹ University of Maryland, Department of Civil & Environmental Engineering, 0147A G.L. Martin Hall, College park, MD 20742. ² ADOJAM LLC, 11100 Kensington Blvd. Kensington, MD 20895.	11. Contract or Grant No. SHA/UM/3-11		
	13. Type of Report and Period Covered Final Report		
12. Sponsoring Organization Name and Address Maryland State Highway Administration Office of Policy & Research 707 North Calvert Street Baltimore MD 21202	14. Sponsoring Agency Code (7120) STMD - MDOT/SHA		
	13. Type of Report and Period Covered Final Report		
15. Supplementary Notes			
16. Abstract Recently Maryland State Highway Administration (SHA) started to explore use of Ground Penetrating Radar (GPR) technology to provide quantitative information for improved decision making and reduced operating costs. To take full advantage of the GPR capabilities, improved analysis techniques need to be developed and implemented. The objective of this study was to assist SHA engineers, technicians, and decision makers in their current effort to explore the use of GPR in assessing the condition of critical infrastructure components and to identify potential improvements in GPR data analysis. The research team closely interacted with representatives from selected divisions of the Office of Materials Technology (OMT) to identify potential GPR applications using existing equipment accessible to SHA, targeting critical high priority areas for analysis and improvement. In regards to pavement structures, a new methodology was suggested to improve the accuracy of GPR data analysis. The initial analysis and results indicated that Multi-scale Pavement GPR data Analysis (MPGA) has significant potential to add value and accuracy to pavement thickness data used in pavement management and rehabilitation analysis. The MPGA results indicate that pavement thickness data trends can be identified based on either automated or semi-automated procedures based on target variability levels of thickness uniformity, and thus can be used to efficiently evaluate pavement material layers. Similarly, for bridge deck analysis, techniques such as migration imaging (for concrete cover depth measurement applications among others) and Fourier analysis of GPR waveforms (for qualitative bridge deck moisture analysis) were used in addition to emerging techniques such as Short Time Fourier Transform analysis (for anticipated quantitative moisture analysis) for improving GPR data interpretation. Migration and Fourier techniques were illustrated corresponding to GPR data collected using a GPR array on selected bridge decks in the Salisbury, MD area. When applied appropriately, such techniques can provide more reliable analysis of bridge deck inspection than conventional means. In terms of precast concrete, this study has shown how GPR can be used to address several of the inspections needed in precast concrete production, including an evaluation of concrete cover depth, reinforcement location, and section thicknesses. The testing and demonstration showed significant potential for quality control using GPR.			
17. Key Words GPR, pavements, bridge decks, precast concrete.	18. Distribution Statement: No restrictions This document is available from the Research Division upon request.		
19. Security Classification (of this report) None	20. Security Classification (of this page) None	21. No. Of Pages 173	22. Price

Form DOT F 1700.7 (8-72) Reproduction of form and completed page is authorized.

University of Maryland, College Park
Department of Civil and Environmental Engineering

**Effective Implementation of Ground Penetrating Radar (GPR) for Condition Assessment
& Monitoring of Critical Infrastructure Components of Bridges and Highways**

Final Research Report

Maryland State Highway Administration

Research Project SP309B4R

Prof. Dimitrios Goulias (PI)

&

Dr. Michael L. Scott (Co-PI)
(ADOJAM)

December 16, 2014

TABLE OF CONTENTS

	Page
EXECUTIVE SUMMARY	iii
LIST OF ACRONYMS	iv
LIST OF FIGURES	v
LIST OF TABLES	vii
CHAPTER 1: INTRODUCTION	
INTRODUCTION	1
RESEARCH APPROACH	1
ORGANIZATION OF THE REPORT	2
CHAPTER 2: GPR APPLICATIONS	3
CHAPTER 3: GPR MULTI-SCALE PAVEMENT ANALYSIS	10
CHAPTER 4: GPR BRIDGE DECK ANALYSIS	23
CHAPTER 5: GPR PRECAST CONCRETE ANALYSIS	40
CHAPTER 6: GPR TESTING PROTOCOLS AND TRAINING MODULES	53
CHAPTER 7: SUMMARY, CONCLUSIONS & RECOMMENDATIONS	
SUMMARY & CONCLUSIONS	54
RECOMMENDATIONS FOR FUTURE DEVELOPMENT	56
REFERENCES	57
APPENDIX A. TESTING PROTOCOLS	
GPR FOR PAVEMENT STRUCTURES	61
GPR FOR BRIDGE DECKS	82
APPENDIX B. TRAINING MODULES	
GROUND PENETRATING RADAR (GPR) FOR PAVEMENT STRUCTURES	96
GROUND PENETRATING RADAR (GPR) FOR BRIDGE DECKS	119
GROUND PENETRATING RADAR (GPR) FOR PRECAST CONCRETE ELEMENTS	150
APPENDIX C. SCI-LAB SCRIPT	162

EXECUTIVE SUMMARY

The objective of this study was to assist State Highway Administration (SHA) engineers, technicians, and decision makers in their current effort to explore the use of Ground Penetrating Radar (GPR) in assessing the condition of critical infrastructure components and to identify potential improvements in GPR data analysis. The research team closely interacted with representatives from selected divisions of the Office of Materials Technology (OMT) to identify potential GPR applications using existing equipment accessible to SHA, targeting critical high priority areas for analysis and improvement.

With regard to pavement structures, a new methodology was suggested to improve the accuracy of GPR data analysis. The initial analysis and results indicate that this new method, Multi-scale Pavement GPR data Analysis (MPGA), has the potential to add value and accuracy to pavement thickness data used in pavement management and rehabilitation analysis.

For bridge deck evaluation, the need to capture moisture effects and detailed depth information are imperative. The use of advanced GPR data analysis techniques such as migration imaging (for concrete cover depth measurement applications among others), Fourier analysis of GPR waveforms (for qualitative bridge deck moisture analysis) and emerging techniques such as Short Time Fourier Transform analysis (for anticipated quantitative moisture analysis) were suggested.

Current quality control (QC) on precast concrete elements is based on plant inspections and periodic audits that have important limitations. Specifically, current precast quality assurance practices include labor intensive activities and sporadic inspections with the potential to miss important problems. This study showed how GPR can be used to address several of the inspection applications needed in precast concrete production, including an evaluation of concrete cover depth, reinforcement location and section thickness.

For the high priority areas of pavement structures and bridge decks, the project team developed the required testing protocols to facilitate implementation of GPR and assist SHA engineers and technicians to conduct surveys. The protocols include information related to the method (background), equipment requirements, calibration guidelines, testing procedures and recommendations for data analysis and reporting. Training material for using GPR on pavement structures, bridge decks and precast concrete elements were also developed

LIST OF ACRONYMS

HMA	Hot Mix Asphalt
GPR	Ground Penetrating Radar
GSSI	Geophysical Survey Systems, Inc.
MPGA	<u>M</u> ulti-scale <u>P</u> avement <u>G</u> PR data <u>A</u> nalysis
MSMT	Maryland Standard Method of Test
OMT	Office of Materials Technology
PMS	Pavement Management System
QA	Quality Assurance
QC	Quality Control
SHA	State Highway Administration
S&S	Sensors & Software Inc.

LIST OF FIGURES

Figure 3.1 US15 – HMA Pavement Data with Global Means (3 Layers)	13
Figure 3.2 US15 – HMA Pavement Data with MPGA Results (3 Layers)	13
Figure 3.3 US15 – HMA Pavement Layer 1 Data with Eight Subdivided Means	14
Figure 3.4 US15 – HMA Pavement Layer 1 Data with MPGA Applied (Using Eight Subdivisions)	14
Figure 3.5 US15 – HMA Pavement Layer 2 Data with Eight Subdivided Means	15
Figure 3.6 US15 – HMA Pavement Layer 2 Data with MPGA Applied (Using Eight Subdivisions)	15
Figure 3.7 US15 – HMA Pavement Layer 2 Data with Sixteen Subdivided Means	16
Figure 3.8 US15 – HMA Pavement Layer 2 Data with MPGA Applied (Using Sixteen Subdivisions)	16
Figure 3.9 US15 – HMA Pavement Layer 3 Data with Eight Subdivided Means	17
Figure 3.10 US15 – HMA Pavement Layer 3 Data with MPGA Applied (Using Eight Subdivisions)	17
Figure 3.11 US15 – HMA Pavement Layer 3 Data with Sixteen Subdivided Means	18
Figure 3.12 US15 – HMA Pavement Layer 3 Data with MPGA Applied (Using Sixteen Subdivisions)	18
Figure 3.13 US15 – HMA Pavement Data with MPGA Results (3 Layers) – Common Interlayer Trend Highlighted in Light Green	19
Figure 3.14 MD675 – Concrete Pavement Data with MPGA Results (2 Layers)	19
Figure 3.15 MD675 – Concrete Pavement Data with Global Means (2 Layers)	20
Figure 3.16 MD675 – Concrete Pavement Layer 1 Data with Sixteen Subdivided Means	20
Figure 3.17 MD675 – Concrete Pavement Layer 1 Data with MPGA Applied (Using Sixteen Subdivisions)	21
Figure 3.18 MD675 – Concrete Pavement Layer 2 Data with Sixteen Subdivided Means	21
Figure 3.19 MD675 – Concrete Pavement Layer 2 Data with MPGA Applied (Using Sixteen Subdivisions)	22
Figure 3.20 15 MD675 – Concrete Pavement Data with MPGA Results (2 Layers) Common Interlayer Trend Highlighted in Light Green	22
Figure 4.1 US 13 Northbound Over Norfolk Southern RR Migration Results (Above) vs. Attenuation Map (Below)	25
Figure 4.2 US 13 Northbound Over Norfolk Southern RR at 1” Depth	26
Figure 4.3. US 13 Northbound Over Norfolk Southern RR at 2” Depth	26
Figure 4.4 US 13 Northbound Over Norfolk Southern RR at 3” Depth	27
Figure 4.5 US 13 Northbound Over Norfolk Southern RR at 4” Depth	27
Figure 4.6 US 13 Northbound Over Norfolk Southern RR at 5” Depth	28
Figure 4.7 US 13 Northbound Over Norfolk Southern RR at 6” Depth	28
Figure 4.8 US 13 Northbound Over Norfolk Southern RR at 7” Depth	29
Figure 4.9 US 13 Northbound Over Norfolk Southern RR at 8” Depth	29
Figure 4.10 US 13 Northbound Over Norfolk Southern RR – Moisture	30
Figure 4.11 Route 290 Over Chester River Migration Results (Above) vs. Attenuation Map (Below)	30
Figure 4.12 Route 290 Over Chester River Migration Results at 1” Depth	31

Figure 4.13 Route 290 Over Chester River Migration Results at 2” Depth	31
Figure 4.14 Route 290 Over Chester River Migration Results at 3” Depth	32
Figure 4.15 Route 290 Over Chester River Migration Results at 4” Depth	32
Figure 4.16 Route 290 Over Chester River Migration Results at 5” Depth	33
Figure 4.17 Route 290 Over Chester River Migration Results at 6” Depth	33
Figure 4.18 Route 290 Over Chester River Migration Results at 7” Depth	34
Figure 4.19 Route 290 Over Chester River Migration Results at 8” Depth	34
Figure 4.20 Route 290 Over Chester River Migration Results – Moisture	35
Figure 4.21 Short Time Fourier Transform (STFT) Analysis of Bridge Deck GPR Data	35
Figure 4.22 Time Domain Bridge Deck GPR Data Comparison (Analytical Waveform Simulation of GPR Response to Wet vs. Dry Concrete)	36
Figure 4.23 Dry Concrete STFT Analysis	36
Figure 4.24 Wet/Moist Concrete STFT Analysis	37
Figure 4.25 Applying STFT Analysis Principles Using a Fourier Transform Filter	37
Figure 4.26 Fourier Transform Filtered Bridge Deck Data (Low Pass) – Rte 346 Bridge Part 1	38
Figure 4.27 Fourier Transform Filtered Bridge Deck Data (Low Pass) – Rte 346 Bridge Part 2	38
Figure 4.28 Plan View Results	39
Figure 4.29 US 13 SB over MD 346 SB FT Filtered Results (Upper) vs Attenuation Map (Lower)	39
Figure 5.1 Grid GPR Data Collected From a Precast Concrete Wall Panel: Integrated 0 to 1 Inch Depth	43
Figure 5.2 Grid GPR Data Collected From a Precast Concrete Wall Panel: Integrated 1 to 2 Inch Depth	44
Figure 5.3 Grid GPR Data Collected From a Precast Concrete Wall Panel: Integrated 2 to 3 Inch Depth	44
Figure 5.4 Grid GPR Data Collected From a Precast Concrete Wall Panel: Integrated 3 to 4 Inch Depth	45
Figure 5.5 Line Scan GPR Data Collected From a Precast Concrete Header Wall Element (Scan 1 – Horiz.): Assumed Velocity/Dielectric	45
Figure 5.6 Line Scan GPR Data Collected From a Precast Concrete Header Wall Element (Scan 1 - Horiz): Correct Velocity/Dielectric	46
Figure 5.7 Line Scan GPR Data Collected From a Precast Concrete Header Wall Element (Scan 1 – Horiz.): Correct Velocity/Dielectric (Hot/Red Color Map)	46
Figure 5.8 Line Scan GPR Data Collected From a Precast Concrete Header Wall Element (Scan 1 – Horiz.): Data Collection Parameters Shown	47
Figure 5.9 Line Scan GPR Data Collected From a Precast Concrete Header Wall Element (Scan 2 – Horiz.)	47
Figure 5.10 Line Scan GPR Data Collected From a Precast Concrete Header Wall Element (Scans 3 and 4 – Vert.)	48
Figure 5.11 Line Scan GPR Data Collected From a Precast Concrete Cylinder Element (Scan 5 – Horiz.)	48
Figure 5.12 Precast Concrete Cylinder Element	49
Figure 5.13 Line Scan GPR Data Collected From Side of a Precast Concrete Manhole Element (Scan 10 – Horiz.)	49

Figure 5.14 Precast Concrete Manhole Element	50
Figure 5.15 Line Scan GPR Data Collected From a Moist Precast Concrete Cylinder Element (Scan 11 – Horiz.)	50
Figure 5.16 Line Scan GPR Data Collected From a Moist Precast Concrete Cylinder Element (Scan 17 – Vert.)	51
Figure 5.17 Line Scan GPR Data Collected From a Sound Wall (Scan 20 – Vert.)	51
Figure 5.18 Line Scan GPR Data Collected From a Sound Wall (Scans 21, 22 – Horiz.)	52

LIST OF TABLES

Table 2.1 Technical Features of GPR Equipment Accessible to SHA	4
Table 2.2 Current & Potential GPR Applications for SHA	5
Table 2.3 MD SHA Priority Ranking	9

CHAPTER 1: INTRODUCTION

INTRODUCTION

State highway agencies are dealing with the evaluation of critical infrastructure components to assess the condition of materials and structures. Maryland State Highway Administration (SHA) can benefit from increased efficiency and reduced life cycle asset costs by taking proactive steps to apply Ground Penetrating Radar (GPR) to civil infrastructure in new and innovative ways. In the past, GPR applications to civil infrastructure have primarily been focused on localized anomaly detection and qualitative evaluations of subsurface features. These types of applications have been identified and evaluated for pavement materials, concrete structures, and other engineered civil infrastructure materials. Recently SHA has started to explore use of GPR technology. GPR can provide quantitative information for improved decision making and reduced operating costs. Efficient GPR data collection and rapid test area coverage are additional advantages discussed and considered for potential MDSHA applications.

The objectives for this research included the following:

1. **Applications.** Identify the specific areas for the application of GPR utilizing the existing equipment either in SHA's inventory and accessible through consultant contracts. Also identify GPR applications of critical interest to SHA where SHA may want to gain access to new equipment;
2. **Testing Standards/ Protocols.** Develop protocols of testing for identified GPR applications;
3. **Data Interpretation & Training.** Suggest potential improvements in GPR data interpretation analysis and develop training procedures for SHA technicians and engineers for each of the identified applications.

RESEARCH APPROACH

To achieve the objectives of this research study the following tasks were undertaken. The tasks were identified and discussed with SHA representatives from the following Office of Materials Technology (OMT) teams: Research and Technology; Soils and Aggregates Technology; Concrete Technology; Structural Materials and Pavement Marking.

Task 1: Define applications of the existing GPR equipment.

The objective of this task was to identify the applications of the existing GPR equipment accessible to SHA. SHA has access to GPR equipment, either available in-house, or through their consultants, including the following:

- Noggin Smart Cart, (250 MHz)
- Conquest (1000, 1500 MHz)

- GSSI SIR-30/ SIR-20
- USRadar

The research team reviewed the capability of such equipment and identified the areas of current and potential applications.

Task 2: Establish current and potential needs and applications.

The objective of this task was to identify a broader set of GPR applications for monitoring the spatial and functional conditions of infrastructure components. The research team identified the required GPR technology for each one of the applications identified in Objective 1 and determined which applications can be fulfilled by the existing GPR equipment identified in Task 1, and provided recommendations of alternative equipment if needed.

Task 3: Protocol and Maryland Standard method of Test (MSMT) Development

The research team identified the required methods of testing and equipment for selected critical applications and developed testing protocols (MSMTs).

Task 4: Data interpretation & training

The objective of this task was to assist SHA technicians and engineers with GPR testing and data interpretation / analysis. The research team developed training guidelines for the data collection and interpretation of GPR surveys for identified applications in Task 2.

Task 5: Final research report

The research results were included in the following chapters of this report.

ORGANIZATION OF THE REPORT

This first chapter presents the introduction, research approach and organization of this report. Chapter 2 presents the broader set of GPR applications for monitoring the conditions of infrastructure components, and the high priority areas for SHA. Chapter 3 covers the GPR post processing data analysis for pavement structures. Chapter 4 provides the methods for enhancing bridge deck analysis. Chapter 5 provides example analysis for GPR testing of precast concrete elements. Chapter 6 provides a brief description of the testing protocols and training manuals included in the appendices of this report. Finally, Chapter 7 provides conclusions and recommendations for future development.

CHAPTER 2: GPR APPLICATIONS

Under task 1, the research team reviewed the capabilities and identified potential applications for the GPR equipment accessible to SHA (including equipment available in-house, or through SHA consultants). The results included in Table 2.1 and 2.2 were discussed and reviewed with SHA representatives from four SHA teams (i.e., Research and Technology, Soils and Aggregates Technology, Concrete Technology, and the Structural Materials and Pavement Marking) and representatives provided their feedback. Priority ranking regarding the applications of interest are presented in Table 3. In order to further examine current and potential GPR needs and applications, the research team prepared and forwarded a questionnaire to the four SHA teams for assessing the current applications. The feedback from the questionnaires was discussed with the four teams along with: (i) the broader set of GPR applications for monitoring the spatial and functional conditions of infrastructure components, and (ii) the needs and required GPR technology for each one of the applications identified.

Table 2.1 Technical Features of GPR Equipment Accessible to SHA

GPR System Feature	GSSI SIR 20/30	S&S Conquest	S&S Noggin	US Radar	Competing Makes/Models
Antenna Center Freq.	400 MHz, 900 MHz, 1.0 GHz, 2.0 GHz	1.0 GHz	100 MHz, 250 MHz, 500 MHz, and 1.0 GHz	250 MHz, 500 MHz, 1.0 GHz	100 MHz to 3.0 MHz
No. of Ant. Channels	SIR 20: 2 ant. channels SIR 30: 4 ant. channels	1 ant. channel	Standard: 2 ant. channels SPIDAR: up to 7 ant. channels	1 ant. Channel	1 to >20 ant. channels
Air Coupled Ant. Avail.	Yes	No	No	No	Yes
Ground Coupled Ant. Avail.	Yes	Yes	No	Yes	Yes
High Speed Avail. >30 mph	Yes	Yes	Yes	No	Yes
Ant. Array (3 or more elements)	SIR 20: No SIR 30: Yes	No	Standard: No SPIDAR: Yes	No	Yes
Multiplex antennas (Tx – Rx combinations)	No	No	Standard: No SPIDAR: Yes	No	Yes
Pulse Repetition Freq.	100 KHz	100 KHz	100 KHz	Unspecified	100 KHz or Adjustable Dwell Time for Step Freq.
Time Range	Up to 8,000 ns	Unspecified	Up to 10,400 ns	Up to 820 ns	Adjustable
Samples/Scan	256 to 8192	Unspecified	Up to 104,000	Unspecified	Up to 104,000
Output	8 bit or 16 bit	16 bit (2's complement)	16 bit (2's complement)	Unspecified	8 bit or 16 bit
Stacking (N average scans)	Unspecified	Unlimited	Unlimited	Unspecified	Unlimited
Operating Temp.	-10 deg. C to 40 deg. C	40 deg. C to 50 deg. C -20 deg. C to 50 deg. C (SL model)	40 deg. C to 50 deg. C	-11 deg. C to 50 deg. C	-10 deg. C to 50 deg. C
Power	12V battery @ 60 Watts	12V battery @ 40 Watts or 120V AC @ 40 Watts	12V battery @ 8 Watts	12V @ 24 Watts	Varies

Table 2.2 Current & Potential GPR Applications for SHA

Application	MD SHA Priority (Rank)	Current GPR System Models Accessible by MD SHA				Other GPR
		GSSI SIR 20/30	S&S Conquest	S&S Noggin	US Radar (Various Models)	Competing Makes/Models
Thickness Detection *+^		<i>Capable:</i> - High resolution - Calibration required - Given dielectric contrast - Can be refined - Semi-auto analysis: 3 rd party software	<i>Limited capability:</i> - Medium resolution - Calibration required - Given dielectric contrast - Can be refined - Semi-auto analysis: Barriers to progress	<i>Capable:</i> - Medium/high resolution - Calibration required - Given dielectric contrast - Can be refined - Semi-auto analysis: 3 rd party analysis/soft.	<i>Limited capability:</i> - Low resolution - Calibration required - Given dielectric contrast - Less refinement available - Semi-auto analysis: Barriers to progress	<i>Capable:</i> - Highest resolution - Calibration required - Given dielectric contrast - Typically can be refined - Semi-automated analysis: 3 rd party analysis/soft.
Subsurface Void Detection [†]		<i>Capable:</i> - Detect various sizes - Categorize type Air filled Water filled - Material dependent	<i>Limited capability:</i> - Detect some sizes only - Categorize type Air filled Water filled - Material dependent	<i>Capable:</i> - Detect various sizes - Categorize type Air filled Water filled - Material dependent	<i>Limited capability:</i> - Detect large sizes only - Categorize type Air filled Water filled - Material dependent	<i>Capable:</i> - Detect various sizes - Categorize type Air filled Water filled - Material dependent
Cracking and Delamination Detection ^{†^}		<i>Potential capability:</i> - Few investigations - Crack size dependent - Crack material dependent - 3 rd party analysis options	<i>Limited capability:</i> - Low resolution - Features too small to detect	<i>Potential capability:</i> - Few investigations - Crack size dependent - Crack material dependent - 3 rd party analysis options	<i>Limited capability:</i> - Low resolution - Features too small to detect	<i>Potential capability:</i> - Few investigations - Crack size dependent - Crack material dependent - 3 rd party analysis options
Corrosion Detection [†]		<i>Potential capability:</i> - Few investigations - Environmental condition dependent	<i>Limited capability:</i> - Low resolution - Features too small to detect	<i>Potential capability:</i> - Few investigations - Environmental condition dependent	<i>Limited capability:</i> - Low resolution - Features too small to detect with this system	<i>Potential capability:</i> - Few investigations - Environmental condition dependent
Rebar: Location, Depth, Orientation *+		<i>Capable:</i> - High resolution - Imaging can be refined - Depth calibration needed - Diameter only estimated	<i>Basic capability:</i> - Medium resolution - Limited refinement avail.	<i>Capable:</i> - High resolution - Imaging can be refined - Depth calibration needed - Diameter only estimated	<i>Limited capability:</i> - Low resolution - Features too small to detect with this system	<i>Capable:</i> - Highest resolution - Imaging can be refined - Depth calibration needed - Diameter only estimated
Rate of Cement Hydration [†]		<i>Potential capability:</i> - Initial investigations completed - New opportunities	<i>Limited capability:</i> - Impractical for medium resolution system	<i>Potential capability:</i> - Initial investigations completed - New opportunities	<i>Limited capability:</i> - Impractical for low resolution System	<i>Potential capability:</i> - Initial investigations completed - New opportunities
Density Monitoring [†]		<i>Potential capability:</i> - Calibration required - Limited investigations	<i>Potential capability:</i> - Calibration required - Limited investigations	<i>Potential capability:</i> - Calibration required - Limited investigations	<i>Limited capability:</i> - Impractical for low resolution System	<i>Potential capability:</i> Calibration required Limited investigations
Drainage Related Issues [†]		<i>Potential capability:</i> - Qualitative detection - Emerging analysis options	<i>Limited capability:</i> - Limited penetration - Impractical coverage area	<i>Potential capability:</i> - Qualitative detection - Emerging analysis options	<i>Limited capability:</i> - Qualitative detection - Few analysis options	<i>Potential capability:</i> - Qualitative detection - Emerging analysis options
Other Applications [†]		- High speed data acquisition available - Precast QC/QA +more	- High speed data acquisition NOT possible - Precast QC/QA + more	- High speed data acquisition available - Precast QC/QA +more	- High speed data acquisition NOT possible - Other	- High speed data acquisition available - Precast QC/QA +more

* Significant body of literature available

† Emerging body of literature available

^ Further new developments supported by theory

‡ Reference standards available for consideration

Range of capabilities:

Poor

Limited capability

Potential capability

Basic capability

Excellent *Capable*

Explanatory Notes for Table 2.2

Thickness detection – refinement methods

Several potential options are available to refine GPR thickness detection measurement:

1. Semi-automated layer interface detection (for enhanced analysis speed and consistency);
2. Multiple options for velocity/dielectric property calibration techniques can be considered;
3. Signal filtering and decluttering for enhanced accuracy.

Void size detection

Detectable void size using GPR can be theoretically estimated using theory/modeling and experimentally tested.

Approximate detectable void sizes based on experience using impulse GPR systems with comparable center frequencies are:

<i>Make/Model</i>	<i>Center Frequency Range</i>	<i>Approx. Void Detection Size</i>
GSSI SIR 20/30	200 MHz – 2 GHz	>1 ft. down to >1 in.
S&S Conquest	1 GHz	>2 in.
S&S Noggin	500 MHz – 1.5 GHz	>4 in. down to >1.5 in.
US Radar (various models)	100 MHz – 1 GHz (MD SHA)	>2 ft. down to >2 in.

Cracking and delamination detection

Cracking and delamination detection using GPR are not always straightforward. In addition, some aspects are not fully understood. Some specific cracking and delamination phenomena have been detected, but their detection is dependent on crack geometry, morphology, depth, and material in addition to parameters of the GPR system of interest. Therefore, it is currently difficult to predict the detectability of cracks for a given GPR application. The effort required to develop such a solution (within a prescribed range in most dielectric materials) may require a future investigation in a separate project. For this project, it might be possible to evaluate conditions that impact capabilities to detect cracks using conventional GPR.

Corrosion detection

Corrosion detection using GPR includes some well understood aspects and several important issues that remain poorly understood. Two phenomena that often occur in a GPR response to corrosion of reinforcing steel in concrete are scattering loss and attenuation (often measured in

dB/meter). If moisture is also present (as when active corrosion is happening) then dispersion phenomena will also occur (which spreads the GPR frequency response spectrum).

One of the key impediments to a more complete understanding of the GPR response to corrosion phenomena is the combination of a GPR response to physical features and a GPR response to chemical features. Each of these GPR response phenomena can include complicated features in its own right. Physical response features frequently involve cracking and chemical response features generally include corrosion products. The combination of these features can produce a complete GPR response that can be hard to interpret.

Developing new ways to analyze and interpret corrosion related physical response features and corrosion related chemical response features has the potential to improve the reliability of GPR inspection where current interpretation is confounded and unclear.

Rebar location, depth, orientation

Using GPR to obtain rebar location, depth, and orientation information is well understood. It begins with the resolution of the GPR system applied. High resolution rebar imaging is achieved using Ultra Wideband (UWB) GPR systems with center frequencies of 1.5 GHz and higher. Medium resolution rebar imaging is achieved using GPR systems with center frequencies between 750 MHz and 1.5 GHz. Low resolution rebar imaging is achieved using GPR systems with center frequencies below 750 MHz. Image refinement is obtained using analysis techniques that focus distributed synthetic aperture radar energy to its original reflector location, such as migration and wave field back-propagation.

Rate of cement hydration

New opportunities exist to measure the rate of cement hydration in distributed areas using GPR in combination with conventional instrumentation. This has the potential to be achieved by correlating GPR sensitivity to moisture with fixed location measurements and complementary measurement of temperature using thermocouples. This approach has the potential to identify areas where uneven or problematic cement hydration issues may be occurring.

Low resolution GPR systems (with center frequencies below 750 MHz) have frequency content that is less efficient in exciting polarized molecules such as water. This reduces the measurable effects of GPR attenuation and dispersion phenomena at low GPR frequencies relative to high GPR frequencies. Therefore, rate of hydration GPR measurements and analysis are anticipated to be most effective at high frequencies (equal to 1.5 GHz or higher) where the response is most pronounced.

Density monitoring

Density monitoring is of interest for pavement evaluation applications where high resolution GPR is needed to detect individual pavement layers. Low frequency GPR smears out responses to pavement layer interfaces, which can also become unclear for successive layers. Therefore

high frequency GPR is desirable to obtain clear, high resolution response features in signals to be analyzed. Current GPR density monitoring techniques are correlated with calibrated cores analyzed in the laboratory.

Drainage related issues

As discussed in the “rate of cement hydration” response above, low frequency GPR is not as effective as high frequency GPR in exciting polarized water molecules (and is therefore somewhat less sensitive to moisture than high frequency GPR). In addition, current techniques require multiple phenomena to be analyzed by an expert to evaluate “qualitative detection” phenomena. Therefore, several obstacles to “quantitative” analysis of moisture exist. In the future, development of “quantitative” techniques that are more consistent and straightforward might become available.

“Limited penetration” is due to medium to high GPR frequency content that does not provide ideal penetration depth for drainage applications. Where deep penetration is desired low GPR frequencies should be used.

Other applications

Precast bridge deck elements and many other precast bridge elements can be practical targets for QC and Quality Assurance (QA) applications using GPR. Thick concrete columns or elements that contain dense reinforcing steel mesh can be difficult to evaluate with GPR due to penetration issues.

Table 2.3 MD SHA Priority Ranking

	CONCRETE TECHNOLOGY DIVISION (Precast Inspection)	FIELD EXPLORATION DIVISION (Bridge/Structure Side)	STRUCTURAL MATERIALS AND PAVEMENT MARKINGS DIVISION	FIELD EXPLORATION DIVISION (Pavement Side)
Thickness Detection	Secondary Concern	Primary Concern	Secondary Concern	Primary Concern
Rebar Location and Depth	Primary Concern	Primary Concern	Primary Concern	Secondary Concern
Subsurface Void Detection	Secondary Concern	Primary Concern	Secondary Concern	Secondary Concern
	Other Concerns	Other Concerns	Other Concerns	Other Concerns
	Portability	Portability	Portability	Speed/Efficiency (large areas)
		Corrosion		

CHAPTER 3: GPR MULTI-SCALE PAVEMENT ANALYSIS

Among the objectives of this research project was to identify potential improvements of GPR post processing data analysis. MPGA was developed to address relevant, diverse Pavement Management Systems (PMS) needs and requirements efficiently. This MPGA approach can be used to accurately evaluate pavement thickness data at appropriate length scales and to produce these results quickly. In addition MPGA can enhance the utility of complementary data for other diverse applications. Relevant to PMS, pavement layer thickness information is a crucial input parameter frequently analyzed in practice based on limited information resources such as: (i) pavement layer design information often assumed to be homogeneous throughout a section of the roadway under evaluation, (ii) measured pavement core data from selected locations and (iii) GPR pavement thickness data with variability issues that can present problems for accurate PMS analysis.

GPR data from an eleven mile section of US-15 HMA pavement and a MD 675 concrete pavement in Maryland was selected for initial analysis using the MPGA algorithm. This pavement GPR data was preprocessed using GPR manufacturer recommended procedures to identify and label three pavement layer interfaces corresponding to the asphalt pavement overlay depth, the asphalt pavement depth and the asphalt pavement base depth, respectively. This pavement data was selected for MPGA analysis due to the variety of characteristics observed. Conventional GPR data interpretation is not designed to capture these characteristics efficiently for subsequent pavement management calculations.

Figure 3.1 shows the data points corresponding to three color coded pavement layers along with horizontal lines representing the mean pavement depth, while Figure 3.2 shows the results from MPGA analysis. Qualitatively, Figure 3.1 pavement layer thickness mean values shown do not appear to represent the overall pavement thicknesses well, and also do not account for the smaller scale trends in pavement thickness of Layer 2 or Layer 3. By contrast, Layer 1 data is more consistent with a representative mean value that corresponds to the entire data section since this layer has a more uniform as-built thickness. MPGA was thus developed and applied in order to account for such broad qualitative thickness data trends, as shown in Figure 3.2. The horizontal lines in Figure 3.2 indicate relatively large scale segments of continuity and shorter discontinuity (based on the observed length characteristics). Figures 3.3 through 3.20 illustrate more details regarding how MPGA works to identify features of interest in the GPR layer data, providing detailed input data to pavement management systems.

The MPGA analysis starts by dividing a project data set into sub-segments of equal length at a scale of interest, as shown in Figure 3.3 for this example. Statistics corresponding to each subdivided data section are compared with the global statistics for the entire pavement project. Using this information, longer continuous data segments are separated from shorter, choppy segments as shown in Figure 3.4.

In automated or semi-automated MPGA procedures (using default or user input criteria), data is further subdivided from larger segment sizes (Figure 3.5 segmented and corresponding Figure 3.6 MPGA output) into smaller subsections in Figure 3.7 and the results from another round of MPGA continuity checks and consolidations are shown in Figure 3.8. The layer 3 MPGA

results shown in Figure 3.12 are relevant in comparison with Figure 3.10, where changes in localized MPGA analysis trends at different scales are evident from one step to the next. More uniform data with less thickness variability can be observed between mileposts 4 and 9. Figures 3.9 and 3.11 show the initially subdivided data segments prior to MPGA consolidation in Figures 3.10 and 3.12 respectively. Figure 3.13 shows a light green highlighted area where MPGA criteria in all three pavement layers indicate pavement layer continuity at a consistent shallow depth (indicating a thin pavement section). This thin, highlighted pavement region contrasts with thicker, more variable pavement areas outside the highlighted region for Layers 2 and 3. Therefore the thin, highlighted region may be considered to control input data for pavement management evaluation purposes in this pavement section. As noted previously, Layer 1 maintains a consistent data trend throughout the analyzed pavement section.

The longest consistent pavement layer thickness data trend shown in Figure 3.13 represents in this specific case the thinnest pavement section. This is particularly relevant to pavement management input data corresponding to Layers 2 and 3, where substantially thicker pavement layer assumptions would have been used with conventional analysis. Without identifying this thinner pavement region the implications on PMS data analysis and identification of alternative rehabilitation strategies could imply a shorter life span for this section than the remaining pavement segments.

In addition, Layer 2 and 3 data show an abrupt transition into the highlighted region at mile 4 and out of the highlighted region at mile 9. This is significant for its consistency of pavement thickness behavior among layers bounded by thickness anomalies. Layer to layer inconsistency at the transitions related to abrupt anomalies may indicate that pavement design, construction, repair, or maintenance issues exist at these boundaries throughout the depth of the pavement section, and particularly beneath the asphalt overlay.

Figures 3.14 through 3.20 provide MPGA results for a section of MD 675 concrete pavement thickness data. The length of this data section is about 1.5 miles, which is significantly shorter than the 11 mile section of US 15 analyzed in Figures 3.1 through 3.13. Figure 3.14 illustrates the final output from the MPGA algorithm for this pavement section, while subsequent figures illustrate how these results were obtained.

Figure 3.14 provides MPGA results and thickness data for a two layer concrete pavement. The near surface layer (Layer 1) indicates two segments of consistent thickness (mile 0 to mile 0.65 and mile 1.15 to 1.45) while segments with deeper Layer 1 thickness (mile 0.65 to 1.15) indicate greater thickness variability. MPGA results (shown in aqua for Layer 1) indicate relatively consistent thickness segments. A continuous line while a broken line indicates shorter localized data trends. Similarly, deeper base layer pavement data results are shown in green (corresponding to Layer 2). Layer 2 information was not detected between 0 and 0.25 miles. Also, there are more discontinuities in Layer 2 results than in Layer 1 results. Even so, two continuous segment trends were identified in Layer 2 (mile 0.5 to 0.8 and mile and mile 1.15 to 1.45). An interlayer relationship trend corresponding to one of these continuous Layer 2 segments was identified and discussed later in this summary of results.

MPGA criteria and length scales of interest were initially selected by a user. Subsequently, analysis results were produced by the algorithm without further user intervention. Identical user selected MPGA criteria were used on both the US 15 pavement and the MD 675 pavement. Different analysis length scales were selected for each pavement to identify relevant data trends. Figure 3.15 illustrates how mean layer thickness values corresponding to the entire MD 675 data analysis section of interest do not capture thickness variability, while global mean trends pass through local discontinuities but fail to accurately represent continuous thickness segments (where data in these segments appear consistently above or below the global mean trend).

Figure 3.16 illustrates how MPGA initially subdivides the MD 675 Layer 1 data section into equal size segments. Subsequently, neighboring local segments with statistical qualities in common are joined together by MPGA, while those that exhibit greater variability in these qualities remain separated, as shown in Figure 17. In a similar manner, subdivision of data into local segments and the subsequent process of joining segments with statistical qualities in common is shown in Figures 3.18 and 3.19 respectively for MD 675 Layer 2 data.

Finally, interlayer trends in MPGA results were examined with respect to significant data segment continuity and discontinuity in Figure 3.20, similar to the Figure 3.13 plot for the US 15 data set. Segments that exhibit interlayer continuity characteristics were highlighted in light green in Figure 3.20 (between mile 1.15 and 1.45). A matching discontinuity appears in both Layer 1 and Layer 2 data immediately before this continuous segment (~mile 1.05 to 1.15). Other interlayer trends in the data can quickly be assessed to have less in common than these highlighted segments based on MPGA.

These initial analysis results indicate that MPGA has the potential to improve accuracy in pavement thickness data that are used in pavement management and rehabilitation analysis. The MPGA results presented herein indicate that pavement thickness data trends can be identified based on either automated or semi-automated procedures using target variability levels of thickness uniformity, and thus can be used to efficiently evaluate pavement material layers. The MPGA approach is able to effectively identify variable and thin pavement thickness subsections, construction pavement thickness discontinuities, and trends among multiple pavement layers which may indicate possible damage, deterioration, or defects.

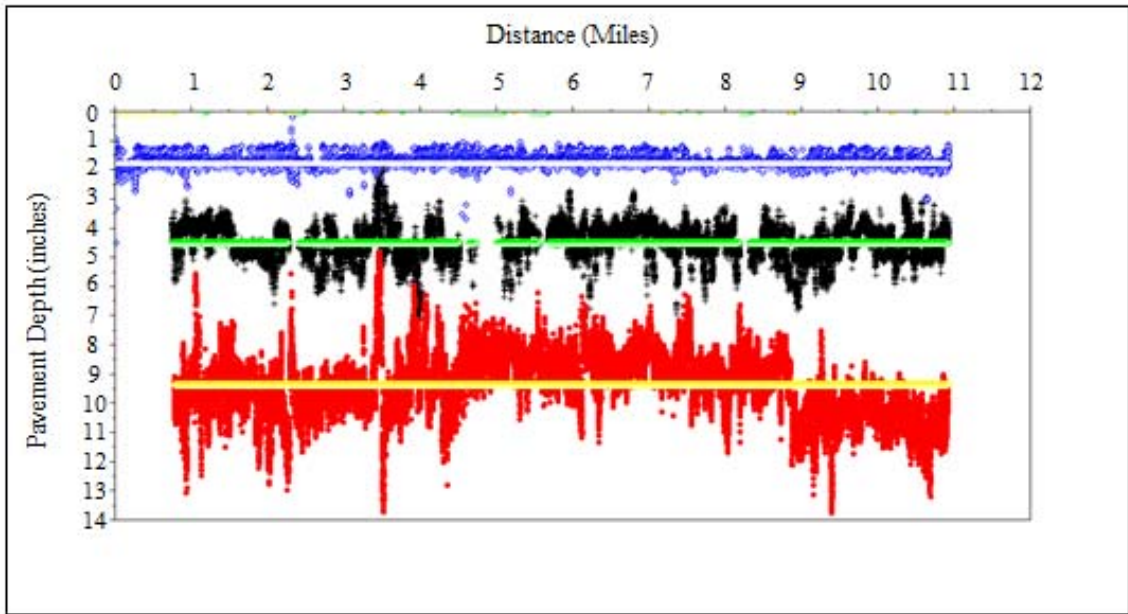


Figure 3.1 US15 – HMA Pavement Data With Global Means (3 Layers)

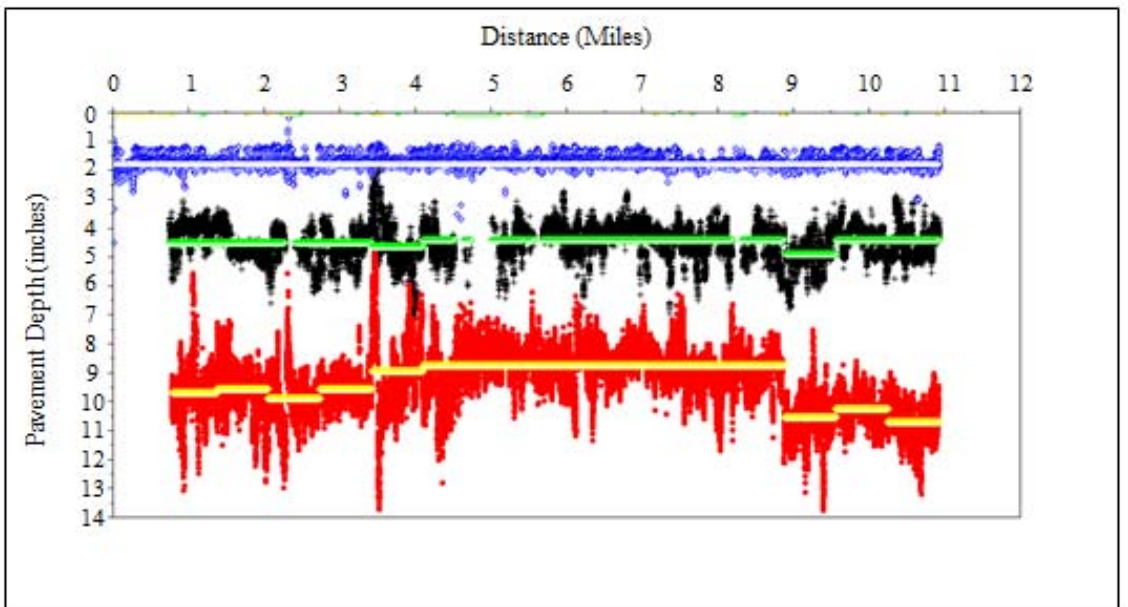


Figure 3.2 US15 – HMA Pavement Data With MPGA Results (3 Layers)

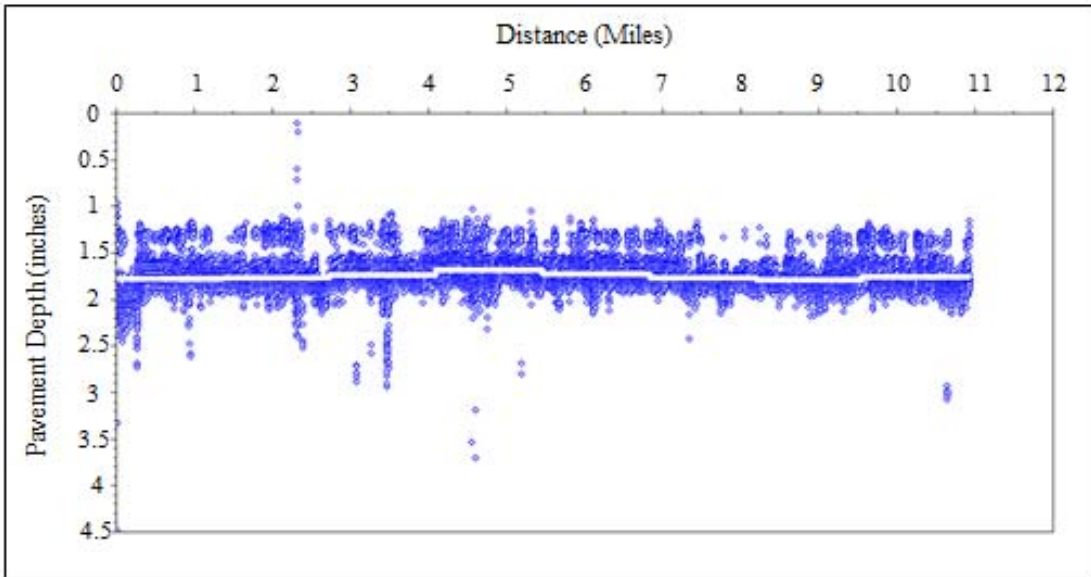


Figure 3.3 US15 – HMA Pavement Layer 1 Data With Eight Subdivided Means

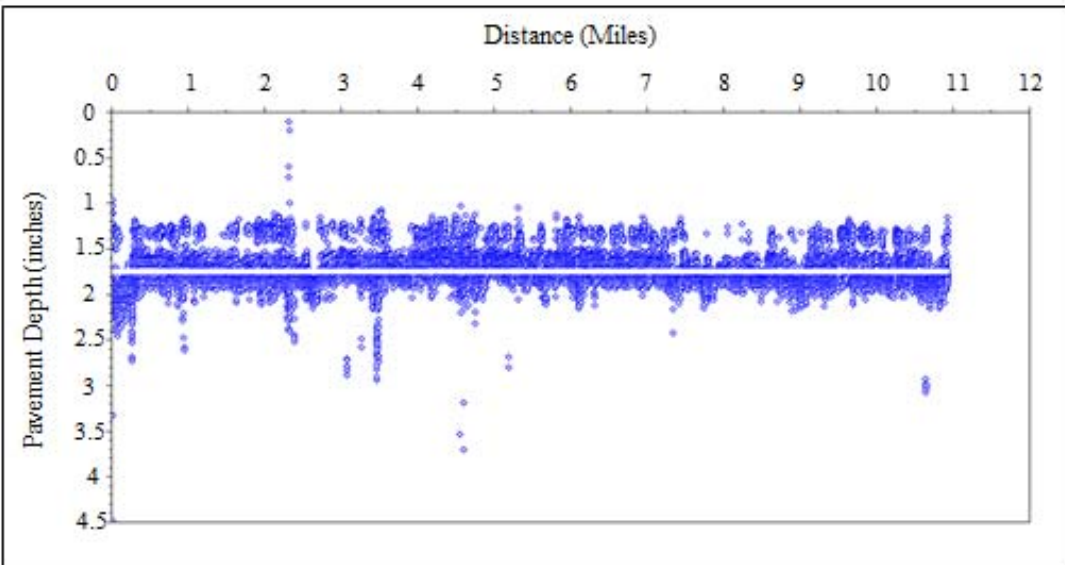


Figure 3.4 US15 – HMA Pavement Layer 1 Data With MPGA Applied (Using Eight Subdivisions)

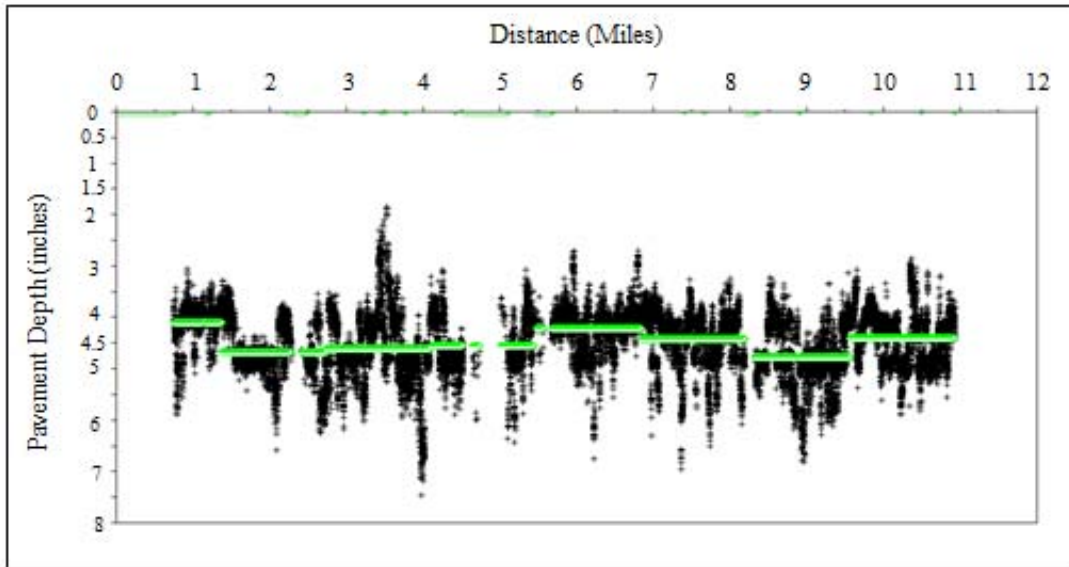


Figure 3.5 US15 – HMA Pavement Layer 2 Data With Eight Subdivided Means

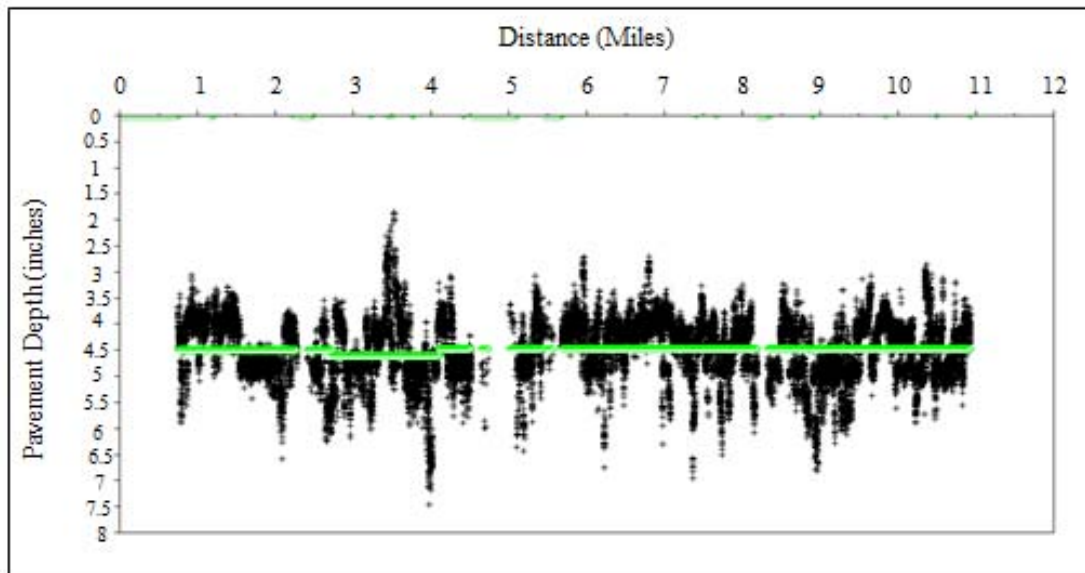


Figure 3.6 US15 – HMA Pavement Layer 2 Data With MPGA Applied (Using Eight Subdivisions)

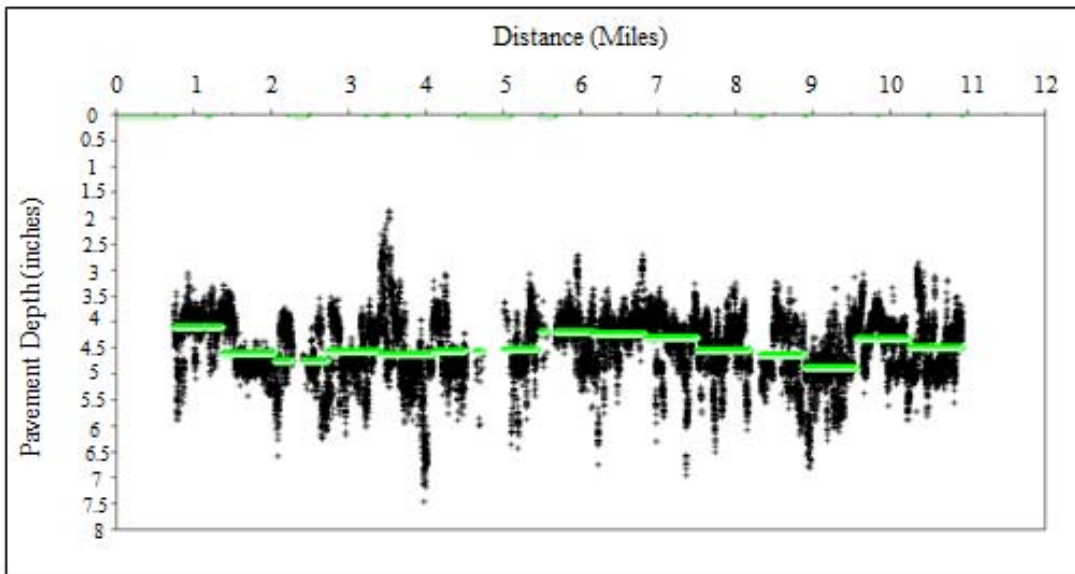


Figure 3.7 US15 – HMA Pavement Layer 2 Data With Sixteen Subdivided Means

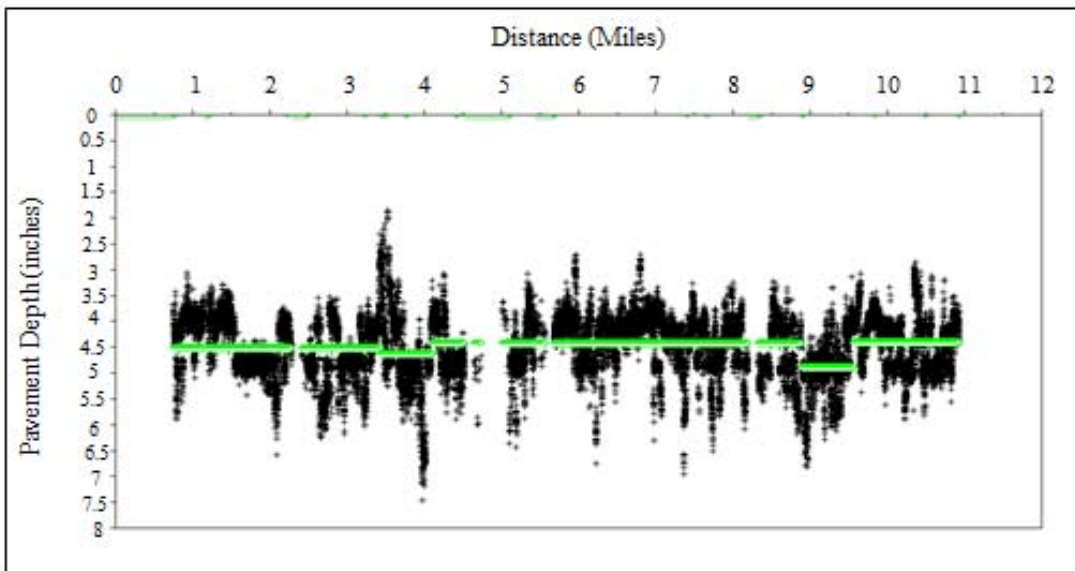


Figure 3.8 US15 – HMA Pavement Layer 2 Data With MPGA Applied (Using Sixteen Subdivisions)

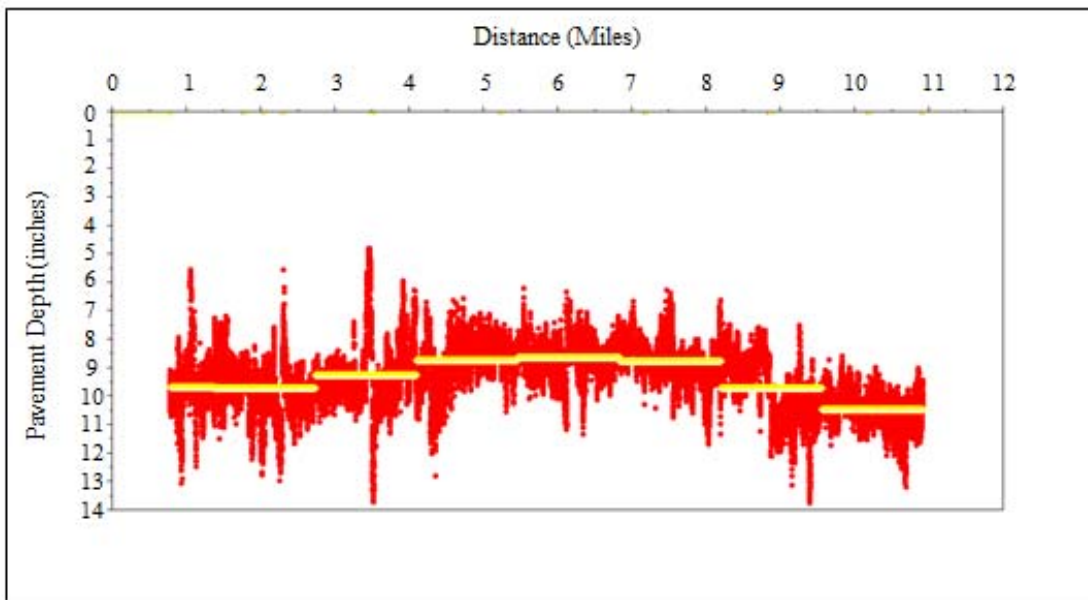


Figure 3.9 US15 – HMA Pavement Layer 3 Data With Eight Subdivided Means

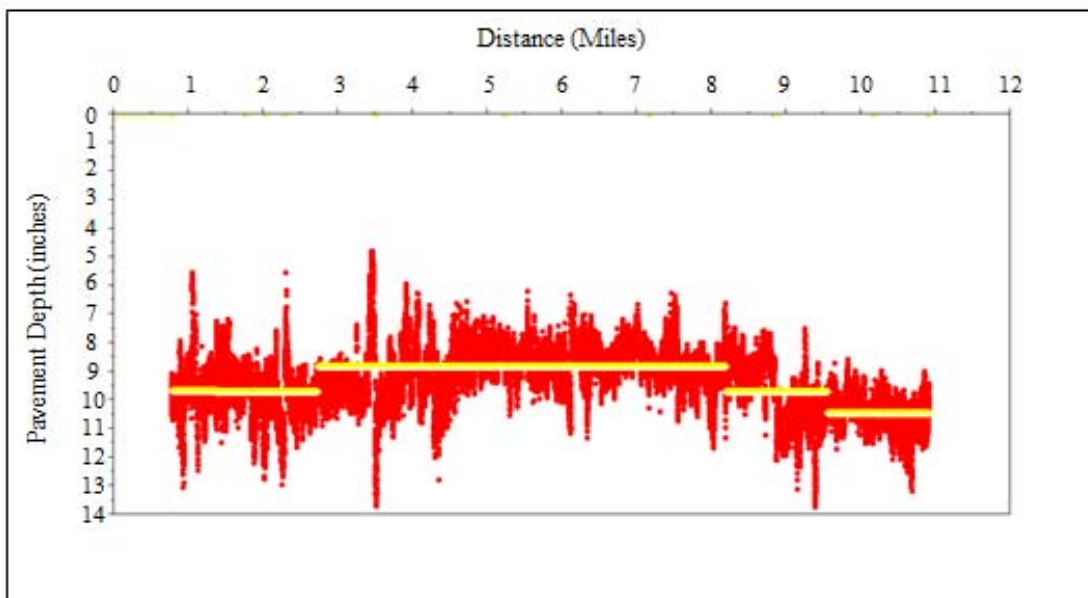


Figure 3.10 US15 – HMA Pavement Layer 3 Data With MPGA Applied (Using Eight Subdivisions)

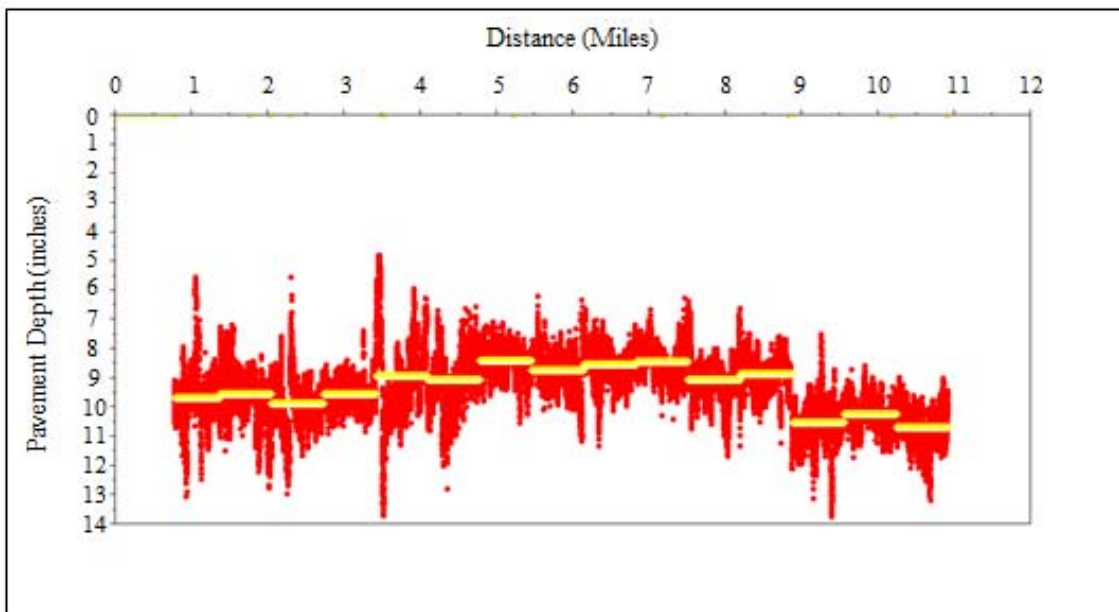


Figure 3.11 US15 – HMA Pavement Layer 3 Data With Sixteen Subdivided Means

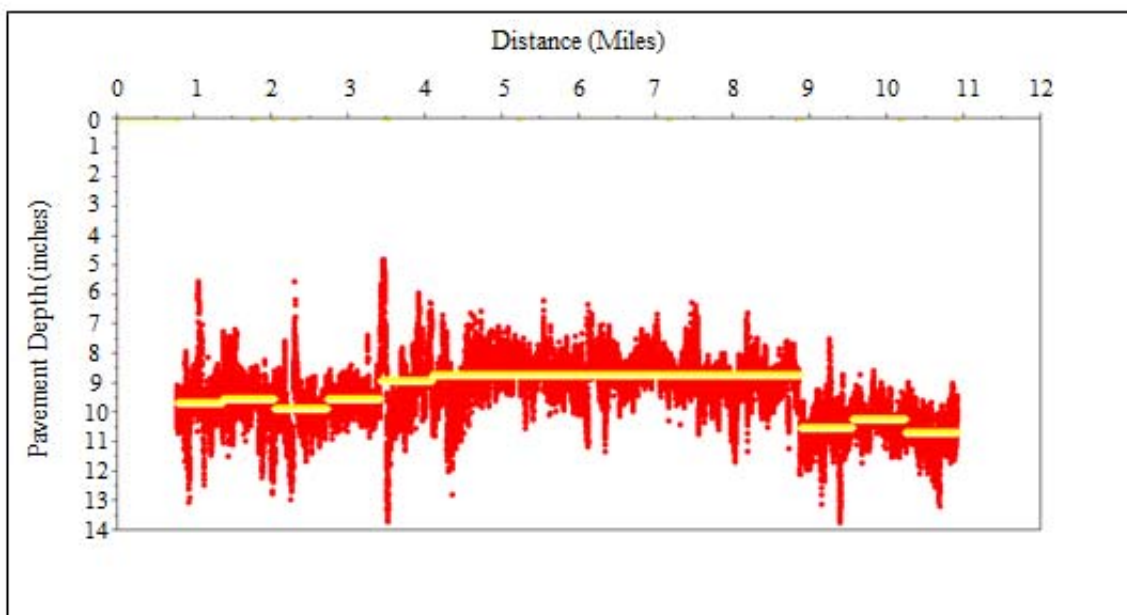


Figure 3.12 US15 – HMA Pavement Layer 3 Data With MPG A Applied (Using Sixteen Subdivisions)

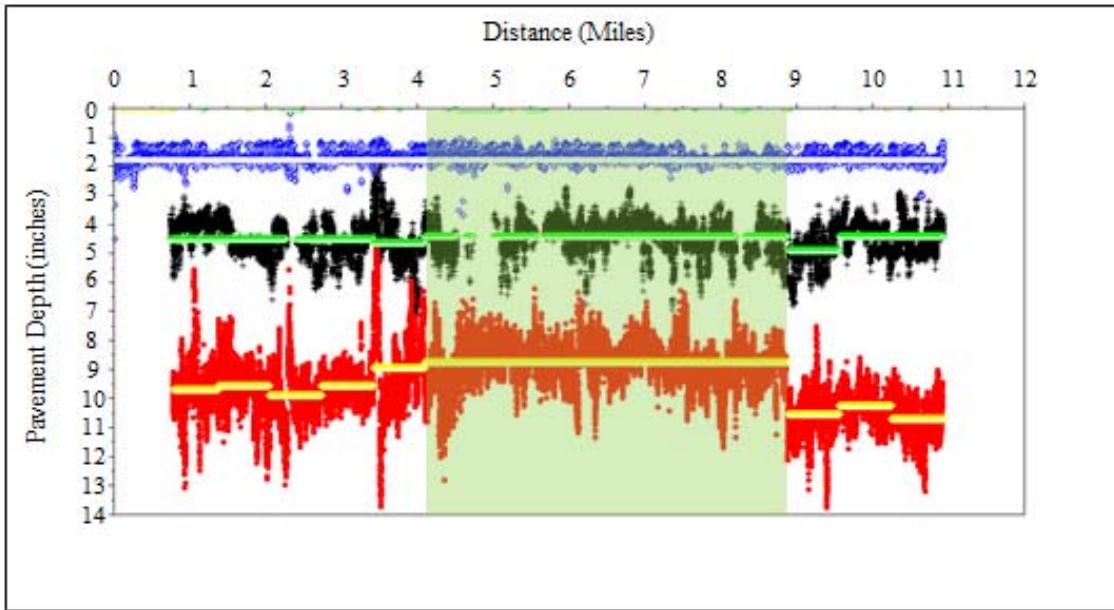


Figure 3.13 US15 – HMA Pavement Data With MPGA Results (3 Layers) – Common Interlayer Trend Highlighted in Light Green

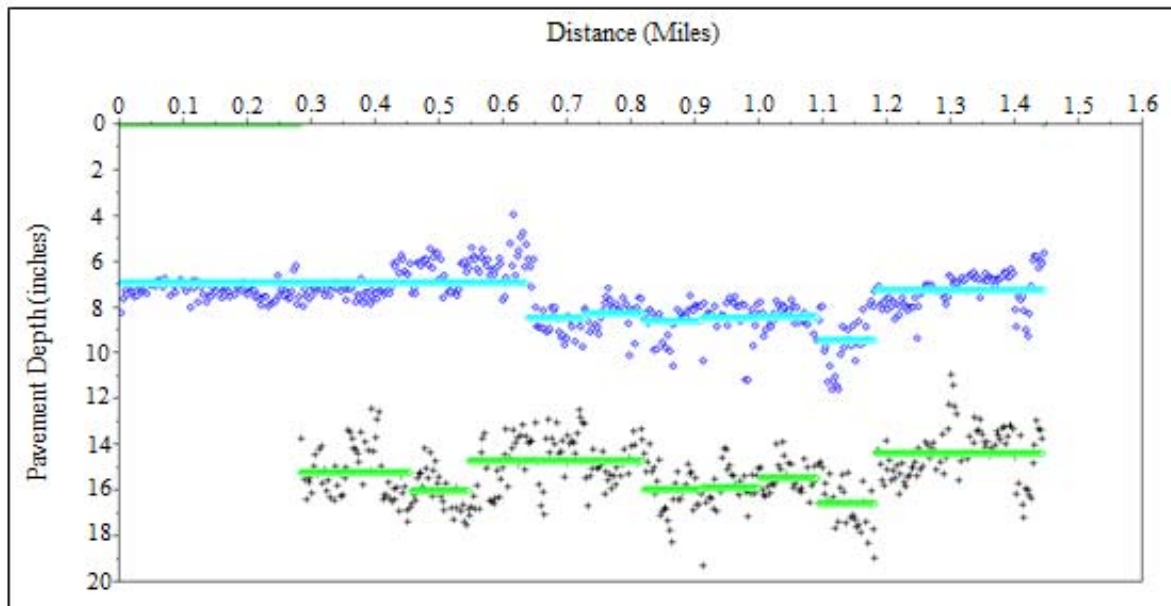


Figure 3.14 MD 675 – Concrete Pavement Data With MPGA Results (2 Layers)

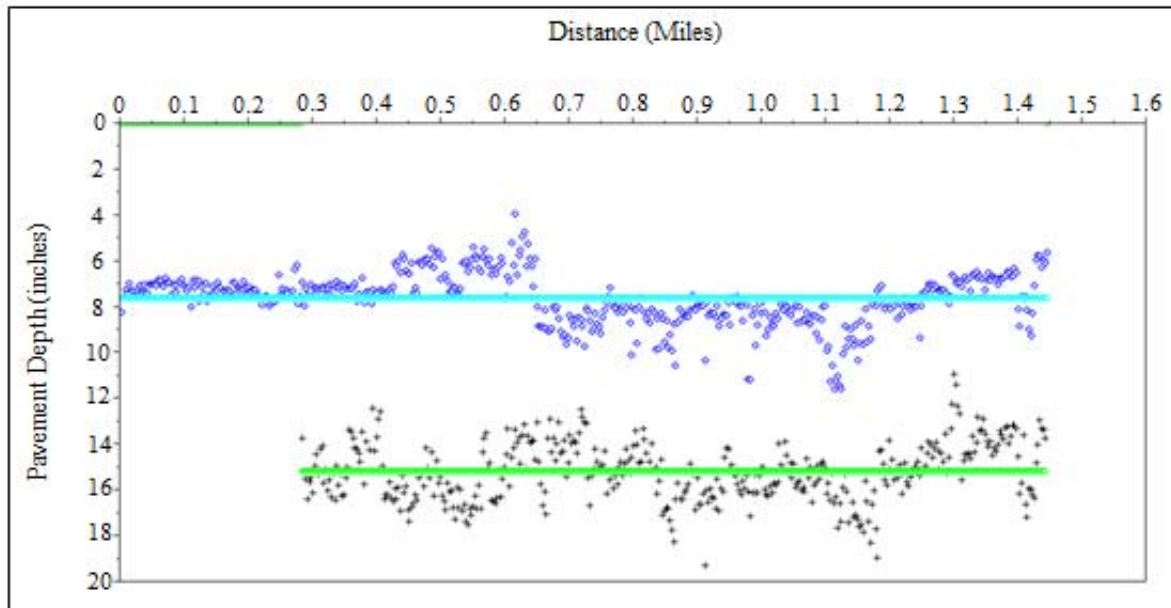


Figure 3.15 MD 675 – Concrete Pavement Data With Global Means (2 Layers)

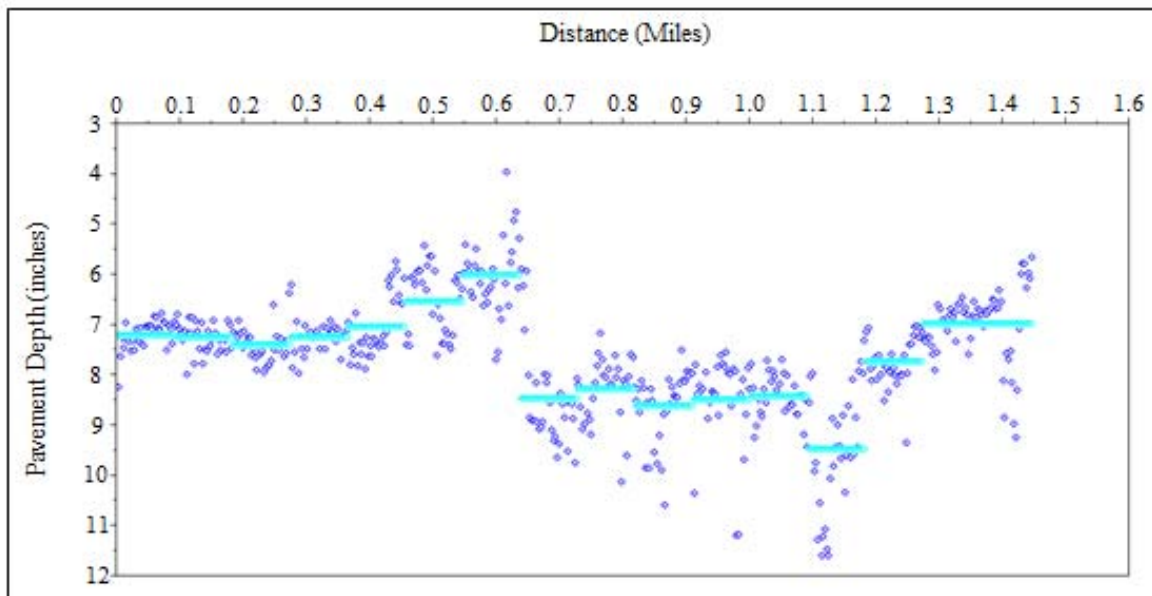


Figure 3.16 MD 675 – Concrete Pavement Layer 1 Data With Sixteen Subdivided Means

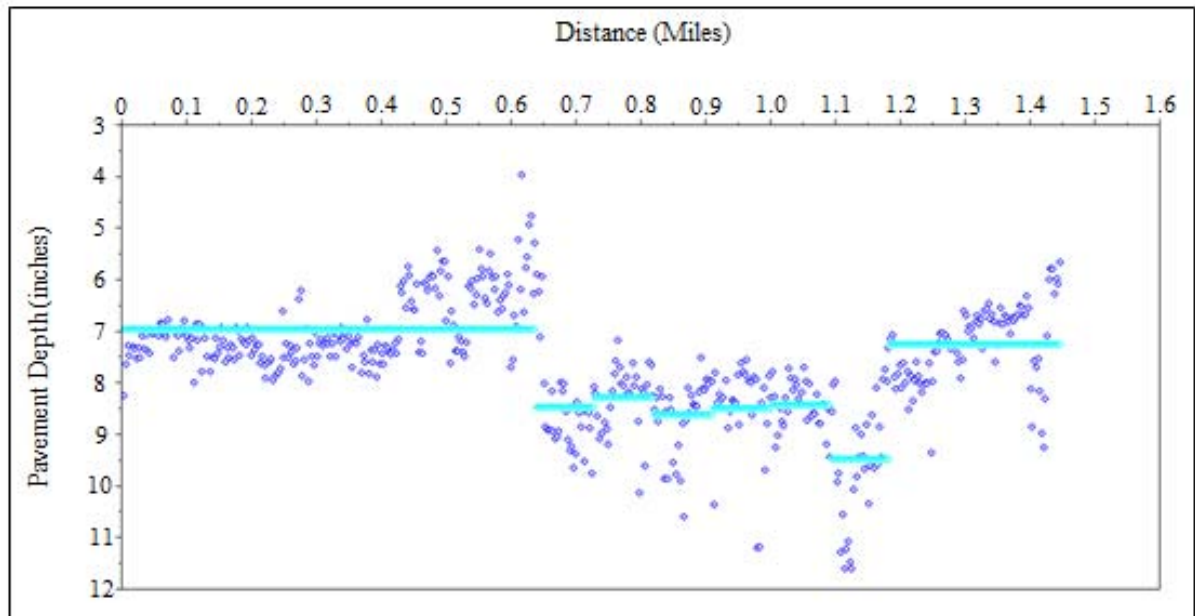


Figure 3.17 MD 675 – Concrete Pavement Layer 1 Data With MPGA Applied (Using Sixteen Subdivisions)

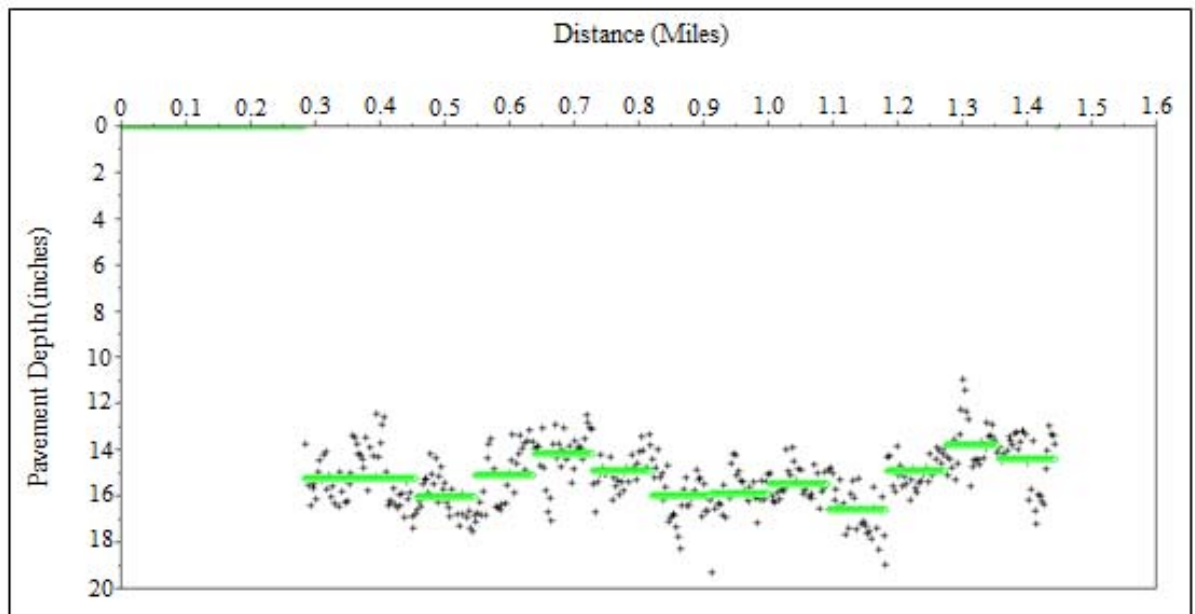


Figure 3.18 MD 675 – Concrete Pavement Layer 2 Data With Sixteen Subdivided Means

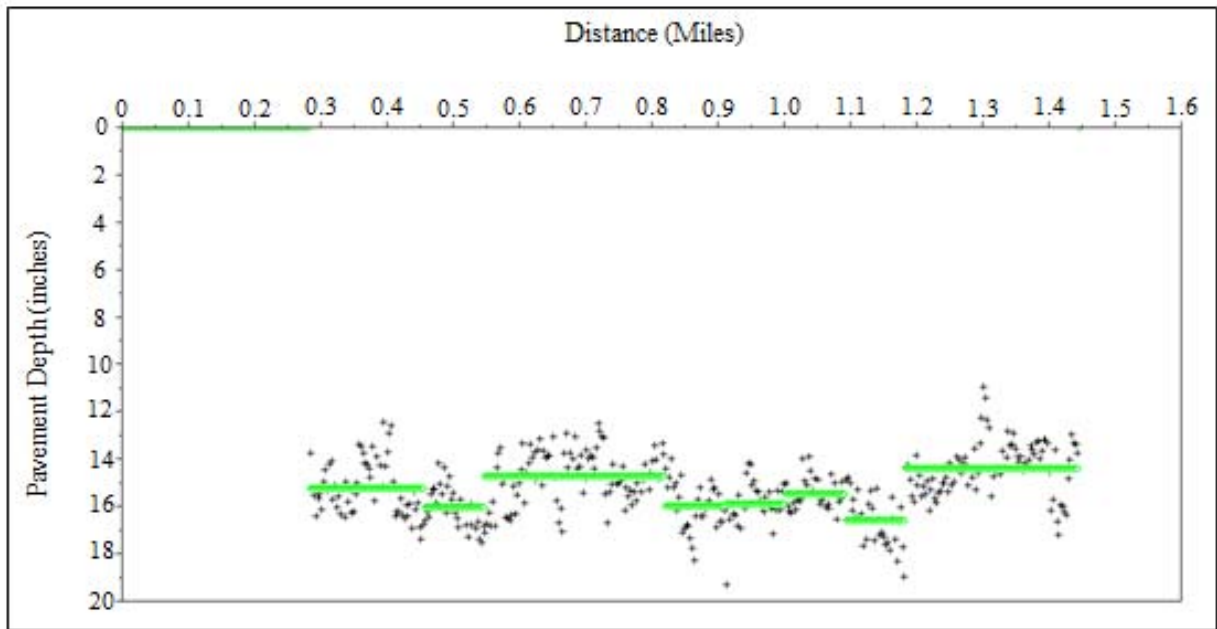


Figure 3.19 MD 675 – Concrete Pavement Layer 2 Data With MPGA Applied (Using Sixteen Subdivisions)

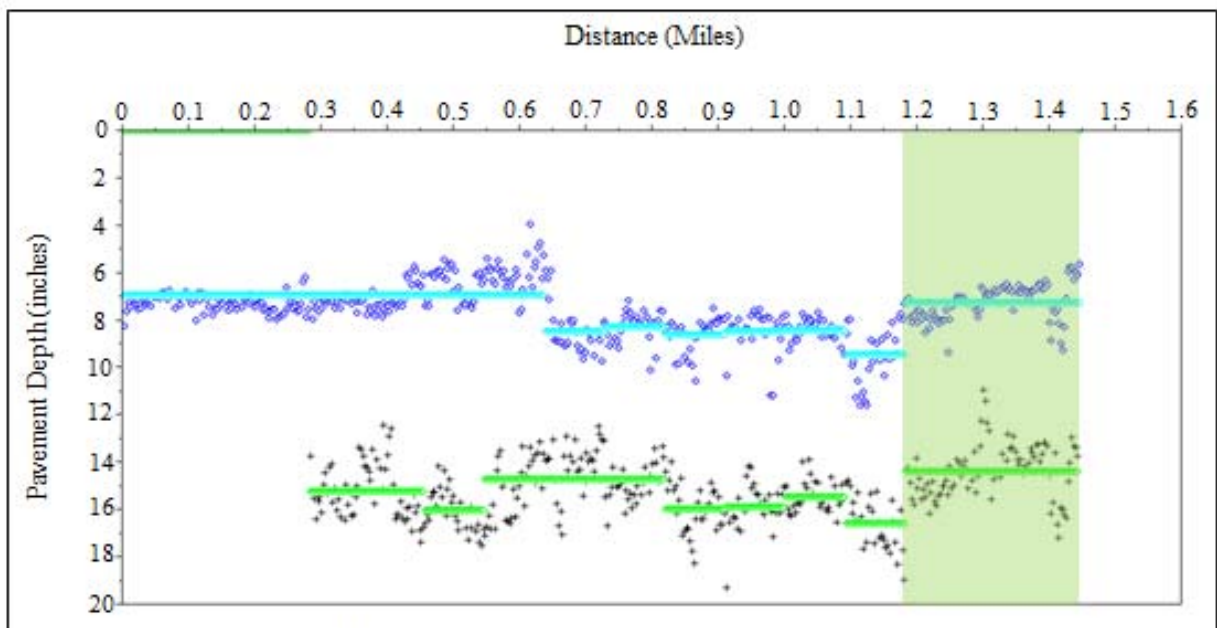


Figure 3.20 MD 675 – Concrete Pavement Data With MPGA Results (2 Layers)
Common Interlayer Trend Highlighted in Light Green

CHAPTER 4: GPR BRIDGE DECK ANALYSIS

Accurate, efficient bridge deck inspection and evaluation is an important aspect of maintaining valuable MD SHA bridge infrastructure assets. Bridge decks usually wear out much faster than other bridge components, motivating a focus on this aspect of bridge inspection. Key problems with the state of practice bridge inspection have been identified in previous studies including bridge rating accuracy and reliability concerns using conventional techniques. Also, bridge inspections and evaluations are required by U.S. Federal rules to address practical needs to identify bridge safety and maintenance issues quickly and cost effectively. Specific reliability problems with qualitative bridge inspection and evaluation practices using existing visual inspection and complementary techniques such as chain drag sounding further motivate development and implementation of new and emerging alternatives. Therefore, there was a need to investigate how MD SHA can address bridge deck inspection problems more effectively with emerging state of the art solutions. Development and study of bridge deck inspection and evaluation techniques using emerging Ground Penetrating Radar (GPR) technologies is a significant technique to consider due to features such as fast data acquisition speed and quantitative measurement capabilities (described below). This study examined ways to develop and implement more reliable bridge inspection and evaluation using GPR techniques.

Currently available GPR data analysis techniques such as migration imaging (for concrete cover depth measurement applications among others), Fourier analysis of GPR waveforms (for qualitative bridge deck moisture analysis) and emerging techniques such as Short Time Fourier Transform analysis (for anticipated quantitative moisture analysis) can be used. Migration and Fourier techniques are illustrated corresponding to GPR data collected using a GPR array on selected bridge decks in the Salisbury, MD area.

Figures 4.1 through 4.9 illustrate GPR migration analysis results from a US 13 north bound bridge over a Norfolk Southern railroad track. Migration results are presented as a series of plan view images at 1 inch depth intervals (corresponding to the upper image in each figure). In the migration images, dark colors represent low magnitude responses (low or no GPR reflection) and light colors represent high magnitude responses (strong GPR reflection). The lower image in each of the Figures corresponds to an amplitude/attenuation map of waveform reflections from the top layer of reinforcing steel in the deck (identical in all nine figures).

An important observation in Figure 4.3 is the GPR migration image corresponding to a 2 inch depth. This image indicates shallow cover depth reinforcing steel in a few key locations (circled in blue). These locations correlate well with several areas in the Figure 4.3 GPR amplitude/attenuation map (where high amplitude responses indicated in red and yellow are associated with a high probability of deterioration). This correlation is consistent with an increased probability of corrosion deterioration in shallow concrete cover depth areas due to fast diffusion of salts and moisture down to the steel depth. The opposite phenomenon is observed where slower diffusion to deeper steel depths typically results in slower corrosion processes corresponding to areas with greater concrete cover depth. Figure 4.4 indicates the remaining migrated reinforcing steel response features around a cover depth of 3 inches. Subsequent Figures 4.5 through 4.9 illustrate responses at increasing depths down to the underside of the bridge deck.

In addition, the top Figure 4.10 image shows a relative moisture map of the US 13 north bound bridge deck over Norfolk Southern Railroad. This relative moisture map was generated by a Fourier analysis of attenuation of migrated GPR response magnitudes through the bridge deck thickness (where the method that produced the top Figure 4.10 image is described later in this section). Probable high moisture content areas are indicated in dark blue while probable low moisture content areas are indicated in aqua. In this Figure 4.10 moisture analysis image, high moisture content areas generally correlate with probable deterioration areas in the corresponding amplitude/attenuation map below it.

Figures 4.11 through 4.19 are migration results from an analysis of GPR data collected on a Route 290 bridge crossing the Chester River. Like prior results, these Figures are presented as plan view images of GPR migration outputs at 1 inch depth intervals (from the surface to an 8 inch depth). For this example case, a very shallow cover depth area appears in Figure 4.12, corresponding to a 1 inch depth and circled in blue. This shallow cover depth area generally coincides with the location of the largest probable deterioration area in the corresponding amplitude/attenuation map in Figure 4.12. This feature further reinforces the hypothesis that shallow reinforcing steel often leads to premature corrosion and subsequent bridge deck deterioration. In addition, a few anomalies in Figure 4.16 through 4.19 depth images correlate well with deterioration areas in the amplitude/attenuation map. Finally, the Figure 4.20 map of relative moisture generally indicates higher moisture content in areas where deterioration is most prevalent.

A summary of the motivation and theoretical support for a Short Time Fourier Transform (STFT) analysis to quantitatively evaluate bridge deck moisture is presented next in Figures 4.21 through 4.24. This is followed by a practical application of a related Fourier analysis to qualitatively evaluate bridge deck moisture in Figures 4.25 through 4.29. Upon further development, the quantitative STFT approach is anticipated to provide a rapid means to evaluate absolute bridge deck moisture content which can account for the significant effects of moisture on GPR responses (which currently present some important challenges to GPR data interpretation and analysis). The related Fourier analysis presented offers a rapid technique to obtain qualitative (relative) moisture information about bridge decks, which can already improve GPR data analysis and interpretation in a few significant ways.

Figure 4.21 shows a ray path diagram corresponding to two theoretical GPR response models, a dry concrete bridge deck and a moist concrete bridge deck. Complex dielectric properties associated with each model are provided and the basic ray path diagrams corresponding to response features of interest (top surface and bottom surface) are shown. Figure 4.22 illustrates how time domain responses to the bridge deck top surface and bottom surface appear in an analytical waveform simulation of moist versus dry concrete. Figure 4.22 shows that the back surface reflection of the moist deck is delayed versus the dry deck and that moisture related dispersion reduces bottom surface GPR response signal energy versus a dry deck. Figures 4.23 and 4.24 show two dimensional STFT responses corresponding to the dry and moist cases respectively. The dominant phenomena revealed by the STFT analysis plot (a frequency versus time representation of the amplitude versus time information) are reduced high frequency content and reduced signal amplitudes (both caused by moisture dispersion phenomena). A time delay associated with the moisture is also observed. In the future an STFT analysis can be developed to quantitatively evaluate bridge deck moisture content based on these response phenomena. Currently, a qualitative Fourier transform analysis of relative moisture content can be performed using related principles and is presented in Figures 4.25 through 4.29.

Figure 4.25 presents an example radargram image (position versus time) in the lower left where a vertical line corresponds to the location of a raw waveform pulse shown to its right. A band pass filtered waveform pulse is shown at the far right, which primarily removes high frequency noise and multi-path scattering phenomena from small features (leaving low frequency response features from larger scale features such as the bridge deck surface and back surface). Example GPR waveform frequency content is shown in red above along with the band pass gain filter profile in blue. The filter profile emphasizes frequencies between 1 GHz and 2.3 GHz, which are the lower frequencies of interest for the relative moisture analysis.

Figures 4.26 through 4.29 provide Fourier analysis plots corresponding to response features at the depth of the bridge deck bottom surface. In these plots, darker blue areas represent areas with more moisture while aqua and other bright colors represent low moisture areas. Multiple views of the results are shown in Figures 4.26 through 4.29. In Figure 4.29 higher moisture content areas are observed to correlate well with many probable deterioration areas in the corresponding amplitude/attenuation plot. Improved information about these moisture phenomena can be used to enhance the interpretation of GPR data, as shown. Additional moisture plots that used the same analysis for other bridge deck examples were already shown in Figures 4.10 and 4.20. Further development of quantitative STFT moisture analysis can make GPR results even more reliable and effective.

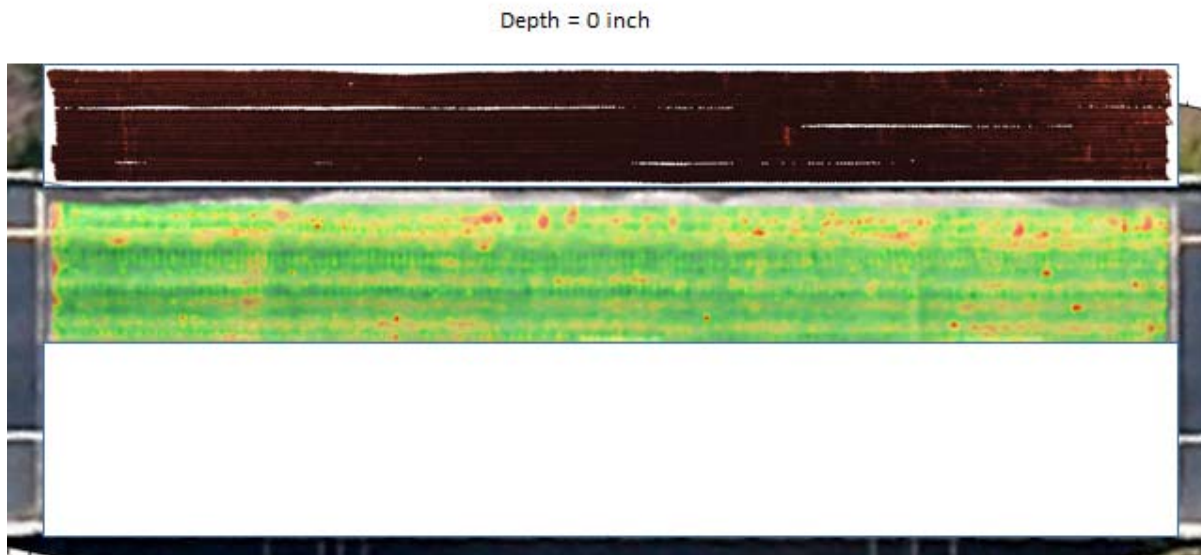


Figure 4.1 US 13 Northbound Over Norfolk Southern RR Migration Results (Above) vs. Attenuation Map (Below)

Depth = 1 inch

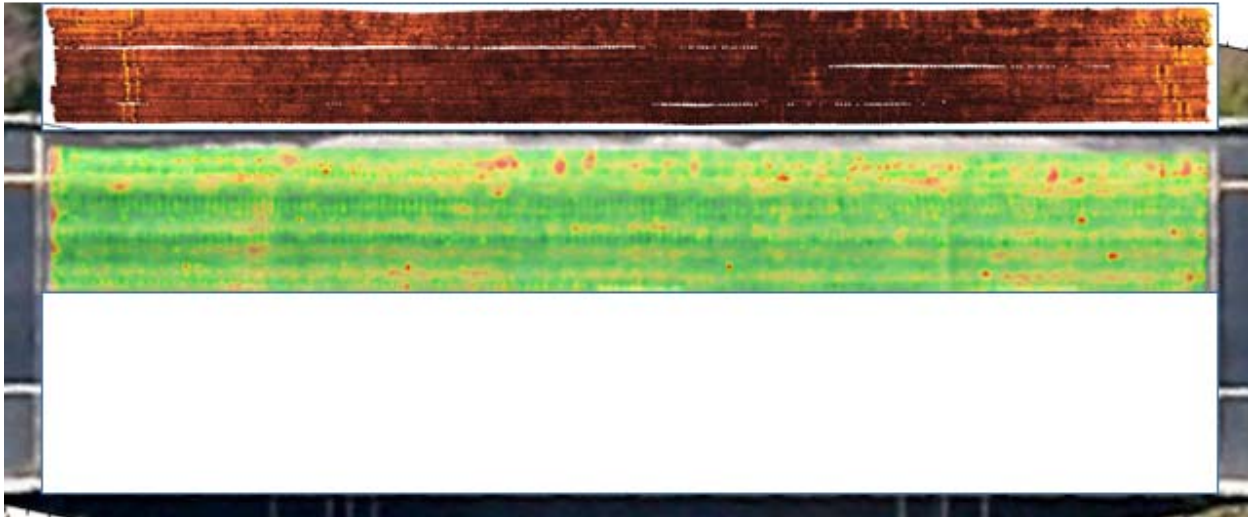


Figure 4.2 US 13 Northbound Over Norfolk Southern RR at 1" Depth

Depth = 2 inch

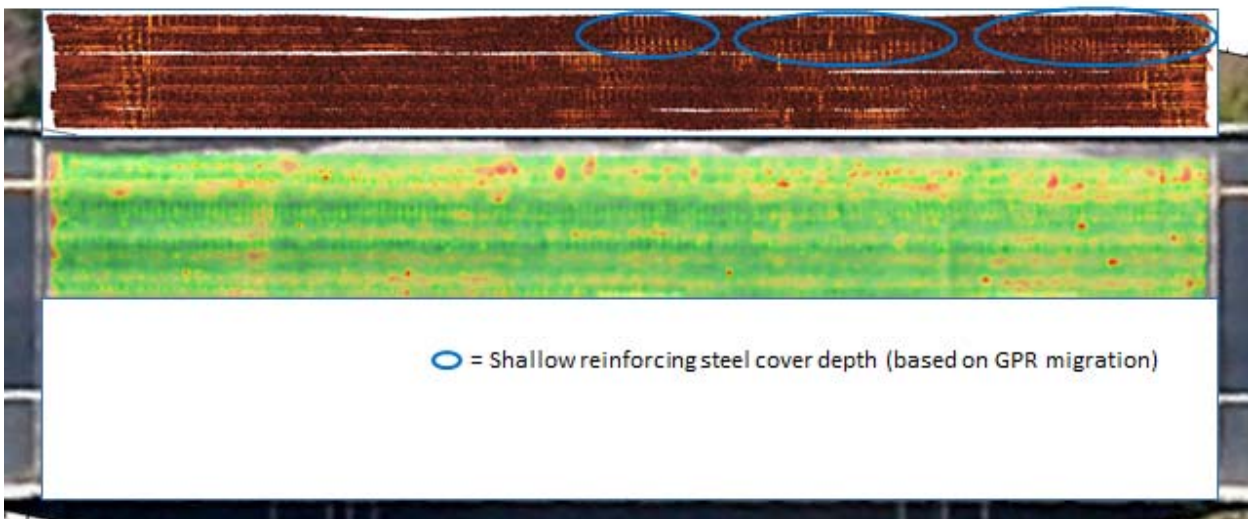


Figure 4.3 US 13 Northbound Over Norfolk Southern RR at 2" Depth

Depth = 3 inch

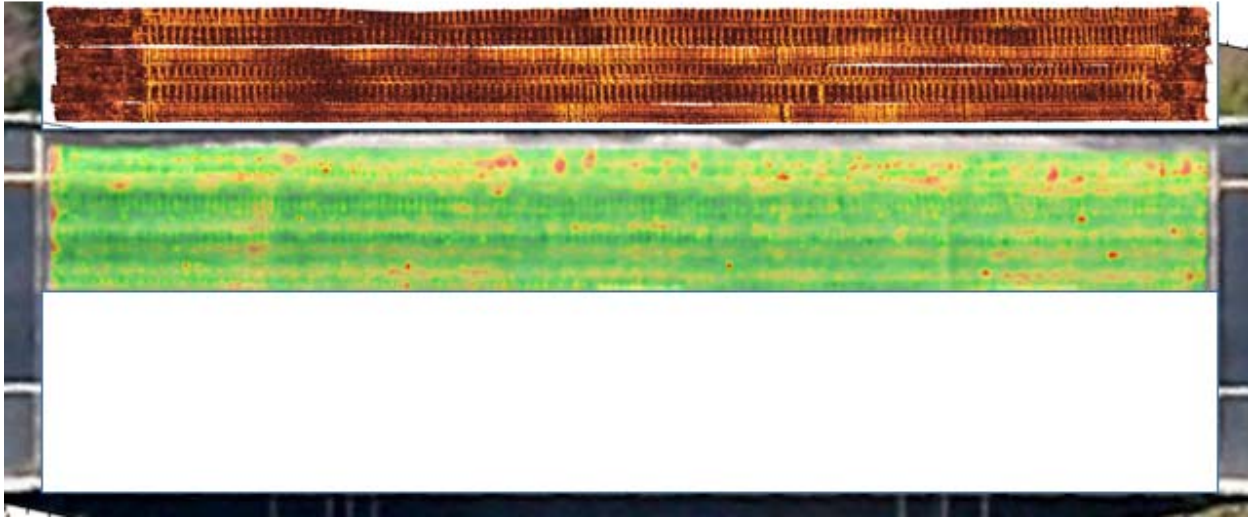


Figure 4.4 US 13 Northbound Over Norfolk Southern RR at 3" Depth

Depth = 4 inch

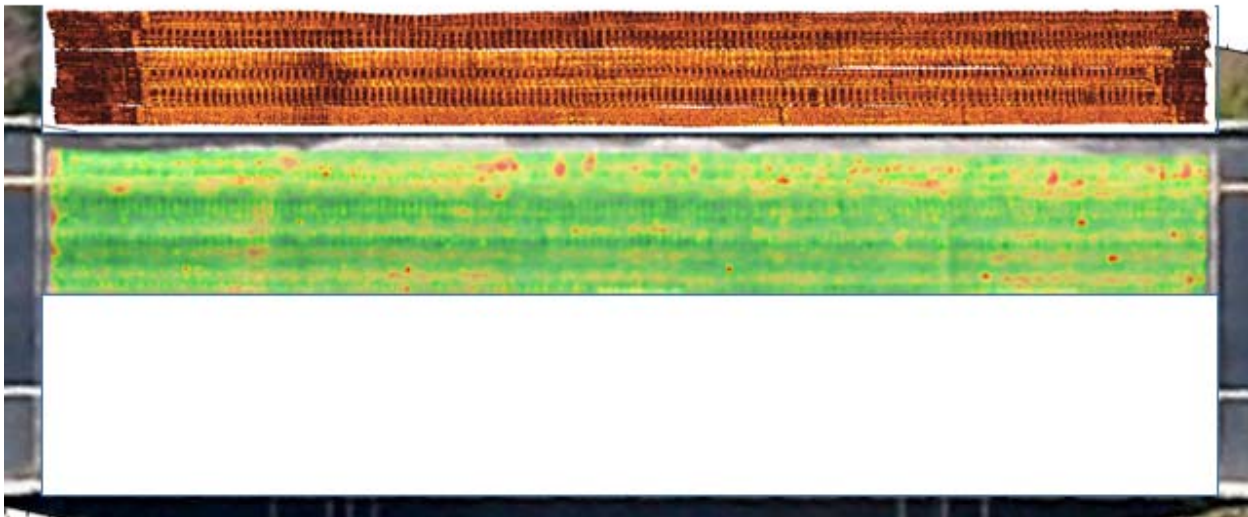


Figure 4.5 US 13 Northbound Over Norfolk Southern RR at 4" Depth

Depth = 5 inch

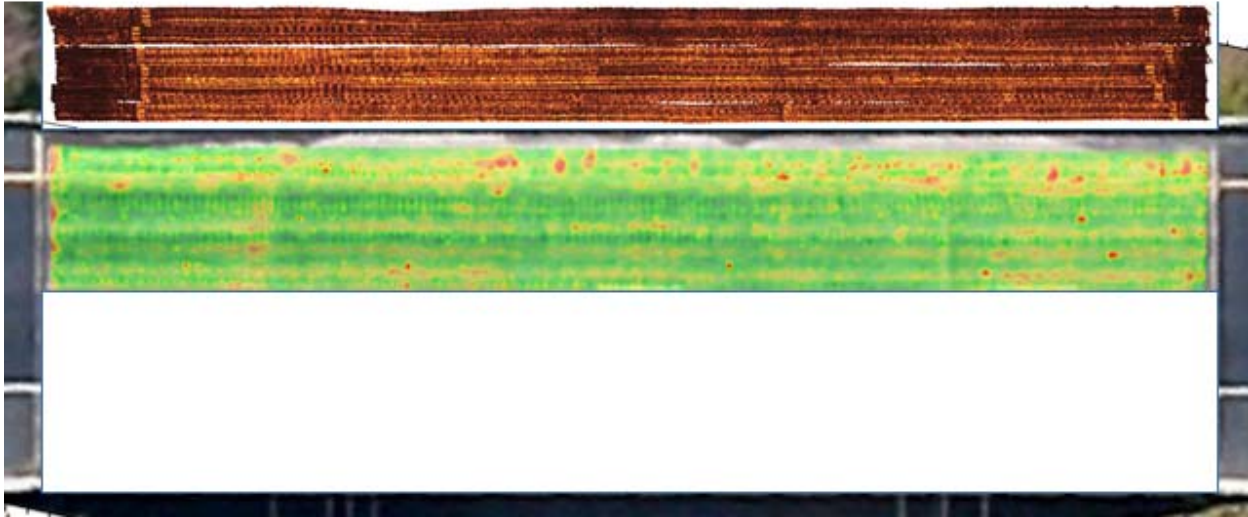


Figure 4.6 US 13 Northbound Over Norfolk Southern RR at 5" Depth

Depth = 6 inch

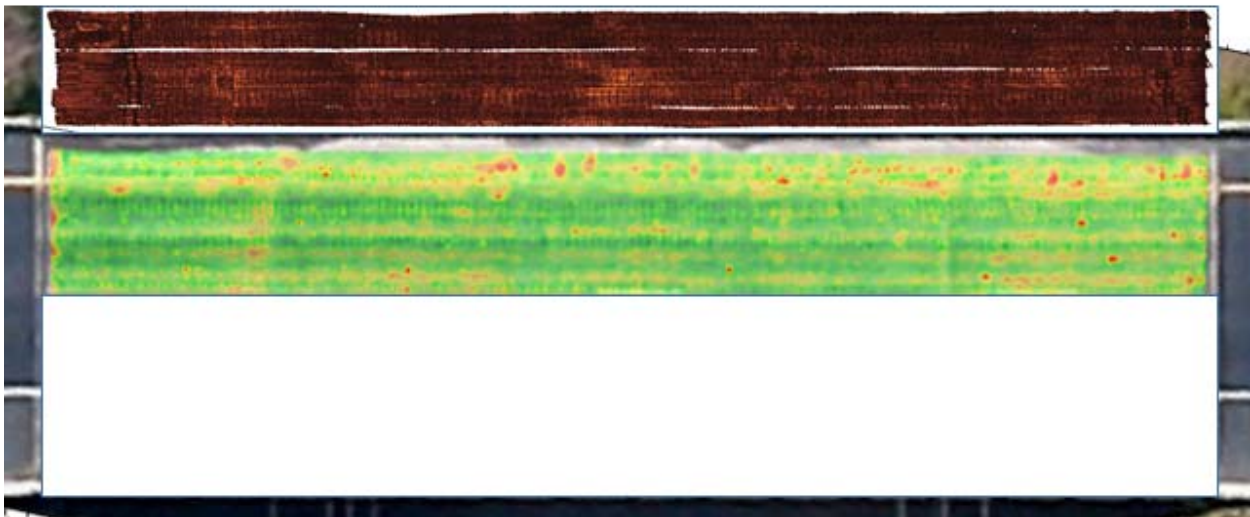


Figure 4.7 US 13 Northbound Over Norfolk Southern RR at 6" Depth

Depth = 7 inch

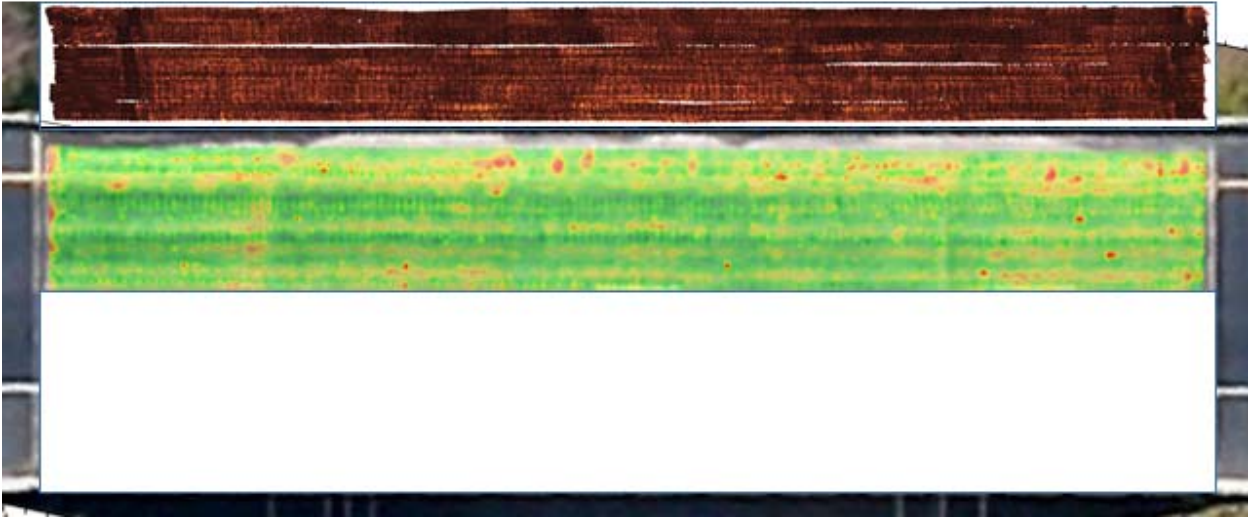


Figure 4.8 US 13 Northbound Over Norfolk Southern RR at 7" Depth

Depth = 8 inch

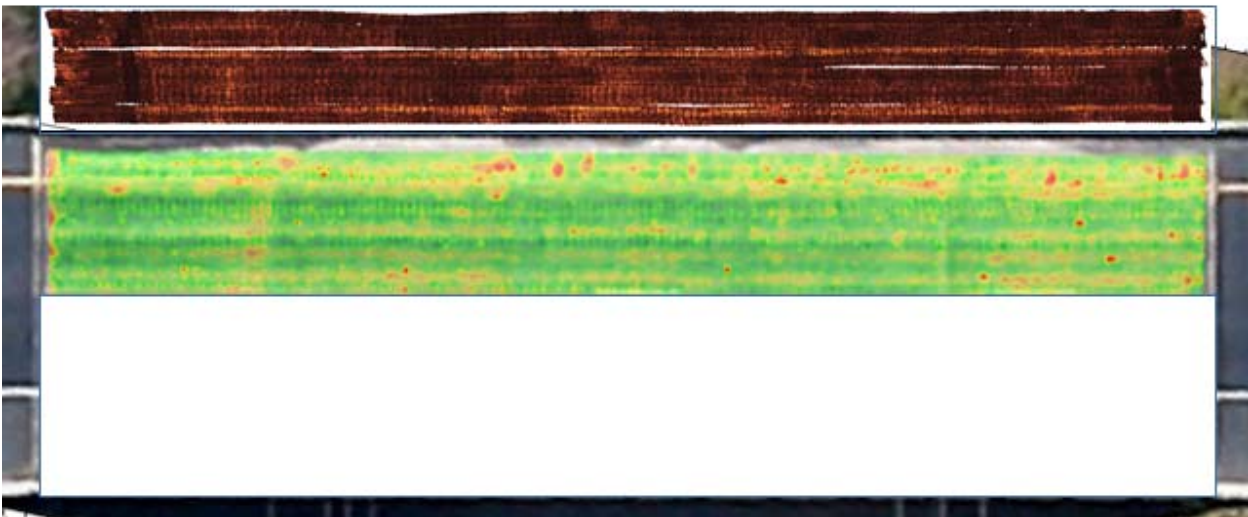


Figure 4.9 US 13 Northbound Over Norfolk Southern RR at 8" Depth

Moisture

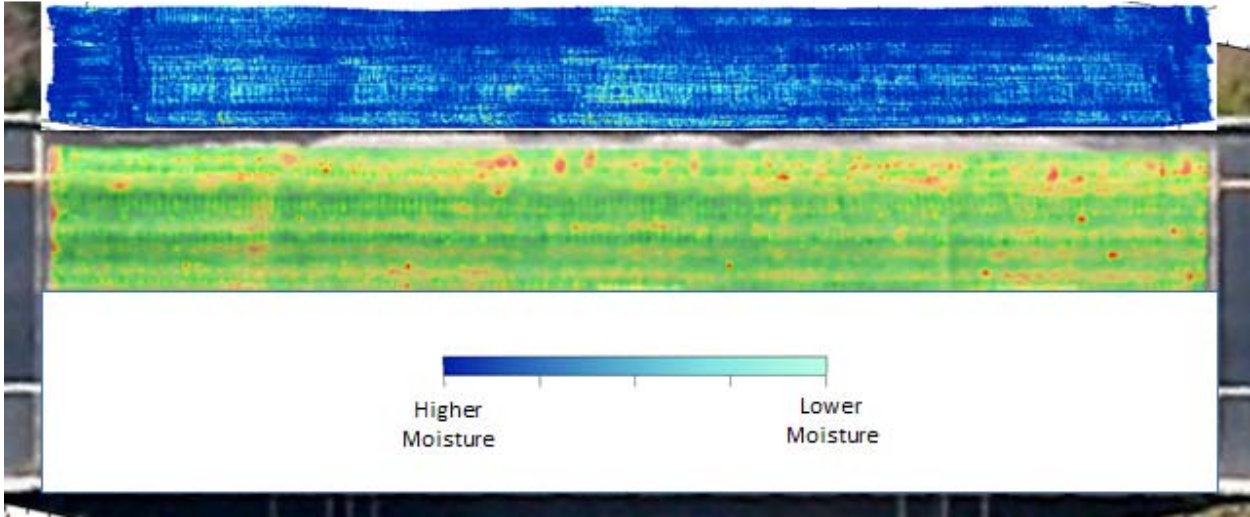


Figure 4.10 US 13 Northbound Over Norfolk Southern RR - Moisture

Depth = 0 inch

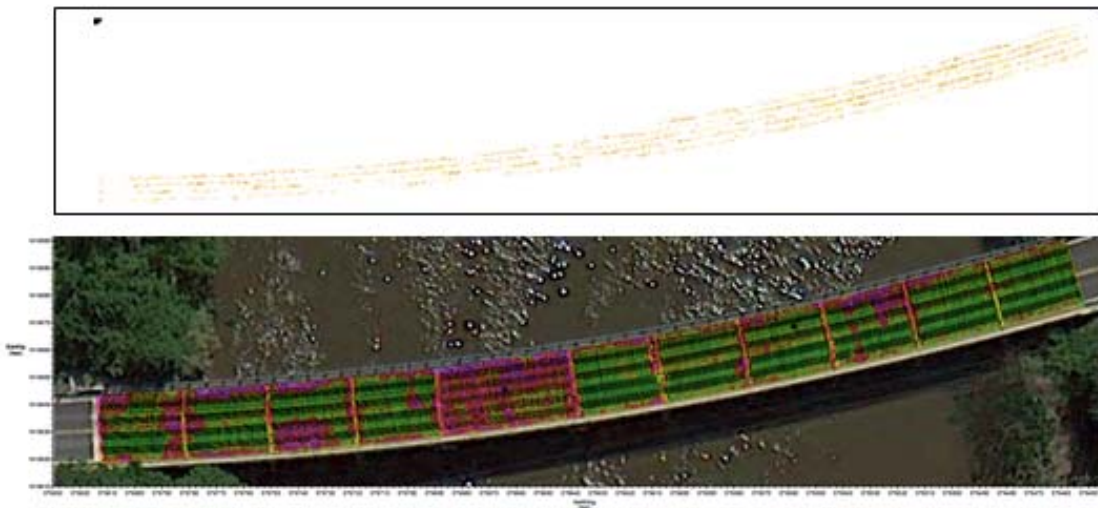


Figure 4.11 Route 290 Over Chester River Migration Results (Above) vs. Attenuation Map (Below)

Depth = 1 inch

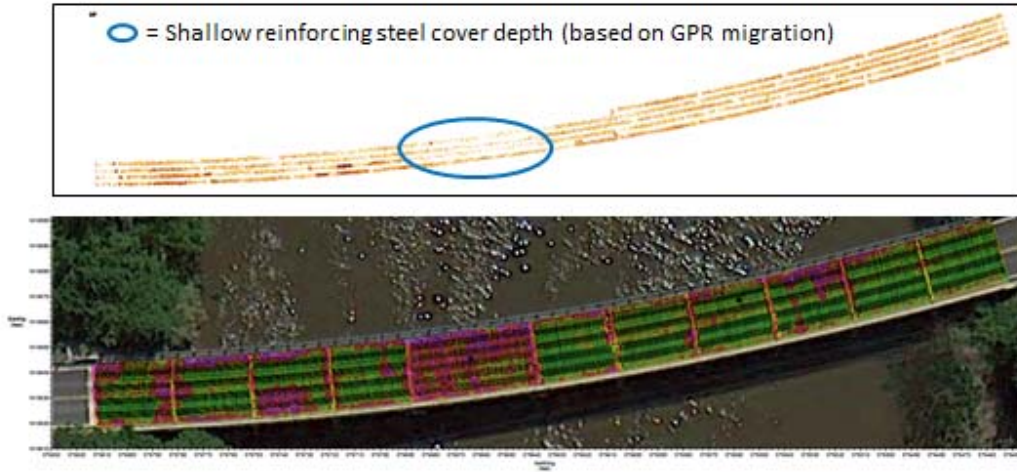


Figure 4.12 Route 290 Over Chester River Migration Results at 1" Depth

Depth = 2 inch

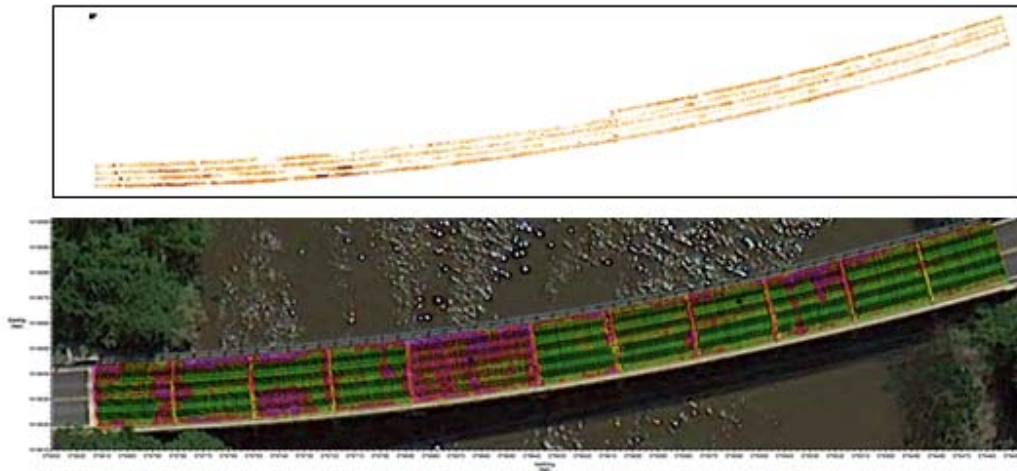


Figure 4.13 Route 290 Over Chester River Migration Results at 2" Depth

Depth = 3 inch

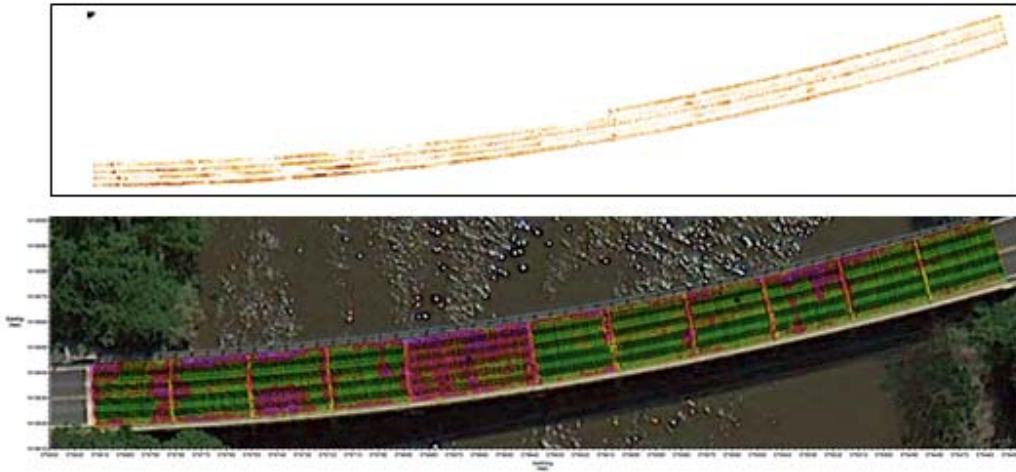


Figure 4.14 Route 290 Over Chester River Migration Results at 3" Depth

Depth = 4 inch

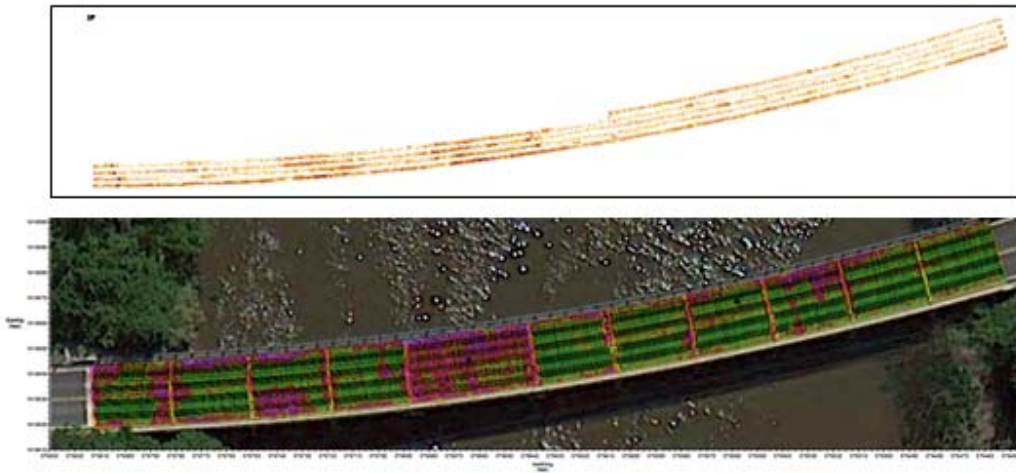


Figure 4.15 Route 290 Over Chester River Migration Results at 4" Depth

Depth = 5 inch

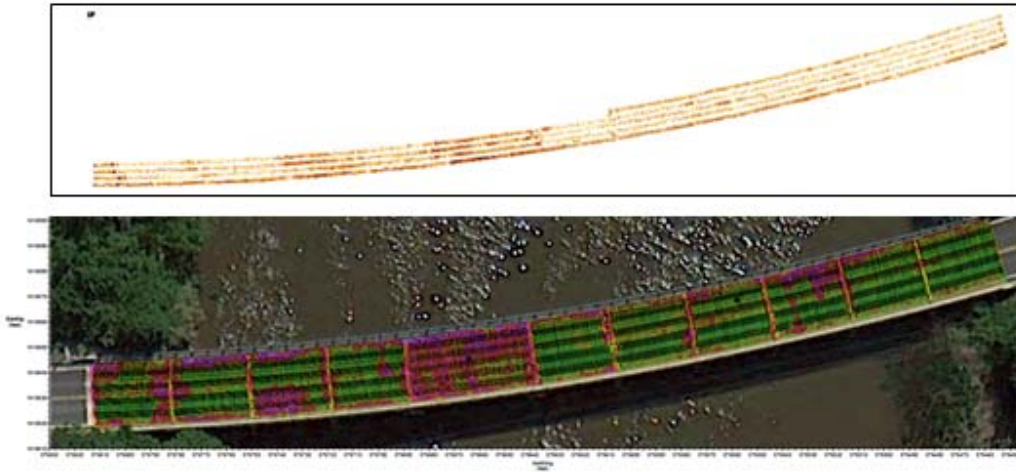


Figure 4.16 Route 290 Over Chester River Migration Results at 5" Depth

Depth = 6 inch

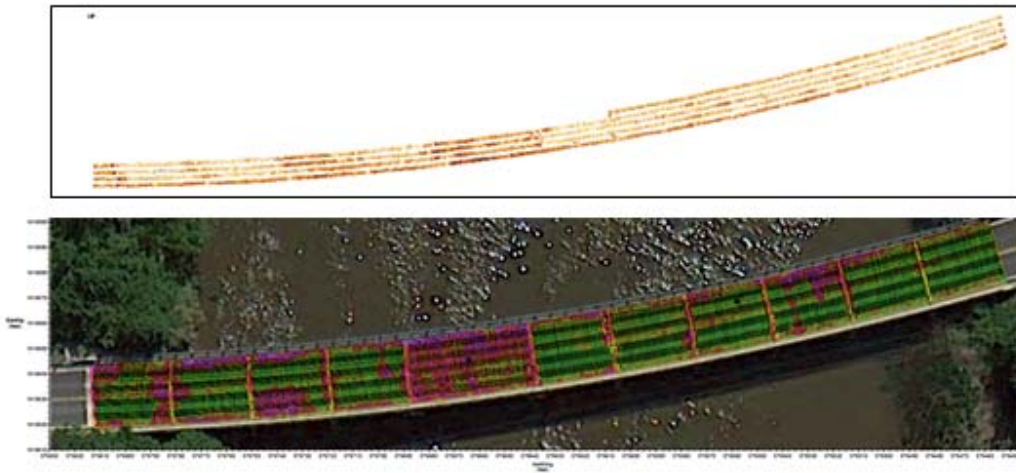


Figure 4.17 Route 290 Over Chester River Migration Results at 6" Depth

Depth = 7 inch

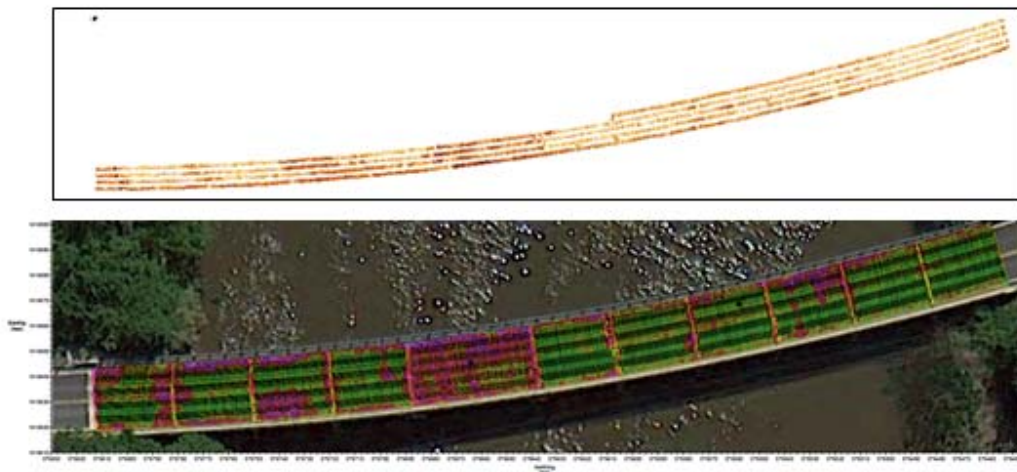


Figure 4.18 Route 290 Over Chester River Migration Results at 7" Depth

Depth = 8 inch

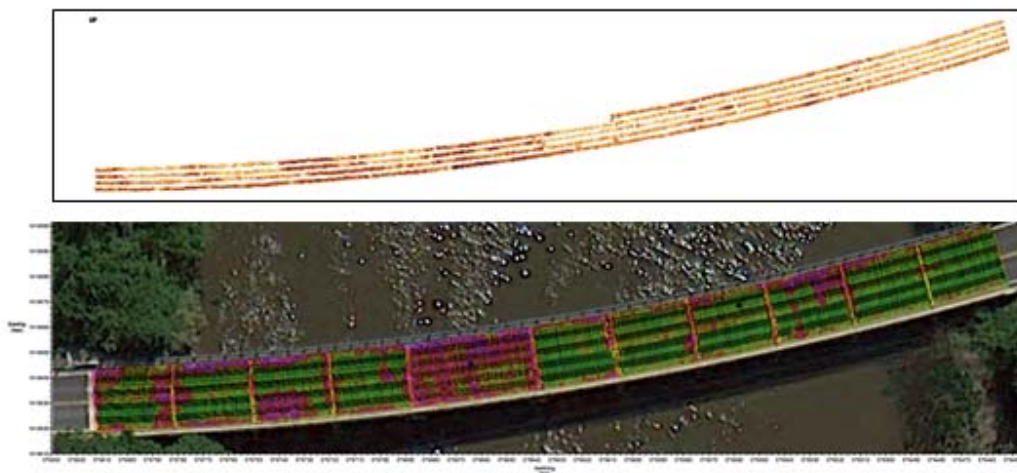


Figure 4.19 Route 290 Over Chester River Migration Results at 8" Depth

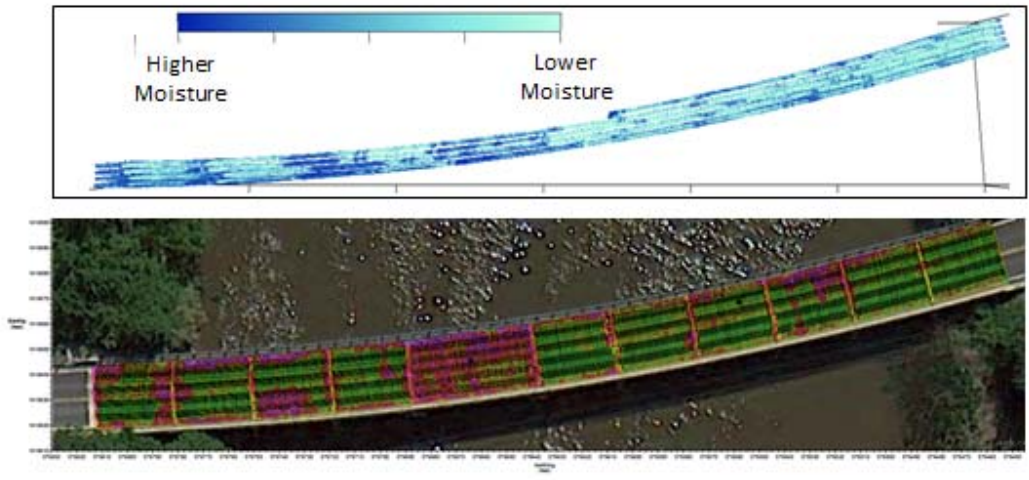


Figure 4.20 Route 290 Over Chester River Migration Results - Moisture

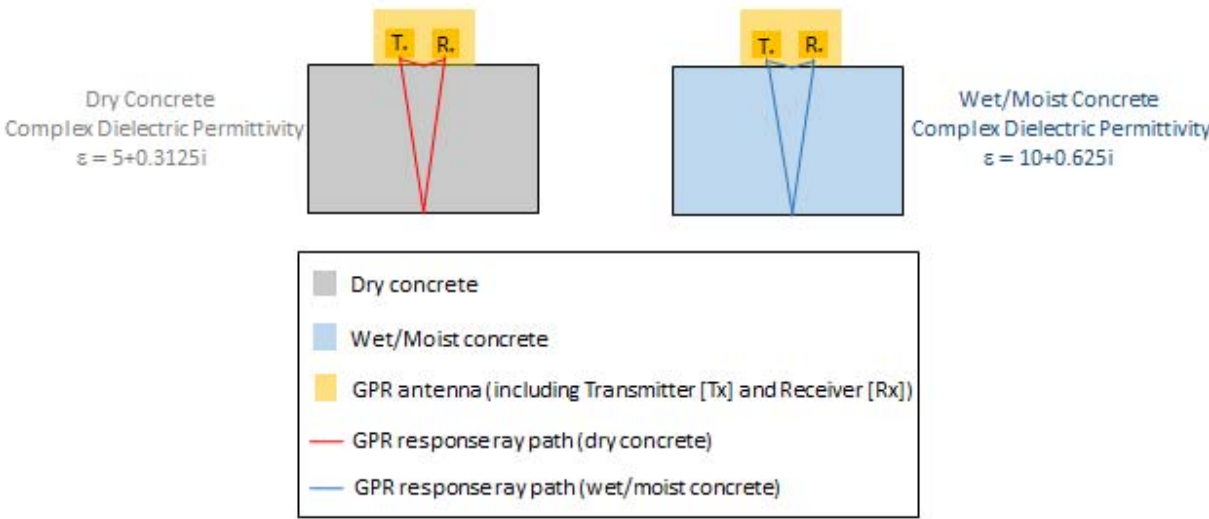


Figure 4.21 Short Time Fourier Transform (STFT) Analysis of Bridge Deck GPR Data

When bridge deck materials are wet/moist:

- The back surface reflection is delayed in time (due to elevated Real dielectric properties)
- Moisture in the deck causes GPR signal dispersion which reduces high frequency content and reduces signal energy versus a dry deck (due to elevated Imaginary dielectric properties)

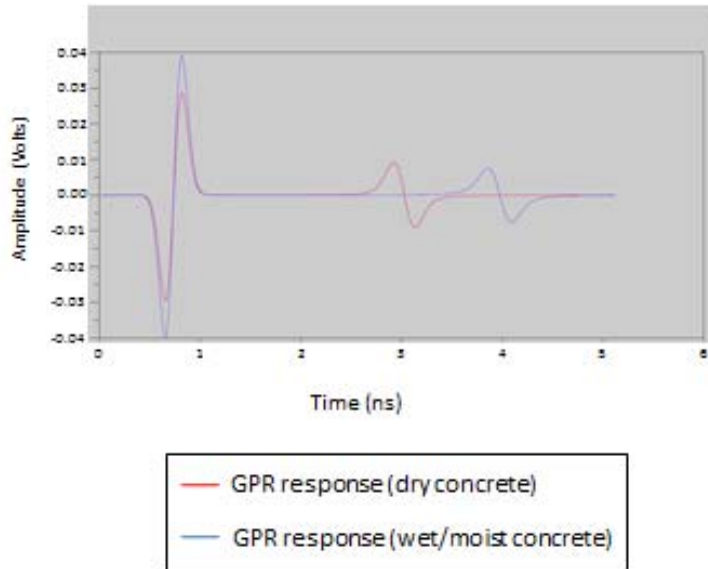
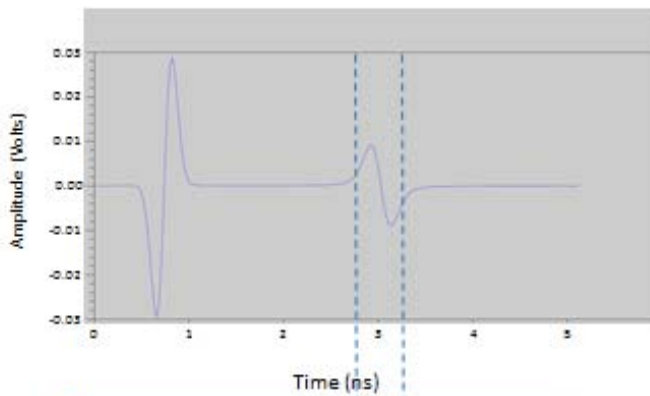


Figure 4.22 Time Domain Bridge Deck GPR Data Comparison (Analytical Waveform Simulation of GPR Response to Wet vs. Dry Concrete)

Time Domain
Bridge Deck GPR Simulated Response
For Dry Concrete



Corresponding STFT of
Bridge Deck GPR Simulated Data
For Dry Concrete

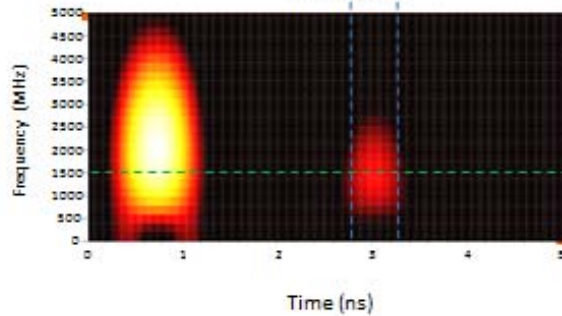
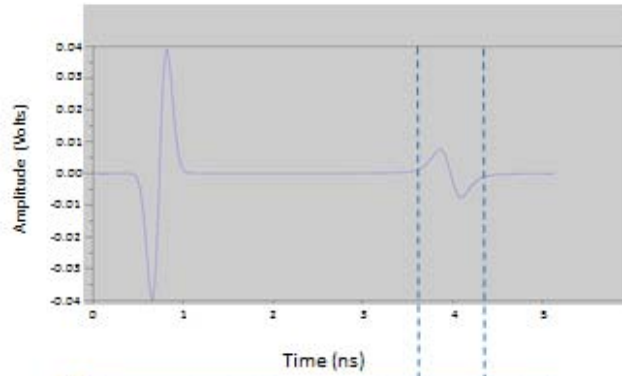


Figure 4.23 Dry Concrete STFT Analysis

Time Domain
Bridge Deck GPR Simulated Response
For Wet/Moist Concrete



Corresponding STFT of
Bridge Deck GPR Simulated Data
For Wet/Moist Concrete

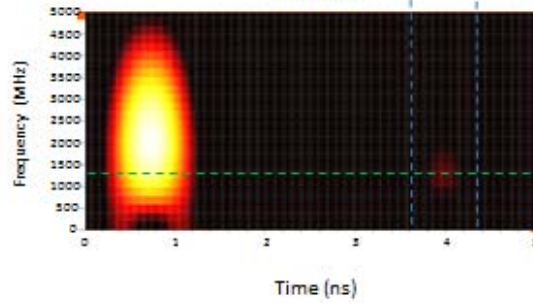


Figure 4.24 Wet/Moist Concrete STFT Analysis

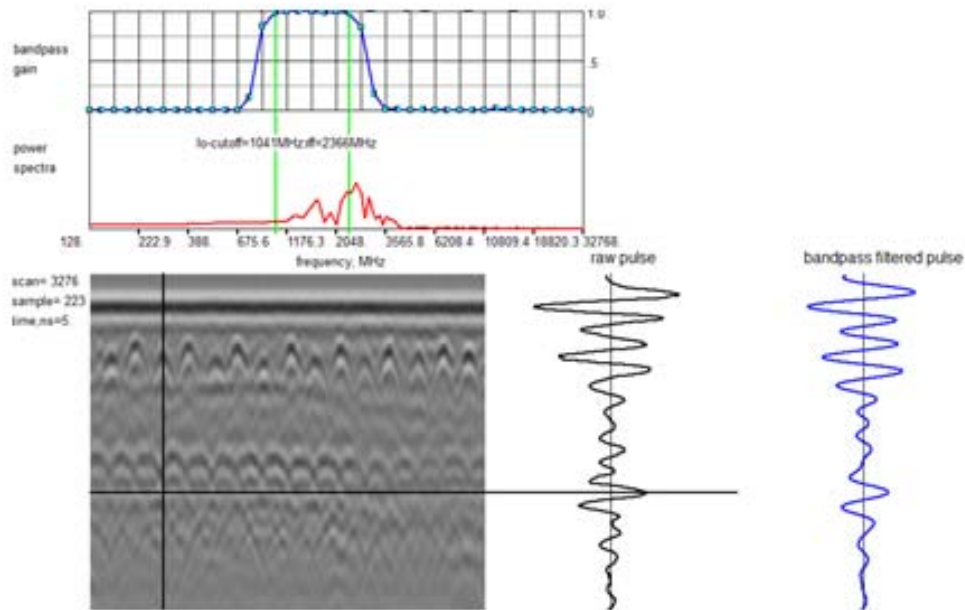


Figure 4.25 Applying STFT Analysis Principles Using a Fourier Transform Filter

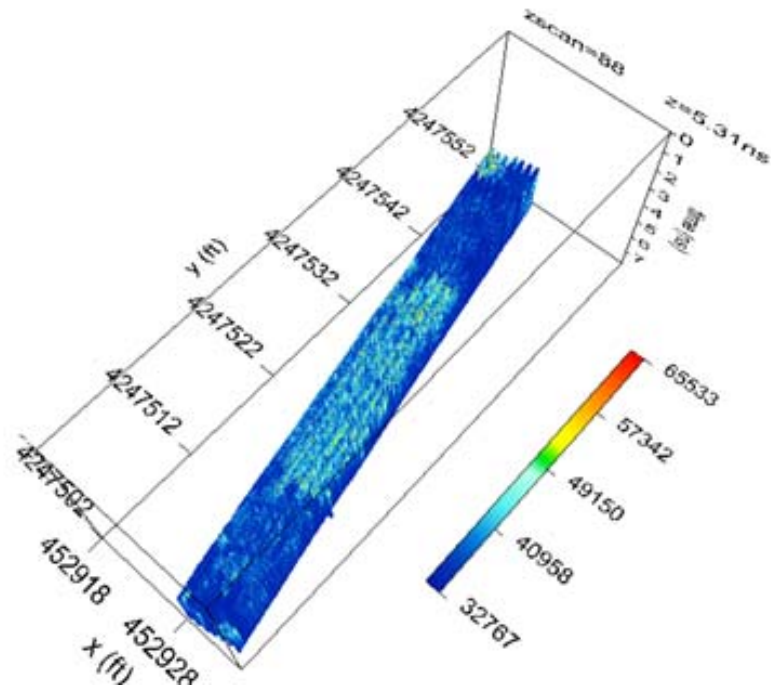


Figure 4.26 Fourier Transform Filtered Bridge Deck Data (Low Pass) – Rte 346 Bridge Part 1

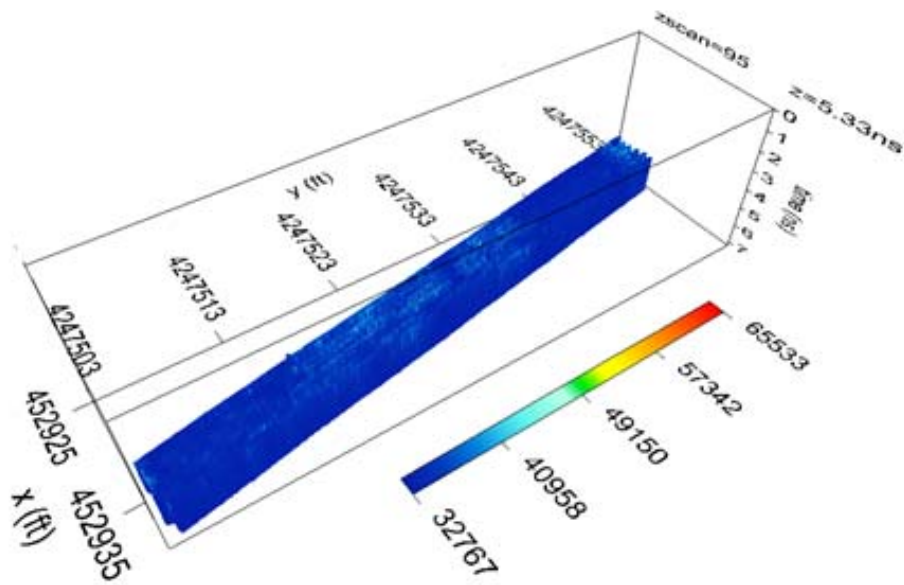


Figure 4.27 Fourier Transform Filtered Bridge Deck Data (Low Pass) – Rte 346 Bridge Part 2

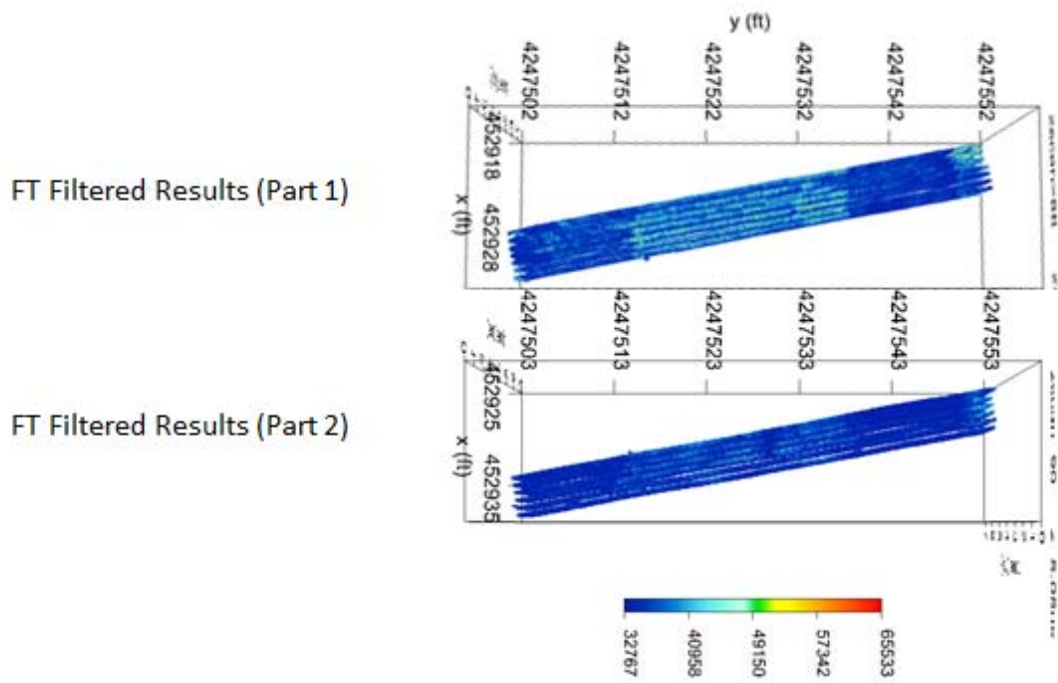


Figure 4.28 Plan View Results

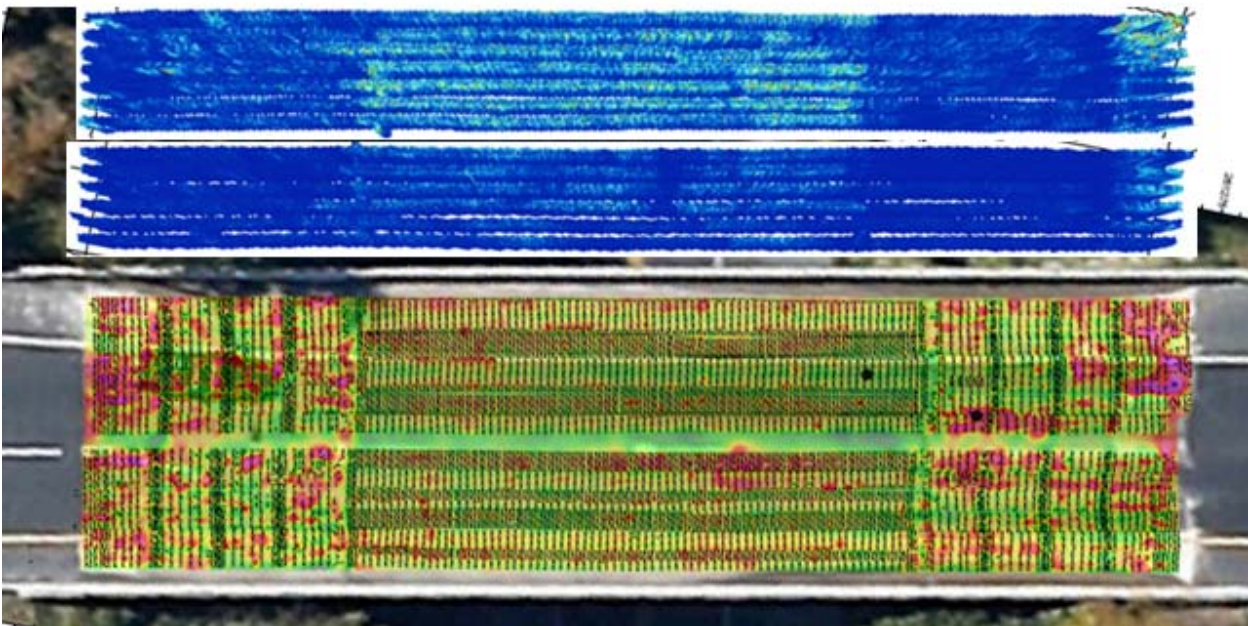


Figure 4.29 US 13 SB over MD 346 SB FT Filtered Results (Upper) vs. Attenuation Map (Lower)

CHAPTER 5: GPR PRECAST CONCRETE ANALYSIS

MD SHA uses precast concrete elements to produce many diverse civil infrastructure components in increasing quantities each year. Using precast concrete elements can be responsive to MD SHA goals to reduce civil infrastructure construction costs, increase construction efficiency, and facilitate quality control improvements versus conventional on site concrete casting. Among these potential benefits, effective implementation of precast concrete element quality control has lagged behind the others for MD SHA applications. Unfortunately, diverse precast concrete element defects and problems have the potential to undermine precast efficiency and cost advantages if they are not addressed. Therefore, precast quality control can benefit from increased MD SHA attention and new tools and methods to address it.

Precast quality control (QC) is currently done using labor intensive, reactive performance audits and sporadic inspections with the potential to miss important problems. In fact, these audits and inspections have not been shown to be effective unless many violations of MD SHA protocols and specifications occur frequently at a given precast facility. Quality control of precast concrete elements should be improved consistent with cost and function benefits of precast concrete elements. If not, benefits of construction using precast concrete elements are at risk due to potential performance issues of undetected defects and issues.

Precast concrete element quality control may lag other benefits due to a lack of information about systematic quality control tools and resources such as Ground Penetrating Radar (GPR). GPR and complementary tools have potential to address quality control issues rapidly and proactively by detecting relevant defects and issues. Without reliable quality control, MD SHA precast concrete elements are susceptible to:

1. Inadequate concrete cover depth to protect reinforcing steel from premature corrosion.
2. Missing or substandard steel reinforcement components to meet MD SHA strength and durability requirements.
3. Material thickness that may not meet MD SHA design specifications (too thin and weak or too thick and heavy).
4. Physical or material issues that do not meet MD SHA specifications.

Using appropriate tools and resources including GPR, precast concrete element testing and evaluation has potential to detect problems before they leave the plant. This can minimize the risk of precast defect or material issues. Appropriate test plans and statistical sampling are also important to achieving desired results. This study included an initial assessment in detecting precast concrete defects using GPR with scans carried out at a precast plant MD SHA sources from.

Introductory aspects of GPR imaging relevant to precast concrete component evaluation are illustrated by example three dimensional data (Figures 5.1 through 5.4). Example two dimensional results are shown in Figures 5.5 through 5.18. Diverse precast concrete specimen geometries were evaluated including a wall panel, a header wall, a cylinder, a manhole, a fresh concrete cylinder, and a sound wall.

Figures 5.1 through 5.4 present a series of four plan view GPR depth slice images of a reinforcing steel grid, increasing in depth from 1 to 4 inches in each successive image. Each of the four figures

includes a side by side comparison between results corresponding to correct dielectric material properties (at left) and assumed/estimated dielectric material properties (at right). This analysis indicates that correct dielectric material properties allow correct GPR depth measurement results to be determined, but further details about features in the images and details of the analysis are explained later. First, a brief summary of principles used to collect and represent each Synthetic Aperture Radar (SAR) image are reviewed immediately below.

In the Figure 5.1 through 5.4 examples, SAR images were built up from a series of GPR antenna scans. During each GPR scan, an antenna consisting of a single transmitter and receiver pair (bistatic) was manually moved along a straight, linear path (following a fixed, marked line). As the GPR antenna moved forward, a GPR encoder wheel turned in proportion to the distance traveled and triggered collection of a GPR waveform approximately three times per inch. Each time of flight GPR waveform measurement includes a series of reflections returned from features with dielectric contrast at increasing depth in the path of the incident GPR wave transmitted by the GPR antenna at a given location. Strong response features in each waveform often correspond to features directly below the antenna pair. However, the incident wave propagates with an approximately cone shaped energy distribution and therefore reflections from some subsurface features adjacent to GPR waveform data collection locations appear in raw GPR waveforms as well. A series of collected waveforms are stacked adjacent to one another to form a SAR image (gray color map images in Figures 5.1 through 5.4).

A SAR image collected on a path orthogonal to the detected reinforcing steel appears as a hyperbola shape (as shown in the lower left gray color map images in Figures 5.1 through 5.4). This distributed hyperbola reflection can be focused back to its original reflection source using a technique called migration imaging (reducing the hyperbola shape to the point like shape corresponding to the original reflector). Seven SAR GPR scans were collected in two orthogonal directions and migrated (focused) in three dimensions to produce the focused image of a reinforcing steel grid at upper left in Figures 5.1 through 5.4 (allowing cover depth to be evaluated). Precise alignment of all fourteen GPR scans was maintained by scanning the GPR antenna along a 2 foot square grid template fixed in position on the wall. Various grid template sizes and shapes are available.

For migration imaging, the dielectric properties (and corresponding propagation velocity) of the concrete material are accounted for to produce a focused result. One approach involves fitting a hyperbola to a point feature in an SAR image as shown in Figures 5.5 and 5.6. The correct propagation velocity corresponds to the fitted hyperbola shape that matches the reinforcing steel response imaged (for an SAR path orthogonal to the steel orientation). Using the correctly calibrated velocity and dielectric properties results in a correct mapping of depth information to GPR time of flight measurements (as shown in Figure 6 for the header wall pictured in Figure 5).

Figure 5.7 presents Figure 5.6 GPR results using an alternative color map (a hot/red Figure 7 color map versus a Figure 5.6 gray color map) illustrating how GPR results can be customized while representing the same underlying information. Figure 5.8 adds a data collection properties window, which specifies parameters such as how many waveform traces make up the SAR image (445 traces) and how far apart each waveform trace sample interval is (0.033 ft). In addition, the center frequency of 1000 MHz is indicated, corresponding to a practical compromise between medium to high resolution and relatively deep penetration capabilities. A parallel scan of the same header wall

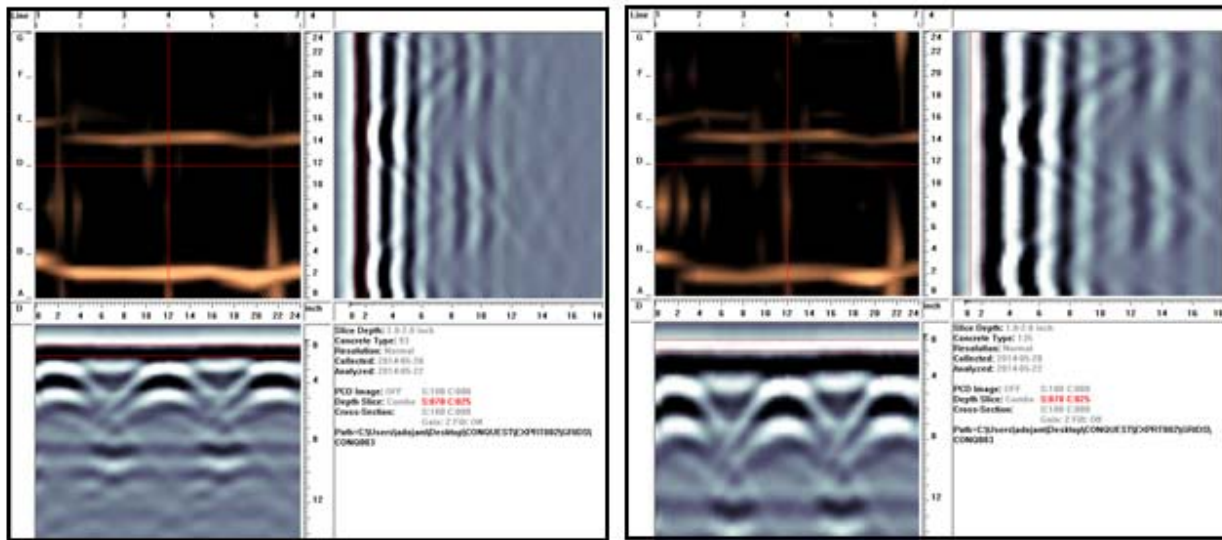
associated with Figures 5.5 through 5.8 is shown in Figure 5.9. The Figure 5.9 scan has the same transverse reinforcing steel spacing as Figure 5.8, indicating vertically oriented reinforcing steel are aligned parallel to each other. Figure 5.10 shows the same header wall reinforcing steel information collected in an orthogonal direction relative to Figure 5.8 and 5.9 scans. Near identical hyperbola features and back wall features between the two scans indicate the precast concrete element was built consistently in the horizontal direction as well.

A precast concrete cylinder can present challenges to practical GPR evaluation versus a flat wall due to curved surfaces. However, some GPR system features can make collecting GPR scan data from these cylinder elements more straightforward and reliable. One of these features is a small antenna head size. A small antenna head size can facilitate consistent contact and orientation between the GPR and the test piece. Another feature is an encoder/trigger wheel centered in the antenna head that can maintain surface contact during small orientation changes while the GPR is scanned tangent to the cylinder surface. An example precast concrete cylinder is pictured in Figure 5.11 (scanned during on-site GPR testing at the precast plant) and a drawing corresponding to this example cylinder is shown as provided by the precast plant (Figure 5.12). The cylinder wall reinforcing steel was imaged using GPR and a back wall depth response is indicated in addition to reinforcing steel hyperbola response features. The small antenna size and the centered GPR trigger wheel position on the antenna scan head provided clear, useful Figure 5.12 data (collected orthogonal to the cylinder axis). In addition, GPR cover depth and wall thickness are accurately represented based on a hyperbola calibration fit.

Figure 5.13 shows a GPR response to a concrete manhole element. Example formwork is also pictured in Figure 5.13 and illustrated in a plan provided by the precast plant (shown in Figure 5.14). The GPR results obtained indicate why this type of test piece presents challenges to address quality control needs. The GPR was scanned along the perimeter of the cylindrical manhole slab to evaluate for adequate cover depth (while directed inward toward its center). Ideally, reinforcing steel bar ends in several orientations should be clearly imaged in addition to other complementary features to obtain quality control metrics from. These bars are observable in the data, but further refinement and testing of antenna data collection paths is recommended due to sensitivity to unique reinforcing steel orientations. This refinement could improve imaging effectiveness and contrast for useful GPR evaluation of this complex shape. Never the less, significant features such as a material property transition (possibly moisture related) and the manhole perimeter were detected in the data as shown in Figure 5.13.

Another concrete cylinder was evaluated inside the precast plant building to show the effects of fresh concrete material properties on GPR response characteristics (Figure 5.15). Hyperbola fitting confirmed GPR wave velocities were reduced to 0.249 ft/ns in fresh, moist concrete versus a velocity of 0.261 ft/ns in more mature, dry concrete (Figure 5.11). Significant GPR signal energy losses were also observed in reinforcing steel responses when Figure 5.11 (dry concrete) and Figure 5.15 (moist concrete) images were compared. It is evident that this was due to GPR energy losses that occur as GPR waves pass through moist material. A vertical scan of the same moist, fresh concrete cylinder in Figure 16 exhibits similar imaging characteristics observed in Figure 5.15, but the thin gage wire mesh produces a diffraction effect rather than a hyperbola response due to its small diameter.

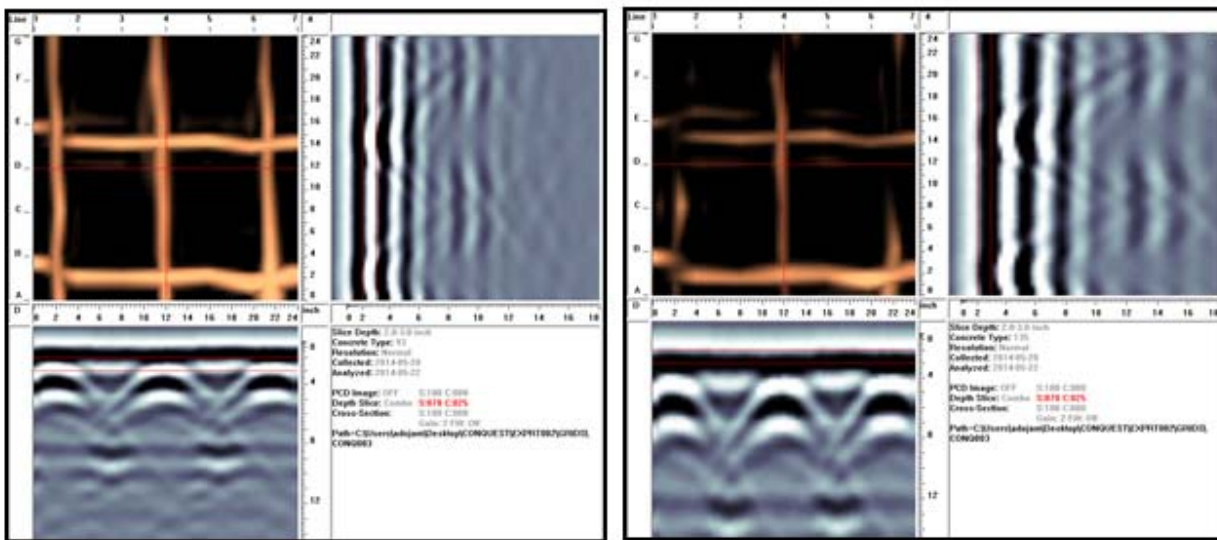
Finally, a sound wall in the field is shown in Figures 5.17 and 5.18. A vertical GPR wall scan is shown in Figure 5.17 and two horizontal scans of the wall are shown in Figure 5.18. Even though the



Correct Velocity/Dielectric

Assumed Velocity/Dielectric

Figure 5.2 Grid GPR Data Collected From a Precast Concrete Wall Panel: Integrated 1 to 2 Inch Depth
 Note: Plan View Migrated Results (Hot/Red Color Map); Individual Alpha Numeric Scans (Gray Color Map)



Correct Velocity/Dielectric

Assumed Velocity/Dielectric

Figure 5.3 Grid GPR Data Collected From a Precast Concrete Wall Panel: Integrated 2 to 3 Inch Depth
 Note: Plan View Migrated Results (Hot/Red Color Map); Individual Alpha Numeric Scans (Gray Color Map)

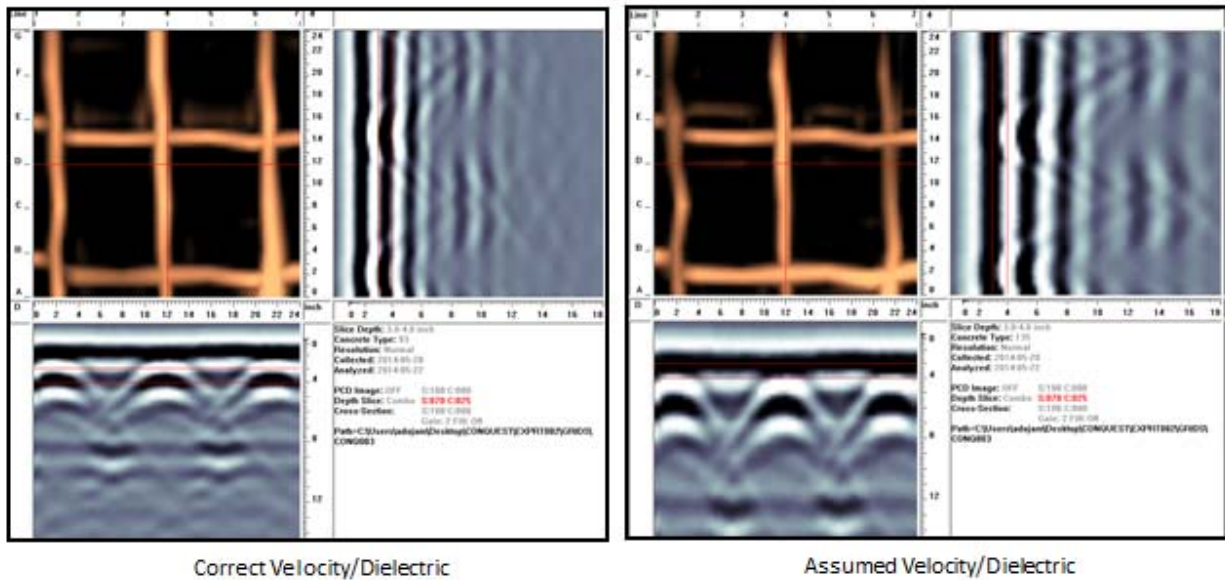


Figure 5.4 Grid GPR Data Collected From a Precast Concrete Wall Panel: Integrated 3 to 4 Inch Depth
 Note: Plan View Migrated Results (Hot/Red Color Map); Individual Alpha Numeric Scans (Gray Color Map)

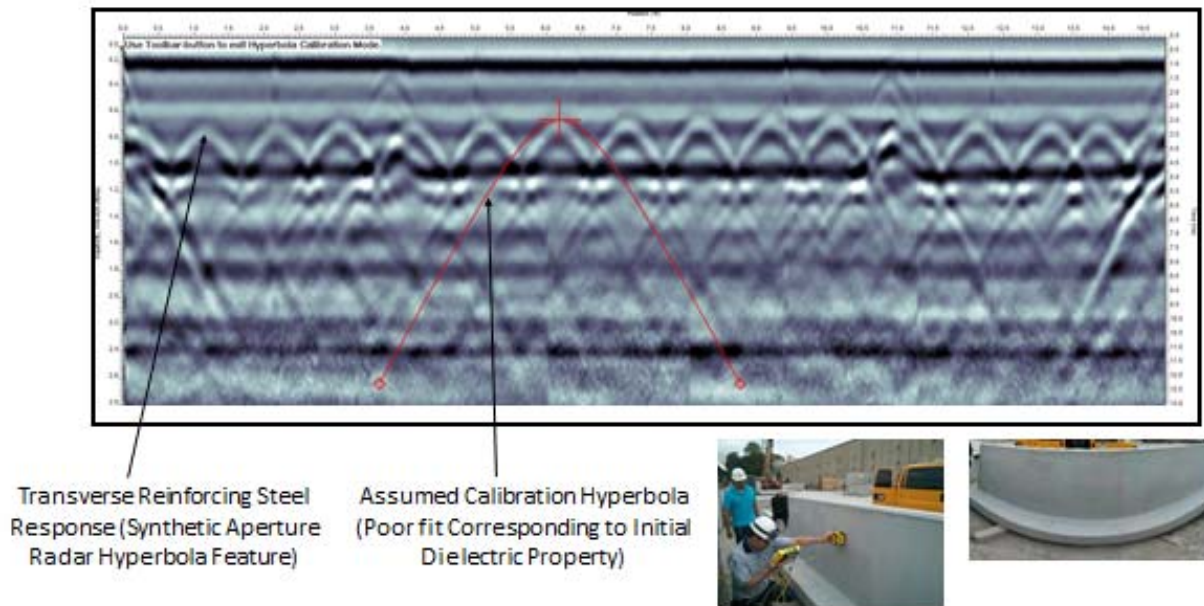


Figure 5.5 Line Scan GPR Data Collected From a Precast Concrete Header Wall Element (Scan 1 – Horiz.): Assumed Velocity/Dielectric

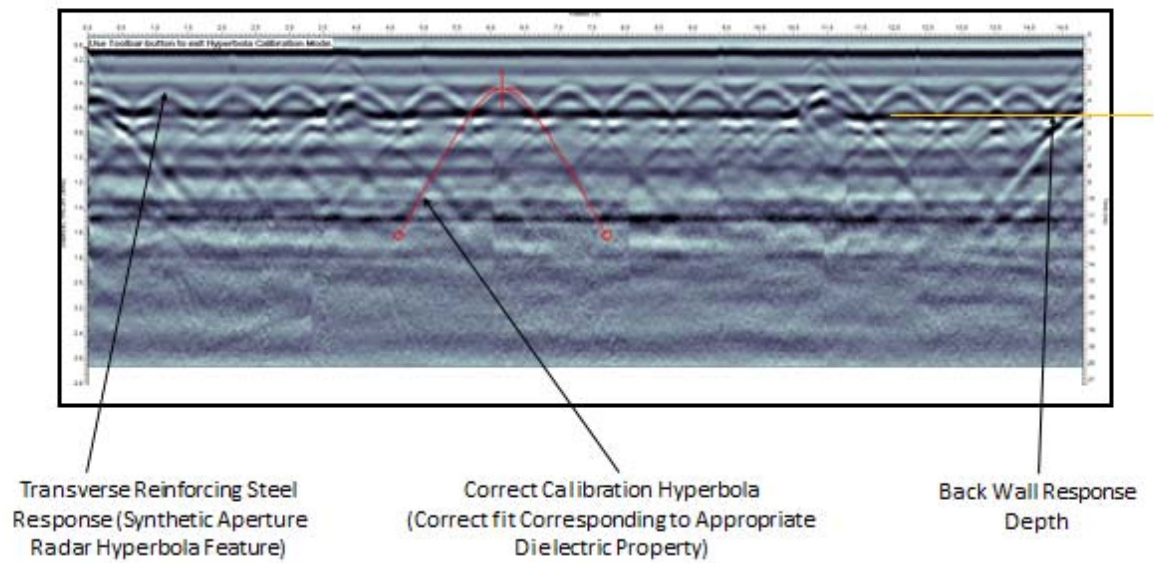
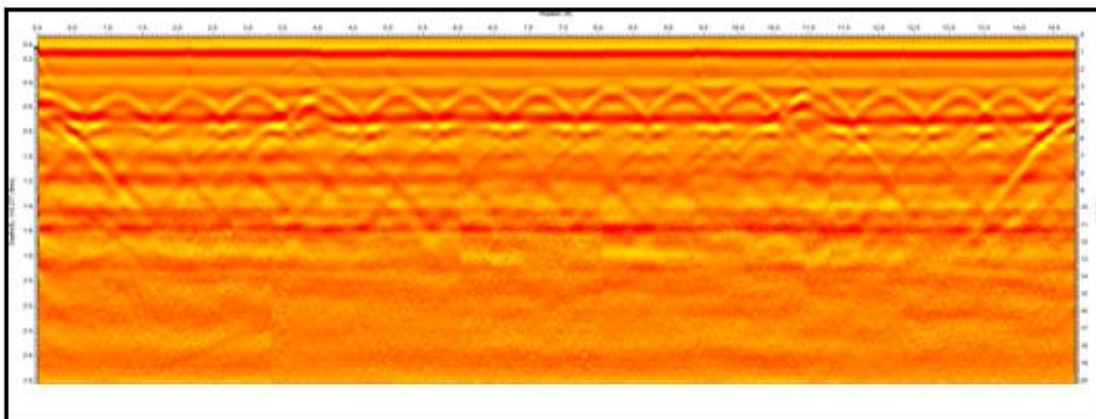
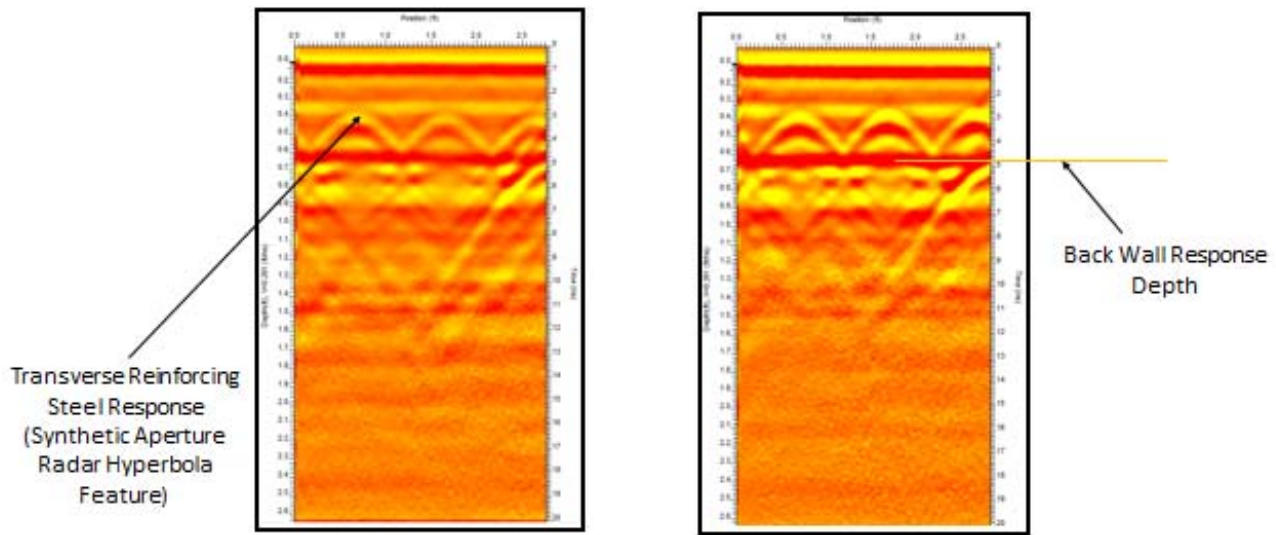


Figure 5.6 Line Scan GPR Data Collected From a Precast Concrete Header Wall Element (Scan 1 - Horiz): Correct Velocity/Dielectric



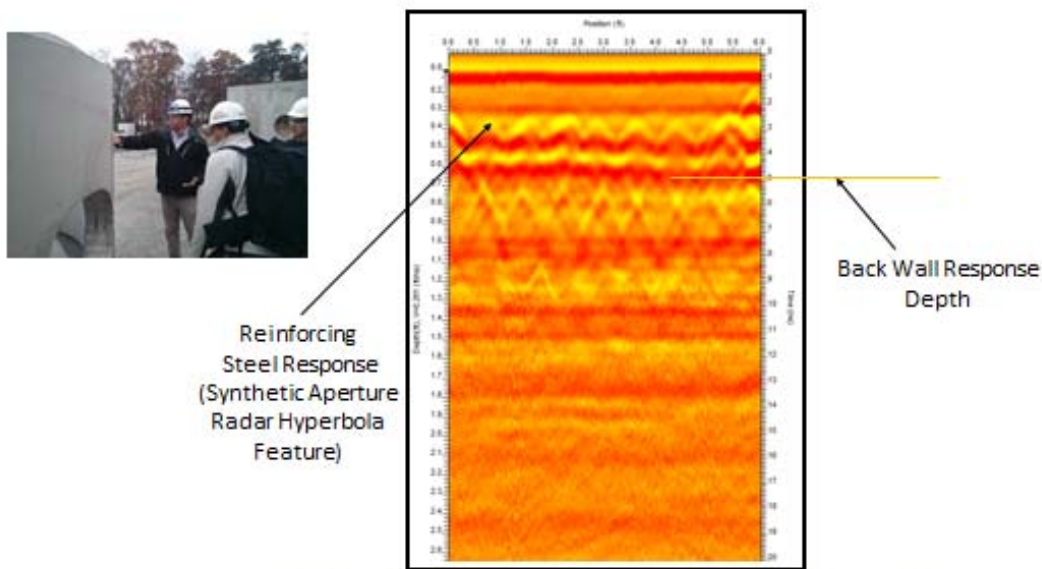
Alternative Color Maps can Improve Contrast and Visualization of Features of Interest

Figure 5.7 Line Scan GPR Data Collected From a Precast Concrete Header Wall Element (Scan 1 - Horiz): Correct Velocity/Dielectric (Hot/Red Color Map)



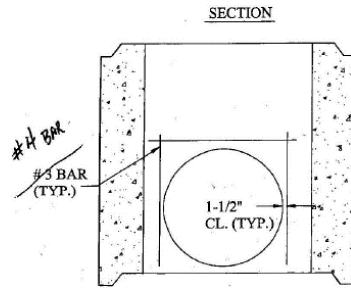
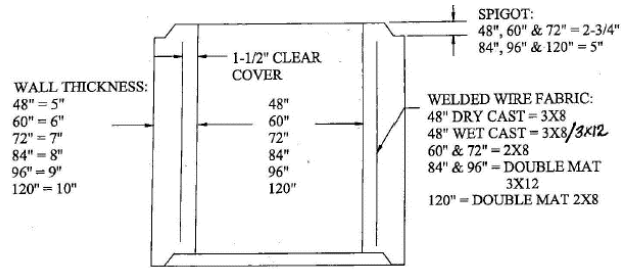
Two Vertical GPR Line Scans From an Example Header Wall Illustrate Orthogonal Reinforcing Steel Symmetry When Compared With Horizontal GPR Line Scans From the Same Wall Element

Figure 5.10 Line Scan GPR Data Collected From a Precast Concrete Header Wall Element (Scans 3 and 4 – Vert.)



Horizontal GPR Line Scan of a Precast Concrete Cylinder Element

Figure 5.11 Line Scan GPR Data Collected From a Precast Concrete Cylinder Element (Scan 5 – Horiz.)



WHEN THE DISTANCE BETWEEN MULTIPLE HOLE OPENINGS IN THE BASE OR ANY RISER IS LESS THAN 6", ADDITIONAL #3 BAR PLACED AROUND HOLE OPENINGS.

Figure 5.12 Precast Concrete Cylinder Element

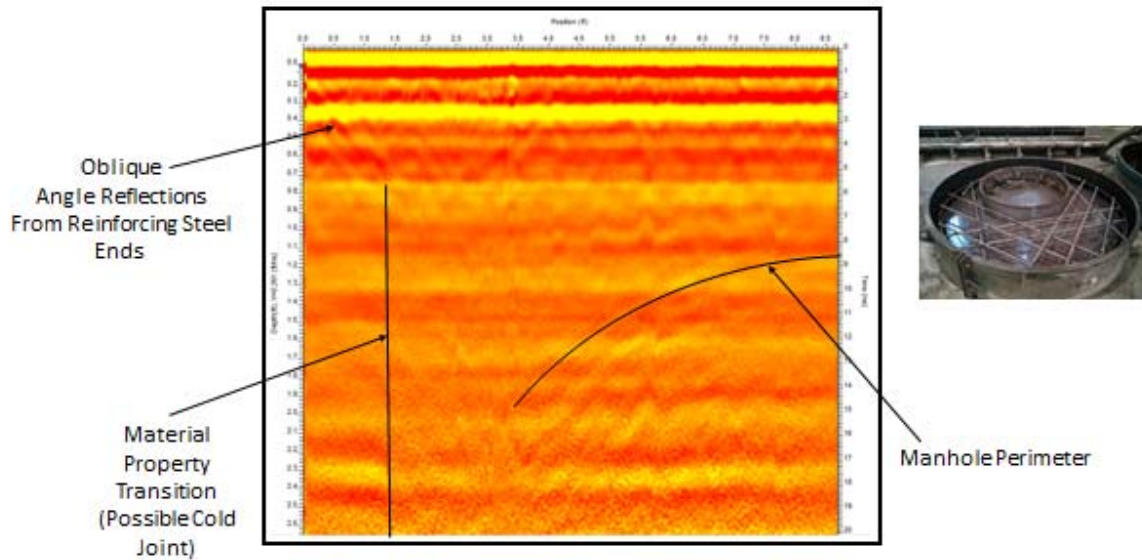


Figure 5.13 Line Scan GPR Data Collected From Side of a Precast Concrete Manhole Element (Scan 10 – Horiz.)

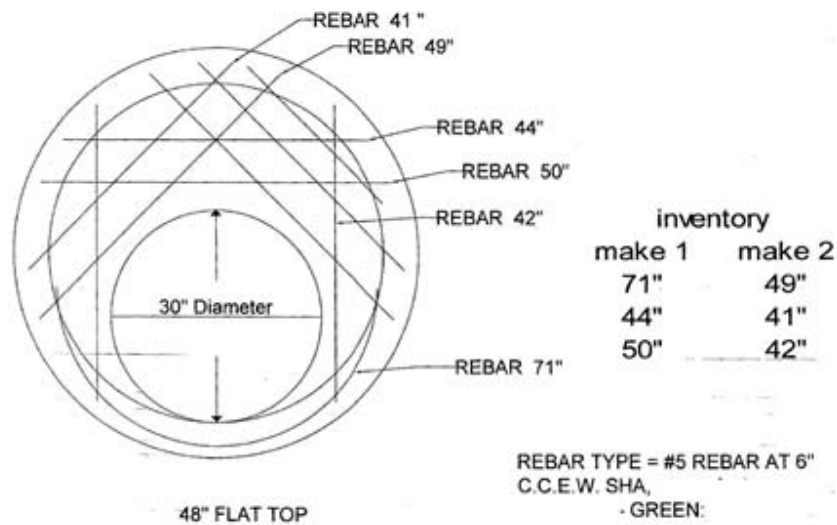


Figure 5.14 Precast Concrete Manhole Element

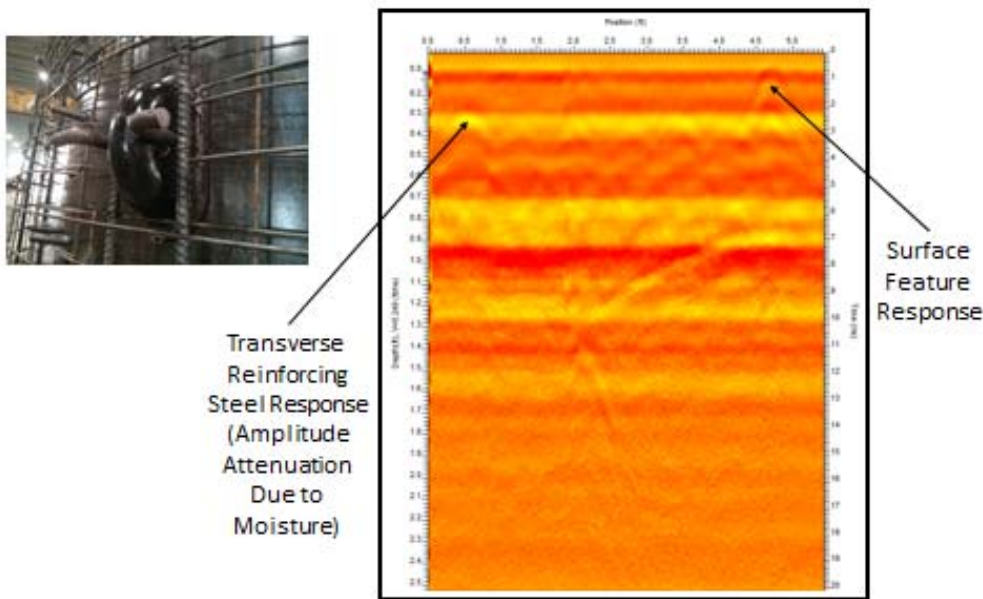


Figure 5.15 Line Scan GPR Data Collected From a Moist Precast Concrete Cylinder Element (Scan 11 – Horiz.)

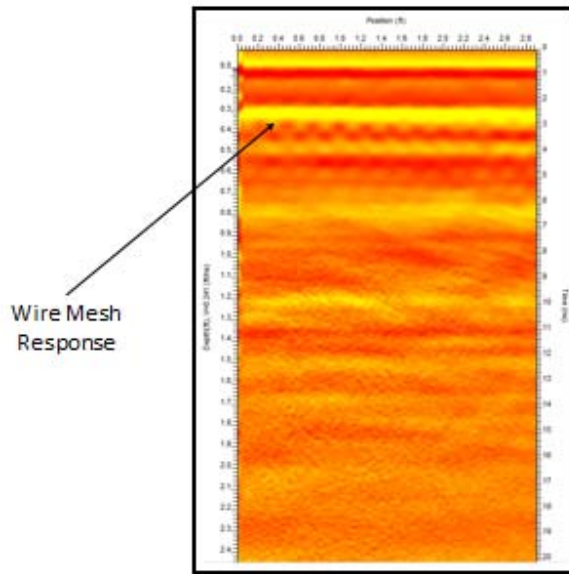


Figure 5.16 Line Scan GPR Data Collected From a Moist Precast Concrete Cylinder Element (Scan 17 – Vert.)

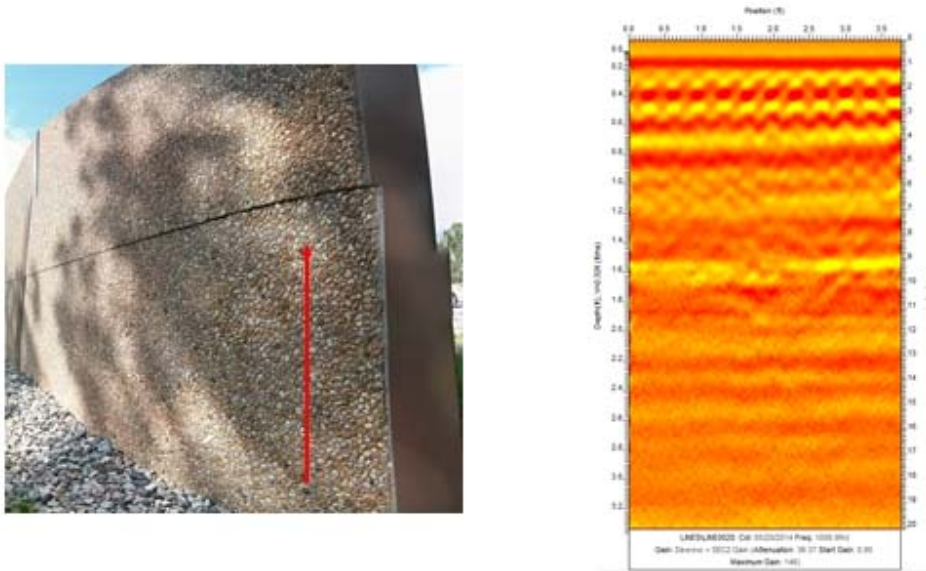


Figure 5.17 Line Scan GPR Data Collected From a Sound Wall (Scan 20 – Vert.)

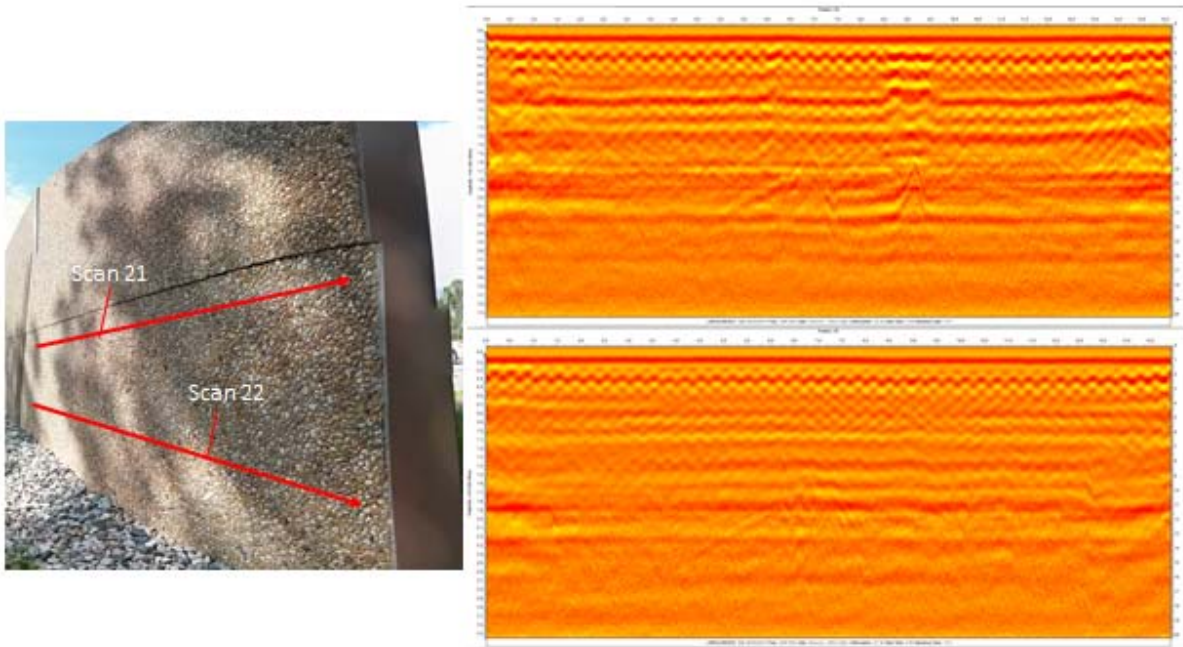


Figure 5.18 Line Scan GPR Data Collected From a Sound Wall (Scans 21, 22 – Horiz.)

CHAPTER 6: GPR TESTING PROTOCOLS AND TRAINING MODULES

The research team developed the testing protocols for GPR evaluation of pavement structures and bridge decks. The testing protocols follow the SHA structure for MSMTs and include sections describing the following:

- Scope;
- Reference Documents;
- Terminology;
- Summary Method (background);
- Apparatus;
- Periodic Calibration;
- Testing Procedure & Data Collection;
- Routine Calibration;
- Data Analysis;
- Reporting;

The protocols are included in the Appendix A.

The research team also developed training modules for the assessment of pavement structures, bridge decks and precast concrete elements. These modules are included in Appendix B and include information related to:

- Summary Method (background);
- Apparatus Characteristics & Applicable Calibrations;
- Examples of Data Analysis.

CHAPTER 7: SUMMARY, CONCLUSIONS & RECOMMENDATIONS

SUMMARY & CONCLUSIONS

The overall objective of this study was to assist SHA engineers, technicians, and decision makers in their current effort to explore the use of GPR in assessing the condition of critical infrastructure components and to identify potential improvements in GPR data analysis. The research team worked closely with representatives from the different divisions of the Office of Materials Technology (OMT) to (i) identify potential GPR applications using existing equipment accessible to SHA, and (ii) identify and target GPR analysis for critical high priority areas. In addition, the research team utilized initial data sets from emerging GPR technologies to evaluate their fundamental capabilities, provide early insights into analysis they can support, and recommend complementary deployment and analysis options for a Phase II study.

Regarding pavement structures, a new methodology was suggested to improve the accuracy of GPR data analysis. The initial analysis and results indicate that MPGA has significant potential to add value and accuracy to pavement thickness data used in pavement management and rehabilitation analysis. The MPGA results indicate that pavement thickness data trends can be identified based on either automated or semi-automated procedures based on target variability levels of thickness uniformity, and thus can be used to efficiently evaluate pavement material layers.

The MPGA approach can effectively identify variable and thin pavement thickness subsections, construction pavement thickness discontinuities, and trends among multiple pavement layers which may indicate relevant damage, deterioration, or defects. Cost savings can be achieved by using this MPGA approach through its rapid, accurate analysis of relevant pavement thickness trends at various length scales. These savings can be realized versus conventional GPR analysis that can eventually produce inaccurate results due to inadequate assumptions about pavement thickness uniformity throughout a pavement section. Savings can also be achieved by using this automated MPGA procedure versus the costly and substantially greater manual analytical work currently used by state highway agencies to achieve similar accuracy in results, using labor and time consuming analysis.

In addition MPGA can enhance the utility of complementary data for other diverse applications. Relevant to PMS, pavement layer thickness information is a crucial input parameter frequently analyzed in practice based on limited information resources such as: (i) pavement layer design information is often assumed to be homogeneous throughout a section of the roadway under evaluation, (ii) measured pavement core data from selected locations, (iii) GPR pavement thickness data with variability issues that can present problems for accurate PMS analysis.

Key problems have been identified with conventional bridge inspection specified by existing Federal requirements, where reliability of bridge deck inspection results is one important aspect. Among these problems are poor reliability of bridge deck inspection techniques to evaluate subsurface distress, such as corrosion induced delamination and subsequent concrete pop-outs. These problems are common due to the prevalence of corrosion phenomena in bridge decks. They are particularly acute where asphalt overlays are applied to bridge decks, making acoustic bridge deck evaluation techniques such as the chain drag method and impact-echo method impractical.

GPR data collection speed, coverage, and material penetration for practical concrete bridge deck applications, has improved steadily over the years due to features such as synchronized antenna arrays (for rapid, parallel path data collection using several antenna elements together) and improved instrument signal to noise ratios (within practical and regulatory limits). These GPR hardware advances have made many potential bridge deck evaluation advances possible, but relatively few GPR systems have been applied broadly in practice by agencies such as MD SHA to the present. In part, this may be due to recognition of needs to improve analysis of GPR data to extract valuable, potentially reliable information (such as locations and quantities of bridge deck deterioration phenomena to scope repair, rehabilitation, or replacement decisions). In addition, there is a need to control for variables such as concrete moisture content, which can impact existing bridge deck GPR results significantly in some scenarios.

Thus, in this study, currently available GPR data analysis techniques such as migration imaging (for concrete cover depth measurement applications among others) and Fourier analysis of GPR waveforms (for qualitative bridge deck moisture analysis) in addition to emerging techniques such as Short Time Fourier Transform analysis (for anticipated quantitative moisture analysis) were applied in novel ways. Migration and Fourier techniques were illustrated corresponding to GPR data collected using a GPR array on selected bridge decks in the Salisbury, MD area. When applied appropriately, such techniques can provide more reliable analysis of bridge deck inspection than conventional means.

Currently precast concrete QC is based on plant inspections and periodic audits. These quality assurance practices include labor intensive activities and sporadic inspections with the potential to miss important problems. In fact, these audits and inspections have not been shown to be effective unless many violations of MD SHA protocols and specifications occur frequently at a given precast facility. This study has shown how GPR can be used to address several of the inspections needed in precast concrete production, including an evaluation of concrete cover depth, reinforcement location, and section thicknesses. The testing and demonstration showed significant potential for quality control using GPR. Further testing and refinement of GPR techniques for evaluation of specific defects is recommended to design more complete data collection scan patterns, hardware settings, and to refine post processing analysis.

For the high priority areas of pavement structures and bridge decks the project team developed the required testing protocols, in MSMT format, to facilitate the implementation of GPR and assist SHA engineers and technicians to conduct such surveys. The protocols include among other information related to the method (background), equipment requirements, calibration guidelines, testing procedure and recommendations for data analysis and reporting. Along with the testing protocols the research team developed training material for pavement structures, bridge decks and precast concrete elements.

In parallel to this project SHA contracted the use of emerging GPR technologies in bridge decks including an efficient ground coupled impulse GPR antenna array system and a high speed, step frequency GPR array system with many configuration options for advanced applications. Initial pilot analysis by the project team included (i) bridge deck deterioration evaluation (where relative moisture content was estimated as a contributing factor), and (ii) quality control/quality assurance parameters (including concrete cover depth) to predict probable deterioration areas. Both technologies provided promising initial information for this study, but high speed (30+ mph) step frequency GPR capabilities and wider coverage area per data collection pass (in addition to potential refinement of versatile

materials evaluation and geometry measurements) were recognized by SHA as high priorities for future work. Therefore, techniques to quantitatively evaluate deterioration factors such as moisture content and active bridge deck corrosion will be developed to leverage step frequency GPR in a Phase II study of bridge decks (at project and network levels) and pavements (at the project level). In addition, step frequency GPR technology can be used to advance MPGA analysis for improved ease of use and further refinement of the analysis.

The expected benefits of the proposed GPR based condition assessment techniques include: i) higher precision and accuracy of the condition assessment of key infrastructure components and materials; ii) higher speed of condition assessment reducing monitoring time and cost; iii) increasing accuracy of the specific locations where failures occur; iv) improving overall condition assessment methods and more accurate performance and life cycle predictions; v) facilitating a method of non-destructive testing for Quality Assurance testing and forensic investigations.

RECOMMENDATIONS FOR FUTURE DEVELOPMENT

The results of this study provide the following recommendations in order to improve and successfully implement GPR surveys within SHA:

- Further refine the post processing analysis techniques for pavement structures for their adoption in the routine GPR analysis by SHA;
- Develop analysis techniques to capture moisture effects more precisely in bridge deck GPR analysis, and better relate moisture with deterioration;
- Develop GPR based deterioration criteria for project level (i.e., density/ location of distress) and network level (i.e., overall condition ranking) analysis of pavement structures and bridge decks;
- Custom tailor testing techniques for different configuration/ shape of precast concrete elements in order to improve accuracy of GPR analysis;
- Develop NDE/GPR based criteria for QA/QC procedures and acceptance of pavements, bridge decks and precast concrete elements;
- Augment existing SHA GPR equipment to expand capabilities and pilot test a universal system for multiple applications;
- Enhance in-house SHA GPR expertise by identifying GPR team leaders within each division and establishing a GPR focus group within OMT.

REFERENCES

- Al-Qadi, I.L., Lahouar, S., Loulizi, A., "Successful Application of GPR for Quality Assurance/Quality Control of New Pavements," Paper No. 03-3512, Proceedings of the Transportation Research Board 2003 Annual Meeting, pp. 1-21, 2003.
- Al-Qadi, I.L., Lahouar, S., Loulizi, A., "Ground-Penetrating Radar Calibration at the Virginia Smart Road and Signal Analysis to Improve Prediction of Flexible Pavement Layer Thicknesses," Report No. FHWA/VTRC 05-CR7, January 2005, pp. 1-65.
- Al-Qadi, I.L., Lahouar, S., "Part 4: Portland Cement Concrete Pavement: Measuring Rebar Cover Depth in Rigid Pavements With Ground Penetrating Radar," Transportation Research Record: Journal of the Transportation Research Board, 2005, pp. 81-85.
- Bois, K., Benally, A., Zoughi, R., "Near-Field Microwave Reflection Property Analysis of Concrete Using Open-Ended Rectangular Waveguides at S- and X-Band", Proceedings of SPIE Vol. 3396, Nondestructive Evaluation of Materials and Composites II, No. 37, March 31, 1998, pp. 37-46.
- Cabrera R. "Optimal GPR Antenna Selection." Geoscanners AB, Environmental Expert Article, May 2012.
- Daniels, D.J., Ground Penetrating Radar, 2nd Edition, IEEE, pp. 1-726, 2004.
- De Souza T., Anna, A., Redman J., Hu, N. "Monitoring the Ground Penetrating Radar Response of Curing Concrete." 16th WCNDT 2004 - World Conference on NDT. Montreal, Canada. Aug 30 - Sep 3, 2004.
- Diefenderfer, B.K., Mokarem, D.W., Sharp, S.R., "Use of Nondestructive Evaluation to Detect Moisture in Flexible Pavements," VTRC Report No. 06-R37., 2006, pp. 1-32.
- Evans, R., "Optimizing Ground Penetrating Radar (GPR) to Assess Pavements." Loughborough University, Thesis, U.K. 2009.
- FHWA. "GPR Measuring Pavement Layer Thickness." FHWA publication HIF 00015. Office of Asset Management., Washington D.C. 2000.
- Finck., F. "Introduction of GPR System for Investigations on Concrete Structures." Otto-Graf-Journal Vol. 14, 2003.
- Gehrig, M., Morris, D., Bryant J. "Ground Penetrating Radar for Concrete Evaluation Studies." Foundation Performance Association Meeting, March 2004.
- GSSI. "GSSI Handbook for RADAR Inspection of Concrete." Geophysical Survey Systems Inc., Salem, New Hampshire. August 2006.
- Huston, D., Fuhr, P., Maser, K., Weedon, W., "Nondestructive Testing of Reinforced Concrete Bridges Using Radar Imaging Techniques," New England Transportation Consortium, NETCR 94-2 Final Report, pp. 1-182, July 1, 2002.
- Kim, S., Surek, J., Baker-Jarvis, J., "Electromagnetic Metrology on Concrete and Corrosion," Journal of Research of the National Institute of Standards and Technology, Vol. 116, No. 3, May-June 2011, pp. 655-669.
- Lahouar, S., "Development of Data Analysis Algorithms for Interpretation of GPR Data," Virginia Polytechnic Institute and State University Thesis, 2003.
- Loken., W. "Use of Ground Penetration Radar to Evaluate Minnesota Roads." Minnesota DOT. Report MN/RC-2007-01. Saint Paul, MN. 2007
- Maser, K., "Use of Ground Penetrating Radar Data for Rehabilitation of Composite Pavements on High-Volume Roads, Transportation Research Record, Vol 1808, 2002, pp. 122-126.
- Maser, K., "Ground Penetrating Radar Data for Pavement Evaluation, Annual Road Profiler Users Group: Pavement Evaluation, Roanoke, VA, 2010.

- Maser, K., Martino, N., Doughty, J., Briken, R., “Understanding and Detecting Bridge Deck Deterioration Using Ground Penetrating Radar,” TRB 91st Annual Meeting, Paper 12-1765, 2012.
- Morey R. “GPR for Evaluating Subsurface Conditions for Transportation Facilities.” Synthesis of Highway Practice 255. TRB, Washington D.C. 1998.
- Minnesota DOT, “Pavement Evaluation Using Ground Penetration Radar.” Technical Summary 2008-10TS, Saint Paul, MN. 2008.
- Olhoeft, G., Smith S. “Automatic Processing and Modeling of GPR Data for Pavement Thickness and Properties.” Eighth International Conference on Ground Penetrating Radar, Gold Coast, Australia, April 2000.
- Pailes, B.M., Gucunski, N., Brown, M., “Correlation of Non-destructive Testing Results to Improve Assessment of Corrosion and Corrosion Damage of a Reinforced Concrete Deck,” Proceedings of the Transportation Research Board 92nd Annual Meeting, Washington, D.C., January 13-17, 2013.
- Perkins, A.D., Amrol, J.J., Romero, F.A., Roberts, R.L., “DOT Specification Development Based on Evaluation of Ground-Penetrating Radar System Performance in Measuring Concrete Cover (Reinforcement Depth) on New Bridge Deck Construction,” Structural Materials Technology IV: an NDT Conference, Editor: Sreenivas Alampalli, New York State Dept. of Transportation, March 2000, pp. 53-60.
- Scott, M., Rezaizadeh, A., Delahaza, A., Santos, C.G., Moore, M., Graybeal, B., Washer, G., “A Comparison of Nondestructive Evaluation Methods for Bridge Deck Assessment,” Nondestructive Testing and Evaluation International, Vol. 36, 2003, pp. 245-255.
- Scott, M., Nondestructive Testing Handbook, Vol. 5, Electromagnetic Testing, Chapter 17, Part 2, Infrastructure Applications of Electromagnetic Testing, American Society for Nondestructive Testing, 2004, pp. 430-436.
- Scullion, T., “Implementing Ground Penetrating Radar Technology Within TXDOT,” Texas Department of Transportation, Report No. FHWA/TX-05/5-1702-01-1, March 2005.
- SHRP 2, Report S2-R06-RW: “A Plan for Developing High-Speed, Nondestructive Testing Procedures for Both Design Evaluation and Construction Inspection.” TRB, Washington D.C., 2009.
- SHRP 2, Report S2-R06A-RR-1: “Nondestructive Testing to Identify Concrete Bridge Deck Deterioration.” TRB, Washington D.C., 2013.
- SHRP 2, Report S2-R06C-RR-1: “Using Infrared and High-Speed Ground Penetrating Radar for Uniformity Measurements on New HMA Layers.” TRB, Washington D.C., 2013.
- SHRP 2 Renewal Project R06D, “Nondestructive Testing to Identify Delaminations between HMA Layers.” TRB, Washington D.C., 2013.
- Smith, S.S., Scullion, T., “Development of Ground-Penetrating Radar Equipment for Detecting Pavement Condition Preventive Maintenance,” Strategic Highway Research Program, Report No. SHRP-H-672, October 1993, pp. 1-178.
- Stolt, R., “Migration by Fourier Transform,” Geophysics, Vol. 43, No. 1, February 1978, pp. 23-48.
- South Dakota DOT. “Feasibility of Using Ground Penetrating Radar (GPR) for Pavements, Utilities, and Bridges.” Report SD2005-05-X. South Dakota Department of Transportation, Pierre, SD. 2006.

- Tinke, Y., Miller, P., Leonard, M., Pott, A., Olson, L., "Bridge Deck Scanning for Condition Assessments of Bare Concrete and Asphalt Overlaid Decks," Proceedings of the Transportation Research Board 92nd Annual Meeting, Washington, D.C., January 13-17, 2013.
- White, J., Wolf, J., Shokouhi, P., Hurlbauss, S., Wimsatt, A., "Concrete Tunnel Lining Evaluation Using Nondestructive Techniques: A Multi-Method Case Study at Eisenhower Tunnel," Proceedings of the Transportation Research Board 92nd Annual Meeting, Washington, D.C., January 13-17, 2013.
- Willett, D., Rister B. "GPR Pavement Layer Thickness Evaluation." Kentucky Transportation Center, Report KTC 02—29, Lexington, Kentucky. 2002
- Zoughi, R., Cone, G.L., Nowak, P.S., "Microwave Non-destructive Detection of Rebars in Concrete Slabs," Materials Evaluation, Vol. 49, No. 11, November 1991, pp. 1385-1388.

APPENDIX A
TESTING PROTOCOLS

Approval:	Maryland Department of Transportation State Highway Administration Office of Materials Technology MARYLAND STANDARD METHOD OF TESTS	
Approved:	GPR FOR PAVEMENT STRUCTURES	MSMT xxx

SCOPE:

This procedure is used to determine the thickness of pavement layers using ground penetration radar. This non-destructive pavement evaluation method could identify defects in pavement materials and structures, such as material property deterioration, voids, moisture concentration, other.

REFERENCE DOCUMENTS:

- ASTM 4748-10, "Standard Test Method for Determining the Thickness of Bound Pavement Layers Using Short-Pulse Radar."
- AASHTO, "Standard Practice for Application of Ground Penetrating Radar (GPR) to Highways," Report No. R037-04-UL, 2009, pp. 12.
- Daniels, D.J., Surface Penetrating Radar, The Institution of Electrical Engineers, pp. 320, December 1996.
- Sebesta, S., Scullion, T., Saarenketo, T., "Using Infrared and High-Speed Ground-Penetrating Radar for Uniformity," Transportation Research Board (TRB), Strategic Highway Research Program (SHRP2) Renewal Research, Report No. S2-R06C-RR-1, pp. 80, 2013.
- Wenzlick, J.D., Scullion, T., Maser, K., "High Accuracy Pavement Thickness Measurement Using Ground Penetrating Radar (Nondestructive Testing for Quality Control of New Pavement)," MoDOT Report No. RDT 99-003, February 1999, pp. 104.
- Zhou, F., Scullion, T., "Guidelines for Evaluation of Existing Pavements for HMA Overlay," Report FHWA/TX-07/0-5123-2, May 2007, pp. 110.

TERMINOLOGY:

Antenna is a transmitting GPR antenna that converts an excitation in the form of a voltage pulse or wave train into EM waves. A receiving GPR antenna converts energy contained in EM waves into voltages, which are regarded as GPR data upon digital sampling of analog voltages, and storage of quantized values.

Bistatic Antenna is an antenna configuration that incorporates two antennas, where the first antenna radiates incident EM waves toward the ground and the second antenna receives the reflected waves.

Bandwidth is the operating frequency range of an antenna, typically the difference between the upper and lower 3-dB frequencies (i.e., upper and lower 3 dB frequencies relative to the antenna's resonant frequency).

Coupling between the GPR antenna and the ground is indicated by the efficiency of the antenna transmitting electromagnetic energy into the ground, where "good" coupling is indicated by efficient transmission of EM energy from the antenna into the ground within the antenna bandwidth and "poor" coupling is indicated by low efficiency transmission of EM energy from the antenna into the ground within the antenna bandwidth.

Depth of Penetration is the maximum depth range a radar signal can penetrate into a given material.

Attenuation is the loss of EM wave energy due to conduction currents.

Scattering is the change in direction of electromagnetic wave propagation that occurs at a change in material properties over a short distance compared to a wavelength for an interval comparable to or greater than a wavelength. Scattering includes reflection (reverse change in direction), refraction (forward change in direction), and diffraction (caused by rapid changes that are small compared to a wavelength in both occurrence and interval).

Time gain is the amplification applied to a trace as a function of time, where the function can be continuous or piecewise depending on data analysis requirements.

Transmit Pulse is the voltage impulse that excites the transmitting antenna.

Polarization (polarization vector) is the orientation of the direction of the vector electromagnetic field. Many GPR antennas are linearly polarized.

Conductivity is the ability of a material to support movement of electrons or ions due to an applied electrical field.

Diffusion is the movement of charges in response to an applied electric field or in response to an applied time-varying magnetic field. Diffusion is the low-frequency, high-loss, limiting behavior of electromagnetic wave propagation and is descriptive of behavior that decays rapidly (exponentially) with distance and time.

Dispersion is a material characteristic where wave velocity is no longer uniquely defined, giving rise to the distinction of phase velocity and group velocity. For example, elevated water content in dielectric civil engineering materials (such as concrete and asphalt) results in increased dispersion effects, where electromagnetic waves become increasingly spread out as a function of frequency.

Dielectric Permittivity is the property that describes the ability of a material to store electric energy by separating opposite polarity charges in space. It relates ability of a material to be polarized in response to the application of an electric field.

Relative Permittivity (relative dielectric permittivity; Dielectric Constant) is the ratio of the dielectric permittivity of a material to the permittivity of free space (or vacuum).

Magnetic Permeability (μ) is the property that describes the ability of a material to store magnetic energy by realignment of electron spin and motion. It relates ability of a material to be magnetized (magnetic polarization).

SUMMARY OF METHOD (background):

This test method provides the means for measuring pavement layer thicknesses of existing, new, or rehabilitated pavements. Furthermore, follow-up data processing could reveal potential defects and deterioration in pavement materials and structures.

As the electromagnetic wave generated by radar propagates through the pavement layers, the wave is attenuated, diffused, and dispersed within material layers and scattered (reflected, refracted, or diffracted) at layer interfaces. The maximum penetration depth depends (among other things): on the ground penetration radar system used (such as transmitted power, receiver sensitivity, center frequency and bandwidth) of the radar system, the electromagnetic properties of the pavement materials; and environmental factors (such as moisture content).

The detection of an interface between two different materials depends upon the partial reflection of incident energy at that interface. The amplitude of the reflected energy at that interface, with respect to the incident energy, is related to the relative dielectric constants of the two materials:

$$\frac{A}{A_0} = \frac{\sqrt{\epsilon_1} - \sqrt{\epsilon_2}}{\sqrt{\epsilon_1} + \sqrt{\epsilon_2}} \tag{1}$$

where:

A = the reflected energy, amplitude

A₀ = the incident energy, amplitude

ε₁ = the dielectric constant material 1, and

ε₂ = the dielectric constant material 2.

The ability to detect the thickness of a layer depends on the contrast between the dielectric constant of that layer and the layer beneath. Layer thickness can be determined using radar technology if the dielectric constant of that material and the two-way travel time for the radar wave to pass through the layer are known. The relationship is defined by the following equation:

$$T = \frac{\Delta t \times c}{2\sqrt{\epsilon_r}} \tag{2}$$

where:

T = layer thickness,

c = speed of light in air, 300 mm/nsec for T in mm (11.8 in/nsec for T in inches),

ε_r = relative dielectric constant of layer, and

Δ_t = two-way pulse travel time through layer (in nanoseconds).

The dielectric constant of a pavement material can vary within a typical range depending on aggregate types, asphalt cement sources, density, cracking, voids, foreign matter, moisture content, and other less common variables. Using an air-coupled horn antenna radar the real part of this

variation may be calculated directly from the radar data by using the known dielectric constant of air and equation (1).

Determining the dielectric constant when using ground coupled dipole antenna radar requires an independent means, such as coring, or a radar based dielectric constant measurement. Radar based dielectric constant measurements can be performed using multi-static antenna pairs positioned at two or more transmitter to receiver location offsets. Using this approach, material properties are subsequently analyzed with techniques such as the Common Midpoint (CMP) method.

APPARATUS:

The radar system for this application should have a resolution sufficient to determine a minimum layer thickness of 40 mm (1.5 in.) to an accuracy of 6.5 mm (0.25 in.). The apparatus consists of an antenna, radar transducer, and display. The radar transducer consists of a transmitter, receiver, and timing and control electronics. The display device includes a personal computer with a data acquisition board. The transducer generates, transmits, and receives broad band radio frequency (rf) signals through the antenna, that are then converted into an audio frequency signal for display and data interpretation. For HMA applications, an air-coupled horn antenna of ≥ 1.5 GHz center frequency is used with the manufacturer suggested distance above the pavement surface. Additional antennas of the same frequency or medium (900 MHz) to low (400 MHz) frequency may be incorporated into the radar system in a cross polarized configuration to evaluate pavement cracking phenomena. A medium to low frequency (≤ 1 GHz) ground coupled GPR in a sled configuration may be used to provide deep penetration. For concrete pavements medium to low frequency (≤ 1 GHz) ground coupled GPR in a sled configuration is used to provide deep penetration. The transmitter has a short-pulse (0.5 to 2.0 ns) rate compatible with United States/FCC restrictions. A wide band receiver is used for processing time signals corresponding to a depth of several feet. The data reduction process has the capability to provide pavement thickness within 7% of actual (as measured using reference pavement cores). The GPR system output includes *.kml format files that include geo-referenced position information.

PERIODIC CALIBRATION

The following GPR system calibrations should be performed at least once annually.

- Time Constant, C_T , Calibration: Perform time constant calibration and stability measurement procedures (such as noise-to-signal ratio, signal stability, and long-term signal stability tests) as described in Appendix A.
- Signal Calibration: Perform calibration and stability measurement procedures (such as signal-to-noise ratio, signal stability, long-term signal stability tests) as described in Appendix A.

TESTING PROCEDURE & DATA COLLECTION:

- Select GPR antenna frequency to penetrate expected depth of pavement structure. A GPR antenna with center frequency of ≥ 2 GHz and wide bandwidth will provide high resolution.

- Mount GPR antenna at manufacturer specified height and vehicle clearance.
- Electronic equipment should be turned on and allowed to warm up and stabilize before any testing is performed. Refer to manufacturer’s manual for the stabilization period.
- Set the GPR configuration to the maximum Pulse Repetition Frequency (PRF) available for the GPR equipment specified for the application. *Select this configuration to maximize the Ground Penetrating Radar (GPR) response waveform Signal to Noise Ratio (SNR).*
- Perform routine calibration described next.
- For flexible pavement surveys collect GPR data using a GPR system with an air coupled antenna (≥ 2 GHz center frequency horn antenna or equivalent) that has stable, calibrated signal characteristics. For rigid concrete pavements, collect GPR data using a high speed ground coupled GPR antenna configuration (ex: antenna sled). Lower frequency GPR antennas (< 2 GHz) may be selected to penetrate concrete materials or thick flexible pavement sections.
- Set GPR waveform sampling interval at ≤ 2 ft.
- Identify project location (mileposts) and spacing of radar scans using markers that can be observed in GPR data such as metal plates positioned on the pavement surface.

ROUTINE CALIBRATION

- Calibrate the data collection triggering device (ex: hub mounted Distance Measurement Instrument [DMI]). A DMI calibration is performed by accurately measuring a length of pavement, driving in a straight line along this path length and correlating the measured length with the corresponding number of DMI pulses recorded by the GPR along this path length. *(Accuracy of DMI measurements is improved for properly inflated and “warmed up” vehicle tires).*
- Calibrate Signal Characteristics. Collect initial metal plate reflection response:
 - i. Use a copper or aluminum plate (minimum 1.21 x 1.21 m - 4 ft. x 4 ft. dimensions) target placed flat on the ground.
 - ii. Collect a metal plate response from the GPR in a stationary configuration and while bouncing the vehicle suspension using an individual’s body weight.

DATA ANALYSIS:

The analysis should include the following steps:

- Perform manufacturer GPR data pre-processing analysis including:
 - a. Adjust zero time offset
 - b. Subtract average background response
 - c. Apply appropriate signal gain for material (linear, piecewise linear, exponential, etc.) to achieve signal processing and analysis objectives by equalizing dynamic range as a function of depth

- Evaluate pavement layer thicknesses based on manufacturer software and using estimated dielectric properties (material specific). Alternatively, use the “*Computation of Layer Relative Dielectric Constant*” technique for computing the layer relative dielectric constants.

- Identify initial set of homogeneous subsections in terms of pavement layer thickness based on initial GPR data and perform iterative alternatives of homogeneous subsections based on the observed statistical variability of the calculated pavement thicknesses. Compare statistical results at successive length scales to determine homogeneous subsections (where layers are consistently identified). Plot thickness results and compute thickness statistics (mean and standard deviation) for each pavement layer at homogeneous subsections. Produce summary plots for pavement layer thickness and layer thickness variability

- Use core data to refine the dielectric layer properties within homogeneous pavement subsections and recalculate the corresponding pavement thickness results.

- Identify areas of concern in error adjusted multi-scale analysis locations. Areas of concern include pavement subsections that may be too thin to meet MD SHA specifications or design requirements.

Computation of Layer Relative Dielectric Constant

System calibration involves a two-step process for GPR measurement quality control and quality assurance (QC/QA). First, the calibration time constant, C_T , is established for the radar system. Subsequently a material with known thickness and dielectric properties is evaluated to confirm accurate dielectric property evaluation based on the calibrated C_T value. C_T is determined by measuring the time interval between reflections from two spaced metal plates (Appendix A, Figure 1). Initially, the time delay between the two reflections from the pair of plates is monitored for stability during a period of two hours (consistent with signal calibration step 2 measurement requirements). The upper plate response time should be determined from this collected data. Next, the upper plate is removed to allow the lower plate response time to be measured alone (consistent with straight line measurement ray paths between the GPR antenna and each respective metal plate). Finally, the relative dielectric constant, ϵ_r , for a pavement layer of interest must be evaluated at a calibration location using equation 3 and compared with a known reference value for the dielectric constant (also using a known reference value for the material thickness in the calculation).

A comparison of the relative dielectric constant measurement at the calibration location with the known reference value of the relative dielectric constant assures the accuracy of the time constant C_T (allowing any significant discrepancy to be detected and corrected via a subsequent measurement as needed).

For subsequent applications of a GPR that meet requirements above, dielectric property variations that occur in civil engineering materials such as HMA pavement and concrete pavement can be evaluated using GPR based on procedures described in Appendix B. Estimates of the dielectric constant may also be used for given materials, depending on measurement accuracy and reliability requirements of the application. In the lack of core data, alternative methods of estimating the dielectric material constants may include: i) GPR testing using on site measurements combined with plate reflection values, or ii) GPR on site testing with the use of multiple antennas for higher accuracy.

As described above, the time interval in nanoseconds, Δ_t , between the surface reflection or top of the layer reflection and the corresponding reflection from the bottom of the known calibration layer of interest is measured. The relative dielectric constant of the known calibration layer is calculated using the following equation:

$$\epsilon_r = \left[\frac{\Delta t \times d_c}{2 \times T \times C_T} \right]^2 \tag{3}$$

where:

ϵ_r = relative dielectric constant of layer,

Δ_t = two-way pulse travel time through layer (in nanoseconds),

d_c = distance between metal plates,

T = Layer thickness (from a known calibration location or obtained from a core), and

C_T = calibration time constant (in nanoseconds).

Identify the signal reflections associated with the surface of the pavement or upper interface of the layer of interest and the lower surface interface of the layer, and determine the time interval, Δ_t , between these two. Calculate the thickness of the layer using the following equation:

$$T = \frac{\Delta t \times d_c}{2 \sqrt{\epsilon_r \times C_T}} \tag{4}$$

where:

T = measured layer thickness,

Δ_t = two-way pulse travel time through layer (in nanoseconds),

d_c = distance between metal plates,

ϵ_r = relative dielectric constant of layer, and

C_T = calibration time constant (in nanoseconds).

REPORT: Quality control/quality assurance results obtained for the C_T calibration value using the above procedure should be reported and evaluated based on comparison with known reference calibration values. If the measured value of the relative dielectric constant of the layer determined using C_T is within acceptable measurement tolerances at the known calibration location, measurement work with the GPR system may proceed.

A report should be provide analysis results in graphical and/or bar chart forms based on referenced analysis steps in Appendix B. Pavement layer thickness results can be reported versus mile post for analysis of overall variability. Statistical variability of pavement layer thickness within homogeneous pavement sections can be specifically reported using procedures in Appendix B.

APPENDIX A.

(from ASTM 4748 and SHRP2 Report S2-R06C-RR1)

TIME CONSTANT, C_T , CALIBRATION

The calibration of the time constant, C_T , is established by measuring the time interval between reflections from two metal plates spaced by a distance, d_c , of approximately 300 ± 5 mm (12 ± 0.2 in.) using four small non-conductive spacers, one attached to each corner of the metal plates, Figure 1. The upper plate is approximately 125 by 125mm (5 by 5 in.) and the lower plate is approximately 300 by 300 mm (12 by 12 in.). The time delay between the two reflections from the pair of plates by observing the received signal on the display device represents the time constant, C_T , in nanoseconds, Figure 2. C_T accuracy can be refined further using the following procedure modification: (a) collect a GPR waveform measurement corresponding to the upper metal plate, (b) remove the upper metal plate and nonconductive spacers from the measurement area, and (c) measure a GPR waveform corresponding to the lower metal plate alone. A modified procedure C_T value (with higher accuracy) is obtained by calculating the time difference between the peak response in waveform "c" and the peak response in waveform "a."

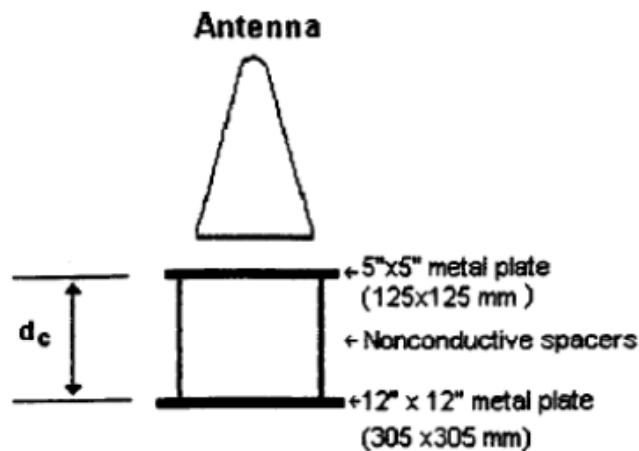


Figure 1. Time Constant, C_T , Calibration Setup (ASTM 4748)

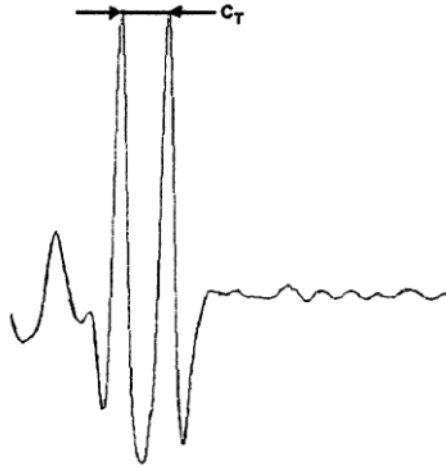


Figure 2. Time Constant, C_T , Measurement (ASTM 4748)

SIGNAL CALIBRATION

Perform the following calibration and signal stability measurements (SHRP2 Report S2-R06C-RR1)

These specifications are based largely on the GPR reflection from a large metal plate. The amplitude of reflection is measured in volts typically from the maximum positive peak to the preceding negative.

Performance Specifications

1. Noise-to-signal ratio test: The antenna will be positioned at its recommended operating height above a minimum 16 square foot (4 ft × 4 ft) metal plate. The radar unit shall be turned on and allowed to operate for a 15-min warm-up period. After warm-up, the unit shall be operated at maximum pulse rate, and 50 radar waveform pulses shall be recorded. The recorded waveforms shall then be evaluated for noise-to-signal ratio. *No averaging or signal cleanup such as sky wave removal (and reflection subtraction) shall be allowed.* The noise-to-signal ratio is described by the following equation:

$$\frac{\text{Noise Level } (A_n)}{\text{Signal Level } (A_{mp})} \leq 0.05 (5\%)$$

The signal level (A_{mp}) is defined as the average metal plate reflection in volts as measured from the peak to the preceding minimum. The noise level (A_n) is defined as the average maximum amplitude in volts occurring between 2 and 10 ns after the surface echo. The noise level is measured from any positive peak to either the preceding or the trailing negative, whichever is greater. The noise-to-signal ratio shall be less than or equal to 0.05 (5%).

2. Signal stability test: The same test configuration shall be used as described in the noise-to-signal ratio test. Fifty traces shall be recorded at the minimum data rate of 25 traces/s. The signal stability shall be evaluated using the following equation:

$$\frac{A_{\max} - A_{\min}}{A_{\text{AVC}}} \leq 0.01 (1\%)$$

where

- A_{\max} = maximum amplitude for all 50 traces,
- A_{\min} = minimum amplitude for all 50 traces, and
- A_{AVC} = average trace amplitude of all 50 traces.

The signal stability test results for the GPR shall be less than or equal to 1%.

3. Long-term signal stability: The same test configuration shall be used as described in the noise-to-signal ratio test. The radar shall be switched on with no warm-up and allowed to operate for 2 h continuously. As a minimum, a single waveform shall be captured every 2 min, 60 in total. The amplitude of reflection shall be calculated and plotted against time. For the system to perform adequately the amplitude should remain constant after a short warm-up period. The stability criterion is as follows:

$$\frac{A_{20\text{y}} - A_{20}}{A_{20}} \leq 0.03 (3\%)$$

where

- A_{20} = amplitude measured at 20 min and
- $A_{20\text{y}}$ = amplitude measured after 20 min.

4. Variations in time-calibration factor: The same test configuration shall be used as described in the noise-to-signal ratio test; 50 traces are collected and the height of the antenna is measured. The test is repeated at two other heights. Typically, heights of approximately 15, 20, and 25 in. are used. The time delay from the end reflection at the tip of the antenna to the metal plate reflection is measured for each trace, and their mean is time t_i (where the subscript represents height position at i). The difference between t_2 and t_1 represents the time to travel a fixed distance in air. For bistatic antennas the travel distance must be calculated based on the system geometry. The factor C_1 is calculated by dividing the distance by the time difference (inches per nanosecond). The factor C_2 represents

the same between heights 2 and 3. The variation in time-calibration factor is as shown below:

$$\frac{C_1 - C_2}{\text{Mean of } C_1 \text{ and } C_2} \leq 0.02 (2\%)$$

The variation in time-calibration factor shall be less than or equal to 2%.

5. End reflection test: The same test configuration and results from the noise-to-signal ratio test shall be used. The amplitude of the end reflection directly preceding the metal plate reflection shall be measured. The size of the end reflection shall be

$$\frac{A_E}{A_{mp}} < 0.15 (15\%)$$

where

A_E = amplitude of end reflection defined as any peak occurring from 1 to 5 ns before the metal plate reflection and

A_{mp} = mean of the amplitude of reflection from the metal plate.

The end reflection in the metal plate test shall be less than 15% of the amplitude of metal plate reflection.

6. Symmetry of metal plate reflection: The same test configuration as used in the signal-to-noise ratio test shall be used. Two different criteria have been established for symmetry, as described below:
 - 6.1 The first criterion is the time from the maximum negative peak following the surface reflection to the zero crossing point. The required specification is

$$t_f \leq 0.7 \text{ ns}$$

- 6.2 The second criterion is based on the symmetry of the "legs" of the metal plate reflection. The amplitude is measured from the positive peak to both the preceding and trailing negative. The required specification is

$$A_{min}/A_{max} > 0.95 (95\%)$$

where A_{min} and A_{max} are the minimum and maximum metal plate reflections measured using the preceding or trailing negatives. The ratio should be at least 95%.

7. Concrete penetration test: The antenna shall be placed at its recommended operating height above a 6-in.-thick concrete block. The concrete block shall be nonreinforced, a minimum age of 28 days, and a minimum 3,000 psi compressive strength. The block shall be 3 ft × 3 ft or greater to ensure that all the GPR energy enters the concrete. The concrete block shall be placed on top of a metal plate. Two hundred traces shall be recorded. The reflection amplitude from the top and bottom of the concrete block shall be measured. The concrete penetration test is defined by the following equation:

$$\frac{A_{bottom}}{A_{top}} \geq 0.25 (25\%)$$

where

A_{top} = mean of the measured return amplitude from the top of the concrete slab and

A_{bottom} = mean of the measured return amplitude from the metal plate.

The concrete penetration test results for the GPR shall be greater than or equal to 25%.

APPENDIX B.

EXAMPLE DATA ANALYSIS:

Step 1. Perform manufacturer recommended GPR data pre-processing steps such as the following:

- a. Adjust zero time offset (focus analysis on target data time window)
- b. Subtract average background response
- c. Apply appropriate signal gain for material (linear, piecewise linear, exponential, etc.) to achieve signal processing and analysis objectives by equalizing dynamic range as a function of depth

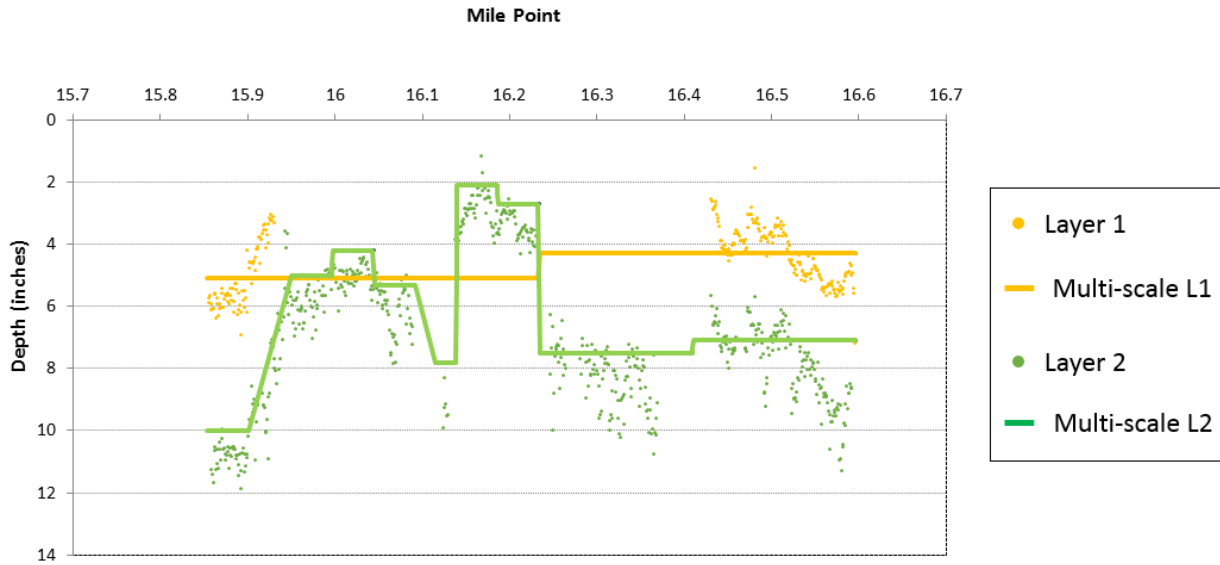
Step 2. Perform semi-automated GPR pavement layer processing in manufacturer software and initially evaluate pavement thickness based on estimated dielectric properties (material specific [Daniels, 1996]).

Step 3. Import initial GPR thickness data into MS Excel to perform multi-scale data analysis and statistical analysis procedures using an ADOJAM MS Excel Macro.

- a. Import pre-processed GPR thickness data into macro spreadsheet
 - i. Estimated pavement thickness information is imported layer by layer
 - ii. Measured pavement core layer thickness is entered manually
- b. Execute spreadsheet macro provided by ADOJAM to analyze layer features at multiple length scales (multi-scale data analysis)
 - i. Compare statistical results from large scales down to successively smaller length scales to determine homogeneous length scales of data subsections (where layers can be consistently identified, Figure 1). In Figures 2 and 3, homogeneous subsection statistics are highlighted in yellow when statistical thickness criteria have been met and are subsequently highlighted in green upon further subdivision.
 - ii. Multi-scale data analysis criteria (user adjustable to address specific needs) include:
 - i. Maximum difference between average pavement layer thickness of adjacent data subsections (layer by layer)
 - ii. Maximum difference between the standard deviation of pavement layer thickness of adjacent data subsections (layer by layer)
 - iii. After minimum length scale subdivisions have been reached, define a minimum standard deviation (or a complete lack of detected data features) within a data subsection to identify a subsection transition zone.

Step 4. Use results from Step 3 in an ADOJAM macro to produce results for decision making (example figures developed using MD SHA data)

- a. Use existing MD SHA plotting spreadsheet to plot thickness results
- b. Extract thickness statistics of each pavement layer at homogeneous length scales, determined in Step 3.b. (Figures 2 and 3, plus Table 1)
 - i. Mean
 - ii. Standard deviation
- c. Produce statistical summary for MD SHA analysis of
 - i. Pavement layer thickness (at homogenous length scales)
 - ii. Pavement layer thickness variability (at homogenous length scales)



MD 213 MP 15.87 to 16.61 MD 213 and MD 313A – Limits of Galena

Figure 1. Multi-scale data analysis showing homogeneous pavement subsections for pavement layer 1 and pavement layer 2 based on current MD SHA GPR pavement layer analysis.

AVG L1	AVG L2	AVG L1 Half	AVG L2 Half	AVG L1 Quart	AVG L2 Quart
4.54	6.1	4.3	7.3	END	7.1
STDEV L1	STDEV L2	5.1	5.2	END	7.5
0.99	2.3	STDEV L1 Half	STDEV L2 Half	#DIV/0!	3.5
		0.9	1.1	5.1	6.5
		1.0	2.6	STDEV L1 Quart	STDEV L2 QUART
				END	1.2
		AVG L1 H Dif	AVG L2 H Dif	END	0.9
		0.2	1.2	#DIV/0!	1.8
		0.5	0.9	1.0	2.5
		STDEV L1 H Dif	STDEV L2 H Dif		
		0.1	1.3	AVG L1 Q Dif	AVG L2 Q Dif
		0.5	0.3	END	0.2
				END	0.2
				#DIV/0!	1.6
				0.0	1.3
				STDEV L1 Q Dif	STDEV L2 Q Dif
				END	0.1
				END	0.2
				#DIV/0!	0.8
				0.0	0.2

Figure 2. Multi-scale analysis structure shown in ADOJAM MS Excel macro(zoom in view).

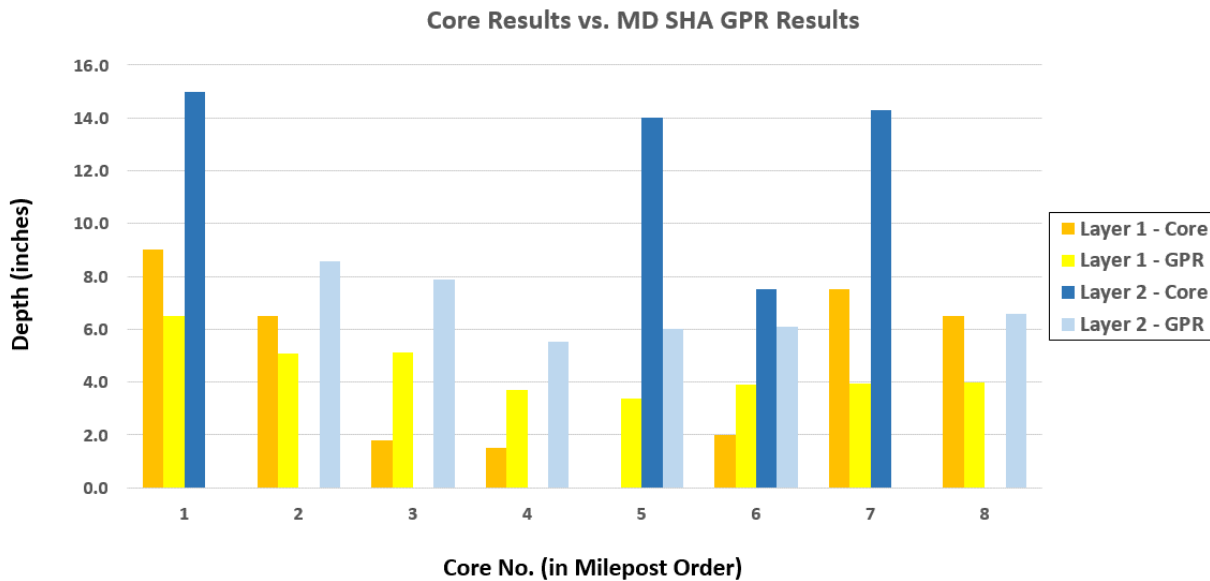
AVG L1	AVG L2	AVG L1 Hsif	AVG L2 Hsif	AVG L1 Quart	AVG L2 Quart	AVG L1 Oct	AVG L2 Oct	AVG L1 Sixt	AVG L2 Sixt
4.54	6.1	4.3	7.3	END	7.1	END	END	END	END
STDEV L1	STDEV L2	5.1	5.2	END	7.5	END	END	END	END
0.99	2.3	STDEV L1 Hsif	STDEV L2 Hsif	#DIV/0!	3.5	END	END	END	END
		0.9	1.1	5.1	6.5	END	END	END	END
		1.0	2.6	STDEV L1 Quart	STDEV L2 QUART	END	2.4	END	END
				END	1.2	END	5.6	END	END
		AVG L1 H Dif	AVG L2 H Dif	END	0.9	END	4.6	END	END
		0.2	1.2	#DIV/0!	1.8	END	8.6	END	END
		0.5	0.9	1.0	2.5	STDEV L1 Oct	STDEV L2 Oct	END	2.7
		STDEV L1 H Dif	STDEV L2 H Dif	AVG L1 Q Dif	AVG L2 Q Dif	END	END	END	2.1
		0.1	1.3	END	0.2	END	END	END	7.8
		0.5	0.3	END	0.2	END	END	END	5.3
				#DIV/0!	1.6	END	END	END	4.2
				0.0	1.3	END	0.6	END	5.0
				STDEV L1 Q Dif	STDEV L2 Q Dif	END	1.2	END	7.2
				END	0.1	END	0.7	END	10.0
				END	0.2	END	1.9	STDEV L1 Sixt	STDEV L2 Sixt
				#DIV/0!	0.8	AVG L1 O Dif	AVG L2 O Dif	END	END
				0.0	0.2	END	END	END	END
						END	END	END	END
						END	END	END	END
						END	1.2	END	END
						END	2.1	END	END
						END	1.3	END	0.4
						END	2.1	END	0.6
						STDEV L1 O Dif	STDEV L2 O Dif	END	1.7
						END	END	END	0.8
						END	END	END	0.5
						END	END	END	0.7
						END	END	END	1.7
						END	1.2	END	0.5
						END	0.5	AVG L1 \$ Dif	AVG L2 \$ Dif
						END	1.7	END	END
						END	0.5	END	END
								END	END
								END	END
								END	END
								END	END
								END	END
								END	END
								END	0.3
								END	0.3
								END	2.2
								END	0.3
								END	0.4
								END	0.4
								END	1.4
								END	1.4
						STDEV L1 \$ Dif	STDEV L2 \$ Dif	END	END
						END	END	END	END
						END	END	END	END
						END	END	END	END
						END	END	END	END
						END	END	END	END
						END	END	END	END
						END	END	END	0.1
						END	END	END	0.0
						END	END	END	0.4
						END	END	END	0.4
						END	END	END	0.2
						END	END	END	0.0
						END	END	END	0.2
						END	END	END	0.2
						END	END	END	1.5

Figure 3. Multi-scale analysis structure shown in ADOJAM MS Excel (zoom out view).

Milepost Range	Layer 1 Depth (in.)		Layer 2 Depth (in.)	
	Average	Std. Dev.	Average	Std. Dev.
15.85-15.90	5.1	1.0	10.0	0.5
15.90-15.95			Transition	Transition
15.95-16.00			5.0	0.7
16.00-16.04			4.2	0.5
16.04-16.09			5.3	0.8
16.09-16.11			Transition	Transition
16.11-16.14			7.8	0.7
16.14-16.19			2.1	1.7
16.19-16.23	4.3	0.9	2.7	0.5
16.23-16.41			7.5	0.9
16.41-16.6			7.1	1.2

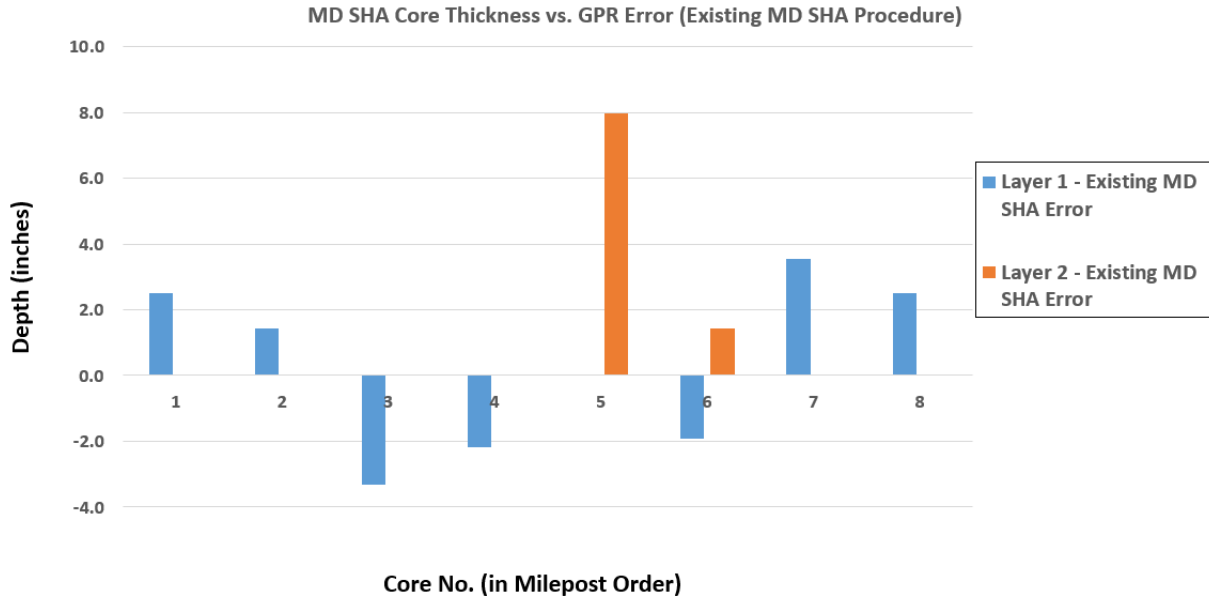
Table 1. Pavement thickness statistics at homogenous length scales.

Step 5. Using core data or alternative calibration information, refine dielectric property results and corresponding pavement thickness results. Refine final outputs accordingly (Figures 3, 4, 5 and 6 plus Table 2).



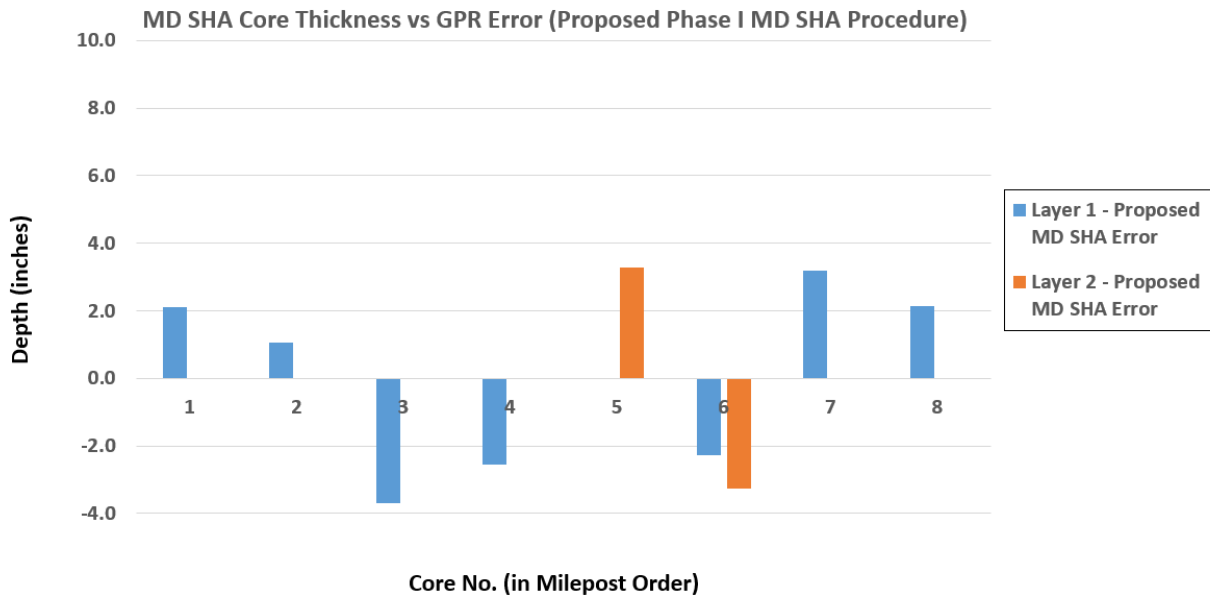
MD 213 MP 15.87 to 16.61 MD 213 and MD 313A – Limits of Galena

Figure 4. Pavement core thickness (layer 1 and layer 2) plotted together with MD SHA pavement GPR thickness (layer 1 and layer 2) determined using existing MD SHA analysis at pavement core locations.



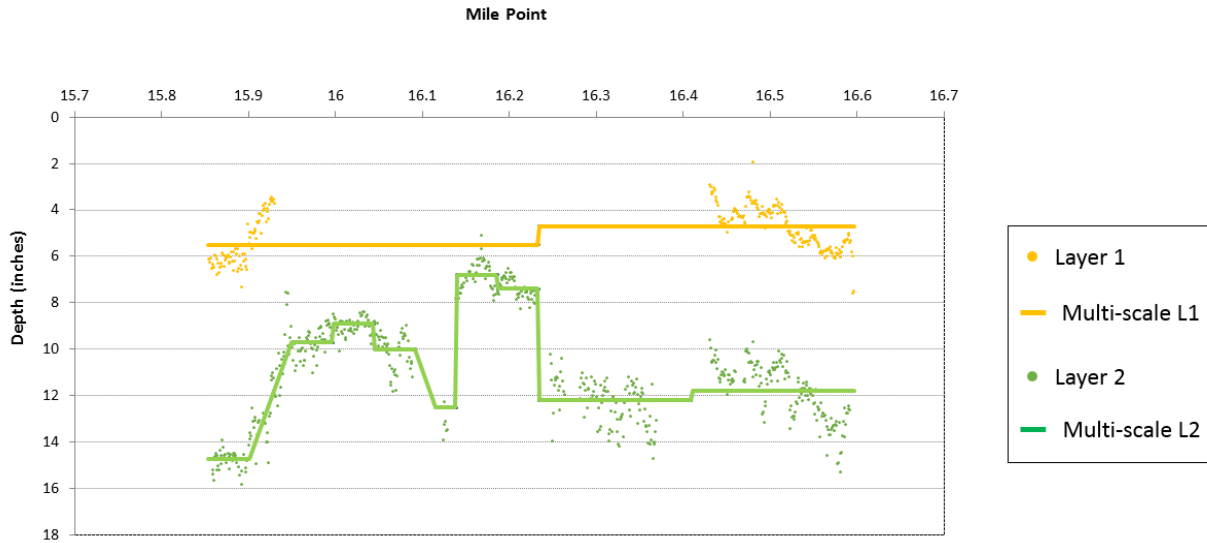
MD 213 MP 15.87 to 16.61 MD 213 and MD 313A – Limits of Galena

Figure 5. Present GPR thickness measurement error with respect to pavement core results based on existing MD SHA analysis procedure at eight core locations.



MD 213 MP 15.87 to 16.61 MD 213 and MD 313A – Limits of Galena

Figure 6. Residual errors after proposed analysis of GPR results and pavement core results (designed to minimize error).



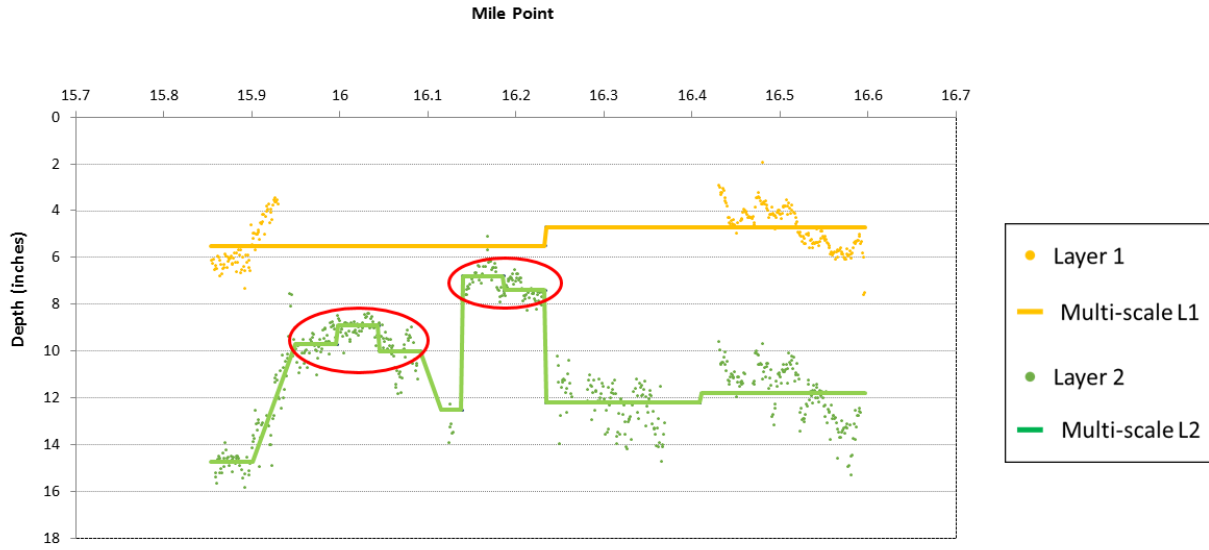
MD 213 MP 15.87 to 16.61 MD 213 and MD 313A – Limits of Galena

Figure 7. Multi-scale analysis adjusted based on proposed error analysis.

Milepost Range	Layer 1 Depth (in.)		Layer 2 Depth (in.)	
	Average	Std. Dev.	Average	Std. Dev.
15.85-15.90	5.5	1.0	14.7	0.5
15.90-15.95			Transition	Transition
15.95-16.00			9.7	0.7
16.00-16.04			8.9	0.5
16.04-16.09			10.0	0.8
16.09-16.11			Transition	Transition
16.11-16.14			12.5	0.7
16.14-16.19			6.8	1.7
16.19-16.23	7.4	0.5		
16.23-16.41	4.7	0.9	12.2	0.9
16.41-16.6			11.8	1.2

Table 2. Pavement thickness statistics at homogenous length scales (adjusted using error analysis).

Step 6. Automatically identify areas of concern in error adjusted multi-scale analysis locations. Areas of concern include pavement subsections that may be too thin to meet MD SHA specifications or design requirements (circled in red in Figure 7).



MD 213 MP 15.87 to 16.61 MD 213 and MD 313A – Limits of Galena

Figure 8. Layer 2 areas of concern circled in red.

APPENDIX C

MULTI-SCALE ANALYSIS MACRO ALGORITHM

For "Lyr" = 1 to # of pavement layer interfaces

Partition current "Lyr" thickness data equally into "part 1" and "part 2" per milepost location

Compute average "part 1" thickness, "L#P1a"

Compute average "part 2" thickness, "L#P2a"

Compute "part 1" thickness standard deviation, "L#P1sd"

Compute "part 2" thickness standard deviation, "L#P2sd"

If $ABS(L\#P1a - L\#P2a) < \text{Threshold average (user specified)}$

Store "L#P1a" and "L#P2a" values and EndIf

Else

Subdivide current "Lyr" # into equally into parts, "p1i," "p2i," "p3i," and "p4i"

Compute average "p1i" thickness, "L#P1ia"

Compute average "p2i" thickness, "L#P2ia"

Compute "p1isd" thickness standard deviation, "L#P1isd"

Compute "p2isd" thickness standard deviation, "L#P2isd"

If $ABS(L\#P1ia - L\#P2ia) < \text{Threshold average (user specified)}$

Store "L#P1ia" and "L#P2ia" values and EndIf

Else

Else subdivide current "Lyr" # subpart equally into four parts and evaluate subparts consistent with established pattern

EndIf

Compute average "p3i" thickness, "L#P3ia"

Compute average "p4i" thickness, "L#P4ia"

Compute "p3i" thickness standard deviation, "L#P3isd"

Compute "p4i" thickness standard deviation, "L#P4isd"

If $ABS(L\#P3ia - L\#P4ia) < \text{Threshold average (user specified)}$

Store "L#P3ia" and "L#P4ia" values and EndIf

Else

If $AVERAGE(p3isd, p4isd) > \text{Threshold st dev (user specified)}$ or null (and minimum subdivision length scale has been reached)

Categorize as "transition" area

Else

Subdivide current "Lyr" # subpart equally into eight parts, evaluate subparts consistent with established pattern until all segments have been categorized

EndIf

EndIf

Endif

Next

Approval:	Maryland Department of Transportation State Highway Administration Office of Materials Technology MARYLAND STANDARD METHOD OF TESTS	
Approved:	GPR FOR BRIDGE DECKS	MSMT xxx

SCOPE:

This procedure is used to determine the condition of concrete bridge decks. Specifically, this non-destructive evaluation method could identify defects related to concrete and rebar deterioration.

REFERENCE DOCUMENTS:

- ASTM D6087-08, "Evaluating Asphalt-Covered Concrete Bridge Decks Using Ground Penetrating Radar."
- ASTM D6432-11, "Standard Guide for Using the Surface Ground Penetrating Radar Method for Subsurface Investigation."
- AASHTO, "Standard Practice for Application of Ground Penetrating Radar (GPR) to Highways," Report No. R037-04-UL, 2009, pp. 12.
- ACI 228.2R-13 "Report on Nondestructive Test Methods for Concrete in Structures," American Concrete Institute, June 2013, pp. 53-61.
- Daniels, D.J., Surface Penetrating Radar, The Institution of Electrical Engineers, pp. 320, December 1996.
- Scott, M.L., Nondestructive Testing Handbook, 3rd Edition, Volume 5, Electromagnetic Testing, Chapter 17. Infrastructure Applications, Part 2. Applications of Ground Penetrating Radar to Bridge Decks, American Society of Nondestructive Testing, 2004, pp. 430-436.
- Scott, M., Rezaizadeh, A., Moore, M., "Phenomenology Study of HERMES Ground Penetrating Radar Technology for Detection and Identification of Common Bridge Deck Features," Report FHWA-RD-01-090, Federal Highway Administration, McLean, VA, 2001, pp 1-27.

TERMINOLOGY:

Antenna is a transmitting GPR antenna that converts an excitation in the form of a voltage pulse or wave train into EM waves. A receiving GPR antenna converts energy contained in EM waves into voltages, which are regarded as GPR data upon digital sampling of analog voltages, and storage of quantized values.

Bistatic Antenna is an antenna configuration that incorporates two antennas, where the first antenna radiates incident EM waves toward the ground and the second antenna receives the reflected waves.

Bandwidth is the operating frequency range of an antenna, typically the difference between the upper and lower 3-dB frequencies (i.e., upper and lower 3 dB frequencies relative to the antenna's resonant frequency).

Coupling between the GPR antenna and the ground is indicated by the efficiency of the antenna transmitting electromagnetic energy into the ground, where "good" coupling is indicated by efficient transmission of EM energy from the antenna into the ground within the antenna bandwidth and "poor" coupling is indicated by low efficiency transmission of EM energy from the antenna into the ground within the antenna bandwidth.

Depth of Penetration is the maximum depth range a radar signal can penetrate into a given material.

Attenuation is the loss of EM wave energy due to conduction currents.

Scattering is the change in direction of electromagnetic wave propagation that occurs at a change in material properties over a short distance compared to a wavelength for an interval comparable to or greater than a wavelength. Scattering includes reflection (reverse change in direction), refraction (forward change in direction), and diffraction (caused by rapid changes that are small compared to a wavelength in both occurrence and interval).

Time gain is the amplification applied to a trace as a function of time, where the function can be continuous or piecewise depending on data analysis requirements.

Transmit Pulse is the voltage impulse that excites the transmitting antenna.

Polarization (polarization vector) is the orientation of the direction of the vector electromagnetic field. Many GPR antennas are linearly polarized.

Conductivity is the ability of a material to support movement of electrons or ions due to an applied electrical field.

Diffusion is the movement of charges in response to an applied electric field or in response to an applied time-varying magnetic field. Diffusion is the low-frequency, high-loss, limiting behavior of electromagnetic wave propagation and is descriptive of behavior that decays rapidly (exponentially) with distance and time.

Dispersion is a material characteristic where wave velocity is no longer uniquely defined, giving rise to the distinction of phase velocity and group velocity. For example, elevated water content in dielectric civil engineering materials (such as concrete and asphalt) results in increased dispersion effects, where electromagnetic waves become increasingly spread out as a function of frequency.

Dielectric Permittivity is the property that describes the ability of a material to store electric energy by separating opposite polarity charges in space. It relates ability of a material to be polarized in response to the application of an electric field.

Relative Permittivity (relative dielectric permittivity; Dielectric Constant) is the ratio of the dielectric permittivity of a material to the permittivity of free space (or vacuum).

Magnetic Permeability (μ) is the property that describes the ability of a material to store magnetic energy by realignment of electron spin and motion. It relates ability of a material to be magnetized (magnetic polarization).

SUMMARY OF METHOD (background):

This test method provides the means for evaluating the condition of concrete bridge decks. Deterioration in concrete bridge decks may include the corrosion of the reinforcement or degradation of the concrete, or both. Corrosion of the steel reinforcement may lead to cracking and delamination (i.e., fracture plane) due to the larger volume steel reinforcement corrosion products occupy versus the steel alone, which creates pressure and subsequent cracking where stress exceeds material strength within the concrete. As the electromagnetic wave generated by radar propagates through the bridge deck materials, the wave is attenuated, diffused, dispersed within the materials, and scattered (reflected, refracted, or diffracted) at layer interfaces (HMA overlay and concrete). The maximum penetration depth depends (among other things): on the ground penetration radar system used (such as transmitted power, receiver sensitivity, center frequency and bandwidth) of the radar system, the electromagnetic properties of the pavement materials; and environmental factors (such as moisture content). Where a GPR with appropriate characteristics has been selected for an application greater penetration will result where dielectric material properties are relatively low, moisture content is minimal, and a small number of material interfaces are present.

For the case of an HMA overlay on top of a concrete bridge deck, the detection of the interface between the two different materials depends upon the partial reflection of incident energy at that interface. The amplitude of the reflected energy at that interface, with respect to the incident energy, is related to the relative dielectric constants of the two materials:

$$\frac{A}{A_0} = \frac{\sqrt{\epsilon_1} - \sqrt{\epsilon_2}}{\sqrt{\epsilon_1} + \sqrt{\epsilon_2}} \quad (1)$$

where:

A = the reflected energy, amplitude

A₀ = the incident energy, amplitude

ε₁ = the dielectric constant material 1, and

ε₂ = the dielectric constant material 2.

The ability to detect the overlay thickness of a layer depends on the contrast between the dielectric constant of the overlay and the concrete bridge deck beneath. Overlay thickness can be determined using radar technology if the dielectric constant of that material and the two-way travel time for the radar wave to pass through the layer are known. The relationship is defined by the following equation:

$$T = \frac{\Delta t \times c}{2\sqrt{\epsilon_r}} \tag{2}$$

where:

T = overlay thickness,

c = speed of light in air, 300 mm/nsec for T in mm (11.8 in/nsec for T in inches),

ϵ_r = relative dielectric constant of layer, and

Δt = two-way pulse travel time through layer (in nanoseconds).

The dielectric constant of a pavement material can vary within a typical range depending on aggregate types, asphalt cement sources, density, cracking, voids, foreign matter, moisture content, and other less common variables. Using an air-coupled horn antenna radar the real part of this variation may be calculated directly from the radar data by using the known dielectric constant of air and equation (1).

Determining the dielectric constant when using ground coupled dipole antenna radar requires an independent means, such as coring, or a radar based dielectric constant measurement. Radar based dielectric constant measurements can be performed using multi-static antenna pairs positioned at two or more transmitter to receiver location offsets. Using this approach, material properties are subsequently analyzed with techniques such as the Common Midpoint (CMP) method.

APPARATUS:

Two alternative GPR systems may be used for this evaluation:

- Air-coupled antennas with central frequencies 1 GHz and greater, with control unit able to transmit at a sufficient rate to collect 20 scans/m (25 scans/ft). The equipment may consist of

either an air-coupled, short-pulse monostatic or bistatic radar(s) with a monocycle pulse 150 mm (6 in.) free space resolution and a 50 scan/s minimum data rate.

- Ground-coupled antennas with central frequencies greater than 1 GHz with control unit able to transmit at a sufficient rate to collect 80 scans/m.

The data acquisition system should be able to gather radar data at the minimum rate of the radar system(s), 50 kHz for one radar, 100 kHz for two radars, and 150 kHz for three radars. The system shall be capable of accurately acquiring radar data with a 60-dB dynamic range. A distance measurement instrument (DMI) with accuracy of 6100 mm/km (66.5 in./mile) and a resolution of 25 mm (1 in.) should be used.

PERIODIC CALIBRATION

For air coupled systems perform calibration and stability measurement procedures (such as signal-to-noise ratio, signal stability, long-term signal stability tests) as described in Appendix A.

PRE-OPERATION MEASUREMENTS:

Free Space Signal (FSP): The equipment manufacturer may require the radar antenna to be mounted in an operational configuration, and 100 waveforms gathered in the absence of the material to be inspected. Use the average of 100 waveforms as a template for clutter removal.

Flat Metal Plate (FMP): Position the radar in an operation configuration, and gather 100 waveforms while illuminating a flat plate with dimensions recommended by the manufacturer. This is a measure of the emitted energy to be used in subsequent measurements, and as a template for correlation or background removal, or both.

DATA COLLECTION PROCEDURE:

Air-Coupled Systems:

- Make radar inspection passes in a longitudinal direction parallel to the centerline of the bridge deck with the antenna mounted to maintain a manufacturer-recommended distance from the bridge deck surface.
- Use a transverse distance (dt) between radar inspection passes <1 m (3 ft).
- Use a longitudinal distance (dl) between radar scans <150 mm (6 in).
- Determine the starting location for passes, that is, at abutments, joints, or a predetermined location.
- Determine the speed of operation for contiguous longitudinal coverage based on the radar range sweep rate and the manufacturer-recommended scan-spacing.

Ground-Coupled Systems:

- Make radar inspection passes either parallel or perpendicular to the direction of traffic, depending on the direction of the top layer of reinforcing. The pass direction should be chosen so that the antenna crosses over the top layer of reinforcing at an angle nearest to 90° .

DATA ANALYSIS:

Two different data processing methodologies are commonly used based on reflection amplitudes. The first method, the “attenuation technique,” calculates deterioration based on the relative reflection amplitudes from the bridge deck bottom relative to the bridge deck surface. The second method, the “top reinforcing reflection technique,” utilizes the relative reflection amplitudes from the top layer of reinforcing to assess deterioration.

Deterioration Measurements at Top Reinforcing Steel—Attenuation Technique:

- Measure and record the applied signal strength, V_t , at the deck surface.
- Measure and record the maximum signal strength of the deck bottom echo, V_{bs} .

- If V_{bs} is $< 0.0264 V_t$ after repeating the longitudinal radar inspection pass, the data are not reliable for determining removal quantities of bridge deck concrete. Processing of the data will require an alternative technique (such as the one used by the Ontario Ministry of Transportation).
- Measure and record the amplitude of the deck bottom echo, V_b , for each waveform.
- Determine delamination at the top reinforcing steel using the attenuation technique as follows:
 - o Consider the concrete delaminated if: $V_b \leq 0.385 V_{bs}$
 where: V_b = bottom echo amplitude, each scan; V_{bs} = bottom echo maximum amplitude, all scans; and 0.385 = a constant derived from research data.
 - o Calculate the percent delaminated at the top steel in each radar inspection pass using the following:

$$X_{tn} = [(W_{dt}) / (W_{dt} + W_{st})] [100] \quad (3)$$

where: X_{tn} = percent delaminated in a radar inspection pass n , at top steel; n = radar inspection pass identification number; W_{dt} = concrete delaminated at top steel, m; and, W_{st} = sound concrete at top steel, m.

- o Calculate the estimated quantity of deck delaminated at top steel for each radar inspection pass using the following:

$$Q_t = (X_{tn}) (L_n) (d_t) \quad (4)$$

where: Q_t = square meters (feet) of deck delaminated at top steel; L_n = length of radar inspection pass, n , m; and d_t = transverse distance between radar inspection passes, m.

- o Calculate the total estimated quantity of deck delaminated at top steel using the following:

$$Q_{Tt} = \sum Q_t \quad (5)$$

where: Q_{Tt} = total square meters (feet) of deck delaminated at top steel for all radar inspection passes.

Deterioration Measurements at or above Top Reinforcing Steel—Top Reinforcing Reflection

Technique:

- Extract the reflection amplitudes from the top layer of reinforcing.

Air-Coupled System:

Data collected with the air-coupled system should be obtained with two antennas (a transmitter and receiver pair) positioned in-line with the longitudinal direction and radiating with a polarization orientation perpendicular to the transverse reinforcing steel direction. The first step in data processing involves clutter removal by normalizing the reflection amplitudes of the metal plate reflections to the asphalt reflection (when HMA overlay exist), then subtracting the free space (FSP) scan from each data scan starting at the mid-point of the asphalt surface reflection. This method may not be reliable for bridge decks containing longitudinal rebar on top of transverse rebar with on-center spacing less than 20 cm (8 in.). For this situation, ground-coupled antenna data should be collected in the direction transverse to traffic flow in addition to longitudinal ground-coupled data, data should be collected and evaluated using the “attenuation technique” or cross-polarized GPR antenna methods may be implemented.

If the orientation of the top layer of reinforcing is not skewed at close to 45° relative to the direction of traffic: (a) normalize the asphalt reflection amplitude of the antenna polarized parallel to the top layer of reinforcing relative to (b) the same reflection amplitude in the other antenna and subtract (b) from (a) for each data scan. This is done to isolate the reflection from the top layer of reinforcing from the asphalt bottom reflection. For top layer of reinforcing angles near 45°, no subtraction should be performed. However, for this case, if the reinforcing reflection amplitudes cannot visually

be differentiated from the asphalt bottom reflection, this method may not be reliable and the data should be analyzed using the “attenuation technique” or ground-coupled antenna data should be collected.

Record the highest amplitude reflections from the top layer of reinforcing in the data from the antenna polarized most nearly perpendicular to the top reinforcing steel orientation.

Ground-Coupled System:

Focus and image the reinforcing reflections using a migration algorithm or an alternative method such as wave field back-propagation to determine their precise locations. Record the corresponding waveform reflection amplitudes from the GPR scan most nearly centered over each reinforcing steel member detected in the data.

Calculate Deterioration Threshold.

- Convert the reflection amplitudes to decibels.

$$A_{db} = 20 \log_{10} (A) \tag{6}$$

where: A_{db} = reflection amplitude in decibels; and A = reinforcing reflection amplitude in data units. The amplitudes of the reinforcing reflections along each pass provide a gradational scale. The lower the reflection amplitude, the higher the likelihood of deterioration. The spatial location of scans containing reflection amplitude less than 6 to 8 dB below the maximum reflection amplitudes recorded typically correspond to deterioration detected using other information, such as (1) bridge deck bottom inspection results, (2) core data when possible, and (3) results from other deterioration assessment techniques to refine the threshold value.

- Create a contour map of the reflection amplitudes versus spatial location on the bridge deck. Locations of deteriorated areas correspond to reflection amplitudes less than the threshold value.

- Calculate the percent deterioration at or above the top steel in each radar inspection pass using the following:

$$X_{tn} = [[W_{dt}]/(W_{dt} + W_{st})] [100] \quad (7)$$

where: X_{tn} = percent deteriorated in a radar inspection pass, n , at or above top steel; n = radar inspection pass identification number; W_{dt} = concrete deteriorated at or above top steel, m, obtained from reflection amplitudes below deterioration threshold value; and W_{st} = sound concrete at top steel, m, obtained from reflection amplitudes above the deterioration threshold value.

- Estimate the quantity of deck deteriorated at or above the top reinforcing using equations 4 and 5.

REPORT:

Report should provide bridge identification and location, survey date and weather conditions, deck status relative to moisture and debris, and any unusual conditions or circumstances. In terms of radar results, the report should include:

- Percent of bridge deck area delaminated, otherwise distressed, or defective for each radar pass, at top steel, in tabular form;
- Bridge deck area, in square meters (feet) delaminated, otherwise distressed, or defective for each radar pass, at top steel, in tabular form;
- Total bridge deck area, in square meters (feet), delaminated, otherwise distresses, or defective for the bridge deck, at top steel, in tabular form;
- Plan view map of bridge deck, depicting radar inspection pass versus longitudinal distance and showing location and extent of detected delamination, other distress, or defects at top steel; and,
- Plan view map of cover depth corresponding to the top layer of bridge deck reinforcing steel.

APPENDIX A.
(per ASTM D6087)

SYSTEM PERFORMANCE COMPLIANCE

1. Signal-to-Noise Ratio Test: Position the antenna at its far field distance approximately equal to maximum dimension of antenna aperture above a square metal plate with a width of 4 times the antenna aperture, minimum. Turn on the radar unit and allow to operate for a 20-min warm-up period or the time. After warming up the unit, record 100 waveforms. Then evaluate the recorded waveform for signal-to-noise ratio. The signal-to-noise ratio is described by the following equation:

$$[\text{Signal Level (} A_{mp} \text{) / Noise Level (} A_n \text{)}] > 20 \text{ (26.0 dB)}$$

This will be performed on each of the 100 waveforms and the average signal-to-noise value of the 100 waveforms will be taken as the “signal-to-noise of the system.” Noise voltage (A_n) is defined as the maximum amplitude occurring between metal plate reflection and region up to 50 % of the time window after the metal plate reflection, normally used with the antenna (that is, 1.0 GHz/20 ns: 10 ns.). The signal level (A_{mp}) is defined as the amplitude of the echo from the metal plate. 6.2.1.3 The signal-to-noise ratio test results for the GPR unit should be greater than or equal to 20 (+26.0 dB).

2. Signal Stability Test: Use the same test configuration as described in the signal-to-noise ratio test. Record 100 traces at the maximum data acquisition rate. Evaluate the signal stability using the following equation:

$$[A_{max} - A_{min} / A_{avg}] \leq 0.01 \text{ (1\%)}$$

where:

A_{max} = the maximum amplitude of the metal plate reflection for all 100 traces,

A_{min} = the minimum amplitude of the metal plate reflection for all 100 traces, and

A_{avg} = the average trace amplitude of all 100 traces.

The signal stability test results for the GPR system should be less than or equal to 1 %.

3. Variations in Time Calibration Factor: Use the same test configuration as described in the signal-to-noise ratio test, except that the metal plate can be replaced by any reflecting object. Collect a single waveform and measure the distance from the antenna to the reflector. Perform this test at three different distances corresponding to approximately 15, 30, and 50 % of the time window normally used with the system. The time delay between the echo from the aperture of the transmitting antenna and that from the reflecting object is measured as time t_1 (where subscript 1 represents position 1, and so forth). The difference between t_2 and t_1 and between t_3 and t_2 represents the travel time for a fixed distance in air. The factor C_i represents the speed between distance i and $i+1$. The allowable variation in measured speed is shown as follows:

$$[C_1 - C_2 / \text{Mean of } C_1 \text{ and } C_2] \leq 0.02 \text{ (2\%)}$$

where:

$$C_1 = \text{distance from Position 2 to Position 1} / t_1$$

$$C_2 = \text{distance from position 3 to Position 2} / t_2$$

The variation in time calibration factor should be less than 2 %.

4. Long-Term Amplitude Variation: Use the same test configuration as described in the signal-to-noise ratio test. Switch on the radar and allow to operate for 2 h continuously. As a minimum, capture a single waveform every 1 min, 120 total. Calculate the amplitude of a metal plate reflection and plot against time for each waveform. For the system to perform adequately, the amplitude of reflection should remain constant after a short warm-up period. The stability criteria is as follows:

$$[A_{\text{max}} - A_{20} / A_{20}] \leq 0.03 \text{ (3\%)}$$

A_{max} = the largest amplitude measured between 20 min and 120 min.

A_{20} = the amplitude measured after 20 min.

APPENDIX B
TRAINING MODULES

Training Module

Ground Penetrating Radar (GPR) for Pavement Structures

- **Summary Method (background)**

Electromagnetic (EM) wave through pavement material layers & interfaces

- Attenuated;
- Diffused;
- Dispersed;
- Reflected and/or Scattered.

Amplitude of reflected to incident energy at Interface:

$$\frac{A}{A_0} = \frac{\sqrt{\epsilon_1} - \sqrt{\epsilon_2}}{\sqrt{\epsilon_1} + \sqrt{\epsilon_2}}$$

A = the reflected energy, amplitude

A₀ = the incident energy, amplitude

ε₁ = the dielectric constant material 1

ε₂ = the dielectric constant material 2.

- **Summary Method (background)**

Maximum penetration depth depends (among other) on:

- GPR system (transmitted power, receiver sensitivity, center frequency & bandwidth);
- Electromagnetic properties of pavement materials;
- Environmental factors (such as moisture content).

Layer Thickness (T):

$$T = \frac{\Delta t \times c}{2\sqrt{\epsilon_r}}$$

c = speed of light in air, 300 mm/nsec for T in mm (11.8 in/nsec for T in inches)

ϵ_r = relative dielectric constant of layer

Δt = two-way pulse travel time through layer (in nanoseconds).

- **Summary Method (background)**

Evaluation of dielectric constant of pavement materials

- **Air-coupled** horn antenna
- Dielectric constant of **air**

Amplitude of reflected to incident energy at Interface:

$$\frac{A}{A_0} = \frac{\sqrt{\epsilon_1} - \sqrt{\epsilon_2}}{\sqrt{\epsilon_1} + \sqrt{\epsilon_2}}$$

A = the reflected energy, amplitude

A_0 = the incident energy, amplitude

ϵ_1 = the dielectric constant of **air**

ϵ_2 = the dielectric constant of the pavement material

- **Summary Method (background)**

Evaluation of dielectric constant of pavement materials

- **Ground - coupled dipole** antenna using hyperbola fit to point-like objects
- **Air – coupled antenna** using metal plate calibration
- **Coring**
or
- Dielectric constant measurements with **multi-static antenna pairs** positioned at two or more transmitter to receiver location offsets.
- Material properties analyzed with **Common Midpoint (CMP)** method technique.

- **Apparatus**

- Resolution sufficient to determine a minimum layer thickness of 40 mm (1.5 in.)
- Accuracy of 6.5 mm (0.25 in.) or better using calibrated techniques at shallow depths (< 2 ft.)
- GPR consists of antenna, radar transducer (transmitter, receiver, timing and control electronics). Display device (PC, DAQ).
- Transducer generates, transmits, and receives broad band radio frequency (rf) signals through antenna, that are then converted into an audio frequency signal for display and data interpretation.

- **Apparatus**

HMA applications

- Air-coupled horn antenna of ≥ 1.5 GHz center frequency.
- Additional antennas of same frequency or paired medium (900 MHz) to low (400 MHz) frequency in a cross polarized configuration to evaluate pavement cracking phenomena.
- Ground coupled GPR medium to low frequency (≤ 1 GHz) in a sled configuration for deep penetration.

Concrete Pavements

- Ground coupled GPR medium to low frequency (≤ 1 GHz) in a sled configuration FOR deep penetration (addressing concrete attenuation).

- **Apparatus**

- Data reduction process with capability to provide pavement thickness within 7% of actual (reference cores).
- GPR system output includes *.kml format that include geo-referenced position.

- **Periodic Calibration**

- GPR system calibrations ([Appendix A](#))
 - Annually
- Time Constant, C_T , Calibration
- Signal Calibration/ Stability
 - Noise-to-signal ratio
 - Signal stability
 - Long-term signal stability
 - Variations in time-calibration factor
 - End reflection test
 - Symmetry of metal plate reflection
 - Concrete penetration test

- **Testing Procedure & Data Collection**

- Allow GPR equipment to warm up and stabilize
- Perform routine calibration
- Set GPR waveform sampling interval at ≤ 2 ft.
- Flexible pavements: air coupled antenna (≥ 2 GHz center frequency horn antenna or equivalent)
- Concrete pavements: high speed ground coupled GPR antenna configuration (ex: antenna sled).
- Lower frequency GPR antennas (< 2 GHz) selected to penetrate concrete materials or thick flexible pavement sections.
- Identify project location and spacing of radar scans on pavement surface.

- **Routine Calibration**

- Distance Measurement Instrument [DMI] Calibration along length of measured distance in pavement.
- Calibrate Signal Characteristics with metal plate reflection response:
 - Use a copper or aluminum plate (minimum 4 ft. x 4 ft. dimensions) target placed flat on the ground.
 - Collect metal plate response from the GPR in a stationary configuration and while bouncing the vehicle suspension.

- **Data Analysis**

- Manufacturer GPR data pre-processing analysis:
 - Adjust zero time offset
 - Subtract average background response
 - Apply appropriate signal gain for material (linear, piecewise linear, exponential, etc.) to achieve signal processing and analysis objectives by equalizing dynamic range as a function of depth
- Evaluate pavement layer thicknesses using estimated dielectric properties
 - or
- Use “Computation of Layer Relative Dielectric Constant” technique

- **Data Analysis**

- Identify initial set of homogeneous subsections in terms of pavement layer thickness based on initial GPR data
- Perform iterative alternatives of homogeneous subsections based on the observed statistical variability of the calculated pavement thicknesses.
- Compare statistical results at successive length scales to determine homogeneous subsections (where layers are consistently identified).

- **Data Analysis**

- Plot thickness results and compute thickness statistics (mean and standard deviation) for each pavement layer at homogeneous subsections.
- Produce summary plots for pavement layer thickness and layer thickness variability
- Use core data to refine the dielectric layer properties within homogeneous pavement subsections and recalculate the corresponding pavement thickness results.
- Identify areas of concern in error adjusted multi-scale analysis locations.
- Areas of concern include pavement subsections that may be too thin to meet MD SHA specifications or design requirements.

Computation of Layer Relative Dielectric Constant

- Two-step process for system calibration:
 - Step 1: Calibration of time constant, C_T , using time delay between reflections from two spaced metal plates (Appendix A, Figure 1)
 - Step 2. Compare measured relative dielectric constant with known material reference value and layer thickness to assess accuracy of the time constant C_T .

Computation of Layer Relative Dielectric Constant

- Two-step process for system calibration:
 - Step 1: Calibration of time constant, C_T , using time delay between reflections from two spaced metal plates (Appendix A, Figure 1)
 - The time delay between the two reflections from the pair of plates is monitored for stability during a period of two hours (signal calibration requirements).
 - Determine upper plate response time.
 - Remove upper plate to allow the lower plate response time to be measured (straight line measurement ray paths between the GPR antenna and each respective metal plate).

Computation of Layer Relative Dielectric Constant

- Evaluate relative dielectric constant, ϵ_r , of the pavement layer (layer thickness needed as well).

$$\epsilon_r = \left[\frac{\Delta t \times d_c}{2 \times T \times C_T} \right]^2$$

ϵ_r = relative dielectric constant of layer,
 Δt = two-way pulse travel time through layer (ns),
 d_c = distance between metal plates,
 T = Layer thickness (from a known calibration location or core), and
 C_T = calibration time constant (ns).

- Step 2. Compare measured relative dielectric constant with known reference value to assess accuracy of the time constant C_T .

Computation of Layer Relative Dielectric Constant

- Identify signal reflections of surface pavement or upper interface of the layer of interest and the lower surface interface of the layer, and determine the time interval, Δt .
- Calculate the layer thickness:

$$T = \frac{\Delta t \times d_c}{2\sqrt{\epsilon_r \times C_T}}$$

T = measured layer thickness
 ϵ_r = relative dielectric constant of layer,
 Δt = two-way pulse travel time through layer (ns),
 d_c = distance between metal plates,
 C_T = calibration time constant (ns).

Computation of Layer Relative Dielectric Constant

- Alternative methods of estimating the dielectric material constants (lack of core data)
- GPR testing using on site measurements combined with plate reflection values;
- GPR on site testing with the use of multiple antennas for higher accuracy.

Draft MSMT

on

Ground Penetrating Radar (GPR) for Pavement Structures

Appendix: Periodic Calibration

- Time Constant, C_2 Calibration
- Noise-to-signal ratio
- Signal Stability
- Long Term Signal Stability
- Variations in time-calibration factor
- End Reflection test
- Symmetry of Metal Plate Reflection
- Concrete Penetration test

APPENDIX	STATE OF MICHIGAN DEPARTMENT OF TRANSPORTATION DIVISION OF HIGHWAY CONSTRUCTION CONSTRUCTION DIVISION
APPENDIX	GPR FOR PAVEMENT STRUCTURES

10/2010
This manual is used to determine the thickness of pavement layers using ground penetrating radar. This manual is for use in conjunction with the Michigan Manual of Standard Specifications and is intended to be used in conjunction with the Michigan Manual of Standard Specifications.

REFERENCES

- 10/2010, Standard Test Method for Determining the Thickness of Road Pavement Layers Using Ground Penetrating Radar.
- 10/2010, Standard Practice for Application of Ground Penetrating Radar (GPR) to Highway Pavement. MS-10-01, 2010, pp. 10.
- Smith, D. L. Ground Penetrating Radar. The International Geophysical Engineers, pp. 100. Denver, CO, 1988.
- Smith, D. L., and T. T. Geyer, Jr., "Using Infrared and High-Speed Ground Penetrating Radar for Pavement Thickness Measurements." Transportation Research Board, TRB, Special Highway Research Program (SHRP) Report of Research Report No. 32-ND-DR-10, pp. 80, 1992.
- Wentzell, J. D., Smith, T. T., and Geyer, Jr., "High Accuracy Pavement Thickness Measurements Using Ground Penetrating Radar." International Training for Quality Control of New Pavement, 1/14/07 Report No. 107-10-023, February 2008, pp. 101.
- Shaw, P., and T. T. "Guidelines for Evaluation of Existing Pavements for MSMT Quality." Report No. 107-10-023, May 2007, pp. 102.

TERMINOLOGY

Ground penetrating radar (GPR) is a non-destructive method for the determination of pavement layer thickness. The GPR system consists of a transmitter and receiver antenna that are buried in the pavement surface. The transmitter antenna sends out a pulse of radio waves that travel through the pavement and are reflected back to the receiver antenna. The time it takes for the pulse to travel through the pavement and be reflected back to the receiver antenna is used to determine the thickness of the pavement layer.

Improved GPR Data Analysis Techniques for Pavement Structures

Current Practice in Identifying Pavement Layer Thickness Analysis

- (i) Design pavement layer information often assumed to be homogeneous throughout a roadway section;
- (ii) Need pavement cores at selected locations to identify pavement layer thicknesses & calibrate GPR response;
- (iii) Neglecting variability dispersion in pavement thickness evaluation within a pavement section may lead to incorrect decisions in PMS rehabilitation strategies

Multi-scale Pavement GPR data Analysis (MPGA)

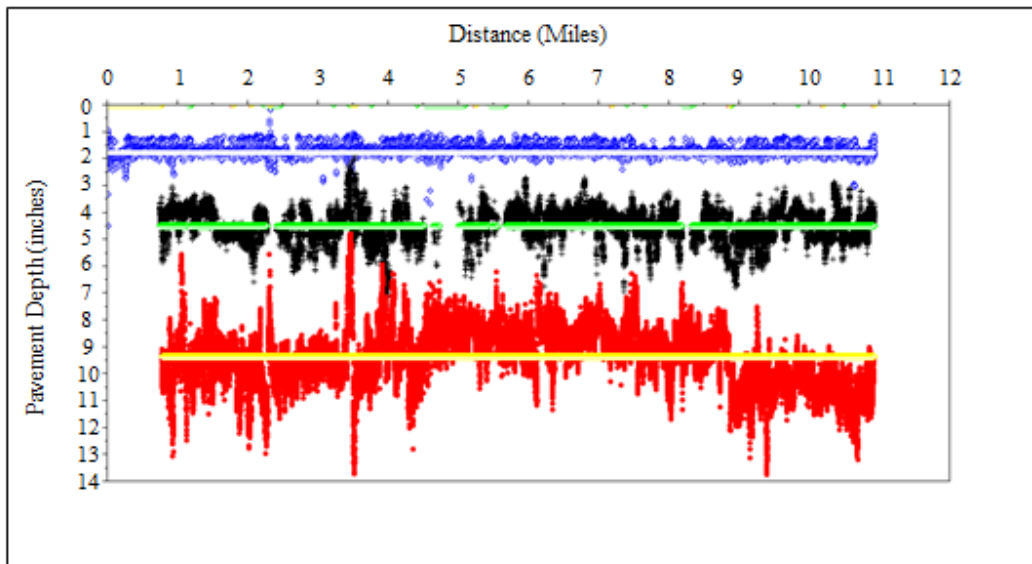
- Improve accuracy of pavement layer thickness data for PMS analysis;
- Improve GPR data analysis in relation to manufacturer recommended procedures;
- Identify reliably homogeneous pavement sections in terms of layer thicknesses;
- Use of default or adjustable user based selection criteria on the level of acceptable thickness variability within a pavement section.

Examples

of

Multi-scale Pavement GPR data Analysis (MPGA)

Figure 1. US15 – HMA Pavement
Data With Global Means (3 Layers)



Multi-scale Pavement GPR data Analysis (MPGA)

Adjustable user based selection criteria on the level of acceptable thickness variability within a pavement section (manual or using scilab script):

- Consecutive segmentation of pavement sections criteria

For a given segment within a data section

- If $\text{MeanDif} > 0.3$ inch & $\text{StDevDif} > 0.1$ inch
then subdivide segment
- else join with adjacent segment and unify adjacent segment statistics

Note:

$\text{MeanDif} = \text{abs}(\text{Segment_Mean} - \text{Global_Mean})$

$\text{StDevDif} = \text{abs}(\text{Segment_St_Dev} - \text{Global_St_Dev})$

Figure 2. US15 – HMA Pavement
Data With MPGA Results (3 Layers)

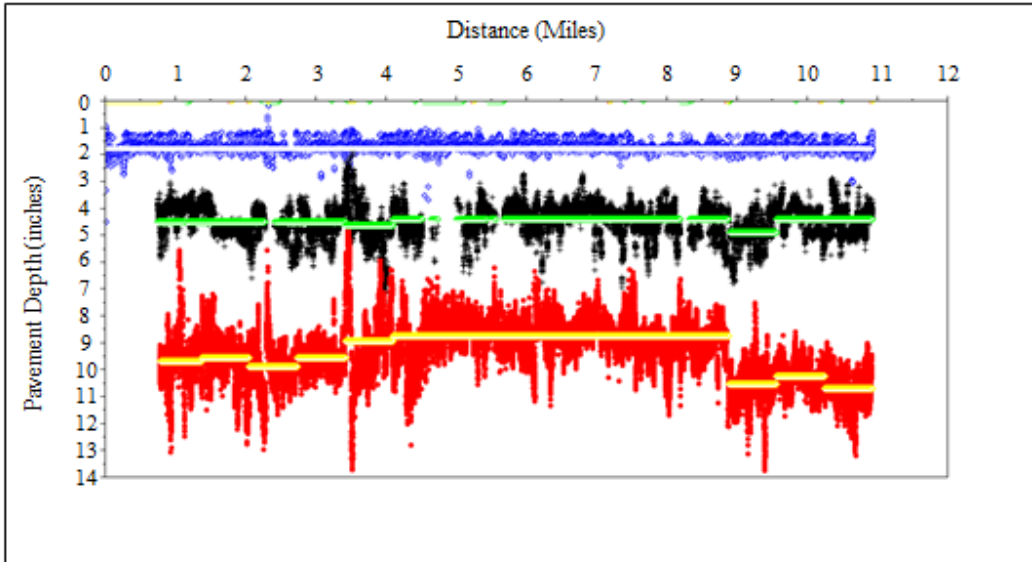


Figure 3. US15 – HMA Pavement
Layer 1 Data With Eight Subdivided Means

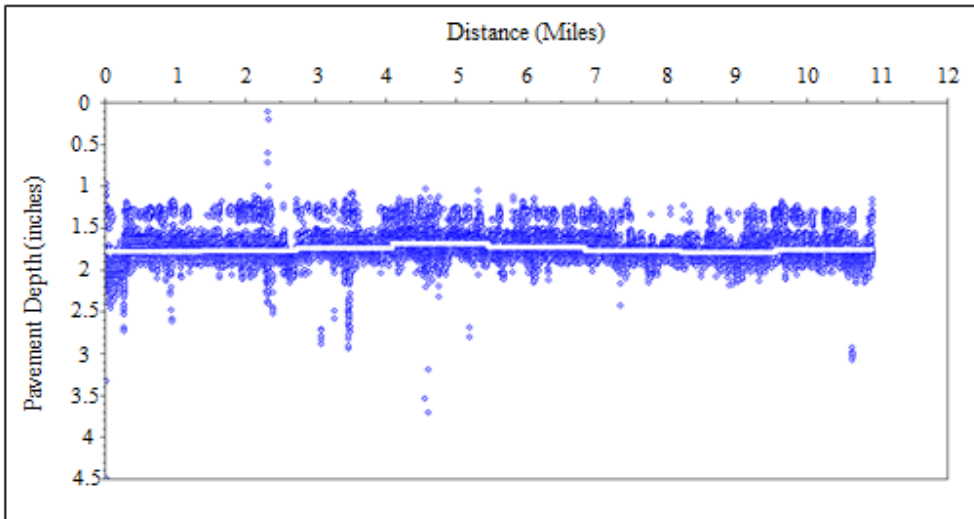


Figure 4. US15 – HMA Pavement
Layer 1 Data With MPGA Applied (Using Eight Subdivisions)

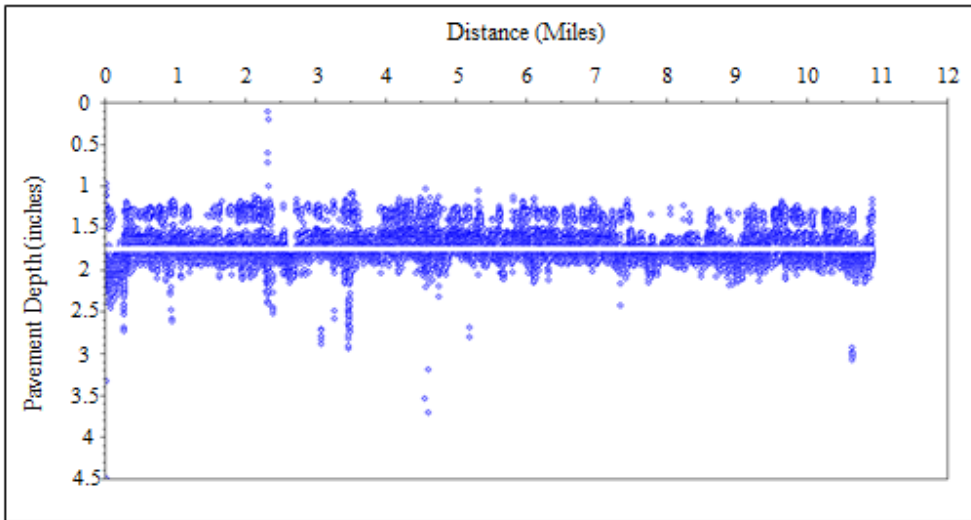


Figure 5. US15 – HMA Pavement
Layer 2 Data With Eight Subdivided Means

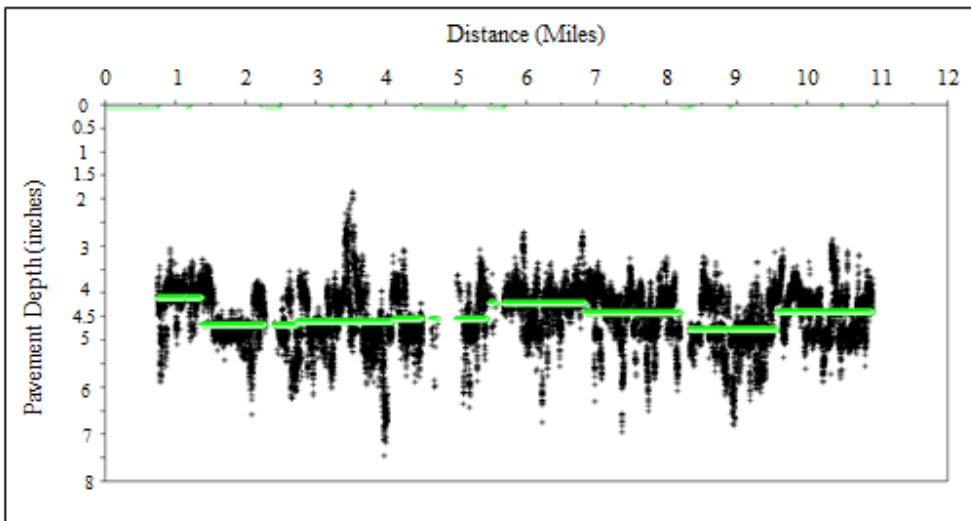


Figure 6. US15 – HMA Pavement
Layer 2 Data With MPGA Applied (Using Eight Subdivisions)

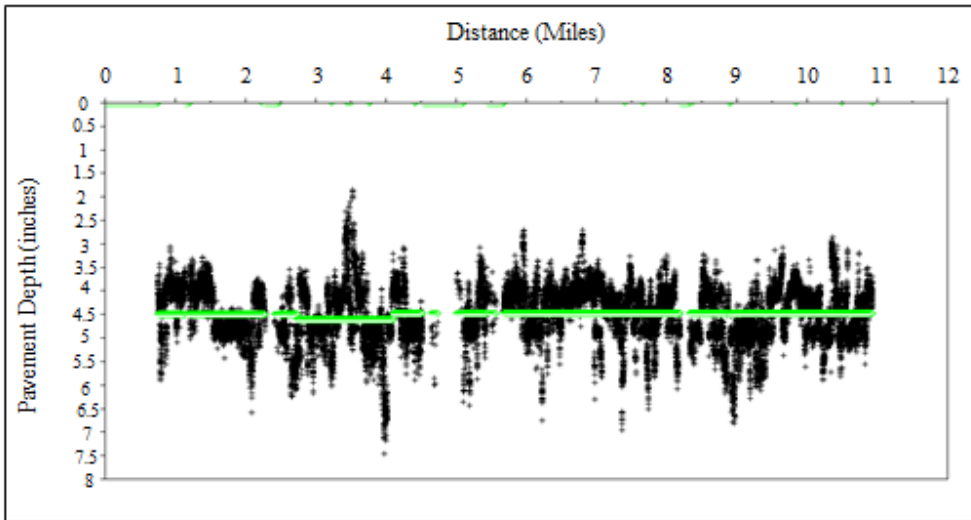


Figure 7. US15 – HMA Pavement
Layer 2 Data With Sixteen Subdivided Means

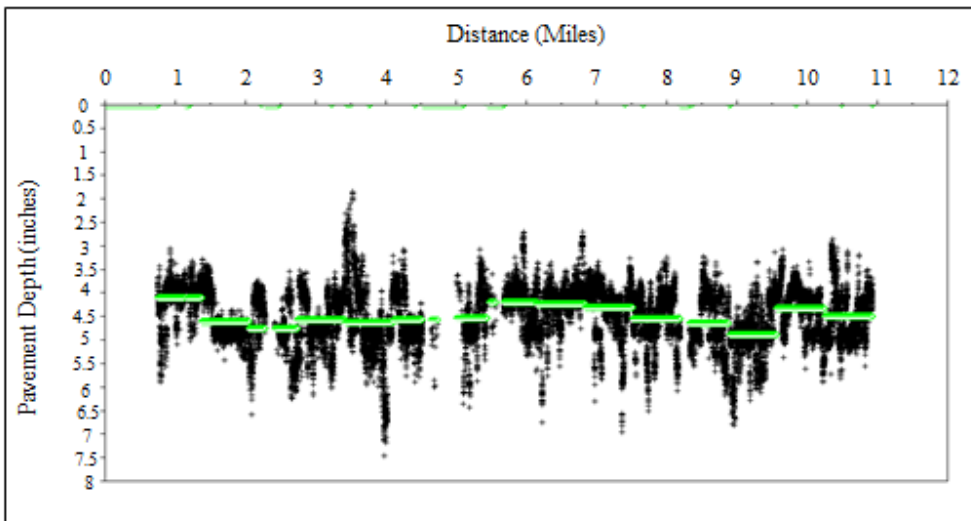


Figure 8. US15 – HMA Pavement
Layer 2 Data With MPGA Applied (Using Sixteen Subdivisions)

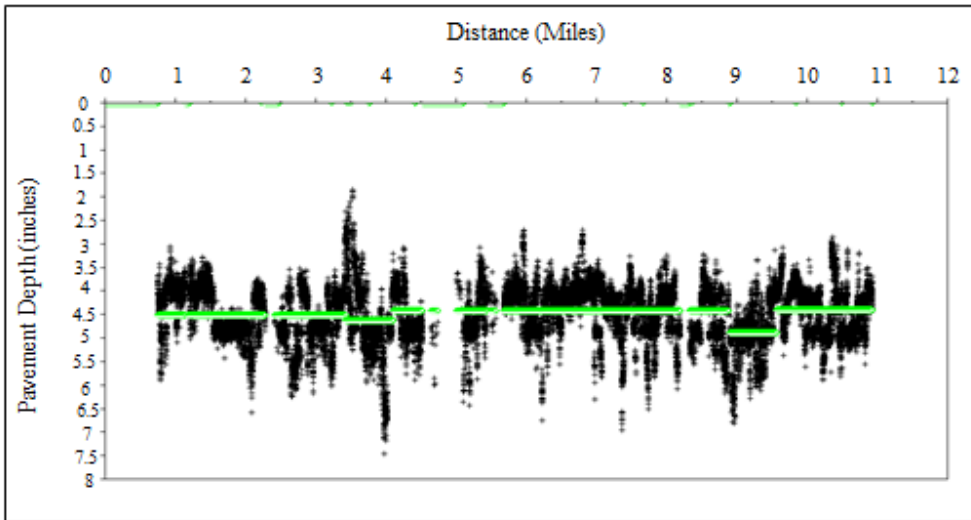


Figure 9. US15 – HMA Pavement
Layer 3 Data With Eight Subdivided Means

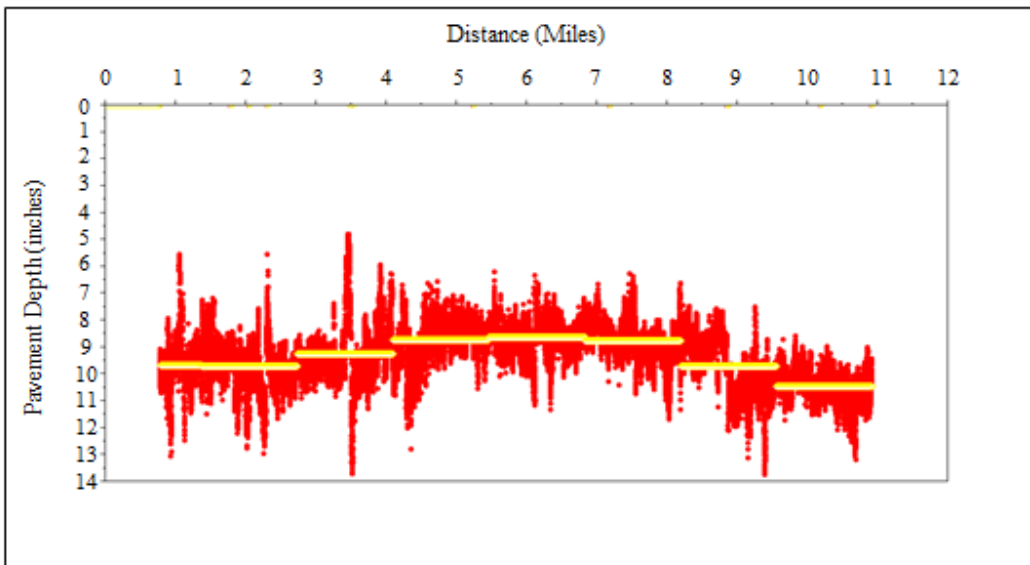


Figure 10. US15 – HMA Pavement
Layer 3 Data With MPGA Applied (Using Eight Subdivisions)

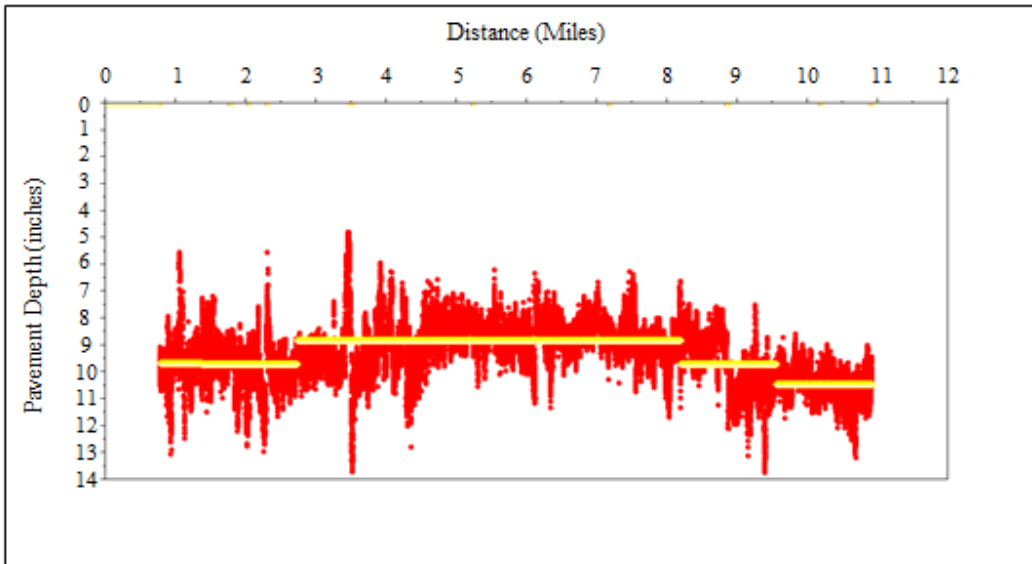


Figure 11. US15 – HMA Pavement
Layer 3 Data With Sixteen Subdivided Means

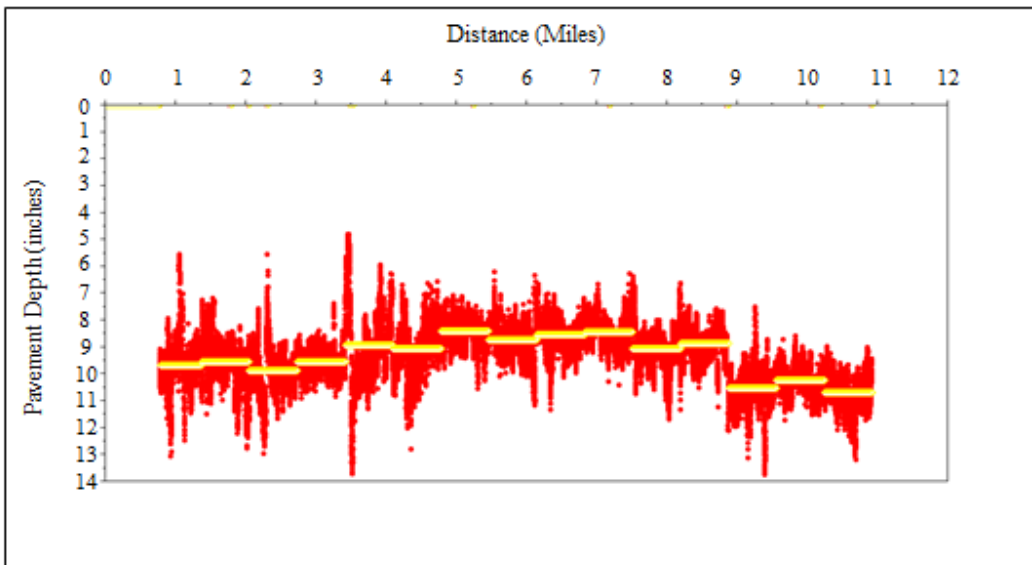


Figure 12. US15 – HMA Pavement
Layer 3 Data With MPGA Applied (Using Sixteen Subdivisions)

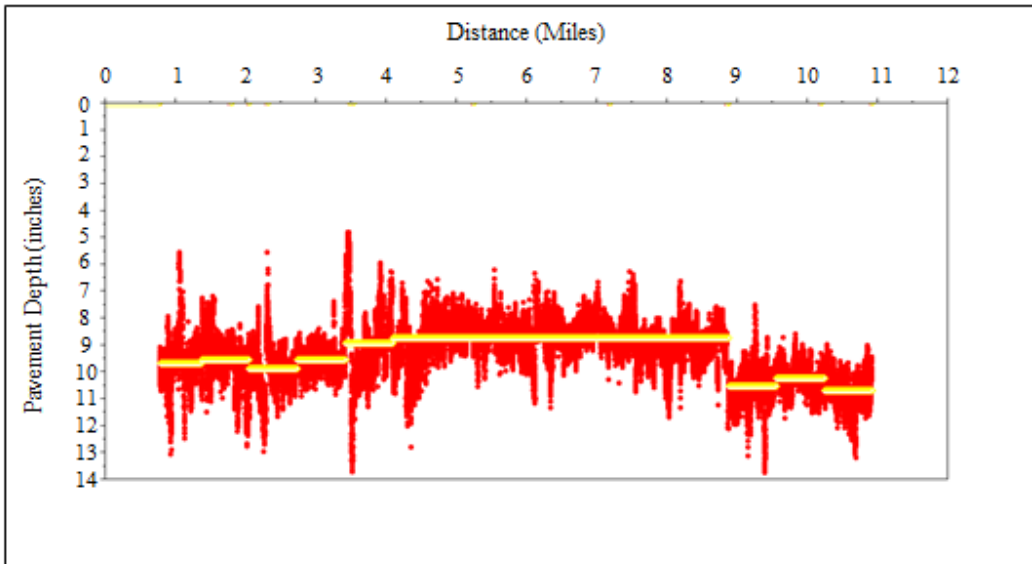


Figure 13. US15 – HMA Pavement
Data With MPGA Results (3 Layers) – Common Interlayer Trend Highlighted in Light Green

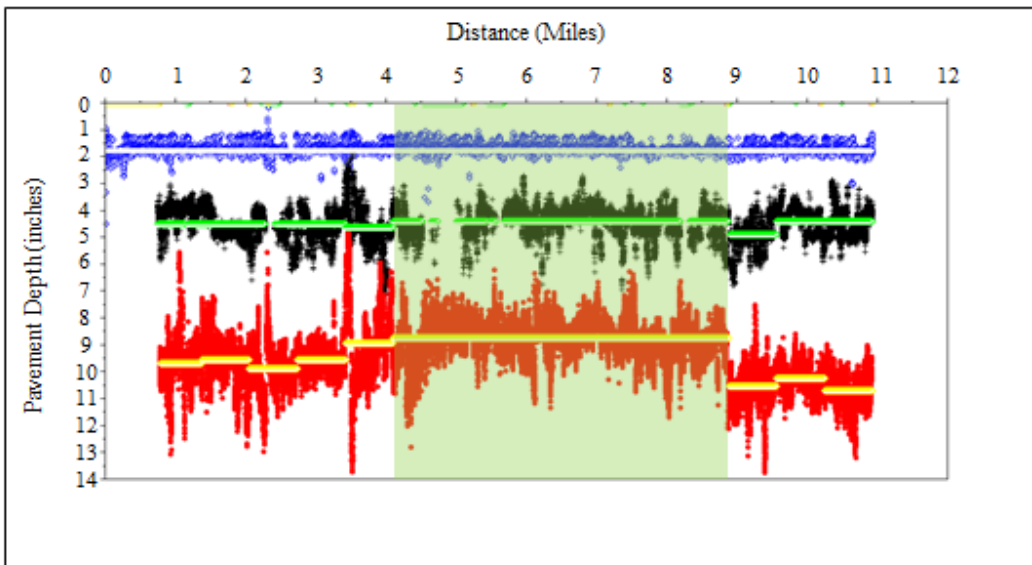


Figure 14. MD 675 – Concrete Pavement
Data With MPG Results (2 Layers)

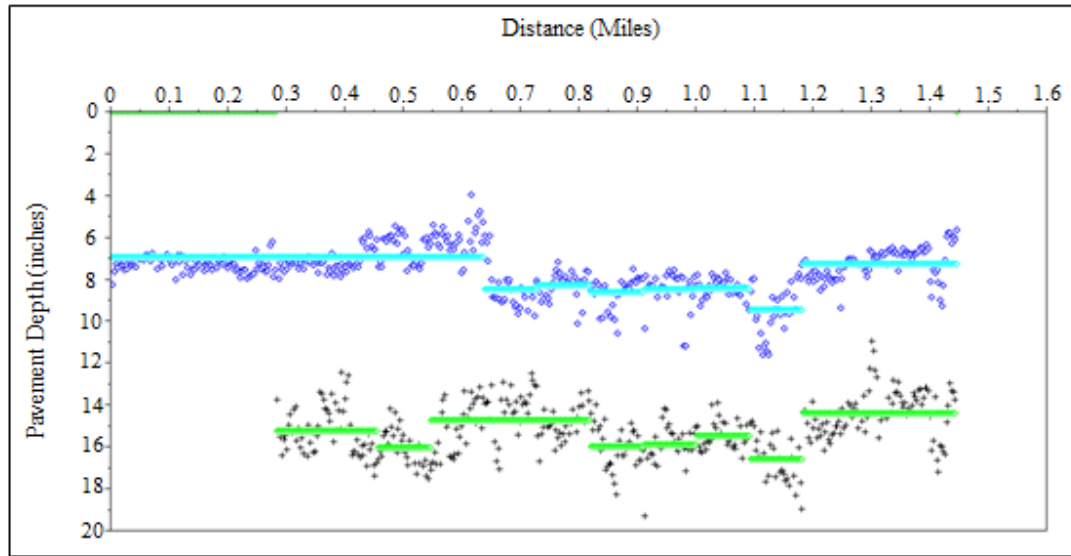


Figure 15. MD 675 – Concrete Pavement
Data With Global Means (2 Layers)

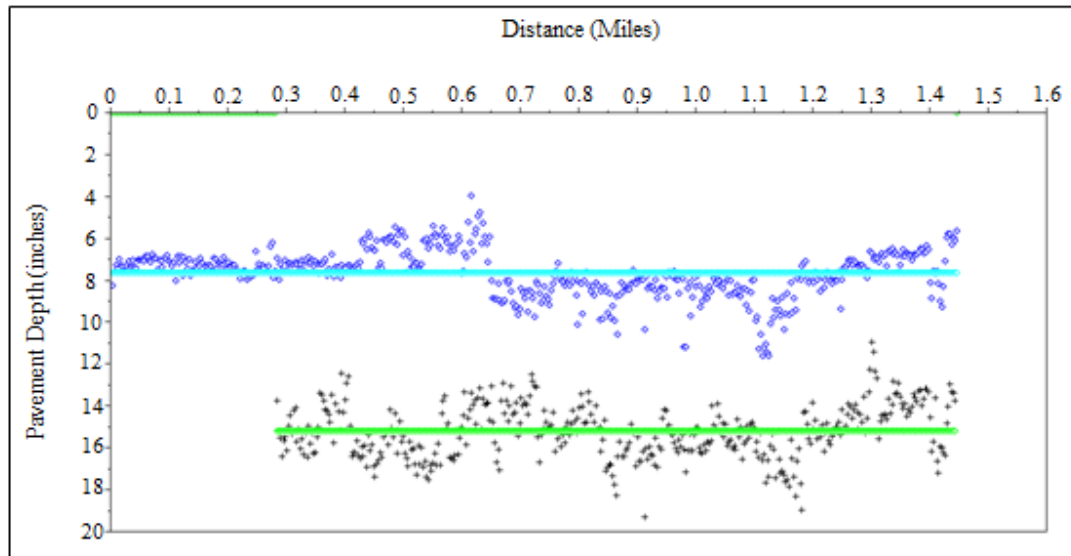


Figure 16. MD 675 – Concrete Pavement
Layer 1 Data With Sixteen Subdivided Means

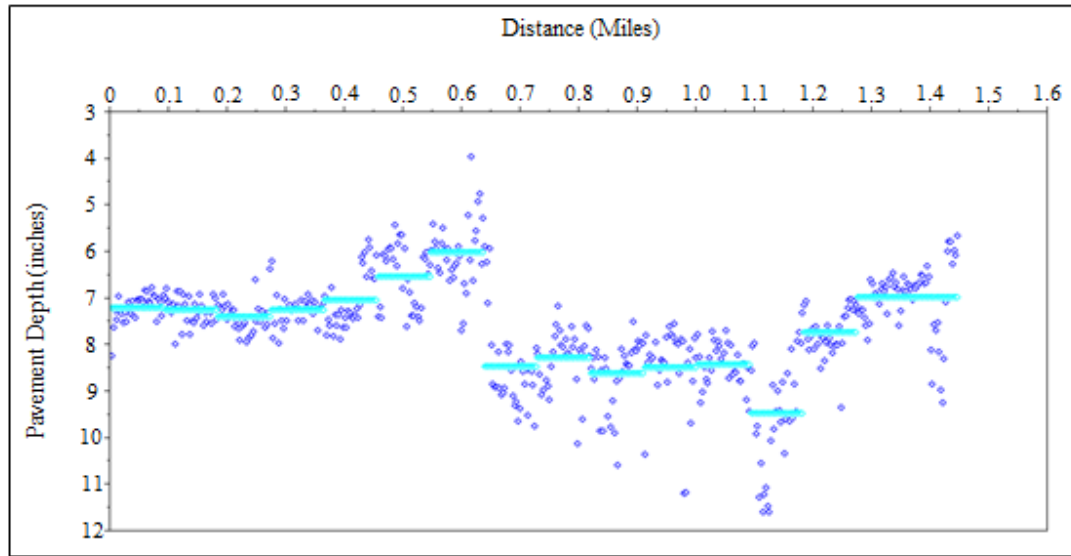


Figure 17. MD 675 – Concrete Pavement
Layer 1 Data With MPGA Applied (Using Sixteen Subdivisions)

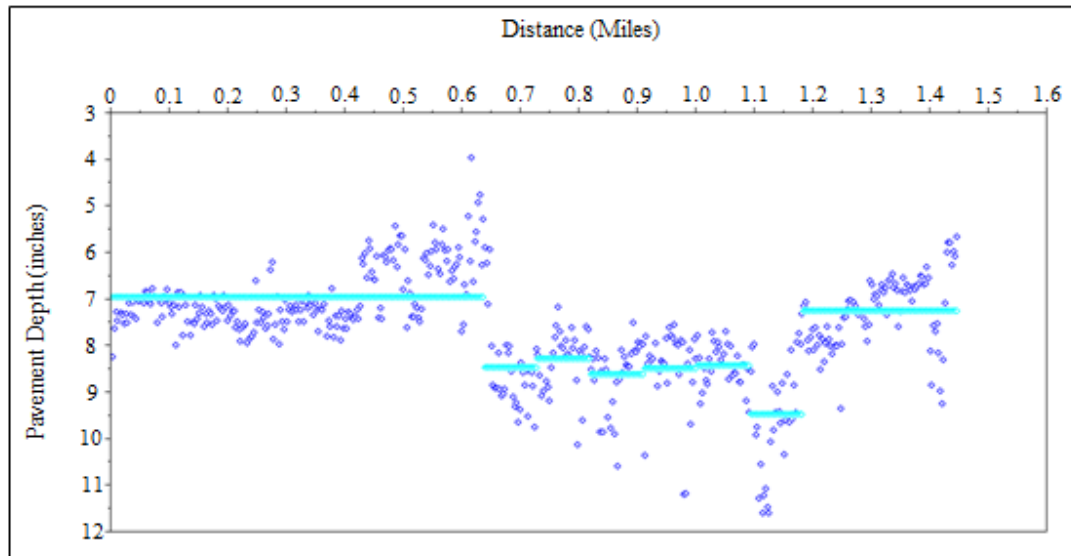


Figure 18. MD 675 – Concrete Pavement
Layer 2 Data With Sixteen Subdivided Means

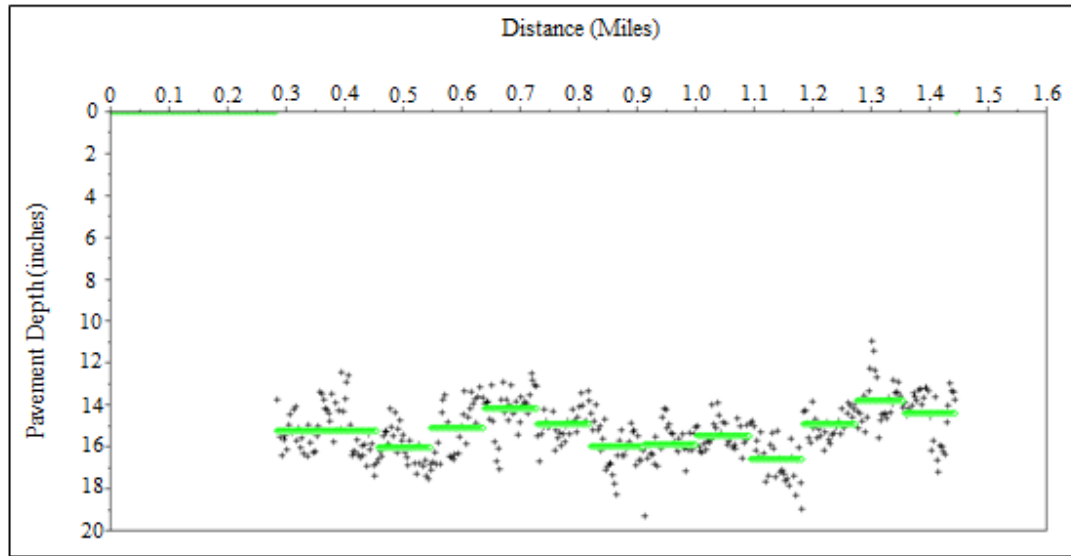


Figure 19. MD 675 – Concrete Pavement
Layer 2 Data With MPGA Applied (Using Sixteen Subdivisions)

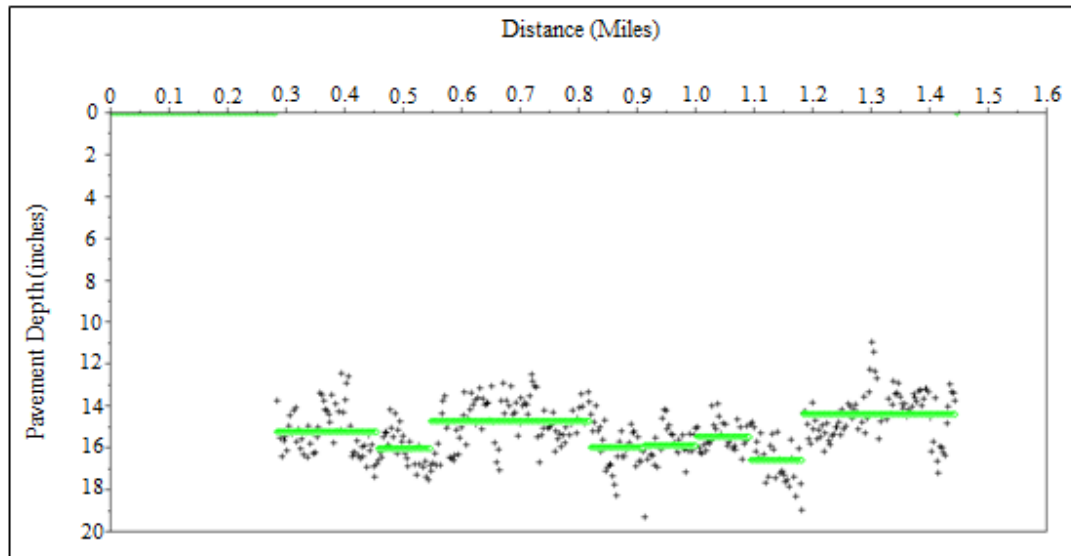
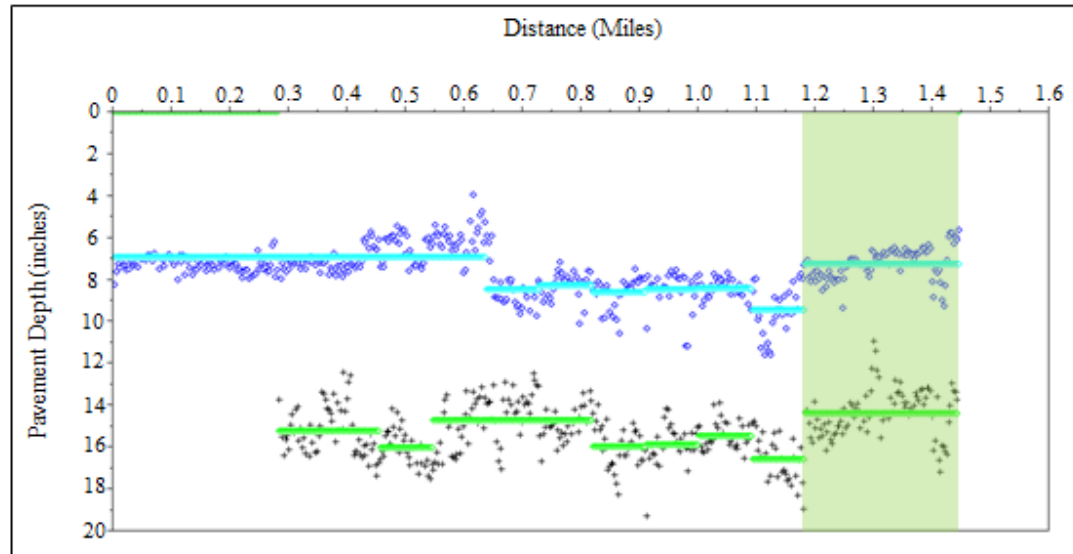


Figure 20. MD 675 – Concrete Pavement
Data With MPGA Results (2 Layers) – Common Interlayer Trend Highlighted in Light Green



Training Module

Ground Penetrating Radar (GPR) for Bridge Decks

- **Summary Method (background)**

HMA overlay on top of a concrete bridge deck

Electromagnetic (EM) wave through pavement material layers & interfaces

- Attenuated;
- Diffused;
- Dispersed;
- Scattered.

Amplitude of reflected to incident energy at interface:

$$\frac{A}{A_0} = \frac{\sqrt{\epsilon_1} - \sqrt{\epsilon_2}}{\sqrt{\epsilon_1} + \sqrt{\epsilon_2}}$$

A = the reflected energy, amplitude

A₀ = the incident energy, amplitude

ε₁ = the dielectric constant material 1

ε₂ = the dielectric constant material 2.

- **Summary Method (background)**

HMA overlay on top of a concrete bridge deck:

Maximum penetration depth depends (among other) on:

- GPR system (transmitted power, receiver sensitivity, center frequency & bandwidth);
- Electromagnetic properties of pavement materials;
- Environmental factors (such as moisture content).

Overlay Thickness (T):

$$T = \frac{\Delta t \times c}{2\sqrt{\epsilon_r}}$$

c = speed of light in air, 300 mm/nsec for T in mm (11.8 in/nsec for T in inches)

ϵ_r = relative dielectric constant of layer

Δt = two-way pulse travel time through layer (in nanoseconds).

- **Summary Method (background)**

Evaluation of dielectric constant of pavement materials

- **Air-coupled** horn antenna
- Dielectric constant of **air**

Amplitude of reflected to incident energy at Interface:

$$\frac{A}{A_0} = \frac{\sqrt{\epsilon_1} - \sqrt{\epsilon_2}}{\sqrt{\epsilon_1} + \sqrt{\epsilon_2}}$$

A = the reflected energy, amplitude

A_0 = the incident energy, amplitude

ϵ_1 = the dielectric constant of **air**

ϵ_2 = the dielectric constant material

- **Summary Method (background)**

Evaluation of dielectric constant of pavement materials

- **Ground - coupled dipole antenna**
- **Coring**
 - or
- Dielectric constant measurements with **multi-static antenna pairs** positioned at two or more transmitter to receiver location offsets.
- Material properties analyzed with **Common Midpoint (CMP)** method technique.

Apparatus

- **Air-coupled antennas**
 - central frequencies 1 GHz and greater;
 - control unit able to transmit at a sufficient rate to collect 20 scans/m (25 scans/ft);
 - short-pulse monostatic or bistatic radar(s) with a monocycle pulse 150 mm (6 in.) free space resolution and a 50 scan/s minimum data rate.
- **Ground-coupled antennas**
 - central frequencies greater than 1 GHz;
 - control unit able to transmit at a sufficient rate to collect 80 scans/m.

Apparatus

- **Data acquisition system**
 - minimum data collection rate of 50 kHz for one radar, 100 kHz for two radars, and 150 kHz for three radars;
 - capable of accurately acquiring radar data with a 60-dB dynamic range;

- **Distance measurement instrument (DMI)**
 - accuracy of 6100 mm/km (66.5 in./mile);
 - resolution of 25 mm (1 in.).

- **Periodic Calibration**
 - **Air coupled system calibrations**
 - **Annually**
 - **System Performance Compliance**
 - Signal-to-noise ratio
 - Signal stability
 - Variations in time-calibration factor
 - Long Term Amplitude Variation

Pre-Operation Measurements

- Free Space Signal (FSP):
 - manufacture recommendations;
 - antenna in operational configuration,
 - 100 waveforms in absence of material to be inspected.
 - Average of 100 waveforms as template for clutter removal.

Pre-Operation Measurements

- Flat Metal Plate (FMP):
 - radar in operation configuration;
 - gather 100 waveforms on a flat plate with dimensions as per manufacturer recommendations;
 - use emitted energy for subsequent measurements, and for correlation or background removal, or both.

Data Collection Procedure

- Air-Coupled Systems
 - radar inspection passes parallel to centerline of bridge deck with antenna mounted at manufacturer recommended distance from bridge deck surface.;
 - Use a transverse distance (dt) between radar inspection passes <1 m (3 ft);
 - Use a longitudinal distance (dl) between radar scans <150 mm (6 in).;
 - Determine starting location for passes (at abutments, joints, or a predetermined location);
 - Determine speed of operation based on the radar range sweep rate and the manufacturer-recommended scan-spacing.

Data Collection Procedure

- Ground-Coupled Systems
 - radar inspection passes either parallel or perpendicular to the direction of traffic, depending on the direction of the top layer of reinforcing;
 - pass direction selected so that antenna crosses over the top layer of reinforcing at an angle nearest to 90°.

Data Analysis

- Attenuation Technique:
 - calculate deterioration based on relative reflection amplitudes from the bridge deck bottom relative to bridge deck surface.
- Top Reinforcing Reflection Technique:
 - use relative reflection amplitudes from the top layer of reinforcing to assess deterioration.

Data Analysis

- Attenuation Technique (*Delamination at Top Reinforcing Steel*)
 - Measure applied signal strength, V_t , at the deck surface;
 - Measure maximum signal strength of the deck bottom echo, V_{bs} ;
 - If V_{bs} is $< 0.0264 V_t$ after repeating the longitudinal radar inspection pass, the data are not reliable (alternative methods recommended - Ontario Ministry of Transportation);
 - Measure and record amplitude of the deck bottom echo, V_b , for each waveform.

Data Analysis

- Attenuation Technique (Delamination at Top Reinforcing Steel)

- Consider concrete delaminated if: $V_b \leq 0.385 V_{bs}$

V_b = bottom echo amplitude, each scan;
 V_{bs} = bottom echo maximum amplitude, all scans;
0.385 = a constant derived from research data.

- Calculate percent delaminated at top steel in each radar inspection pass:

$$X_{tn} = [(W_{dt}) / (W_{dt} + W_{st})] [100]$$

X_{tn} = percent delaminated in a radar inspection pass n, at top steel;
n = radar inspection pass identification number;
 W_{dt} = concrete delaminated at top steel, m;
 W_{st} = sound concrete at top steel, m.

Data Analysis

- Attenuation Technique (Delamination at Top Reinforcing Steel)

- Calculate estimated quantity of deck delaminated at top steel for each radar inspection pass:

$$Q_t = (X_{tn}) (L_n) (d_t)$$

Q_t = square meters (feet) of deck delaminated at top steel;
 L_n = length of radar inspection pass, n, m;
 d_t = transverse distance between radar inspection passes, m.

- Calculate total estimated quantity of deck delaminated at top steel :

$$Q_{Tt} = S Q_t$$

Q_{Tt} = total square meters (feet) of deck delaminated at top steel for all radar inspection passes.

Data Analysis

- *Deterioration Measurements at or above Top Reinforcing Steel—Top Reinforcing Reflection Technique:*
 - Extract the reflection amplitudes from the top layer of reinforcing.

Data Analysis

- *Deterioration Measurements at or above Top Reinforcing Steel—Top Reinforcing Reflection Technique:*

Air-Coupled System

- data collected with two antennas (transmitter - receiver pair) positioned in-line with longitudinal direction;
- antennas radiating with polarization orientation perpendicular to the transverse reinforcing steel direction;
- clutter removal by normalizing the reflection amplitudes of the metal plate reflections to the asphalt reflection (if HMA overlay exist);
- subtract the free space (FSP) scan from each data scan starting at the mid-point of the asphalt surface reflection*

* Further consideration on data analysis is needed for bridge decks containing longitudinal rebar on top of transverse rebar with on-center spacing less than 20 cm (8 in.), and when the orientation of the top layer of reinforcing is not skewed at close to 45° relative to the direction of traffic.

Data Analysis

- Deterioration Measurements at or above Top Reinforcing Steel—Top Reinforcing Reflection Technique:

Ground- Coupled System

- Focus and image the reinforcing reflections using a migration algorithm or an alternative method such as wave field back-propagation to determine their precise locations;
- Record the corresponding waveform reflection amplitudes from the GPR scan most nearly centered over each reinforcing steel member detected in the data.

Data Analysis

- Deterioration Measurements at or above Top Reinforcing Steel—Top Reinforcing Reflection Technique:

Calculate Deterioration Threshold.

- Convert the reflection amplitudes to decibels.

$$A_{db} = 20 \log_{10} (A)$$

A_{db} = reflection amplitude in decibels;
 A = reinforcing reflection amplitude in data units.

- Lower reflection amplitude* corresponds to higher likelihood of deterioration.

*location with reflection amplitude less than 6 to 8 dB below the maximum reflection amplitudes correspond to deterioration detected using other information, such as (1) bridge deck bottom inspection results, (2) core data when possible, and (3) results from other deterioration assessment techniques to refine the threshold value.

Data Analysis

- Deterioration Measurements at or above Top Reinforcing Steel—Top Reinforcing Reflection Technique:

Calculate Deterioration Threshold.

- Create contour map of reflection amplitudes versus spatial location on the bridge deck;
- Locations of deteriorated areas correspond to reflection amplitudes less than threshold value.
- Calculate percent deterioration at or above the top steel in each radar inspection pass:

$$X_{tn} = [(W_{dt}) / (W_{dt} + W_{st})] [100]$$

X_{tn} = percent deteriorated in a radar inspection pass, n , at or above top steel;

n = radar inspection pass identification number;

W_{dt} = concrete deteriorated at or above top steel, m , obtained from reflection amplitudes below deterioration threshold value;

W_{st} = sound concrete at top steel, m , obtained from reflection amplitudes above deterioration threshold value.

Draft MSMT

on

Ground Penetrating Radar (GPR) for Bridge Decks

Appendix: System Performance Compliance

- Signal-to-noise ratio
- Signal stability
- Variations in time-calibration factor
- Long Term Amplitude Variation

Approved:	Missouri Department of Transportation State Highway Administration Office of Materials Technology Institution of Standards Methods (ISM 1015)
Approved:	GPR FOR BRIDGE DECKS

NOTE:

This procedure is used to determine the condition of concrete bridge decks. Specifically, this non-destructive evaluation method could identify defects related to concrete and other deterioration.

REFERENCE DOCUMENTS:

ASTM D6971-05, "Measuring Asphalt-Covered Concrete Bridge Decks Using Ground Penetrating Radar."

ASTM D6952-11, "Standard Guide for Using the Surface Ground Penetrating Radar Method for Subsurface Investigation."

ASHTO, "Standard Practice for Application of Ground Penetrating Radar (GPR) to Highways," Report No. R017-04-01, 2009, pp. 12.

ACI 208.2R-02 "Report on Nondestructive Test Methods for Concrete in Structures," American Concrete Institute, June 2012, pp. 10-41.

Demko, D.J., Surface Penetrating Radar, The Institution of Electrical Engineers, pp. 221, December 2006.

Sunk, M., Nondestructive Testing Handbook, 2nd Edition, Volume 5, Electromagnetic Testing, Chapter 17, Infrastructure Applications, Part 2, Applications of Ground Penetrating Radar to Bridge Decks, American Society of Nondestructive Testing, 2004, pp. 400-430.

Sunk, M., Neuzilstein, A., Shous, M., "Phenomenology Study of HERMES Ground Penetrating Radar Technology for Detection and Identification of Common Bridge Deck Features," Report FHWA-RD-01-200, Federal Highway Administration, McLean, VA, 2001, pp. 1-17.

Improved GPR Data Analysis Techniques for Bridge Decks

Current Practice in Bridge Deck Inspection Analysis

- (i) Subjective Bridge Deck Inspection Surveys with Visual Inspections;
- (ii) Location specific measurements:
 - time consuming, costly, labor intensive and destructive objective measurements (coring);
 - subjective measurements (chain drag sounding);
 - traffic control & safety
- (iii) Lack of capability to accurately identify deterioration variability within a bridge deck;
- (iv) Lack of capability to accurately detect subsurface deterioration.

GPR based Bridge Deck Inspection

- Accurate and efficient bridge deck inspection;
- Provide objective bridge deck deterioration ratings
- Accurate detection of location specific deterioration problems;

Improvements in GPR Analysis

- Account for bridge deck concrete moisture content effects on GPR signal attenuation and thus data analysis using Short Term Fourier Transform (SFTF) analysis;
- Use of Migration techniques for examining concrete cover & reinforcement features with bridge deck depth.

GPR Migration

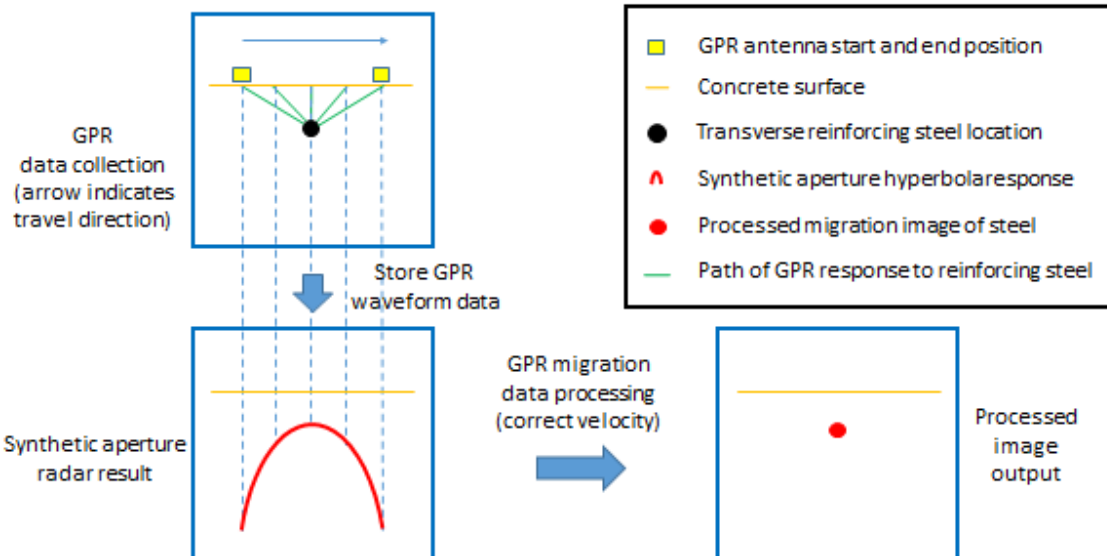
• *GPR Migration Analysis - Concept*

- Provides intuitive subsurface geometry information based on GPR data
- Maps GPR waveform data from the time domain (time units) into the spatial domain (depth units)
 - Inputs:
 - Synthetic Aperture Radar (SAR) time domain data
 - GPR calibration information (including data sampling information)
 - Dielectric material properties (measured, calibrated, or assumed)
 - Distance measurement instrument position, GPS position, etc.
 - Outputs:
 - Range dimension information in depth units
 - Subsurface feature of interest geometries/shapes including
 - + Point objects (example: transverse reinforcing steel)
 - + Dielectric material interfaces (example: bridge deck pavement layer interfaces)
 - + Linear features of interest (examples: bridge beams or long reinforcing steel)
 - + Anomalies (voids, deterioration/distress features)
 - Relative magnitude of feature reflection (reflection strength)

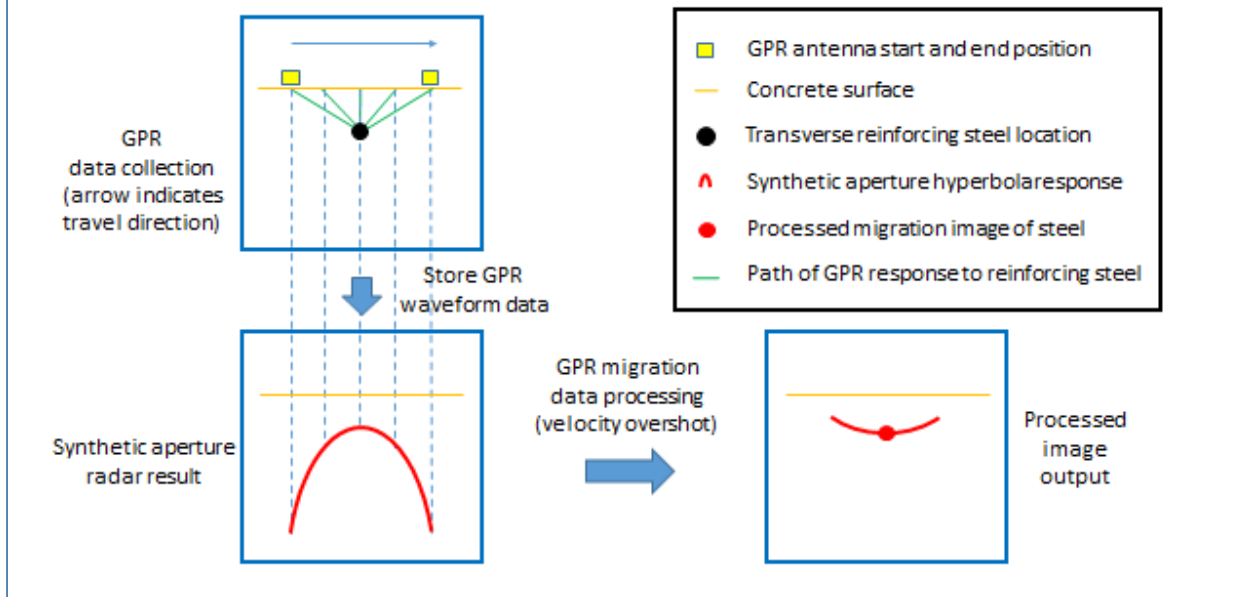
How GPR Migration is Performed

- *GPR Migration Analysis – How to Perform*
 - Select a migration method:
 - Kirchoff (fast, very accurate)
 - Frequency wavenumber (fastest, accurate)
 - Hyperbolic summation (slow, accurate)
 - Other
 - Each technique uses the Exploding Source Model (ESM) concept to:
 - Extrapolate received waveform signals back to "exploding source" reflection points
 - Form migrated images by back extrapolating incident GPR waves to $t=0$
 - Basic Migration Steps (Conceptual):
 - A hyperbola shaped summation template (computed using material property information) is conceptualized at each wave field data point
 - All wave field data that falls on the hyperbola corresponding to a given data point is summed and stored for that point (within a selected aperture)
 - Geometric and computational details differ in important but often subtle ways for each migration method
 - For Efficient Real World Migration Computation:
 - Data is transformed into the frequency domain before processing
 - Migration processing is performed in the frequency domain (to minimize computational requirements)
 - Frequency domain results are inverse transformed to obtain migration output

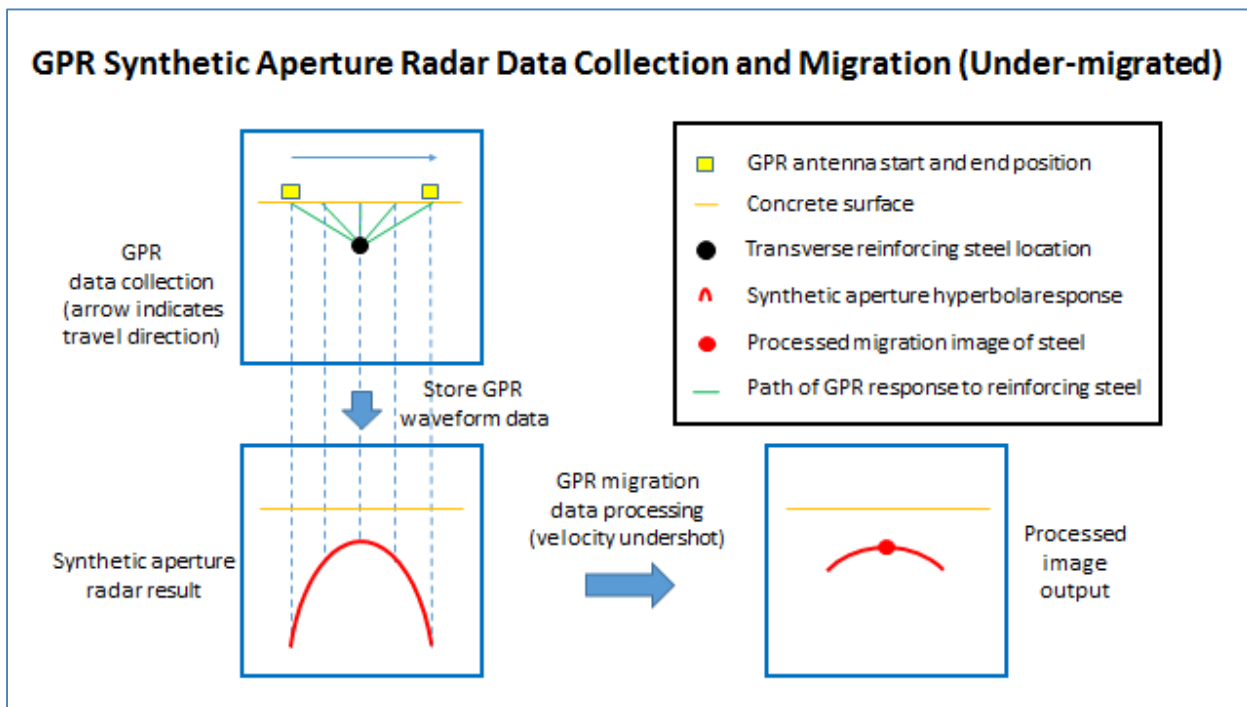
GPR Synthetic Aperture Radar Data Collection and Migration Data Processing



GPR Synthetic Aperture Radar Data Collection and Migration (Over-migrated)



GPR Synthetic Aperture Radar Data Collection and Migration (Under-migrated)



Examples
of
Bridge Deck GPR Data Analysis

Figure 1. US 13 Northbound Over Norfolk Southern RR
Migration Results (Above) vs. Attenuation Map (Below)

Depth = 0 inch

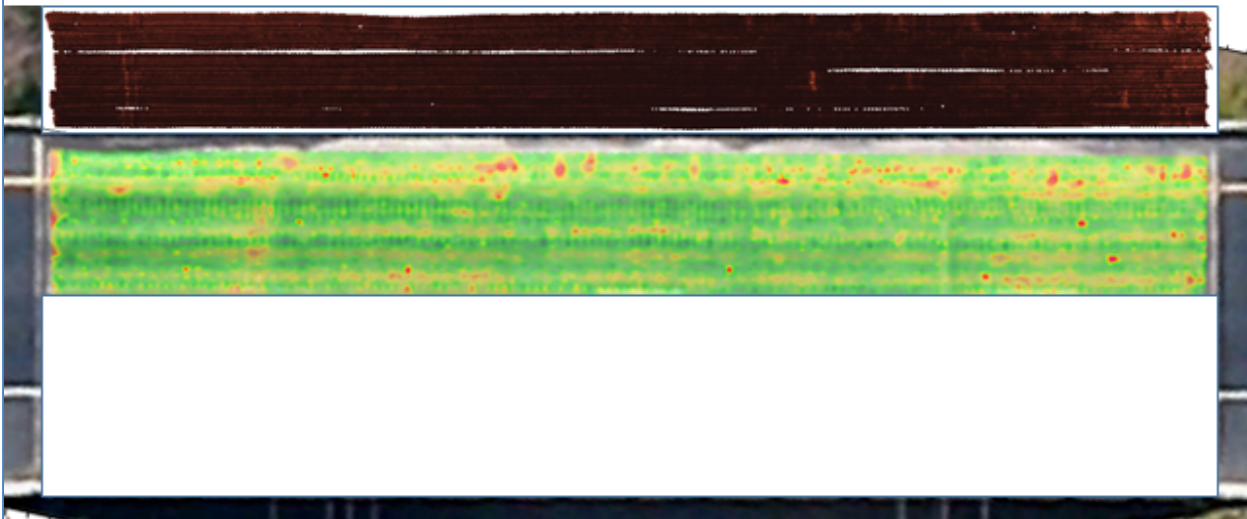


Figure 2. US 13 Northbound Over Norfolk Southern RR

Depth = 1 inch

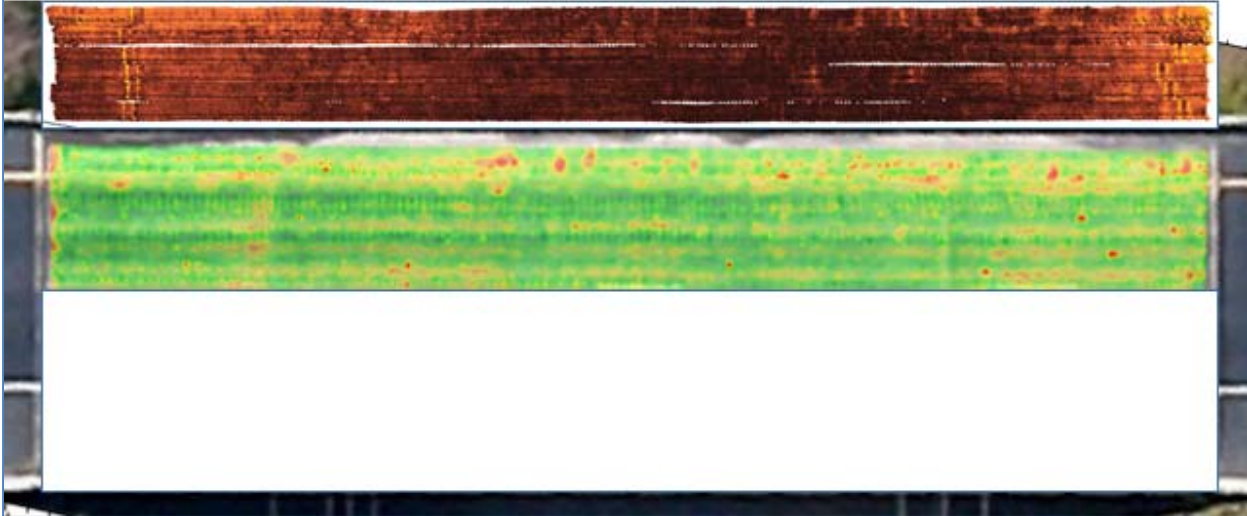


Figure 3. US 13 Northbound Over Norfolk Southern RR

Depth = 2 inch

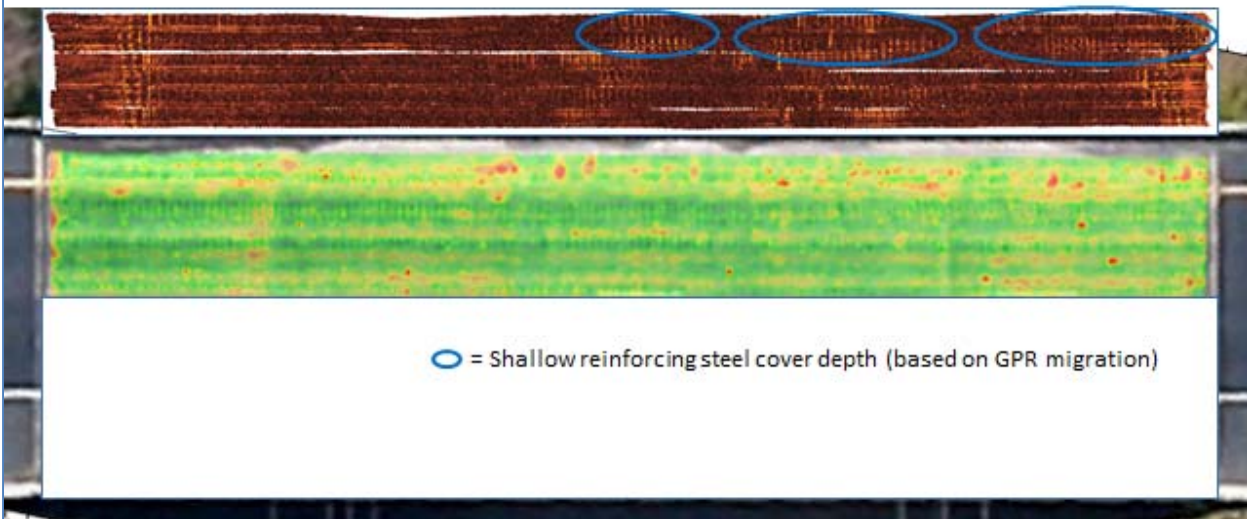


Figure 4. US 13 Northbound Over Norfolk Southern RR

Depth = 3 inch

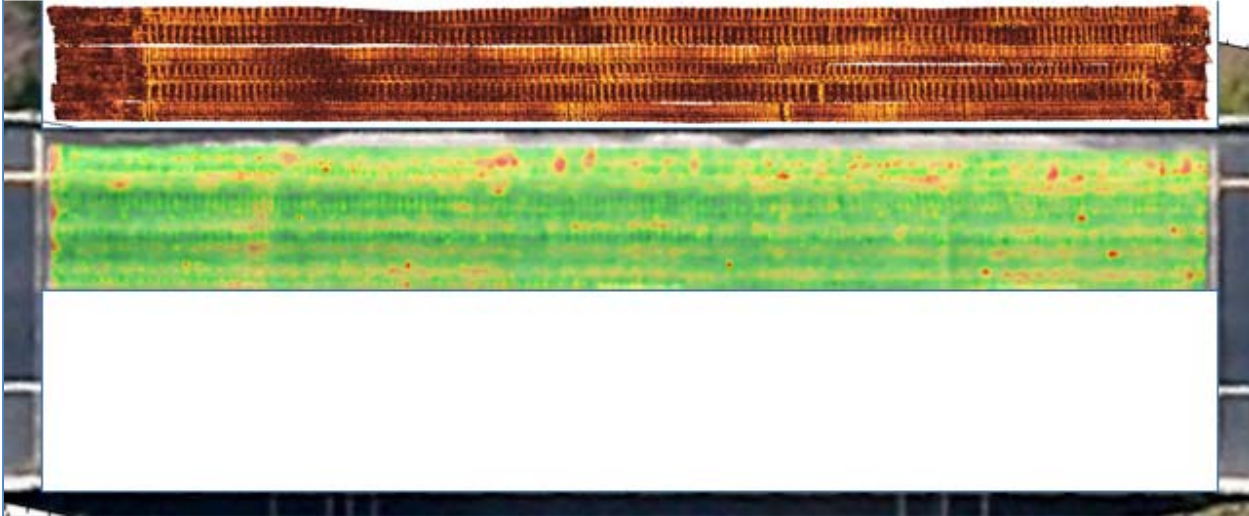


Figure 5. US 13 Northbound Over Norfolk Southern RR

Depth = 4 inch

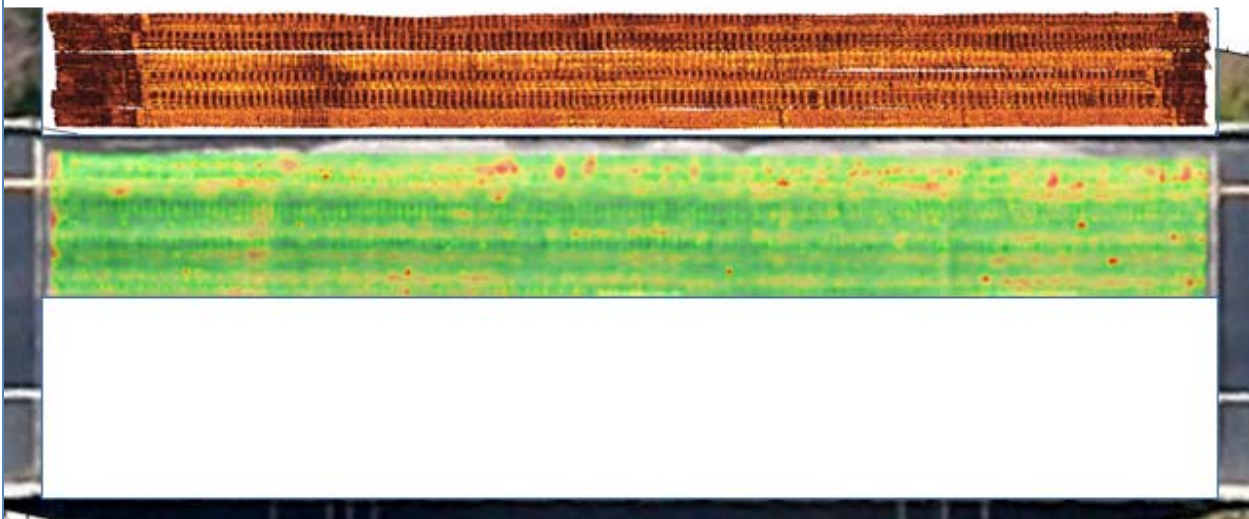


Figure 6. US 13 Northbound Over Norfolk Southern RR

Depth = 5 inch

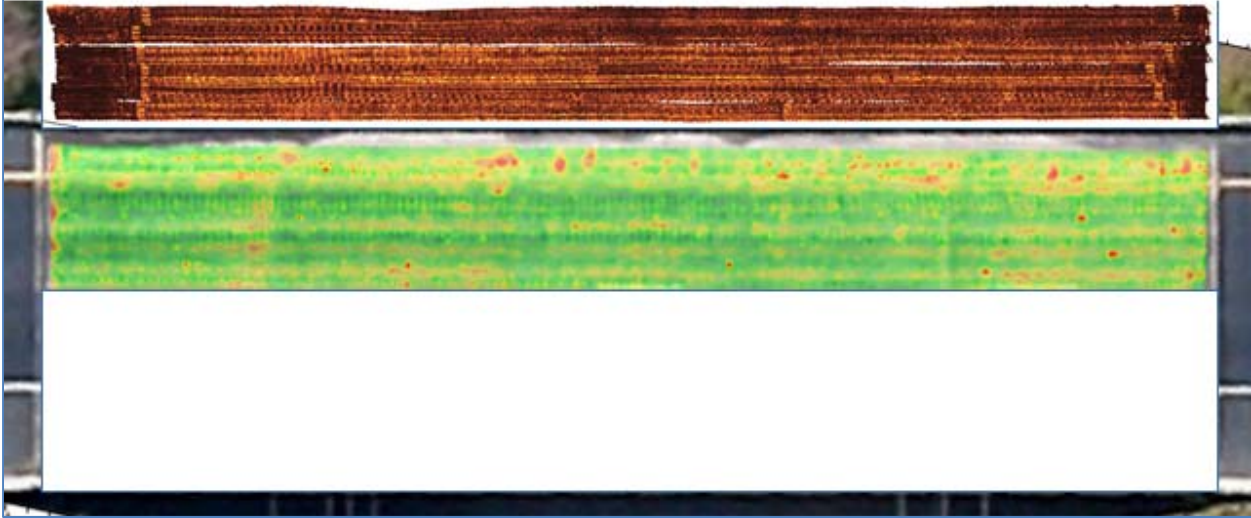


Figure 7. US 13 Northbound Over Norfolk Southern RR

Depth = 6 inch

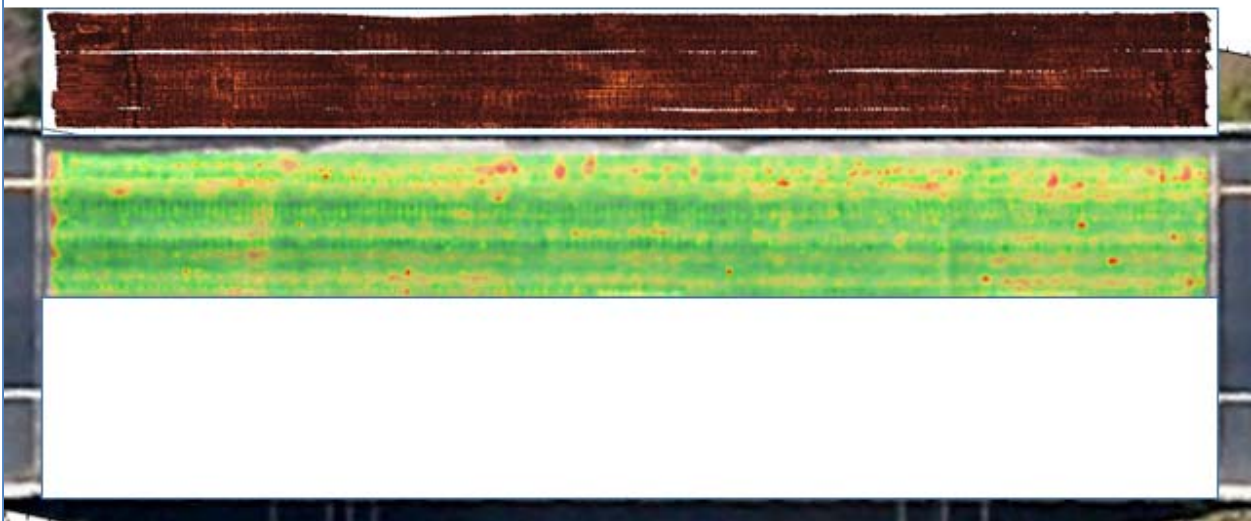


Figure 8. US 13 Northbound Over Norfolk Southern RR

Depth = 7 inch

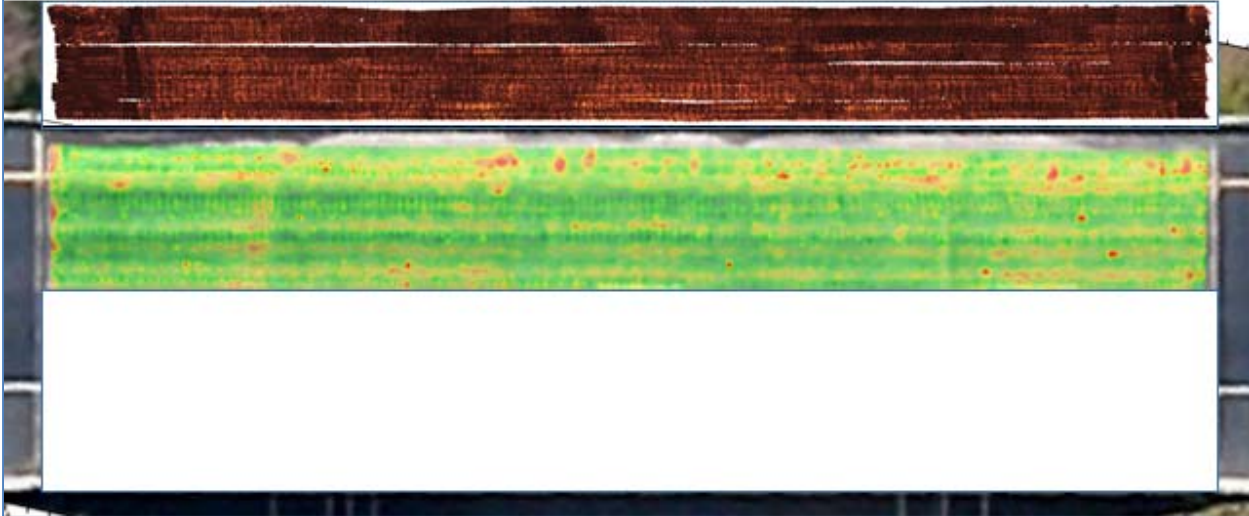


Figure 9. US 13 Northbound Over Norfolk Southern RR

Depth = 8 inch

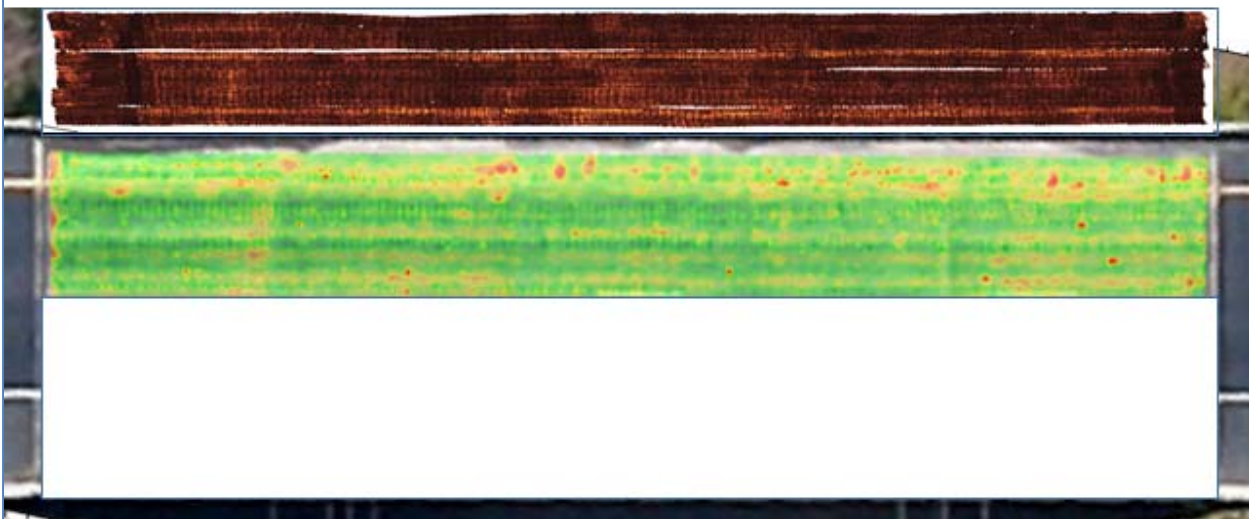


Figure 10. US 13 Northbound Over Norfolk Southern RR
Moisture

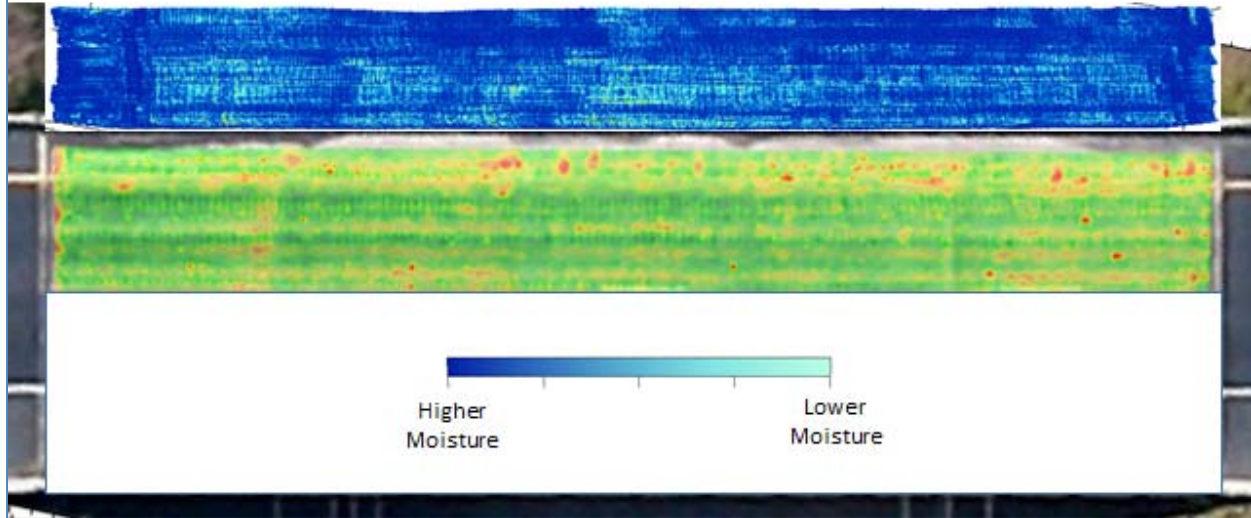


Figure 11. Route 290 Over Chester River
Migration Results (Above) vs. Attenuation Map (Below)

Depth = 0 inch

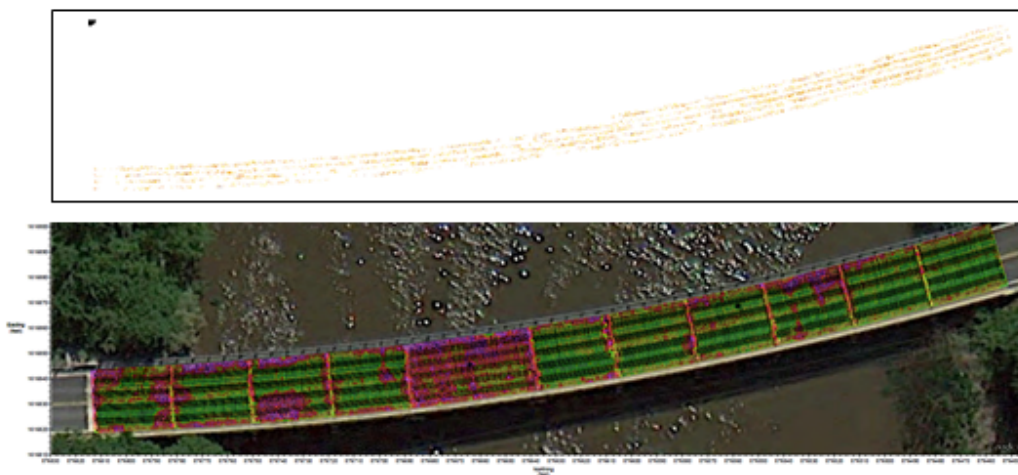


Figure 12. Route 290 Over Chester River

Depth = 1 inch

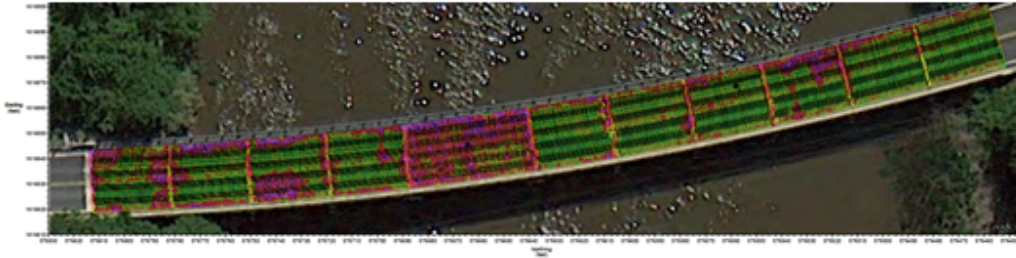
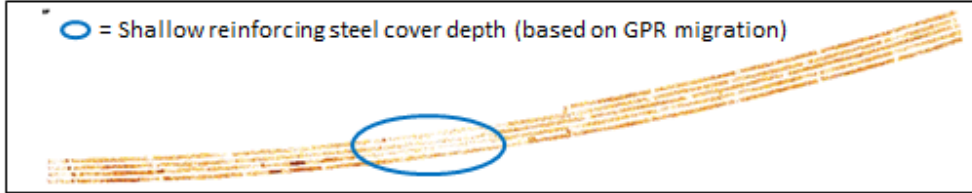


Figure 13. Route 290 Over Chester River

Depth = 2 inch

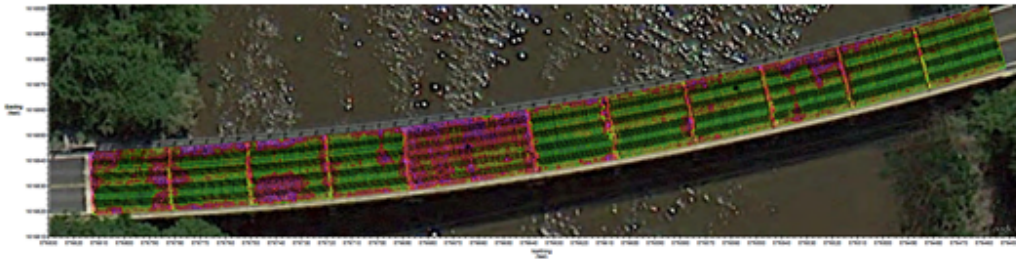
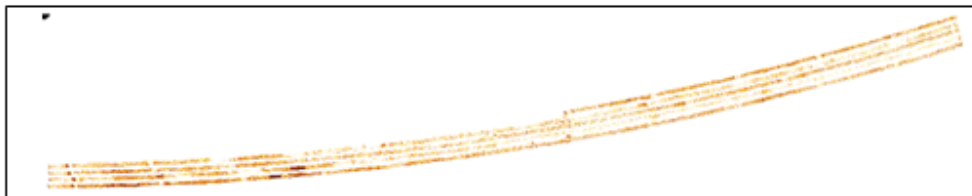


Figure 14. Route 290 Over Chester River

Depth = 3 inch

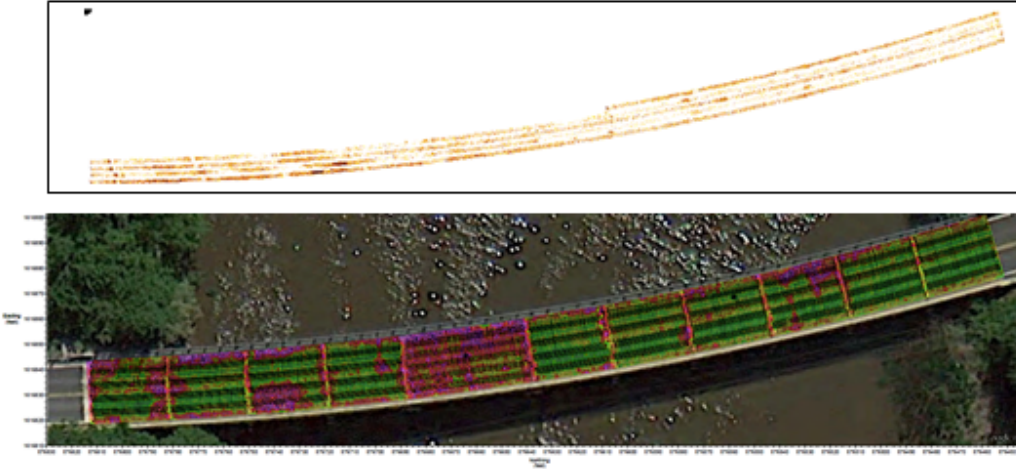


Figure 15. Route 290 Over Chester River

Depth = 4 inch

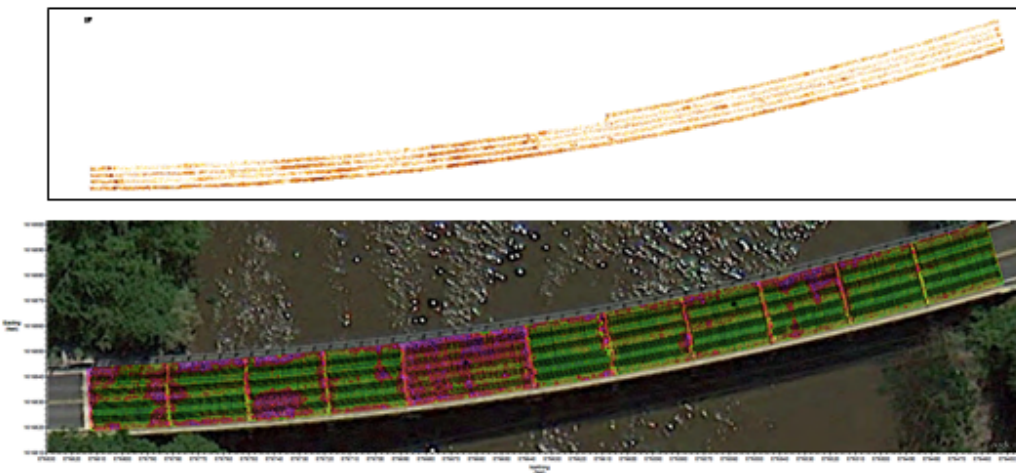


Figure 16. Route 290 Over Chester River

Depth = 5 inch

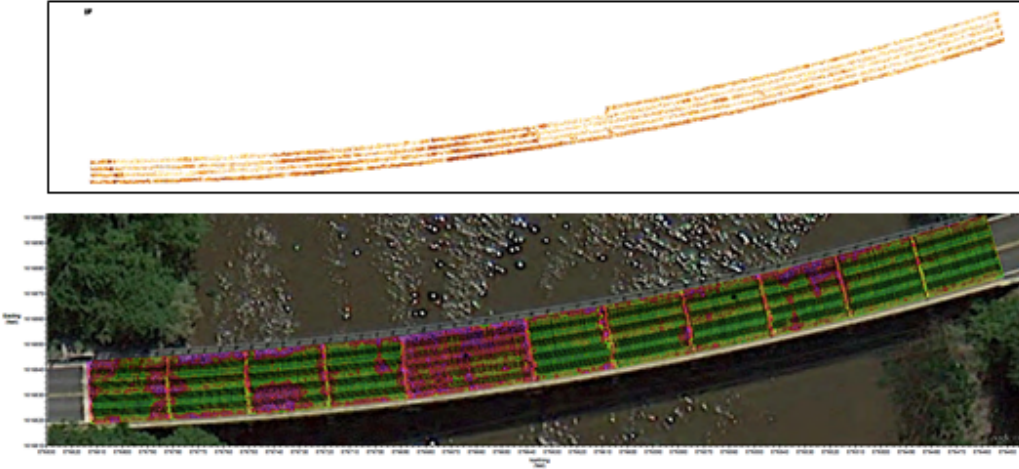


Figure 17. Route 290 Over Chester River

Depth = 6 inch

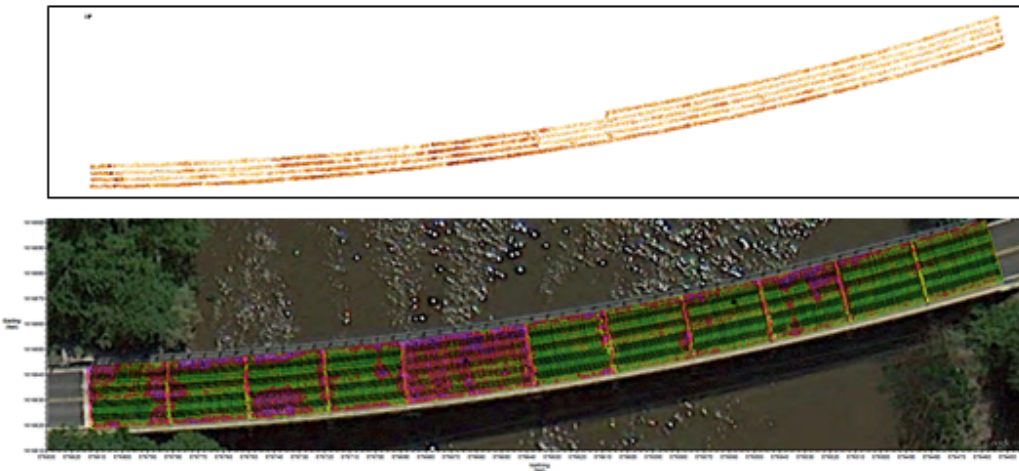


Figure 18. Route 290 Over Chester River

Depth = 7 inch

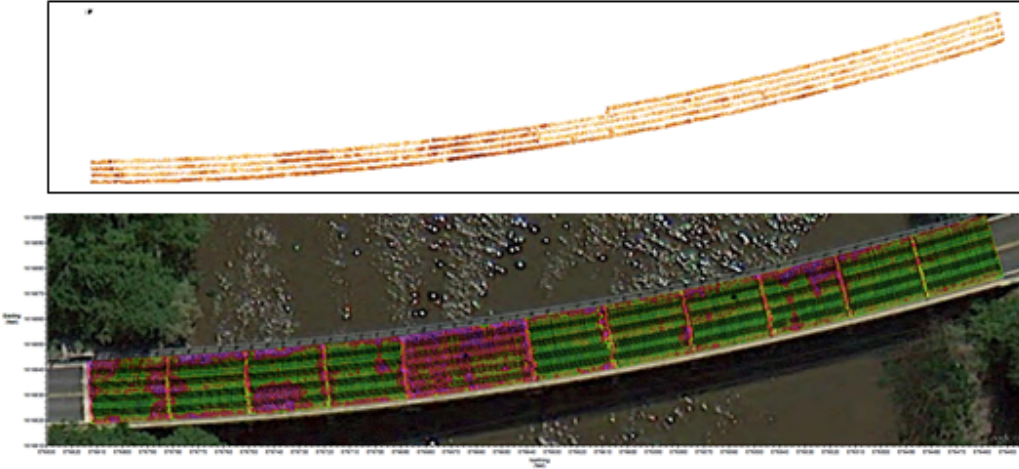


Figure 19. Route 290 Over Chester River

Depth = 8 inch

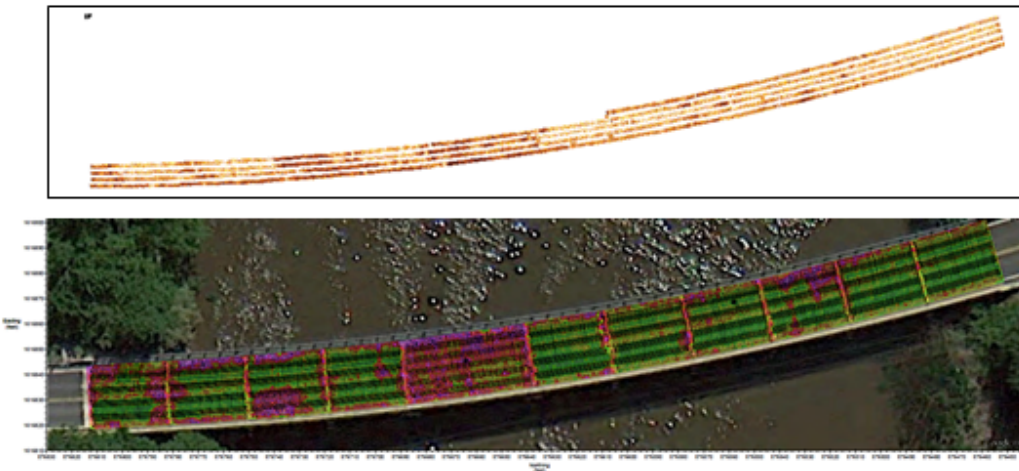
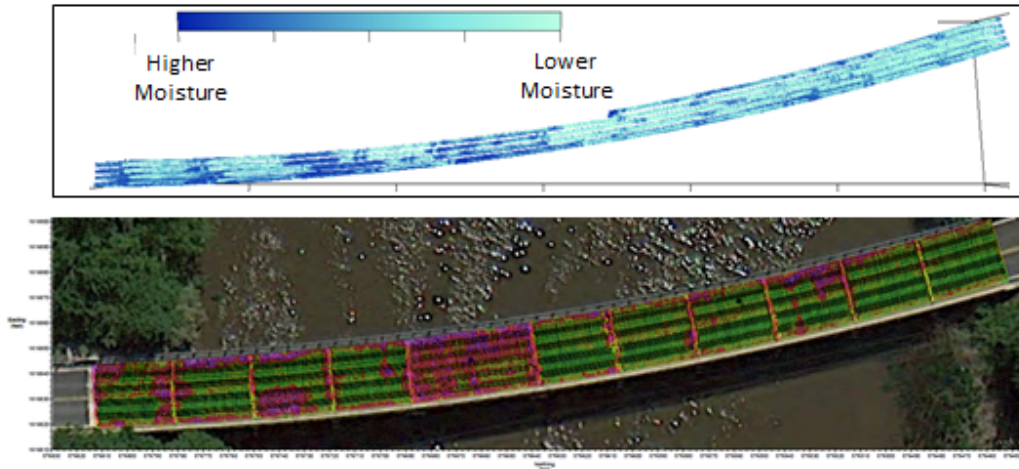


Figure 20. Route 290 Over Chester River
Moisture



Short Time Fourier Transform (STFT) Analysis

- STFT evaluation of wet/moist bridge deck GPR data allows dispersion phenomena to be observed and evaluated (characteristic of a wet/moist GPR response with elevated Imaginary dielectric properties) including:
 - Reduced frequency content
 - Reduced center frequency
- STFT results also show the time delay caused by wet/moist materials consistent with elevated Real dielectric properties
- Most environmental issues impacting GPR measurement consistency involve water/moisture
- STFT analysis can:
 - Detect and evaluate typical wet/moist bridge deck materials
 - Provide an estimated measurement effect due to wet/moist material issues
 - Offer additional insights for bridge deck GPR material evaluation

Figure 21. Short Time Fourier Transform (STFT) Analysis of Bridge Deck GPR Data

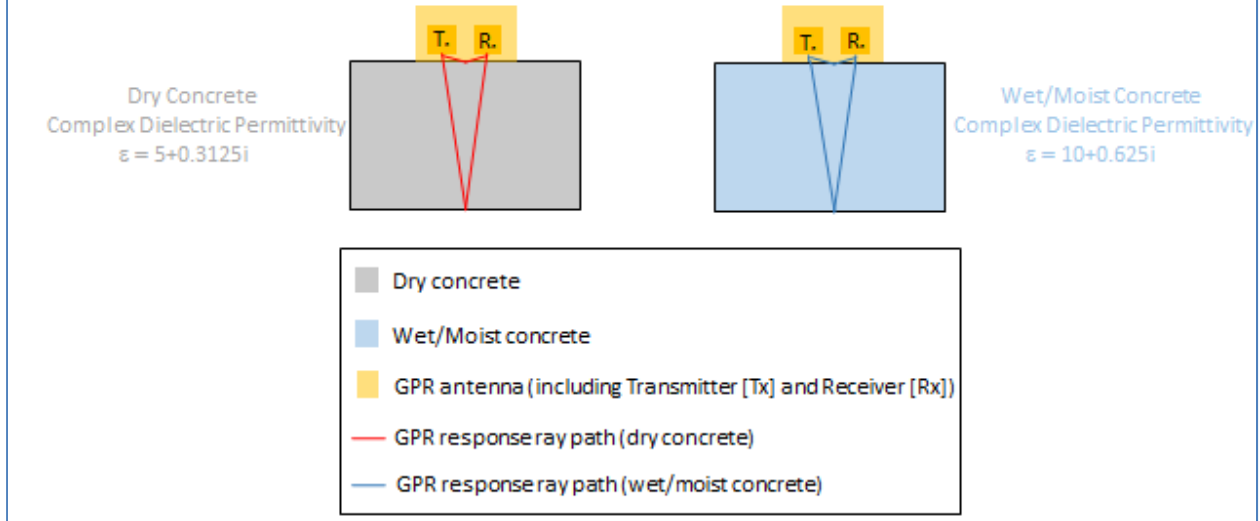


Figure 22. Time Domain Bridge Deck GPR Data Comparison (Analytical Waveform Simulation of GPR Response to Wet vs. Dry Concrete)

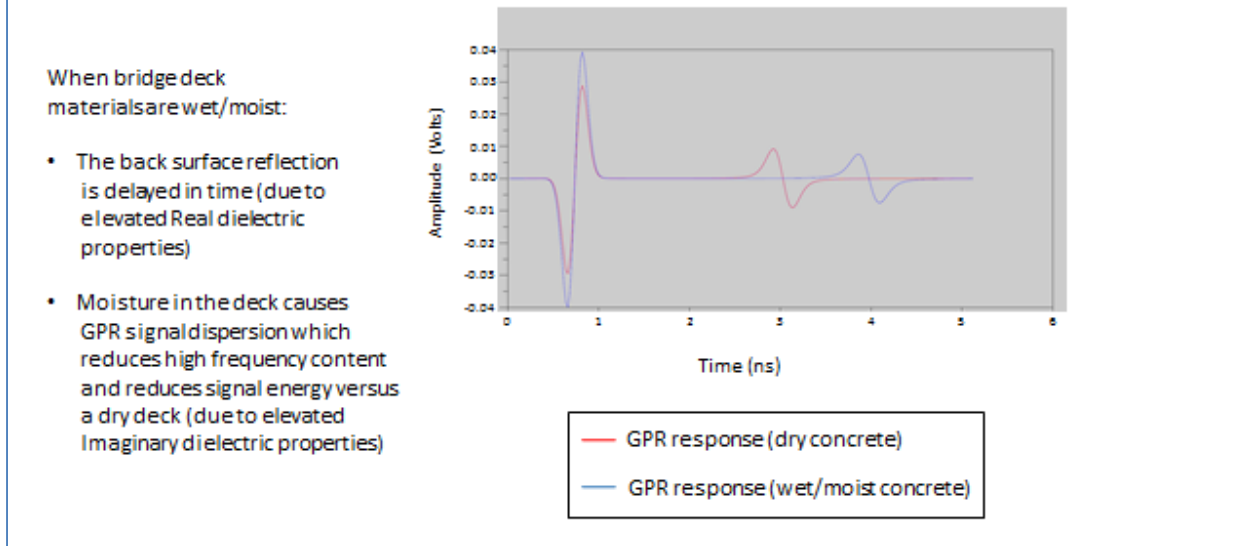
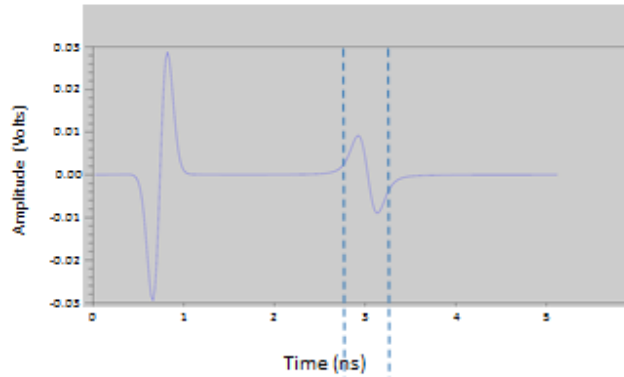


Figure 23. Dry
Concrete STFT Analysis

Time Domain
Bridge Deck GPR Simulated Response
For Dry Concrete



Corresponding STFT of
Bridge Deck GPR Simulated Data
For Dry Concrete

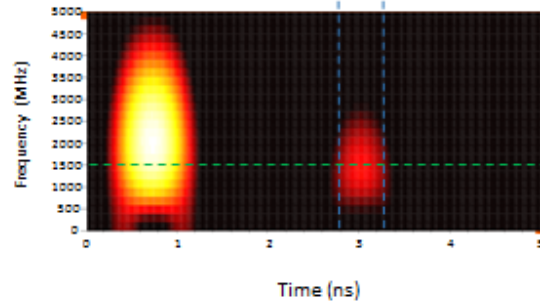
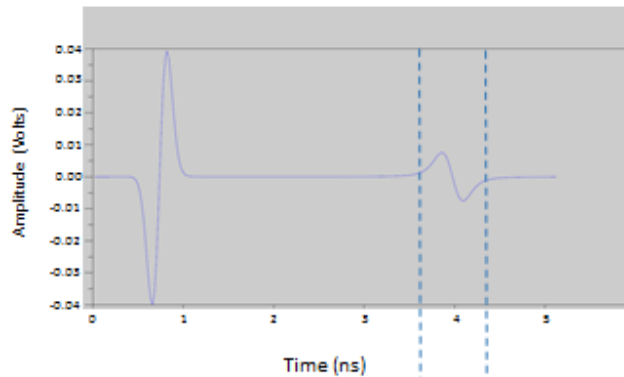


Figure 24. Wet/Moist
Concrete STFT Analysis

Time Domain
Bridge Deck GPR Simulated Response
For Wet/Moist Concrete



Corresponding STFT of
Bridge Deck GPR Simulated Data
For Wet/Moist Concrete

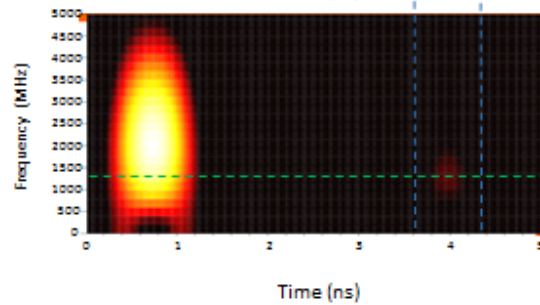


Figure 25. Applying STFT Analysis Principles Using a Fourier Transform Filter

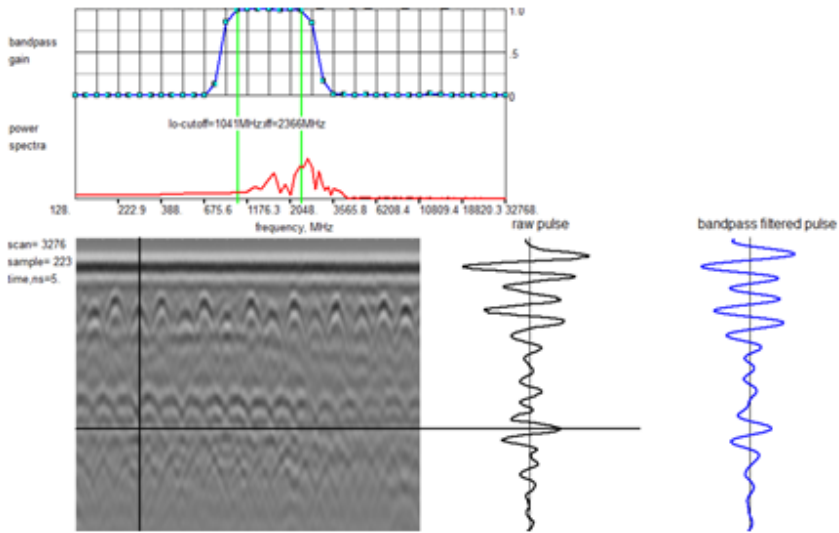


Figure 26. Fourier Transform Filtered Bridge Deck Data (Low Pass) – Rte 346 Bridge Part 1

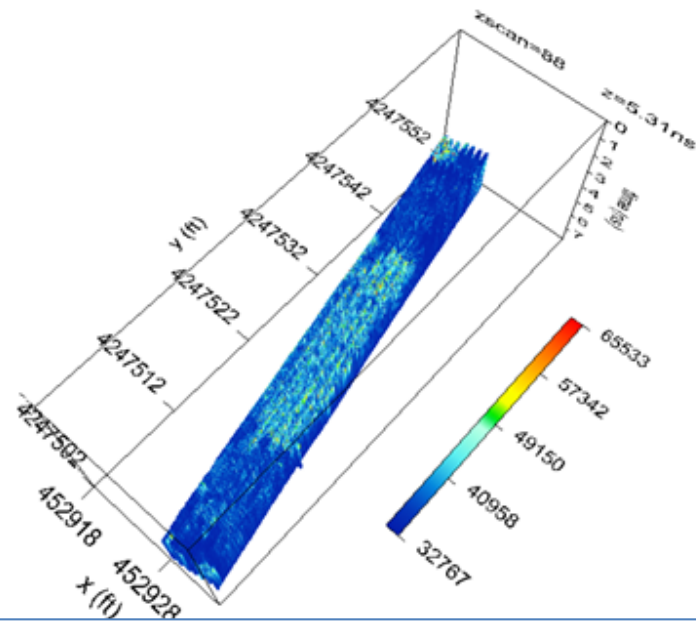


Figure 27. Fourier Transform Filtered Bridge Deck Data (Low Pass) – Rte 346 Bridge Part 2

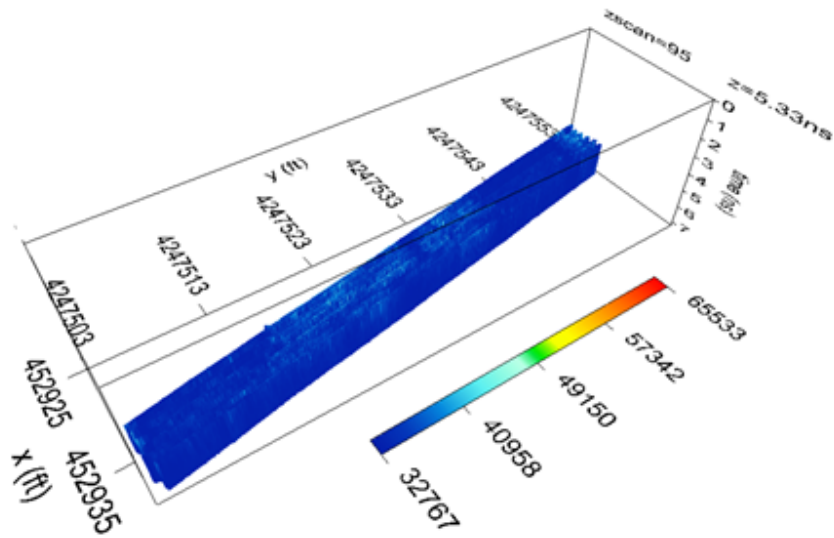


Figure 28. Plan View Results

FT Filtered Results (Part 1)

FT Filtered Results (Part 2)

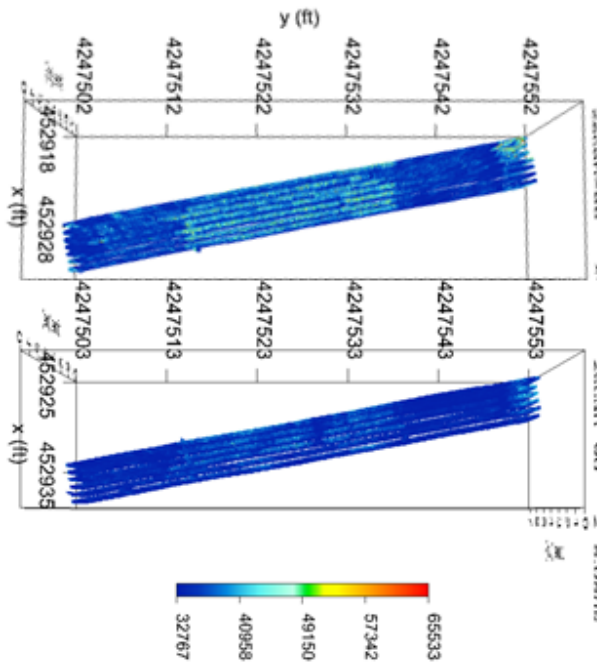
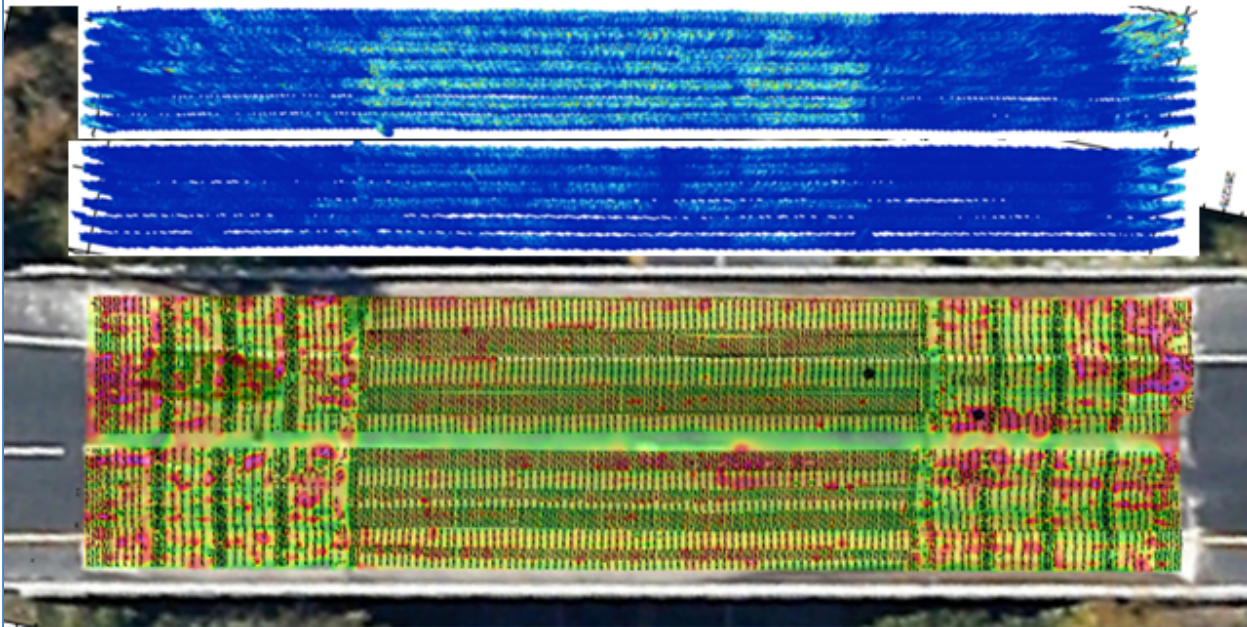


Figure 29. US 13 SB Over MD 346 SB FT Filtered Results (Upper) vs Attenuation Map (Lower)



Interpreting Fourier Transform Analysis

- Part 1 response indicates low moisture content
 - Generally high amplitude (shown in aqua colors)
 - Consistent low frequency response
 - Moisture effects will not have a significant impact on results
- Part 2 response indicates higher moisture content
 - Generally lower amplitude (shown in deeper blue colors)
 - Less consistent low frequency response
 - Moisture effects can have a significant impact on results (including the attenuation map)
- A full spectrum magnitude plot does separate out moisture related phenomena (as the following slide illustrates)

Training Module

Ground Penetrating Radar (GPR) for Precast Concrete Elements

GPR in QA/ QC Process

- GPR Capabilities
 - detect concrete cover;
 - detect substandard steel reinforcement;
 - assess physical dimensions;
 - identify reinforcement orientation and spacing;
 - detect subsurface deterioration.

- **Summary Method (background)**

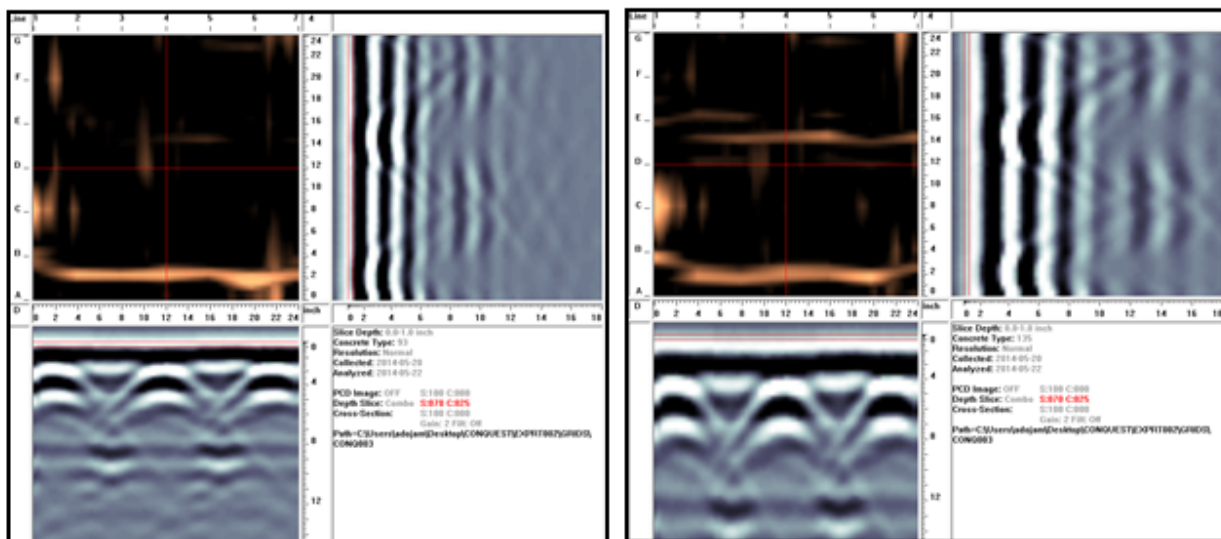
- Handheld GPR evaluation of precast concrete elements
 - Single antenna (transmitter, receiver pair) configuration
 - Collect synthetic aperture radar (SAR) data manually along precisely defined linear paths
 - Collect data along at least two separate linear paths when collecting 2D data (more as appropriate/needed)
 - Collect complementary data along parallel and orthogonal paths when collecting 3D data
 - For each concrete element category, use a detailed data sampling and evaluation plan based on probability of detection of defect or distress features of interest

GPR Apparatus

- **Ground-coupled antenna**
 - Central frequencies greater than 0.9 GHz;
 - Higher frequencies offer greater resolution to image smaller feature details
 - Lower frequencies offer better penetration depth
 - Moderate to high frequency antenna offer a useful compromise (1 GHz)
 - Small, maneuverable antenna sizes are recommended
- **Distance measurement instrument (DMI) trigger wheel features**
 - The DMI trigger wheel should be centrally located to remain in contact on curved surfaces
 - A spring loaded DMI wheel suspension should provide continuous contact on rough surfaces
- Control unit should transmit at a sufficient rate to collect greater than 50 scans/m.
- Compact control unit with integrated display screen recommended
- Scan templates and/or scan location marking equipment should be standardized

Examples
of
GPR Data Analysis in Precast Concrete Elements

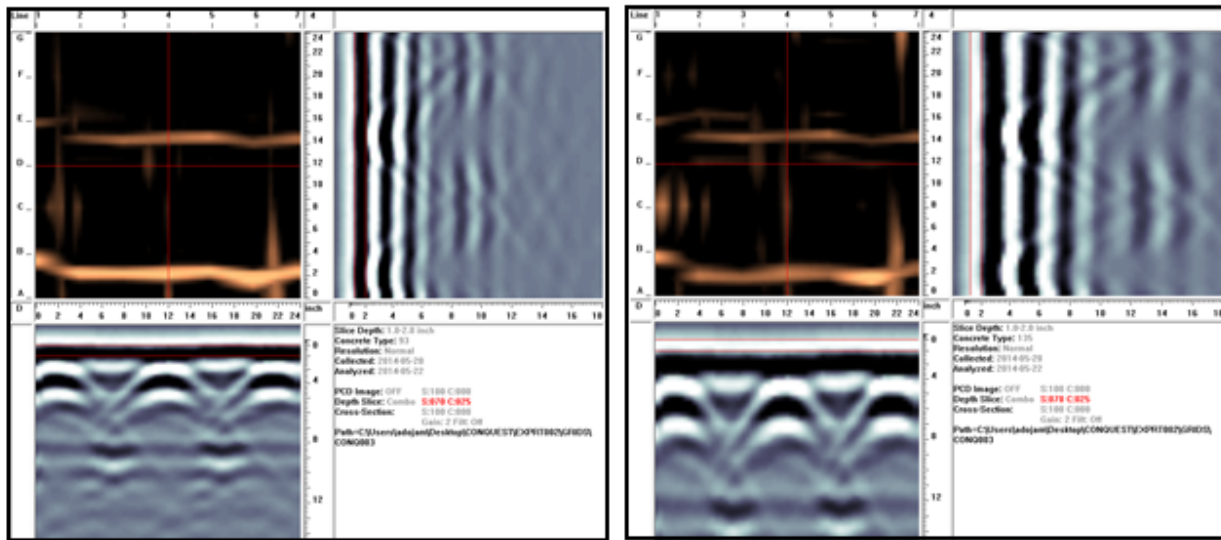
**Figure 1. Grid GPR Data Collected From a Precast Concrete Wall Panel:
Integrated 0 to 1 Inch Depth Plan View Migrated Results (Hot/Red Color Map)
and Individual Alpha Numeric Scans (Gray Color Map)**



Correct Velocity/Dielectric

Assumed Velocity/Dielectric

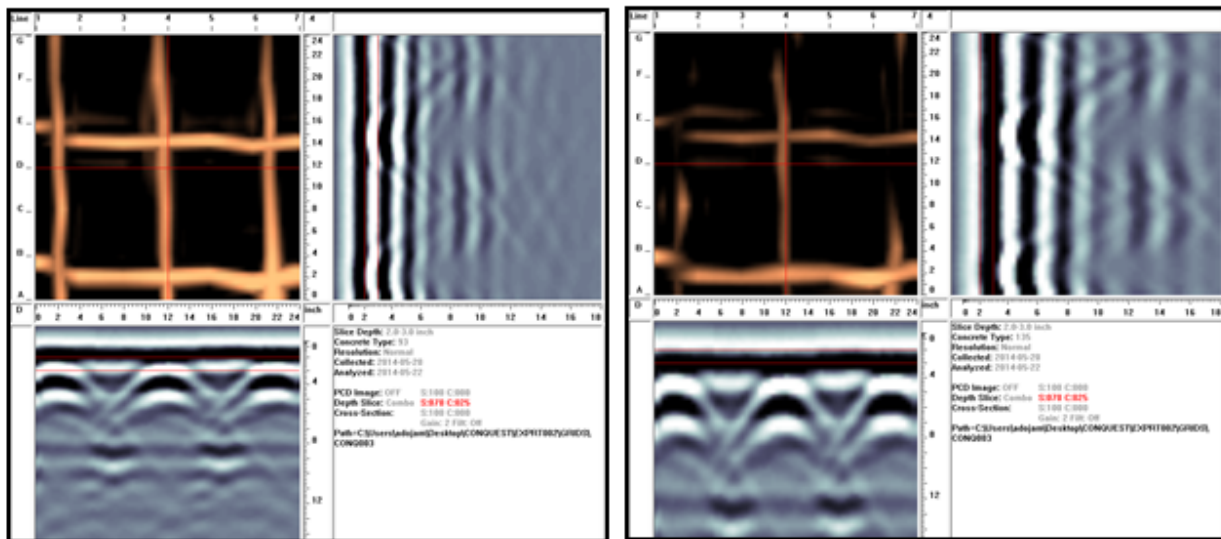
Figure 2. Grid GPR Data Collected From a Precast Concrete Wall Panel:
 Integrated 1 to 2 Inch Depth Plan View Migrated Results (Hot/Red Color Map)
 and Individual Alpha Numeric Scans (Gray Color Map)



Correct Velocity/Dielectric

Assumed Velocity/Dielectric

Figure 3. Grid GPR Data Collected From a Precast Concrete Wall Panel:
 Integrated 2 to 3 Inch Depth Plan View Migrated Results (Hot/Red Color Map)
 and Individual Alpha Numeric Scans (Gray Color Map)



Correct Velocity/Dielectric

Assumed Velocity/Dielectric

Figure 4. Grid GPR Data Collected From a Precast Concrete Wall Panel:
 Integrated 3 to 4 Inch Depth Plan View Migrated Results (Hot/Red Color Map)
 and Individual Alpha Numeric Scans (Gray Color Map)

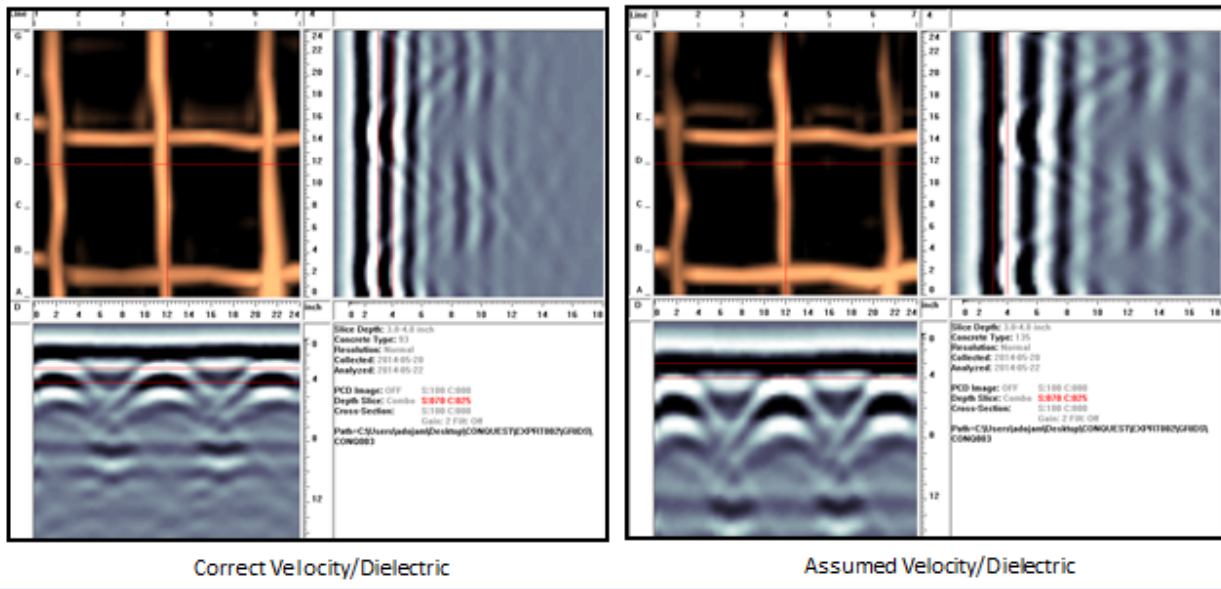
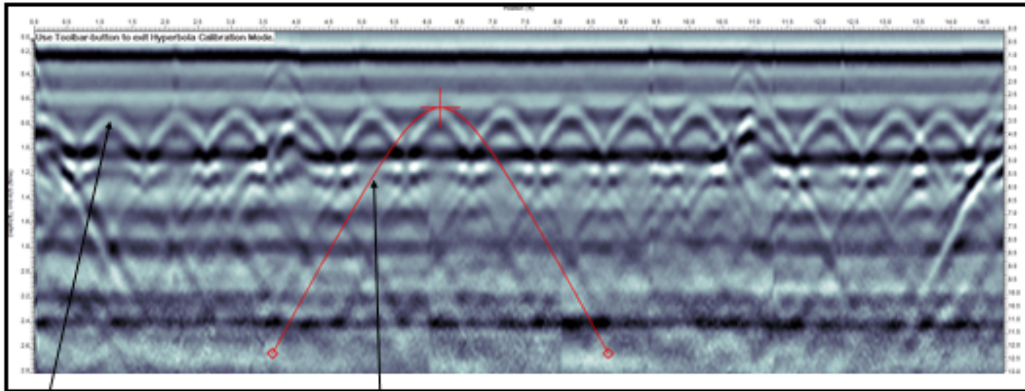


Figure 5. Line Scan GPR Data Collected From a Precast Concrete Header Wall Element (Scan 1 – Horiz.):
 Assumed Velocity/Dielectric

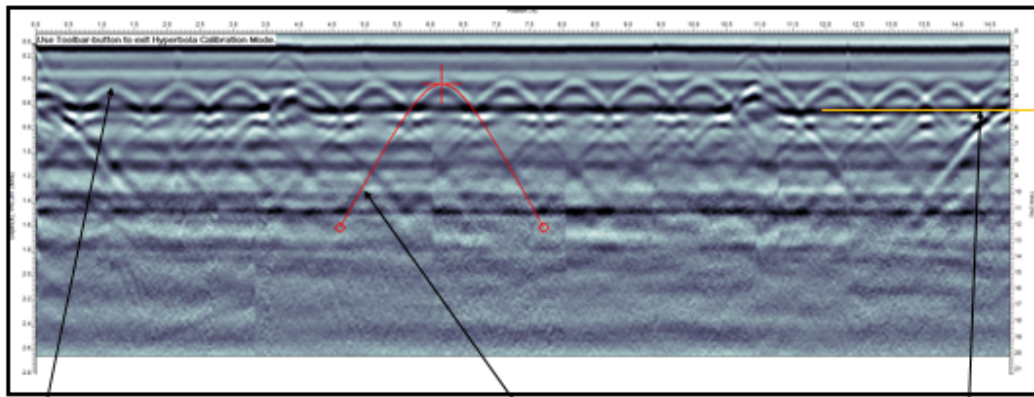


Transverse Reinforcing Steel
 Response (Synthetic Aperture
 Radar Hyperbola Feature)

Assumed Calibration Hyperbola
 (Poor fit Corresponding to Initial
 Dielectric Property)



**Figure 6. Line Scan GPR Data Collected From a Precast Concrete Header Wall Element (Scan 1 - Horiz):
Correct Velocity/Dielectric**

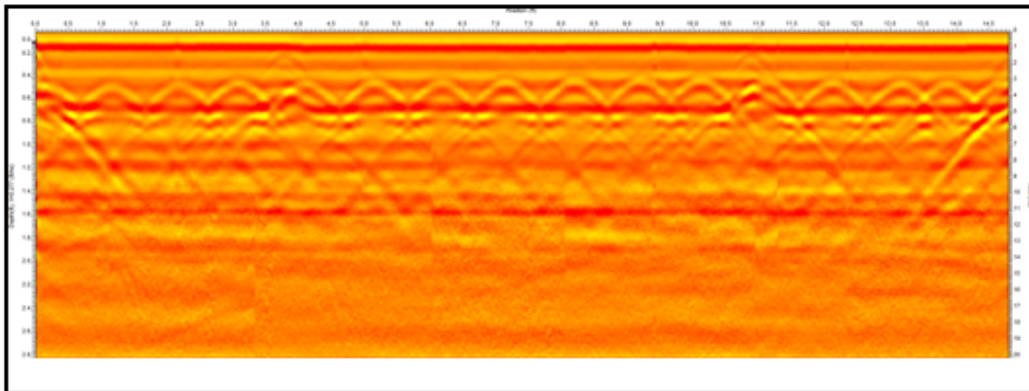


Transverse Reinforcing Steel
Response (Synthetic Aperture
Radar Hyperbola Feature)

Correct Calibration Hyperbola
(Correct fit Corresponding to Appropriate
Dielectric Property)

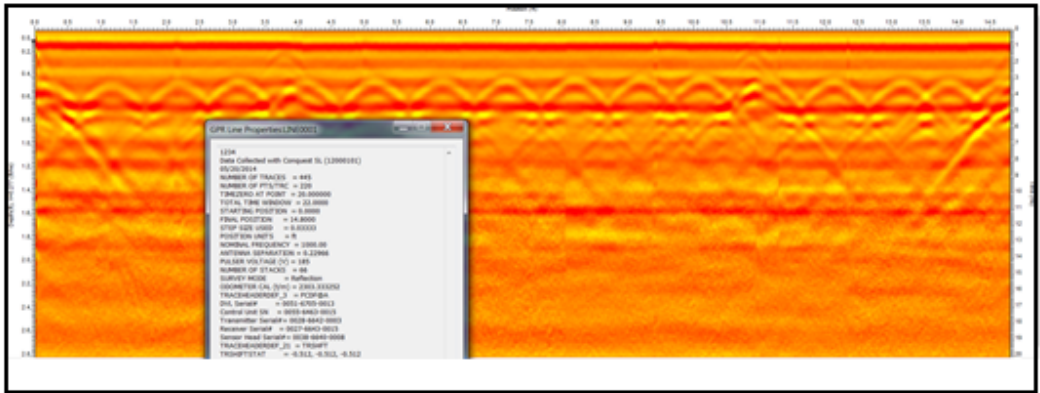
Back Wall Response
Depth

**Figure 7. Line Scan GPR Data Collected From a Precast Concrete Header Wall Element (Scan 1 – Horiz.):
Correct Velocity/Dielectric (Hot/Red Color Map)**



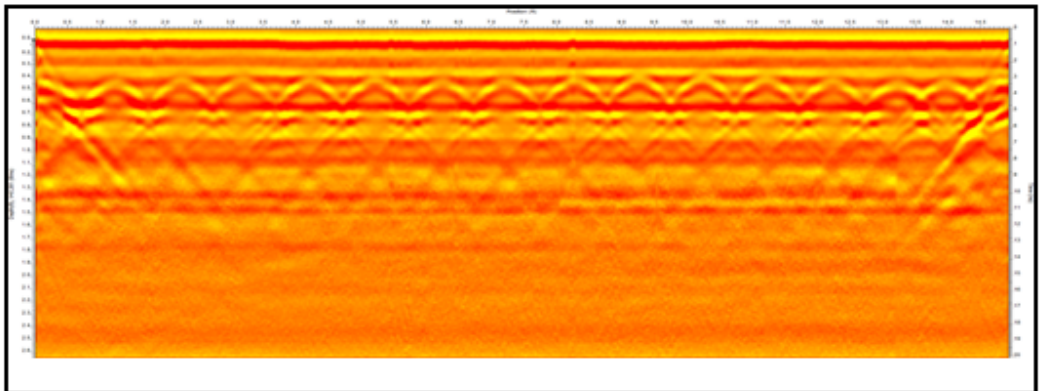
Alternative Color Maps can Improve Contrast and Visualization of Features of Interest

**Figure 8. Line Scan GPR Data Collected From a Precast Concrete Header Wall Element (Scan 1 – Horiz.):
Data Collection Parameters Shown**



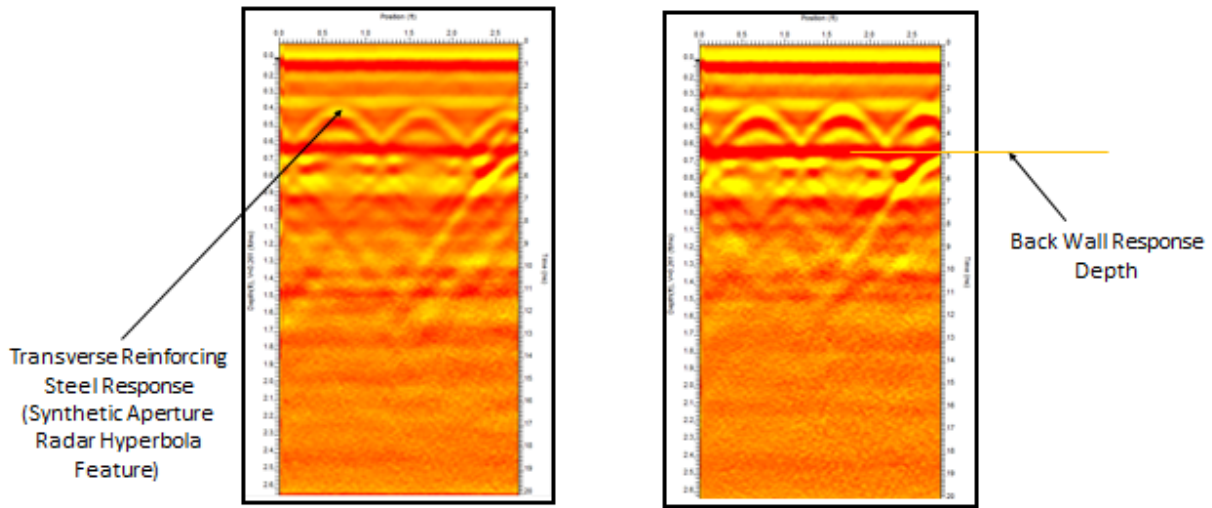
GPR Parameters Stored With Each Collected File can be Used to Confirm Correct
Data Collection Configuration

Figure 9. Line Scan GPR Data Collected From a Precast Concrete Header Wall Element (Scan 2 – Horiz.)



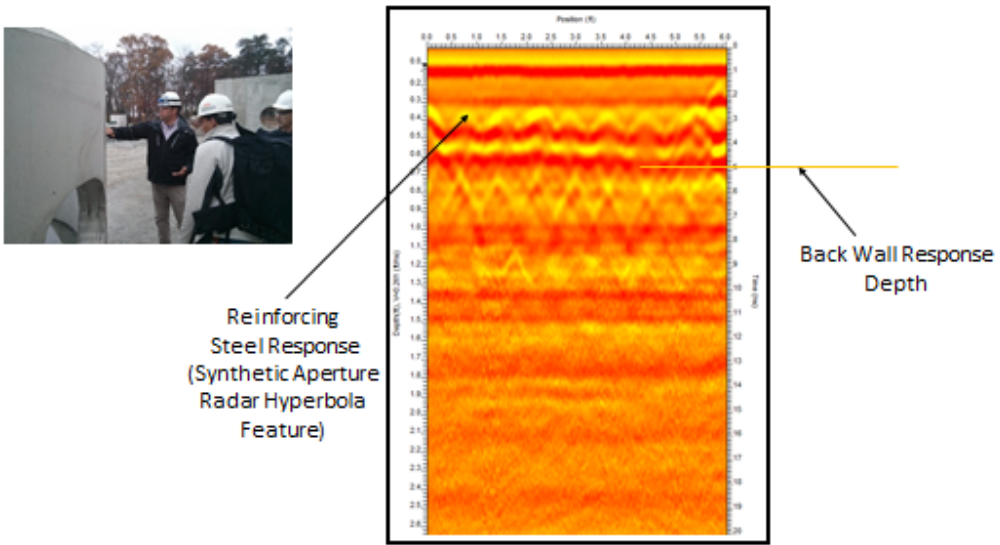
GPR Line Scan 2 Indicates Features Consistent With Scan 1

Figure 10. Line Scan GPR Data Collected From a Precast Concrete Header Wall Element (Scans 3 and 4 – Vert.)



Two Vertical GPR Line Scans From an Example Header Wall Illustrate Orthogonal Reinforcing Steel Symmetry When Compared With Horizontal GPR Line Scans From the Same Wall Element

Figure 11. Line Scan GPR Data Collected From a Precast Concrete Cylinder Element (Scan 5 – Horiz.)



Horizontal GPR Line Scan of a Precast Concrete Cylinder Element

Figure 12. Precast Concrete Cylinder Element

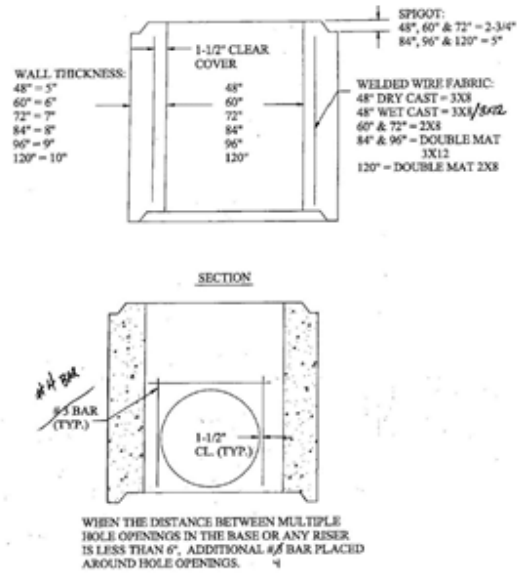


Figure 13. Line Scan GPR Data Collected From Side of a Precast Concrete Manhole Element (Scan 10 – Horiz.)

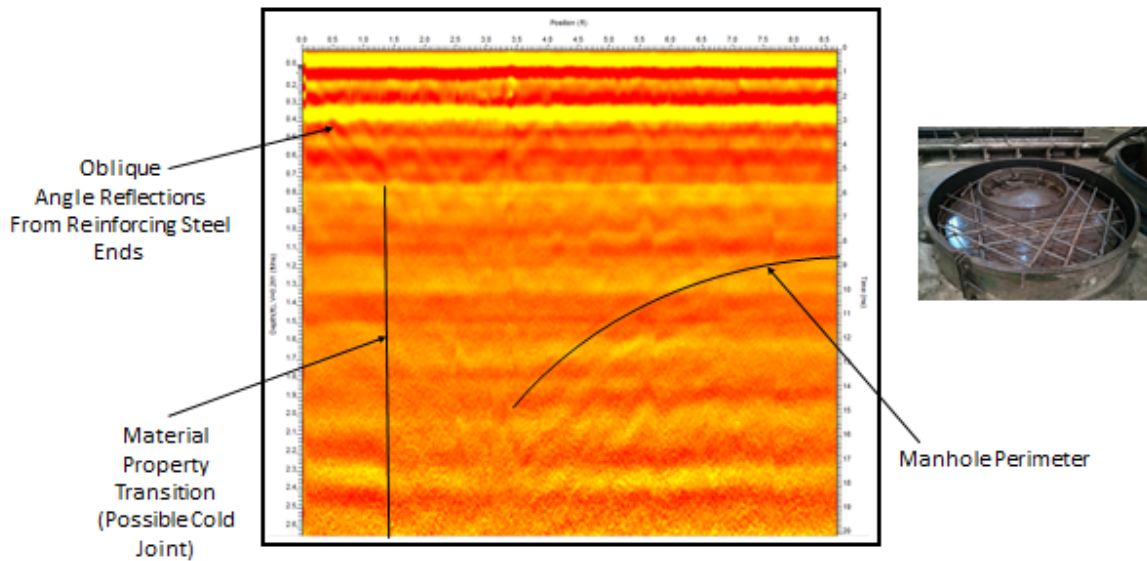


Figure 14. Precast Concrete Manhole Element

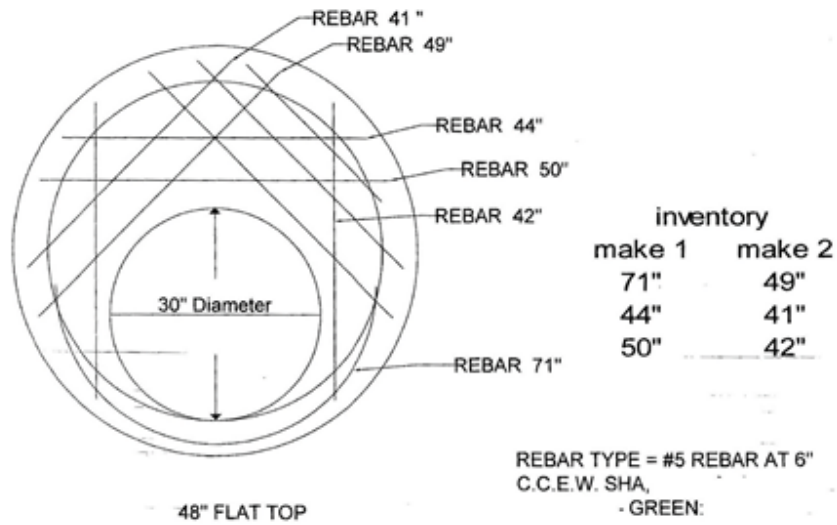


Figure 15. Line Scan GPR Data Collected From a Moist Precast Concrete Cylinder Element (Scan 11 – Horiz.)

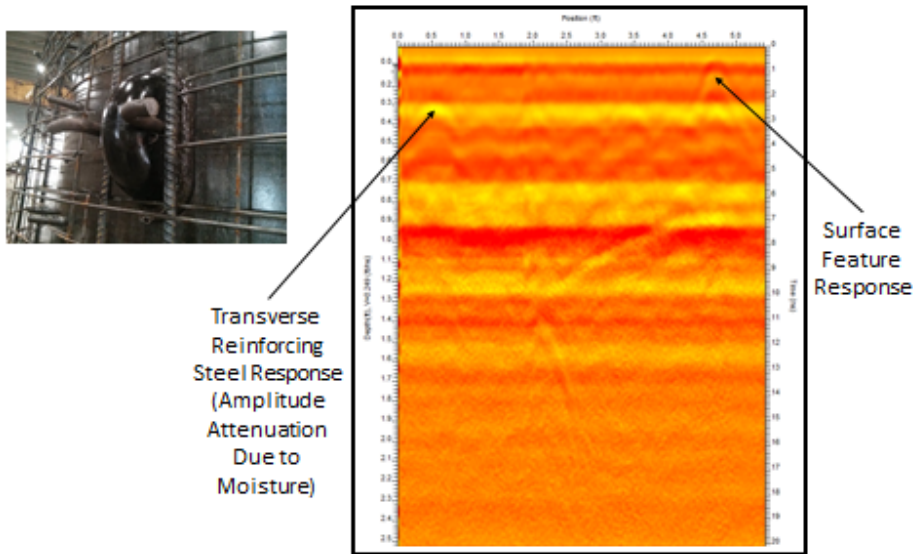


Figure 16. Line Scan GPR Data Collected From a Moist Precast Concrete Cylinder Element (Scan 17 – Vert.)

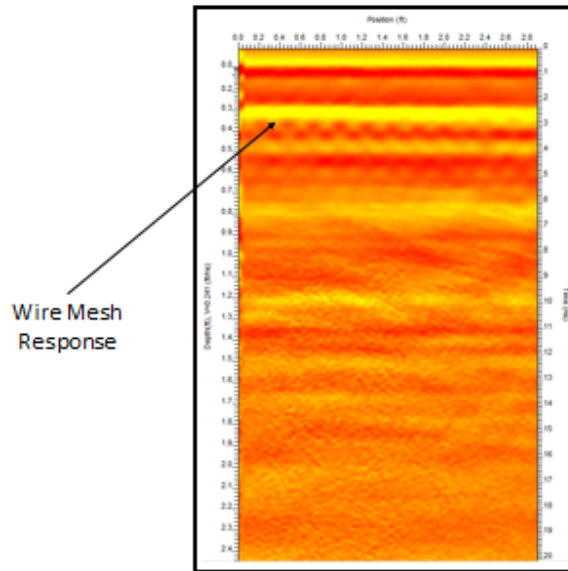


Figure 17. Line Scan GPR Data Collected From a Sound Wall (Scan 20 – Vert.)

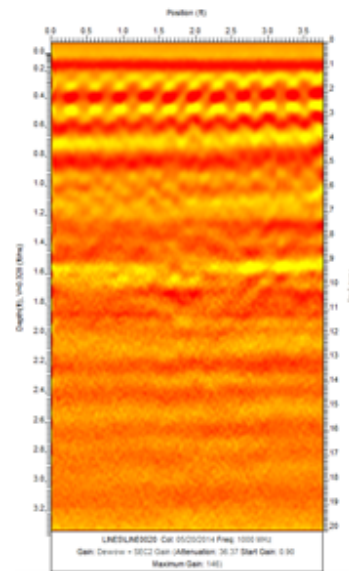
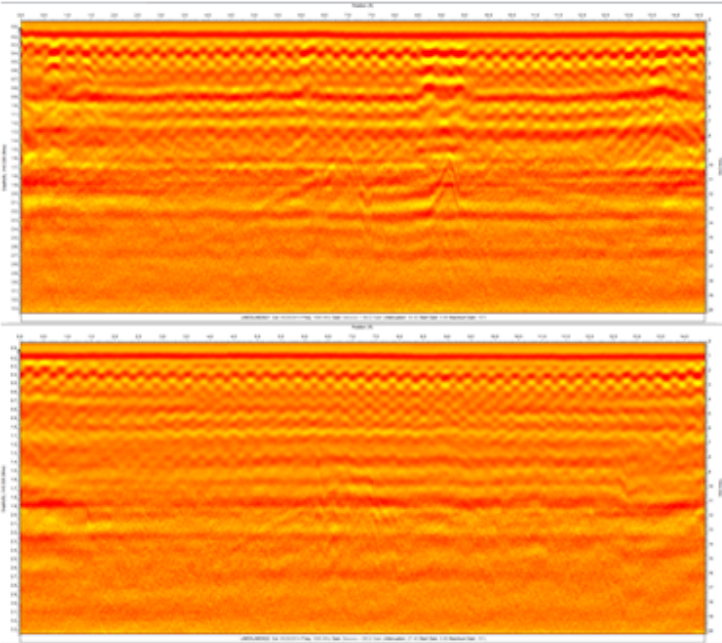
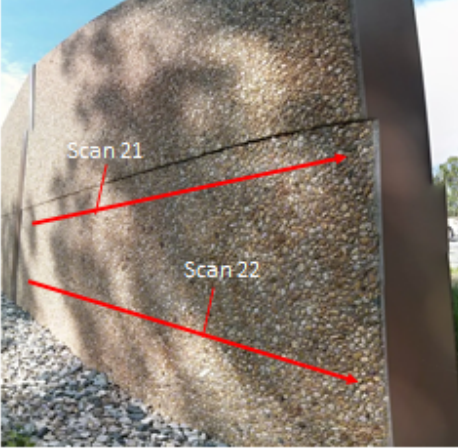


Figure 18. Line Scan GPR Data Collected From a Sound Wall (Scans 21, 22 – Horiz.)



APPENDIX C
SCI-LAB SCRIPT

The SciLab script code beta version 3 is composed of an executable file (MSA25.sce and two custom functions (compscript1.sci and Rmsf2.sci) called by the executable file. The purpose of each script is described next.

1. MSA25.sce SciLab executable script.

Purpose: Evaluates and summarizes GPR pavement layer data trends and features using automated or semi-automated techniques.

```
/* Multi Scale Analysis (Revision 3 Beta)
/*
/* Purpose:
/* Evaluates and summarizes GPR pavement layer data trends and
/* features using automated or semi-automated techniques
/*
/* Inputs:
/* Milepost data filename: pathai definition (Line 24)
/* Layer1 depth data filename: patha definition (Line 25)
/* Layer2 depth data filename: pathb definition (Line 26)
/* Layer3 depth data filename: pathc definition (Line 26)
/*
/* Final Output:
/* Plot presenting multi-scale results corresponding to three
/* GPR pavement data layers
/*
/* User adjustable parameters:
/* 1. path = Current directory (where all data files, executables
/* and subroutines are stored)
/* 2. initsub = number of multi-scale analysis (MPGA) subdivisions
/* desired by the user for analysis

mode(0)
clear all;

***Adjust number of multi-scale subdivisions by defining initsub
initsub=16.0;
***Change path string below to match directory selected
path='C:\test\Rev3\';
***Change file names to reflect input file names
pathai='MP.csv';
patha='US15L1.csv';
pathb='US15L2.csv';
pathc='US15L3.csv';

//Set current directory to path
cd(path);
//Initialize *.sci functions to use as program subroutines
funcprot(0);
exec("rmsf2.sci");
exec("compcrit1.sci");
```

```
//Load Data Strings
```

```
samp=35832;
```

```
path1i=strcat([path,pathai]);  
fd_ri=mopen(path1i,'rt');  
txti=mgetl(fd_ri, samp);  
//mprintf('%s\n',txti);  
di=strtod(txti);  
[di,endstr]=strtod(txti);  
clear(txti);  
erri=mclose([fd_ri]);
```

```
path1=strcat([path,patha]);  
path2=strcat([path,pathb]);  
path3=strcat([path,pathc]);
```

```
fd_r=mopen(path1,'rt');  
txt=mgetl(fd_r, samp);  
//mprintf('%s\n',txt);  
d=strtod(txt);  
[d,endstr]=strtod(txt);  
clear(txt);  
err=mclose([fd_r]);
```

```
fd_r2=mopen(path2,'rt');  
txt2=mgetl(fd_r2, samp);  
//mprintf('%s\n',txt2);  
d2=strtod(txt2);  
[d2,endstr]=strtod(txt2);  
clear(txt2);  
err2=mclose([fd_r2]);
```

```
fd_r3=mopen(path3,'rt');  
txt3=mgetl(fd_r3, samp);  
//mprintf('%s\n',txt3);  
d3=strtod(txt3);  
[d3,endstr]=strtod(txt3);  
clear(txt3);  
err3=mclose([fd_r3]);
```

```
//Threshold Values for Difference in Mean and Standard Dev Between Segments and initial subdivision size
```

```
MeanDif1=0.3;  
StDevDif1=0.1;  
MeanDif2=0.3;  
StDevDif2=0.1;  
MeanDif3=0.3;  
StDevDif3=0.1;
```

```

szd=size(d);
szdone=szd(1);
szd2=size(d2);
szd2one=szd2(1);
szd3=size(d3);
szd3one=szd3(1);

```

//Initial Layer 1 Statistics (Full Data Set)

```

x2=0;
for x=1:szdone
    if isnan(d(x)) then
        d(x)=0;
    end
    if d(x)<>0|d(x)<>%nan then
        x2=x2+1;
        ds(x2)=d(x);
    end
end
end
[ij, v, mn]=spget(sparse(ds));
dstdev=stdev(v);
dmean=mean(v);

```

//Initial Layer 2 Statistics (Full Data Set)

```

y2=0;
for x=1:szd2one
    if isnan(d2(x)) then
        d2(x)=0;
    end
    if d2(x)<>0|d2(x)<>%nan then
        y2=y2+1;
        d2sa=d2(x);
        d2s(y2)=d2sa;
    end
end
end
[ij, v, mn]=spget(sparse(d2s));
dstdev2=stdev(v);
dmean2=mean(v);

```

//Initial Layer 3 Statistics (Full Data Set)

```

z2=0;
for x=1:szd3one
    if isnan(d3(x)) then
        d3(x)=0;
    end
    if d3(x)<>0|d3(x)<>%nan then
        z2=z2+1;
        d3sa=d3(x);
        d3s(z2)=d3sa;
    end
end

```

```

    end
end
[ij, v, mn]=spget(sparse(d3s));
dstdev3=stdev(v);
dmean3=mean(v);

// Filter significant layer crossover phenomena

for x=1:szd2one
    if d2(x)<>0&d2(x)<dmean then
        d2(x)=0.;
    end
end

for x=1:szd3one
    if d3(x)<>0&d3(x)<dmean2 then
        d3(x)=0.;
    end
end

//Initial plot with three data layers and mean values presented

for x=1:szdone
    if d(x)<>0 then
        mn1(x)=dmean;
        di1(x)=di(x);
    else
        mn1(x)=0.;
    end
end

for x=1:szd2one
    if d2(x)<>0 then
        mn2(x)=dmean2;
        di2(x)=di(x);
    else
        mn2(x)=0.;
    end
end

for x=1:szd3one
    if d3(x)<>0 then
        mn3(x)=dmean3;
        di3(x)=di(x);
    else
        mn3(x)=0.;
    end
end

//[dmeans,dmean2s,dmean3s,dstdvs,dstdv2s,dstdv3s]=substat(d,d2,d3);

```

```

figure(2);

plot(di,d,'bd',di,d2,'k+',di,d3,'r. ');
plot(di,mn1,'wd');
plot(di,mn2,'gd');
plot(di,mn3,'yd');

for x=1:szd3one
// plot(di3,mn3,'y- ');
end

xlabel("Milepost");
ylabel("Depth (inches)");

//Initial Multi-Scale Subdivision Function Call - Layer 1

[L1subm,L1substd,mn1seg,std1seg]=rmsf2(szd3one,initsub,di,d,MeanDif1,StDevDif1);
figure(100);
plot(di,d,'d');
plot(di,L1subm,'wd');

//Initial Multi-Scale Subdivision Function Call - Layer 2

[L2subm,L2substd,mn2seg,std2seg]=rmsf2(szd2one,initsub,di,d2,MeanDif2,StDevDif2);
figure(101);
plot(di,d2,'k+');
plot(di,L2subm,'gd');

//Initial Multi-Scale Subdivision Function Call - Layer 3

[L3subm,L3substd,mn3seg,std3seg]=rmsf2(szd3one,initsub,di,d3,MeanDif3,StDevDif3);
figure(102);
plot(di,d3,'r. ');
plot(di,L3subm,'yd');

//Initial layer 1 subdivision criteria evaluation

[L1submo1,mn1sega,std1sega,crit1,lbl]=compcrit1(szd3one,mn1seg,std1seg,initsub,L1subm,MeanDif1,StDevDif1,dmean,dstdev);
figure(200);
plot(di,d,'d');
plot(di,L1submo1,'wd');

//Initial layer 2 subdivision criteria evaluation

[L2submo2,mn2sega,std2sega,crit2,lbl2]=compcrit1(szd2one,mn2seg,std2seg,initsub,L2subm,MeanDif2,StDevDif2,dmean2,dstdev2);
figure(400);
plot(di,d2,'k+');
plot(di,L2submo2,'gd');

//Initial layer 1 subdivision criteria evaluation

```

```

[L3submo3,mn3sega,std3sega,crit3,lbl3]=compcrit1(szd3one,mn3seg,std3seg,initsub,L3subm,MeanDif3,StDev
Dif3,dmean3,dstdev3);
figure(600);
plot(di,d3,'r. ');
plot(di,L3submo3,'yd');

//Plot final multi-scale output results
figure(1000);
plot(di,d,'bd',di,d2,'k+',di,d3,'r. ');
plot(di,L1submo1,'wd');
plot(di,L2submo2,'gd');
plot(di,L3submo3,'yd');

```

2. compscrit1.sci

Purpose: Evaluate multiscale phenomena based on statistical criteria at a user selected scale of interest. Consistent data trends and data variability are detected and passed to the main program script as output via the Lsubmo2 variable based on the analysis scale selected.

```

function [Lsubmo2, mnsegn, stdsegn, crit, lbl]=compcrit1(sz, mnseg, stdseg, initsub, Lsubm, MeanDif1cr,
StDevDif1cr, dmean, dstdev)

```

```

/** Function call for MSA25.sce SciLab script
/**
/** Purpose: Evaluate multiscale phenomena based on statistical
/** criteria at a user selected scale of interest. Consistent data
/** trends and data variability are detected and passed to the main
/** program script as output via the Lsubmo2 variable based on
/** the analysis scale selected.

```

```

//Evaluate initial segmented results versus multiscale criteria

```

```

for xi=1:initsub
    mndif1=mnseg(xi)-dmean;
    stddif1=stdseg(xi)-dstdev;
    if mndif1<MeanDif1cr&stddif1<StDevDif1cr then
        mnsegn(xi)=dmean;
        stdsegn(xi)=dstdev;
        crit(xi)=1;
    else
        mnsegn(xi)=mnseg(xi);
        stdsegn(xi)=stdseg(xi);
        crit(xi)=0;
    end
end

```

```

incr=round(sz/initsub);
sbst=0;
lblinc=1;

```

```

for xi=1:initsub
  clear subset;
  clear mn1;
  clear std1;
  clear dep;
  sbst=sbst+incr;
  ref=1;
  if xi>1 then;
    ref=sbst-incr+1;
  end
  if xi==initsub then
    ref=sz-incr+1;
    sbst=sz;
  end
  for y=ref:sbst
    if Lsubm(y)<>0 then
      if crit(xi)==1 then
        Lsubmo(y)=dmean;
        lbl(y)=lblinc;
      else
        Lsubmo(y)=Lsubm(y);
        lbl(y)=0;
      end
    else
      Lsubmo(y)=0;
      lbl(y)=0;
    end
  end
  if crit(xi)==0 then
    lblinc=lblinc+1;
    lbl(y)=0;
  end
end
end

```

```

incr=round(sz/initsub);
sbst=0;
lblinc=1;
for xi=1:initsub
  sbst=sbst+incr;
  ref=1;
  if xi>1 then;
    ref=sbst-incr+1;
  end
  if xi==initsub then
    ref=sz-incr+1;
    sbst=sz;
  end
  for y=ref:sbst
    if Lsubm(y)<>0 then
      if lbl(y)>=1 then
        lblcur=lbl(y);
      end
    end
  end
end

```

```

        vals(lblcur,y)=Lsubm(y);
    end
end
end
end

valsmn(1:lblcur)=0;
incrm(1:lblcur)=0;
incr=round(sz/initsub);
sbst=0;
for xi=1:initsub
    sbst=sbst+incr;
    ref=1;
    if xi>1 then;
        ref=sbst-incr+1;
    end
    if xi==initsub then
        ref=sz-incr+1;
        sbst=sz;
    end

    for y=ref:sbst
        if lbl(y)>=1 then
            valsmn(lbl(y))=valsmn(lbl(y))+vals(lbl(y),y);
            incrm(lbl(y))=incrm(lbl(y))+1;
            lblinc=lbl(y);
            lblr(y)=lbl(y);
        end
        if lbl(y)==0 then
            lblr(y)=50;
        end
    end
end
end
mnlbl=min(lblr);

for incs=mnlbl:lblinc
    mn(incs)=(valsmn(incs)/incrm(incs));
end

```

*//substitute local means for broad calculated means where
//apropriate*

```

sbst=0;
for xi=1:initsub
    sbst=sbst+incr;
    ref=1;
    if xi>1 then;
        ref=sbst-incr+1;
    end
    if xi==initsub then
        ref=sz-incr+1;
        sbst=sz;
    end

```

```

end
for y=ref:sbst
    if lblr(y)>=1&lblr(y)<50 then
        Lsubmo2(y)=mn(lbl(y));
    else
        Lsubmo2(y)=Lsubmo(y);
    end
end
end
end

```

```
endfunction
```

3. **Rmsf2.sci** SciLab script.

Purpose: Evaluate statistical parameters of pavement layer depth data corresponding to data segments at user defined scale.

```
function [mns1, stds1, mn1seg, std1seg]=rmsf2(sz, initsub, milepost, depth, MeanDif, StDevDif)
```

```
/* Function call for MSA25.sce SciLab script
```

```
/*
```

```
/* Purpose: Evaluate statistical parameters of pavement layer depth
```

```
/* data corresponding to data segments at user defined scale
```

```

clear mns1;
clear stds1;
incr=round(sz/initsub);
sbst=0;
for xi=1:initsub
    clear subset;
    clear mn1;
    clear std1;
    clear dep;
    sbst=sbst+incr;
    ref=1;
    if xi>1 then;
        ref=sbst-incr+1;
    end
    if xi==initsub then
        ref=sz-incr+1;
        sbst=sz;
    end
    dep=depth;
    incr=0;
    totz=1;
    tot=0;
    for zi=ref:sbst

```

```

if isnan(dep(zi)) then
    dep(zi)=0;
end
if dep(zi)>0|dep(zi)<>%nan then
    incr=incr+1;
    subset(incr)=dep(zi);
end
end
[ij, v, mn]=spget(sparse(subset));
mn1=mean(v);
mn1seg(xi)=mn1;
std1=stdev(v);
std1seg(xi)=std1;
for y=ref:subst
    if dep(y)<>0 then
        mns1(y)=mn1;
        stds1(y)=std1;
    else
        mns1(y)=0.;
        stds1(y)=0.;
    end
end
end
endfunction

```